E/MJ THIS MONTH IN MINING

In-situ uranium leaching operations flourish in southern Texas

ONLY TWO YEARS after the first commercial operation came on stream near George West, in-situ uranium leaching has established a strong foothold in southern Texas. (See E/MJ, July 1975, p 73.) Four leaching operations are now on stream in the area, with four more in various phases of development and pilot testing.

The Clay West mine, near George West, Tex., was started up in April 1975 by joint venturers Atlantic Richfield (50% owner and operator), Dalco Oil (25%), and US Steel (25%). The operation is currently being expanded from 250,000 to 1 million lb per year of yellowcake. The expanded plant, due to come on stream next year, is now a joint venture of US Steel and Niagara Mohawk. Dalco and Arco have sold their shares. Arco is operating the facility until August 1, when US Steel will take over.

Clay West was the first commercial in-situ mine to tap U_3O_8 from the Texas uranium province that extends from north of Houston to Brownsville. At nearby Burns Ranch, an operation owned 100% by US Steel came into production last December, with a 150,000-lb-per-year capacity. In a radical departure from Clay West, where pregnant solution is pumped to a central processing plant, Burns is designed with an ion exchange column at the wellfield. After uranium is extracted, the laden resin is trucked in 10,000- to 12,000-g lots to a central plant for processing. This system provides great flexibility and is more economical than piping, according to US Steel officials. Satellite fields have been set up. When one field is exhausted, a new one can be opened by rerouting the trucks.

Near Bruni, Wyoming Mineral Corp. is completing a development phase of 100,000 lb per year and expects to reach full production of 250,000 lb per year by yearend. At the Bruni plant, about 10 acres are in production, with 120 wells per 5 acres, at 40- to 60-ft intervals in a five-spot pattern—four injection wells surrounding each production well. A weak ammonia leach and proprietary ion exchange extraction are used. Current operations will recover more than 50%, and in some areas more than 75%, of the uranium from the wells. The solution produced contains 100 to 200 ppm in initial leaching stages, but concentration may fall as low as 25 ppm as the ore is depleted in a well, indicating the need for wellfield realignment or expansion.

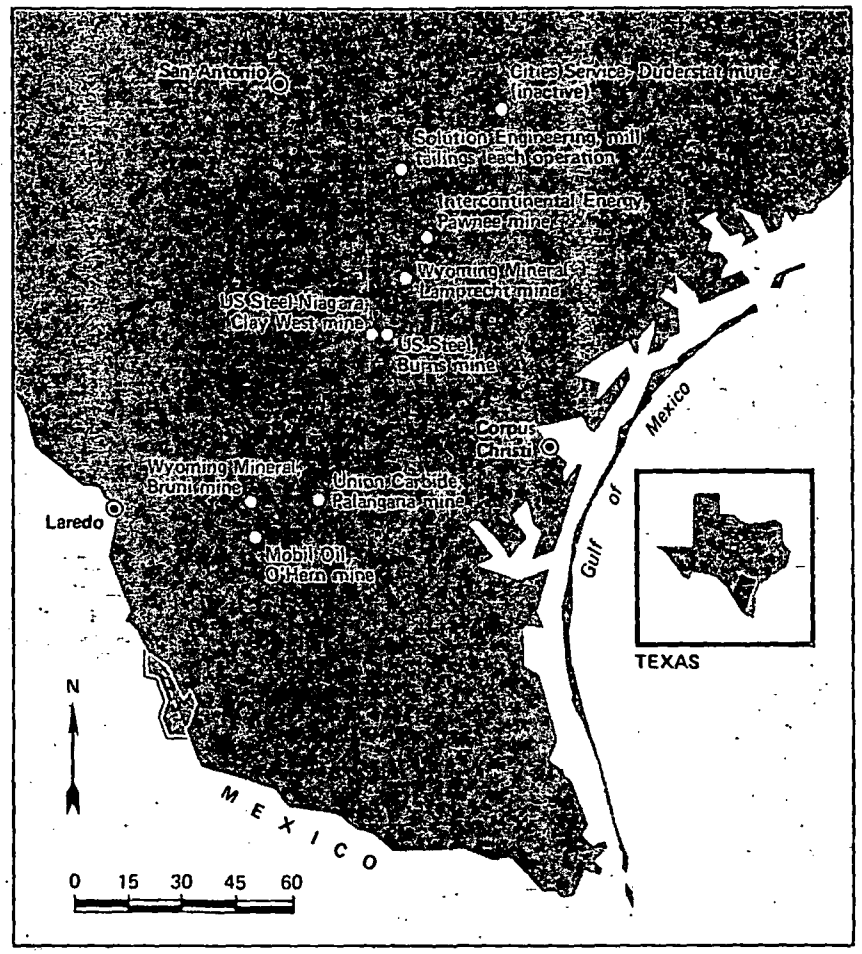

Control of the Bruni operation is manual, guided by in-plant instrumentation and a flow meter on each wellhead. The levels of injection and recovery surge tanks also are monitored to assure that injection does not exceed withdrawal. Monitoring wells on the periphery are sampled biweekly; if there are indications of an excursion, the situation is corrected either by halting injection and overpumping the

(Continued on p 27)

In-situ uranium operations in Texas

Company	Location	Capacity (lb per year U_3O_8)	Status
US Steel, Niagara Mohawk	George West	250,000	Expanding to 1 million lb per year.
US Steel	Burns Ranch	150,000	In production.
Wyoming Mineral	Bruni	100,000	Full production will be 250,000 lb per year.
Wyoming Mineral	Ray Point	500,000	Being developed.
Union Carbide	Duval County		Pilot testing.
International Energy	Pawnee mine	180,000	On stream.
International Energy	Ray Point	300,000	On stream in March 1978.
Solution Engineering	Alice	1 million lb total production	Recovery from tailings.

production wells or by changing the pumping balance in that portion of the field.

Experience at Bruni facilitated construction of the company's second production unit—the Lamprecht plant at Ray Point, north of George West. This installation is designed for a capacity of 500,000 lb per year of yellowcake. Development at Lamprecht has been done under a temporary order of the Texas Water Quality Board. Wyoming Mineral expected to receive permits from the board in May to allow full operation of the plant. The company says that the Lamprecht mine is virtually a duplicate of the facilities at Bruni except in capacity, and that bringing the plant on stream should present few problems because of the lessons learned at Bruni.

In Duval County, Union Carbide has been pilot-testing its plant for the past 18 months. The company pumped at a total rate of 120 gpm last July, and in January 1977 began injecting 32 wells at 10 gpm each. No production figures are available.

International Energy Co. came on stream this spring with a 180,000-lb-per-year facility whose output will go to Virginia Electric Power. At the Pawnee mine in Bee County, the basic process is similar to other operations in the area—alkaline leach and a fixed resin reactor—but design of the well pattern is unique. IEC uses a computer-generated wellfield design, which takes into account hydrological conditions for maximum sweep efficiency and control of the leachate. Injection and production wells are laid out in a nonuniform pattern, depending on the underground conditions. The computer, located in Denver, also monitors pressure and flow rate, although it does not physically control the operation.

IEC plans a second plant, at Ray Point in Live Oak County, with an initial design capacity of 300,000 lb per year, to be in operation by March 1978.

Another leaching process, although not exactly in-situ mining, is a unique venture of Solution Engineering Co. near Alice. The company is gearing up to recover uranium values from the tailings of the Susquehana mine, which operated from 1961 to 1973, depositing some 3 million tons of tailings. The plan is to recover about 30%, or 1 million lb, of uranium from ponds and by injecting dry tailings. The company estimates that there are 40 million g of solution available in seven sites—three former open-pit mines and four impoundments. Most of the solution contains 60 to 70 ppm of uranium oxide. The company is using old mill tankage in setting up a facility to process 500 to 1,000 g per min. If a water quality permit is received in time, commercial operations will begin in the fall.

One hurdle faced by all the Texas in-situ operations is obtaining permits from the Texas Water Quality Board. Because the technology is relatively new, the board originally had no precedent to guide it, and obtaining permits has been a tedious and drawn-out affair. Wyoming Mineral is working with the board to develop permit guidelines less complicated than the present 30-page permit document. A standard form of perhaps only a couple of pages is envisaged, with references to other documents that spell out performance details of government regulations. The permit form would specify only exceptions unique to the mining site.

There is strong interest in the procedural question of restoring the mining aquifers because many water quality parameters must be considered. For example, there are questions about meeting the overall toxicity of the original baseline condition. Can and should this be done by element-by-element restoration, or are variations in each element permissible as long as the original toxicity quotient is reestablished?

The board has the authority to specify aquifers that have more value as mineral resources than as water resources. After mining, such aquifers may not have to be totally restored to meet every original parameter. The Texas uranium producers are confident that restoration can be done where necessary to meet the requirements, and R&D work by all companies is reportedly producing encouraging results. □

New Arizona commission to determine complex water rights in Santa Cruz Valley

A BILL signed into law early in May has removed the immediate threat of injunctive action to prevent pumping and transportation of water in Arizona. The bill authorizes a commission to study and make recommendations on the future use of Arizona's water resources by Dec. 31, 1979. If the Arizona legislature fails to enact a ground-water management code by September 1981, the commission's recommendation will become law.

Cyprus Pima Mining Co. and several other companies that operate mines south of Tucson are defendants in a suit brought by Farmers Investment Co. (Fico), an agricultural corporation that pumps water to irrigate its lands in the Santa Cruz valley. Fico sought to enjoin the mines from pumping water and claimed $70 million in damages. The City of Tucson also asked for a declaration of rights to certain ground water and sought to enjoin agricultural and industrial users from returning to the ground water that would make the water supply undesirable for domestic use.

The Arizona Supreme Court ruled in August 1976 that if pumping of water may injure the wells of neighboring owners, water cannot be taken "off the land" or "to another parcel," even though both parcels overlie the common source of supply. In another case, several landowners sought to enjoin Cyprus Bagdad from pumping and transporting water from the Big Sandy ground-water and drainage basin and the Big Sandy River, on the grounds that this would cause irreparable damage to the plaintiffs and that it was an unlawful and unreasonable use.

An injunction against Bagdad would have caused curtailment or suspension of mine expansion, which will increase concentrator capacity from about 6,000 tpd to 40,000 tpd. The new concentrator is slated to start up in September at a cost of $15 million.

In view of the new legislation, Cyprus says that it intends to proceed with full pumping in August or September and anticipates no drawdown of the water table because former use of the land for agriculture required more water than industrial use.

In two other civil suits, the US government and certain Indians seek a declaration of their water rights in the Santa Cruz River basin. The defendants are Cyprus Pima, other mining companies, Fico, and the City of Tucson. The new law banning injunctions will not affect this case, but no trial date has yet been set. □

(Continued on p 31)

Minerals on March cover

K. Fukumoto of Dresser Minerals' Cookeville, Tenn., office correctly identified 10 of the minerals pictured on the cover of the March 1977 issue of E/MJ, in response to a challenge published in the April issue. He has been rewarded with one giant pterodactyl egg and a copy of *Continents in Motion*, by Walter Sullivan.

INTERFACING TECHNOLOGIES IN HYDROMETALLURGY

Milton E. Wadsworth
Associate Dean, College of Mines and Mineral Industries
and Professor of Metallurgy, Department of Metallurigcal Engineering
University of Utah, Salt Lake City, Utah

1977

SME-AIME vol 29 no 12 p. 30-33

INTERFACING TECHNOLOGIES IN HYDROMETALLURGY

Milton E. Wadsworth
Associate Dean, College of Mines and Mineral Industries
and Professor of Metallurgy, Department of Metallurigcal Engineering
University of Utah, Salt Lake City, Utah

ABSTRACT

Hydrometallurgical processing of ore deposits by solution mining or in-situ techniques requires the interfacing of several well developed technologies. The means of bringing broadly diverse concepts together represents one of the main challenges in in-situ processing. Important related technologies and some suggestions regarding interfacing are presented.

INTRODUCTION

This paper is presented to illustrate the complex nature of many hydrometallurgical processes which require the interfacing of several fields of technology. Unfortunately these technologies often have barriers resulting from inherent technical complexity, vocabulary, and mutual awareness of the depth of knowledge and endeavor in each separate field. No better example exists than that of the hydrometallurgical processing of low grade or remote ore bodies as in dump leaching and in-situ or solution mining. The very complexity of such processes emphasizes the need for instrumentation for purposes of monitoring and control.

INTERFACING TECHNOLOGIES

Figure 1 illustrates several technologies which interface in solution mining. How well these technologies interface depends upon the size of the operation and its financial capability to bring to bear the optimal use of information, processing, etc. available. It is inconceivable that any one individual can optimize each potential contribution alone. Consequently some areas are usually neglected of necessity or simply are not fully appreciated. The point seems apparent when one examines what must be done at some future date to develop and exploit a remote solution mining system with maximum chance for success.

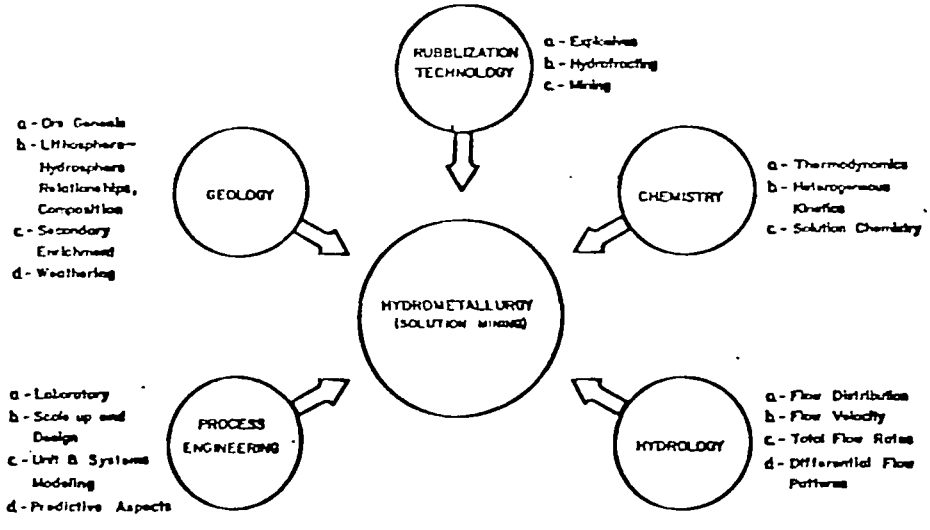

SCIENCE AND TECHNOLOGY INTERFACES
IN HYDROMETALLURGY

Figure 1

It is necessary for each discipline to communicate needed background information so a process of optimal design may be developed.

As illustrated in Fig. 1 important interfacing technologies for understanding and developing a complex solution mining system are Geology, Rubblization Technology, Chemistry, Hydrology and Process Engineering. The process engineer must bring existing factual information and laboratory data together so predictions of some reliability can be developed for needed scale-up in the field. The task of scale-up often is overwhelming considering the order of magnitude changes from laboratory to the field. Typically this may refer to about six orders of magnitude change. The lack or impracticability of intermediate staging or pilot plant equivalent represents the weakest link in process design of solution mining systems.

It is not within the scope of this paper to discuss these technologies in depth. A few examples of important background information and suggested ways of interfacing will be presented.

GEOLOGY

The field of geology provides important background information regarding ore genesis, lithosphere-hydrosphere reactions, secondary enrichment and weathering. Following formalizations originally proposed by Pourbaix[1], the geologist presents important thermodynamic relations[2] particularly suitable to analyzing lithosphere and hydrosphere relations in the form of E_h-pH diagrams. While these diagrams fail to predict rates of reaction they are very useful in predicting final phases, oxidation potentials associated with certain mineral phases, and solution reactions as a function of voltage (E_h) and acidity (pH). These diagrams provide rapid evaluation of oxygen potentials associated with certain minerals and immediately draw attention to the very low oxidation potential at or near the water table. Regions where oxidation and secondary enrichment can occur are clearly apparent. An analysis of oxygen potential relative to the water table and patterns of oxidation of secondary enrichment suggest unique types of solution mining systems. While highly idealized, Fig. 2 illustrates the classical array of oxidized and secondarily enriched zones relative to the water table. Interfaces are not clearly delineated but general relations associating oxidation potential and

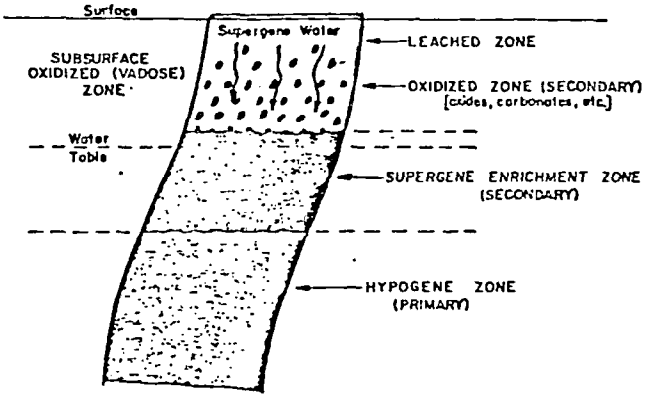

Figure 2. Cross-section illustrating regions of oxidation and secondary enrichment relative to the primary ore source.

mineralization become apparent. Using copper as an example, Fig. 3 illustrates the type of mineralization found in each zone[3]. The geometric and chemical relationship of the oxidized secondary (supergene) enrichment zones and primary (hypogene) zones lead to the three general types of in-situ, solution mining systems. As will be shown the types of in-situ, solution mining systems delineated above as a broad base may be applied to a variety of mineral deposits, copper merely being an example.

Secondary enrichment occurs when oxidized ores release soluble constituents which migrate downward and react to form new mineral phases. These reactions may be simple metathesis, precipitation or may involve oxidation-reduction couples. Again using copper as an example, sulfide supergene enrichment forming covellite (CuS) and chalcocite (Cu_2S) from the primary chalcopyrite ($CuFeS_2$) and pyrite (FeS_2) may occur by the following reactions[4]:

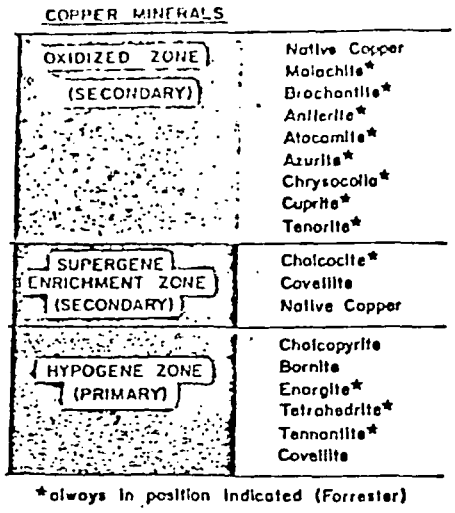

Figure 3. Sequence of copper mineralization as a result of weathering and secondary enrichment.

Covellite (CuS)

(1) $PbS + CuSO_4 = CuS + PbSO_4$

(2) $CuFeS_2 + CuSO_4 = 2\ CuS + FeSO_4$

Chalcocite (Cu_2S)

(3) $5\ FeS_2 + 14\ CuSO_4 + 12\ H_2O = 7\ Cu_2S + 5\ FeSO_4 + 12\ H_2SO_4$

(4) $5\ CuFeS_2 + 11\ CuSO_4 + 8\ H_2O = 8\ Cu_2S + 5\ FeSO_4 + 8\ H_2SO_4$

Reactions (1) and (2) represent simple metathesis while (3) and (4) involve oxidation-reduction couples. It is interesting to note that reaction (3) involving FeS_2/Cu_2S will occur at E_h of approximately 0.05 volts at pH = 2 and a total sulfur activity of 0.1. This voltage corresponds to an oxygen partial pressure for which log P(atm) = -79. The importance of the oxygen consuming ability of sulfides with apparent slow O_2 diffusion emphasizes the importance of the water table as a barrier to oxygen infusion.

Secondary reactions, as illustrated above, may occur during leaching. This was evident in the studies of Braun, et al.[5], where released copper values migrated into ore fragments forming CuS according to reaction (2). In our own laboratories the kinetics of reaction (2) have been found to be surprisingly rapid. One micron particles of chalcopyrite will react essentially completely in 70 hours at 90°C.

Weathering reactions are very important since natural weathering provides access paths for solution penetration due to cracking and bulk volume changes. Also accelerated weathering occurs during leaching causing particle fragmentation and clay slime formation. Such in-situ weathering may enhance or retard dissolution depending upon the particle sizes resulting from weathering. Modeling of in-situ systems over long periods of time will undoubtedly have to include artificial weathering kinetics since porosity and particle size are predominant factors in the leaching mechanism. Figure 4 illustrates the typical weathering sequence for feldspar showing dramatic variations in pore space[4]. Leach[7] lists the relative rates of weathering according to the sequence:

Hornblend > Biotite > Plagioclase > K-spar > K-mica

A typical sequence in the case of K-feldspar is

$$\text{K-feldspar} \xrightarrow{(a)} \text{K-mica} \xrightarrow{(b)} \text{Kaolinite} \xrightarrow{(c)} Al^{+3} + H_4SiO_4$$

$$\text{(5)}\quad 3\underset{\text{K-feldspar}}{KAlSi_3O_8} + 2H^+ + 12\,H_2O = \underset{\text{K-mica}}{KAl_3Si_3O_{10}(OH)_2} + 2K^+ + H_4SiO_4 \quad \text{(a)}$$

$$\text{(6)}\quad 2\underset{\text{(K-mica)}}{KAl_3Si_3O_{10}(OH)_2} + 2H^+ = 3\underset{\text{(Kaolinite)}}{Al_2Si_2O_5(OH)_4} + 2K^+ \quad \text{(b)}$$

$$\text{(7)}\quad \underset{\text{(Kaolinite)}}{Al_2Si_2O_5(OH)_4} + 6H^+ = 2Al^{+3} + H_2O + 2H_4SiO_4 \quad \text{(c)}$$

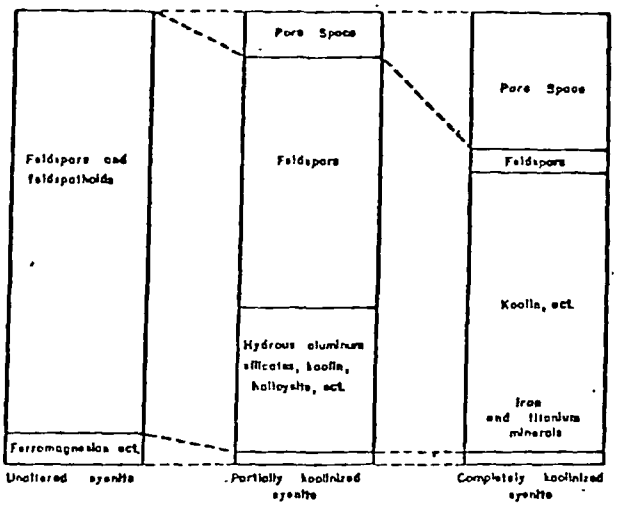

Diagram showing changes of volume and of minerals in the weathering of syenite. (W.J. Mead, Econ. Geol.)

Figure 4.

SOLUTION MINING SYSTEMS

Based upon weathering patterns and change in oxidation with depth, three general types of solution mining systems are suggested. These are presented in Fig. 5 and may be summarized as:

Type (I); surface dumps or deposits having one or more sides exposed and deposits within the lithosphere but above the natural water table,

Type (II); deposits located below the natural water table but accessible by conventional underground or bore hole mining techniques, and

Type (III); deposits below the natural water table and too deep for economic mining.

Type I is representative of systems which are leached by passing thin films introduced by pumping into bore holes, surface flooding, or surface spraying. In each case similar hydrological and chemical conditions prevail. Solutions of high ionic strength, containing suitable lixiviant, are involved with associated precipitation of salts according to limits of solubility. Control of the hydrology is very difficult and channeling occurs leading to surface blockage and long diffusion paths from by-pass zones into zones of active fluid flow. Leaching may be carried out continuously for oxides and secondary sulfides, or in the case of certain sulfides, alternate oxidation, drain, and leach cycles may be most effective. In the case of sulfides the active lixiviant is ferrous ion and requires good aeration, supported by bacterial activity to maintain effect ferric ion levels. In the case of oxides the lixiviant is usually sulfuric acid. The leaching of oxides is first order with respect to hydrogen ion. Since gangue minerals usually consume acid, increasing acidity may simply result in excessive gangue dissolution. One of the major challenges of oxide leaching is to find a means of introducing acid to minimize the consumption by gangue and at the same time avoid excessive acidity in the effluent which would be unsuitable for solvent extraction.

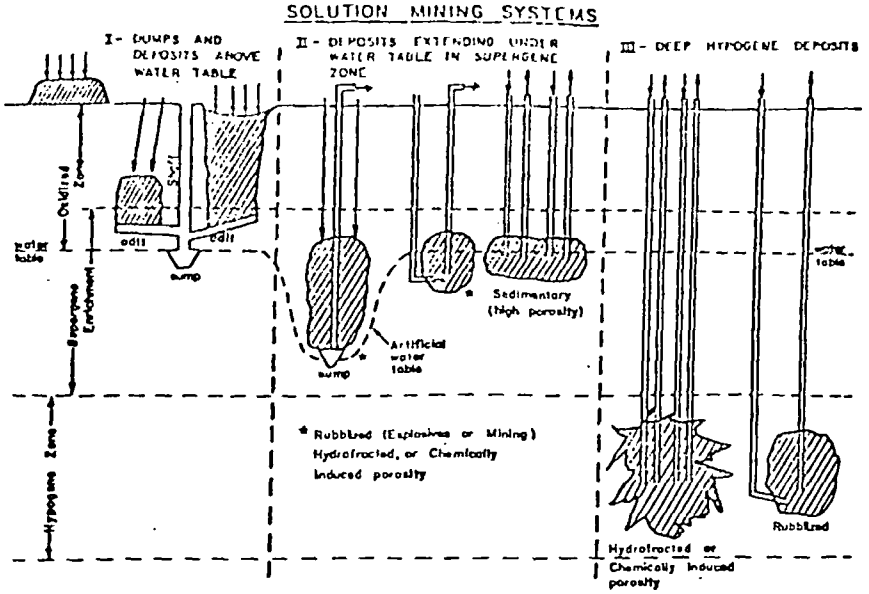

Figure 5.

Type II systems apply to deposits below the water table extending normally to less than 1000 ft. Certain oxides such as uranium may extend much deeper but secondary enrichment usually falls within 1000 ft in depth. Bore hole mining of uranium is typical of a Type II system. In In this case the "roll front" deposit of reduced uranium in a finely disseminated deposit is mined by down-hole and up-hole pumping using a grid pattern. Figure 6 illustrates such a deposit and Fig. 7 shows a typical bore hole pattern as was used at Clay West(8).

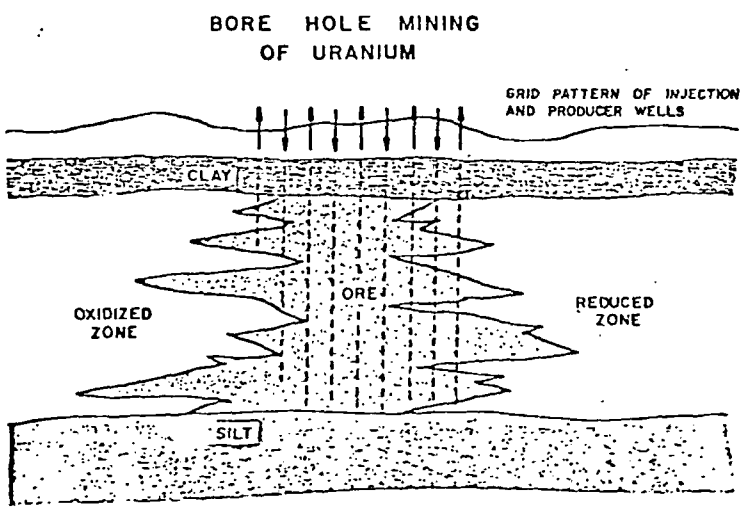

Figure 6. Illustration of "roll-front" uranium deposit suitable for bore hole mining.

Type II also is represented by deposits requiring extensive shattering or fracturing. Rubblization may be accomplished as in the case of Type I, by use of conventional explosives and mining. In the latter case the deposit would have to be dewatered during mining producing an artificial water table as illustrated in Fig. 5. Once rubblized the deposit may be leached by percolation as in Type I systems; however, ingress of water may cause appreciable and even unacceptable dilution. As in the case of Type I effective recovery of leach solution is

accomplished by pumping from a sump at the water table level. A second, and potentially important, approach is to allow the rubblized deposit to refill and then leach by pumping air, oxygen, ferric ion solutions (or some other oxidant) into the inundated deposit. Significant

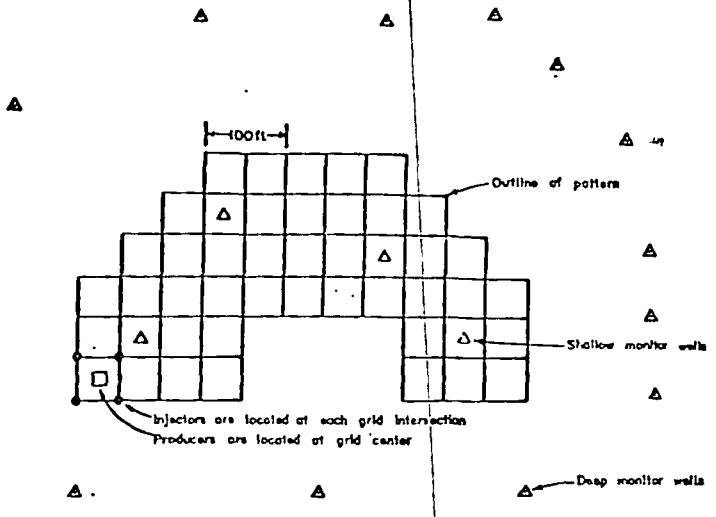

Clay West uranium leaching pattern [White,1975]

Figure 7.

advantage may result from the hydrostatic head which increases oxygen solubility and the corresponding kinetics of reaction. Figure 8 compares the relative effectiveness of ferric ion and oxygen at various depths based upon a uniform ferric ion concentration but variable oxygen concentration enhanced with depth. For pure oxygen, a hydrostatic head of approximately 1000 ft would make oxygen competitive with the ferric ion. For air, approximately 600 ft hydrostatic head would be required. At even greater depths the effectiveness of oxygen far exceeds ferric ion as the effective lixiviant. The inundated deposit has the added advantage that the leaching may be carried out at elevated temperatures from heats of reaction and/or external heating.

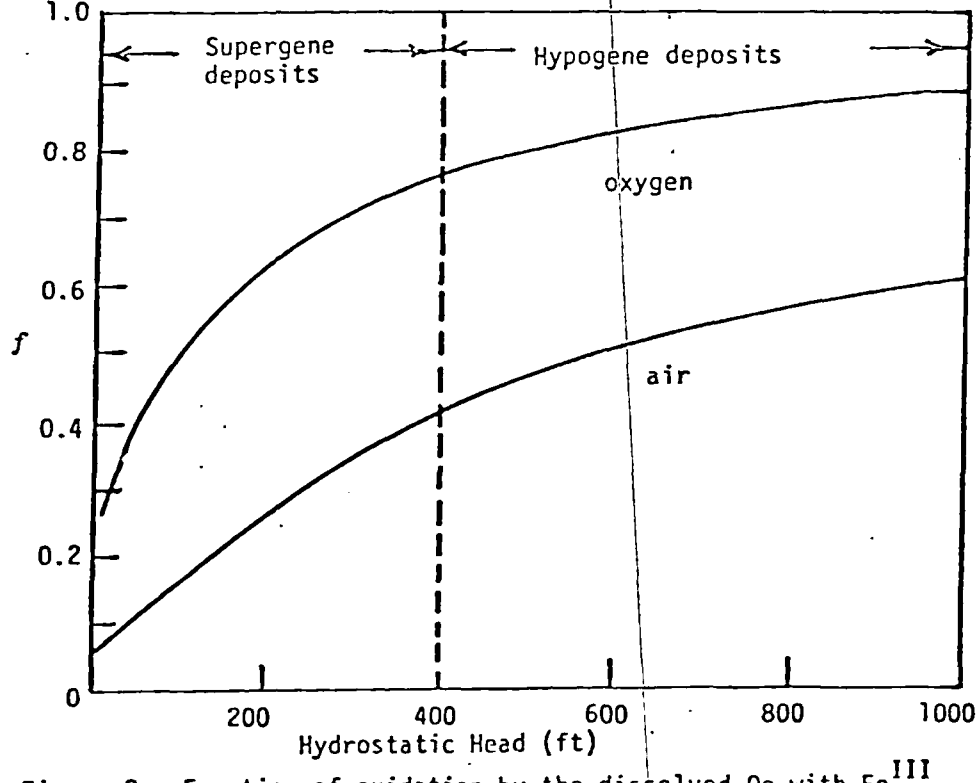

Figure 8. Fraction of oxidation by the dissolved O_2 with Fe^{III} present at 0.018 molar for various hydrostatic heads.

Type III deposits are typical of those considered by Lawerence Livermore researchers[5]. In this case a porous ore body induced by explosives fracturing, hydrofracturing, or chemical dissolution is leached under high hydrostatic head leading to conditions which may be suitable to leach normally refratory sulfide and oxide minerals. The greatest deterent to effective leaching in Type III systems is technology to provide rubblization or penetration under controlled, predictable conditions. Much must be done to render such systems amenable to competent scale-up analysis. It is apparent that the hydrology of Type II and III systems must be known and predictable. In some instances, as in uranium solution mining, this may be done effectively. Quantifying flow patterns in rubblized and hydrofracted ore deposits remains a difficult problem requiring extensive study from the laboratory to testing in the field under conditions amenable to accurate monitoring.

HYDROLOGY

Interfacing hydrology, solution chemistry with process engineering involves a task of major proportions. Modeling of one or two phase flow systems over long flow paths past ore fragments of varying size and composition requires a detailed knowledge of heterogeneous kinetics, hydrology, solution thermodynamics, porosity variation, weathering and physical characteristics of the deposit. In the laboratory only simple isolated conditions may be effectively simulated. These results must then be extrapolated by orders of magnitude rarely attempted by the process engineer. The lack of adequate field data make this task even more difficult. The common denominator linking laboratory tests to in-situ extraction rates upon the ability to predict solution velocity at each point in a deposit coupled to the chemical history of the residual ore and transported solution. In a given element within a deposit the solution through that zone must be known. Figure 9 illustrates such an incremental volume within an ore deposit for rubblized and hydrofracted ore. The effective flow path may be around individual particles or particle domains into which relatively long-range diffusion must occur. The ore fragment sizes or effective diameter of particle domains must be known for successful prediction of leaching results.

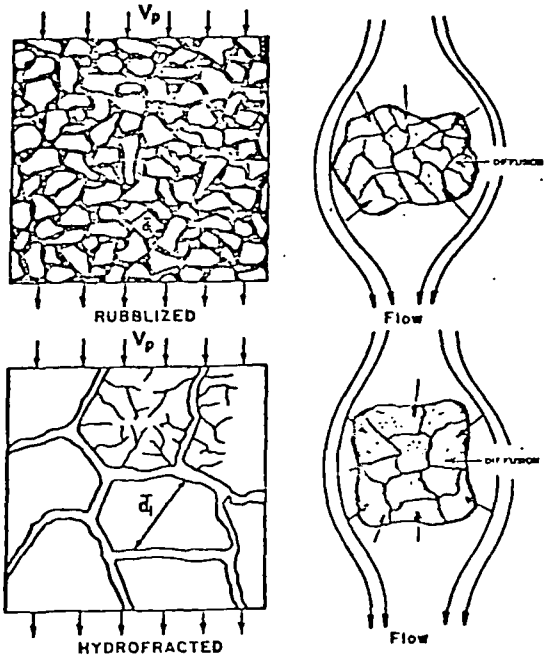

Figure 9. Flow of solution through a volume increment within an ore deposit.

Needed information of solution flow, solution chemistry and rate processes for a simple single phase system, neglecting side diffusion effects, may be represented by the following equations applied to some jth volume increment within the deposit.

FOR THE jth INCREMENT

$$(8) \qquad \left(\frac{\partial c}{\partial t}\right)_L = \frac{V_p}{\epsilon'} \frac{\partial c}{\partial q} + \dot{R}^L$$

$$(9) \quad \dot{R}^L = \sum_i A_{io} C_i (fK_c + K_g) + \left(\frac{\partial c}{\partial t}\right)_p$$

(surface flush reaction)(particle penetration)

$$(10) \quad \epsilon\left(\frac{\partial c}{\partial t}\right) = \dot{R}^p + D^L_{eff} \nabla^2 C$$

$$(11) \quad \dot{R}^p = \sum_m G_m C f(m)$$

where V_p is solution velocity ϵ' is the void space between ore fragments or particles and q is the coordinate in the direction of flow. The term $\dot{R}^L$ represents all reactions in the jth volume causing a change in concentration of lixiviant c. Equation (9) includes surface flush reactions involving gange and mineral constituents for each ith ore fragment size where A is the area and K_c and K_g are rate constants for the surface flush reaction and f is the fraction of the surface exposed to mineral capable of releasing the desired metal value. The flush reaction may or may not be needed depending upon whether or not fracture zones follow mineralized zones preferentially. The right hand term of Equation (9) represent reaction by particle penetration. Equation (10) represents coupled diffusion and chemical reaction within an ore fragment where ϵ is the ore fragment porosity D^L_{eff} is the effective diffusivity of lixiviant and $\dot{R}^p$ includes the heterogeneous rate processes for all mineral types m present as indicated in equation (11). The term G_m is the geometric term related to particle shape and extent of reaction and $f(m)$ is the intrinsic rate constant. An additional set of equations may be written for each metal value released. The solution chemistry including pH, concentration and E_h will predict saturation levels and the onset of precipitation. Clearly the coupling of all of these effects presents a challenge of major proportion to the process engineer. Reliable predictability will require intensive scale-up and testing from laboratory to field block testing before reliable results may be predicted for a major remote ore body.

INSTRUMENTATION

Instrumentation for in-situ extraction will be required to monitor lixiviant, metal content in solution, pH, E_h and flow velocity of influent and effluent as well as gas flow velocity where needed. Control components of an in-situ mining system logically therefore will include solution and gas velocity control and reagent addition control. Monitoring instrumentation in peripheral areas undoubtedly will also be routinely required to ensure compliance with environmental constraints associated with any in-situ solution mining system.

BIBLIOGRAPHY

1. Pourbaix, M., 1966, Atlas of Electrochemical Equilibria in Aqueous Solutions, Pergamon Press, New York.

2. Garrels, R.M., and Christ, C.L., 1965, Solution, Minerals, and Equilibria, Harper and Row, New York.

3. Forrester, J.D., 1946, Principles of Field and Mining Geology, pp. 136, 137, John Wiley & Sons, New York.

4. Bateman, A.M., 1951, The Formation of Mineral Deposits, pp. 229-230, John Wiley and Sons, New York.

5. Braun, R.L., Lewis, A.E., and Wadsworth, M.E., 1974, "In-Place Leaching of Primary Sulfide Ores: Laboratory Leaching Data and Kinetics Model," Met. Trans., vol. 5, pp. 1717-1726.

6. Sohn, H.J. 1977, Primary and Secondary Reactions Important in Copper Hydrometallurgy, Ph.D. thesis, in preparation, University of Utah.

7. Leach, D.L., 1975, "Mineralogical Considerations in Leaching of Primary Copper Sulfides at Elevated Temperature and Pressure," In Place Leaching and Solution Mining, Symposium, Mackay School of Mines, University of Nevada, Reno, Nev.

8. White, L., 1975, "In-Situ Leaching Opens New Uranium Reserves in Texas," E & MJ., vol. 176, No. 7, pp. 73-81.

Interfacing Technologies in Solution Mining

Milton E. Wadsworth, University of Utah

Hydrometallurgical processing of ore deposits by solution mining or in situ techniques requires the interfacing of technologies as diverse as hydrology, geology, chemistry, and rubblization. This synthesis represents one of the main challenges to in situ processing due to the inherent complexity and vocabulary of these well-developed technologies, and to the general lack of appreciation for the depth of knowledge and endeavor in each separate field. No better example of the need for such interfacing of technologies exists than that of solution mining.

How well these technologies interface depends upon the size of the operation and its financial capability to use the information and technology available. It is inconceivable that any one individual can optimize each potential contribution alone; consequently, some areas are usually neglected or simply are not fully appreciated. When one examines what must be done at a future date to develop and exploit a remote solution mining system, it becomes obvious that each discipline must effectively communicate the needed background information to make the project a synthesized whole.

In technological interfacing, the process engineer must bring existing factual information and laboratory data together so reliable predictions can be developed for scale-up in the field. This represents the weakest link in solution mine design due to the impracticality of pilot-plant staging. Thus, the task of scale-up is often overwhelming, typically in the range of six orders of magnitude from the laboratory to the field.

This article provides a few examples of the type of background information needed, and suggests means of interfacing that information into a well-designed solution mining system.

Using Geology to Predict Solution Reactions

When studying solution mining systems, geology provides important background information regarding ore genesis, lithosphere-hydrosphere reactions, secondary enrichment, and weathering. Certain thermodynamic relations are particularly suited to analyzing lithosphere and hydrosphere relations in the form of E_h-pH diagrams.[1,2] While these diagrams fail to predict rates of reaction, they are very useful in predicting final phases, oxidation potentials associated with certain mineral phases, and solution reactions as a function of voltage (E_h) and acidity (pH). These diagrams provide rapid evaluation of oxygen potentials associated with certain minerals, immediately drawing attention to the very low oxidation potential at or near the water table, as well as clearly pointed out regions where oxidation and secondary enrichment can occur.

An analysis of oxygen potential relative to the water table and oxidation patterns of secondary enrichment suggests unique types of solution mining systems. The highly idealized figure below illustrates the classical array of oxidized and secondarily enriched zones relative to the water table. Interfaces are not clearly delineated but general relations associating oxidation potential and mineralization become apparent. Using copper as an example, the next diagram illustrates the type of mineralization found in each zone.[3] The geometric and chemical relationship of the oxidized secondary (supergene) enrichment zones and primary (hypogene) zones must each be solution mined by a different approach.

Secondary enrichment occurs when oxidized ores release soluble constituents which migrate downward and react to form new mineral phases. These reactions may be simple metathesis, precipitation, or may involve oxidation-reduction couples. Again using copper as an example, sulfide supergene enrichment forming covellite (CuS) and chalcocite (Cu_2S) from the primary chalcopyrite ($CuFeS_2$) a pyrite (FeS_2) may occur by the following reactions:[4]

Covellite (CuS)

$$PbS + CuSO_4 = CuS + PbSO_4 \quad (1)$$

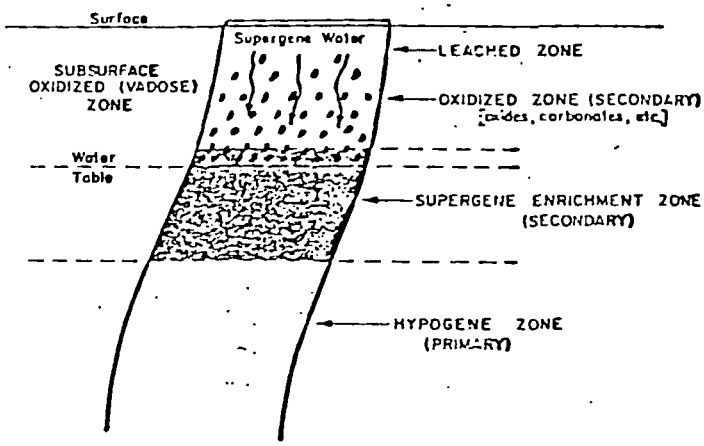

Cross-section illustrating regions of oxidation and secondary enrichment relative to the primary ore source.

OXIDIZED ZONE (SECONDARY)	Native Copper Malachite★ Brochantite★ Antlerite★ Atacamite★ Azurite★ Chrysocolla★ Cuprite★ Tenorite★
SUPERGENE ENRICHMENT ZONE (SECONDARY)	Chalcocite★ Covellite Native Copper
HYPOGENE ZONE (PRIMARY)	Chalcopyrite Bornite Enargite★ Tetrahedrite★ Tennantite★ Covellite

★always in position indicated (Forrester)

Sequences of copper mineralization as a result of weathering and secondary enrichment.

$$CuFeS_2 + CuSO_4 = 2CuS + FeSO_4 \quad (2)$$

Chalcocite (Cu_2S)

$$5FeS_2 + 14CuSO_4 + 12H_2O = 7Cu_2S + 5FeSO_4 + 12H_2SO_4 \quad (3)$$

$$5CuFeS_2 + 11CuSO_4 + 8H_2O = 8Cu_2S + 5FeSO_4 + 8H_2SO_4 \quad (4)$$

Reactions (1) and (2) represent simple metathesis, while (3) and (4) involve oxidation-reduction couples. Reaction (3), involving FeS_2/Cu_2S, occurs at an E_h of approximately −0.5 v and pH of 2, with a total sulfur activity of 0.1. This voltage corresponds to an oxygen partial pressure for which log P_{atm} equals −79. This oxygen-consuming capability of sulfides with apparent slow O_2 diffusion emphasizes the importance of the water table as a barrier to oxygen infusion.

The secondary reactions illustrated above may occur during leaching as evidenced in studies by Braun, et al., where released copper values migrated into ore fragments to form CuS according to reaction (2).[5] The kinetics of this reaction have been found to be surprisingly rapid: One-micron particles of chalcopyrite will react essentially to completion in 70 hours at 90°C (194°F).

Natural weathering is another important aspect of ore body assessment since it provides access paths for solution penetration. Accelerated leaching also occurs during leaching, causing particle fragmentation and clay slime formation. Such in situ weathering may enhance or retard dissolution depending upon the particle sizes resulting from weathering reactions. Modeling of in situ systems over long periods of time will undoubtedly have to include artificial weathering kinetics since porosity and particle size are predominant factors in the leaching mechanism.

Three General Types of Solution Mining Systems

Based upon weathering patterns and changes in oxidation with depth, three general types of solution mining systems will be considered:

Type I ore bodies have one or more sides exposed, such as a surface dump. Deposits within the lithosphere but above the water table may also be classified as Type I.

Type II deposits are located below the natural water table but are accessible by conventional underground or borehole techniques.

Type III are below the natural water table, too deep for economic mining.

Type I deposits are leached by pumping solvent into boreholes, surface flooding, or surface spraying, but in each case similar hydrological and chemical conditions prevail. Solutions of high ionic strength, containing suitable lixiviant, are involved with associated precipitation of salts according to limits of solubility. Hydrology is very difficult to control in Type I deposits: channeling occurs, leading to surface blockage and long diffusion paths from by-pass zones into zones of active fluid flow. Leaching may be carried out continuously for oxides and secondary sulfides, or in the case of certain sulfides, a system of alternate oxidation, drain, and leach cycles may be most effective. The active lixiviant for sulfides is ferrous ion, coupled with good aeration and bacterial activity; sulfuric acid is usually used on oxides. The leaching of oxides is

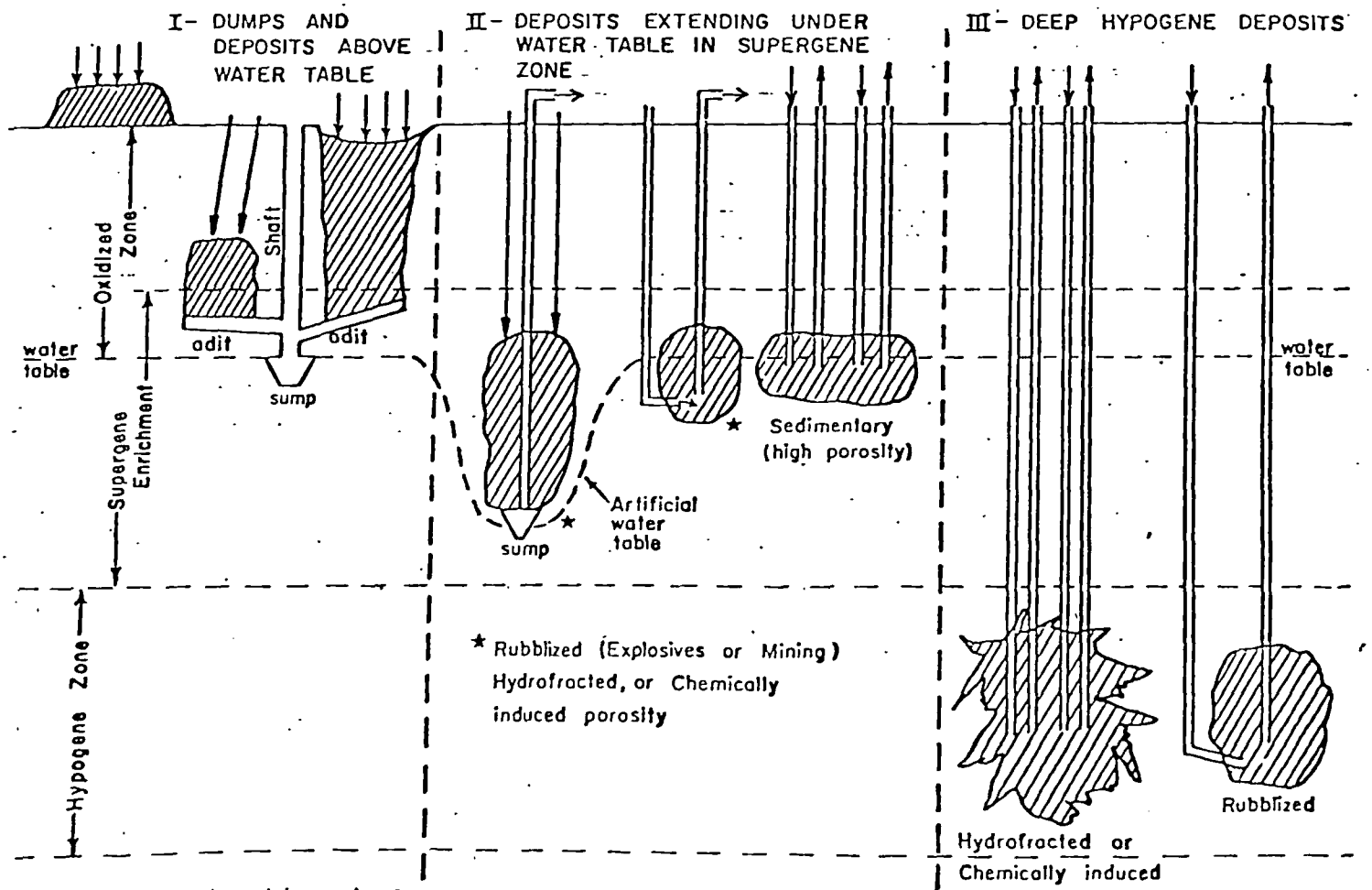

Three types of solution mining systems.

first order with respect to hydrogen ion and since gangue minerals usually consume acid, increasing acidity may simply result in excessive gangue dissolution. A major challenge to oxide leaching is to find a means of introducing acid which will minimize the consumption by gangue and at the same time avoid excessive acidity in the effluent.

Type II systems apply to deposits below the water table but rarely more than 300 m (1000 ft) below the surface. Certain oxides, such as those of uranium, may extend much deeper, but secondary enrichment usually falls within 1000 feet in depth. Borehole mining of uranium is typical of a Type II system, in which case the roll front deposit of reduced uranium is mined by down-hole and up-hole pumping in a grid pattern.

Type II deposits may require extensive shattering or fracturing by conventional explosives and mining. In the latter case, the deposit would have to be dewatered during mining to produce an artificial water table. Once rubblized, the deposit may be leached by percolation as in Type I systems; however, ingress of water may cause appreciable and even unacceptable dilution. As in Type I systems, effective recovery of leach solution is accomplished by pumping from a sump at the water table level. A second, and potentially important, approach is to allow the rubblized deposit to refill and then leach by pumping air, oxygen, and ferric ion solutions (or some other oxidant) into the inundated deposit. Significant advantage may result from the hydrostatic head which increases oxygen solubility and the corresponding kinetics of the reaction. A comparison of the relative effectiveness of ferric ion and oxygen at various depths based upon a uniform ferric ion concentration but variable oxygen concentration shows that, for pure oxygen, a hydrostatic head of approximately 1000 ft would make oxygen competitive with the ferric ion; at greater depths, oxygen can far exceed ferric ion in effectiveness as a lixiviant. For air, approximately 180 m (600 ft of hydrostatic head would be required. An inundated deposit has the added advantage that leaching may be carried out at elevated temperatures by heat of reaction and/or external heating.

Type III deposits are typical of those considered by Lawrence Livermore researchers.[8] A porous ore body induced by explosive fracturing, hydrofracturing, or chemical dissolution is leached under high hydrostatic head leading to conditions which may be suitable to leach normally refractory sulfide and oxide minerals. The greatest deterrent to effective leaching in Type III systems is technology to provide rubblization or penetration under controlled and predictable conditions. Quantifying flow patterns in rubblized and hydrofracted ore deposits remains a difficult problem that requires extensive study in the laboratory and testing in the field.

Interfacing Hydrology in the Study

Interfacing hydrology and solution chemistry with process engineering involves a task of major proportions. Modeling of one or two phase flow systems over long flow paths past ore fragments of varying size and composition requires a detailed knowledge of heterogeneous kinetics, hydrology, solution thermodynamics, porosity variation, weathering, and physical characteristics of the deposit. In the laboratory, only isolated conditions can be effectively simulated, and then these results must be extrapolated by orders of magnitude rarely attempted by process engineers. The lack of adequate field data makes this task even more difficult.

Linking laboratory tests to in situ extraction requires an accurate prediction of solution velocity at each point in a deposit, along with a chemical history of the residual ore and transporting solution. The effective flow path may be

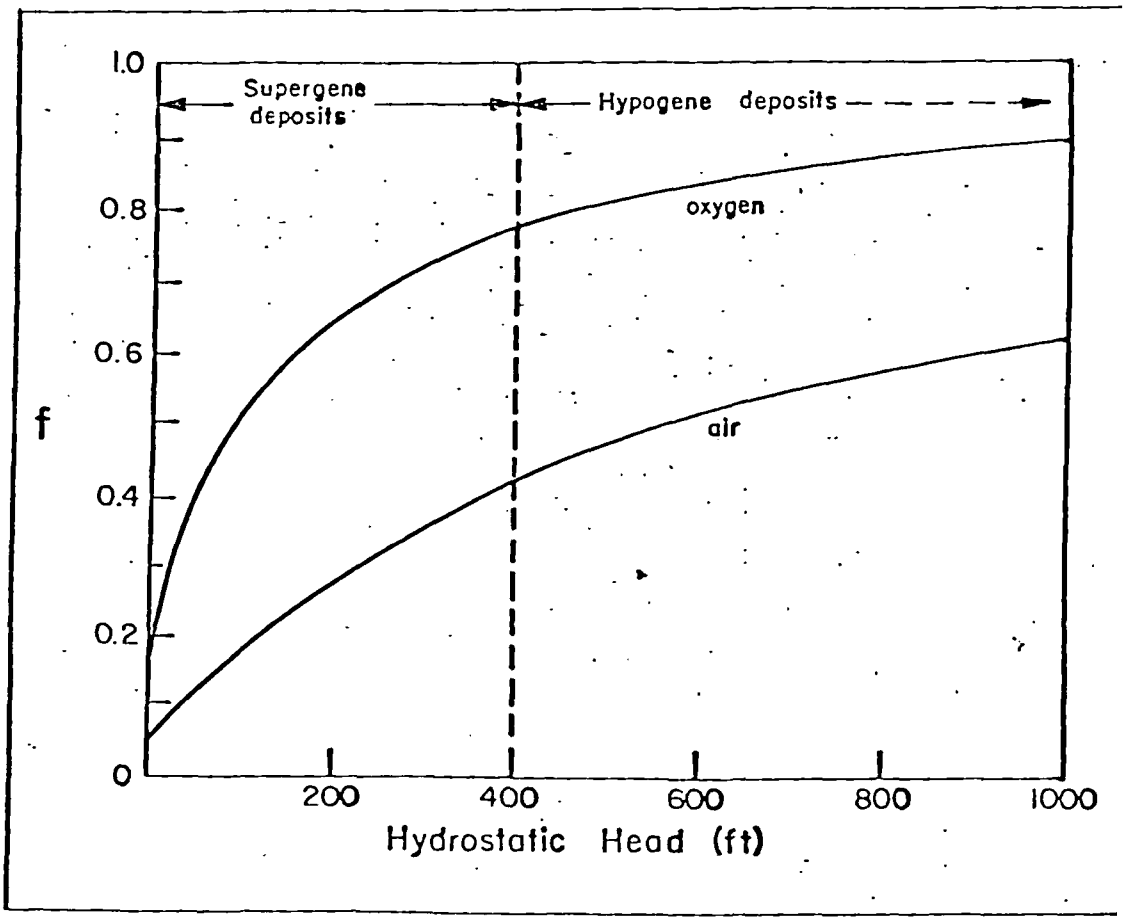

Fraction of oxidation by the dissolved O_2 with Fe^{III} present at 0.018 molar for various hydrostatic heads.

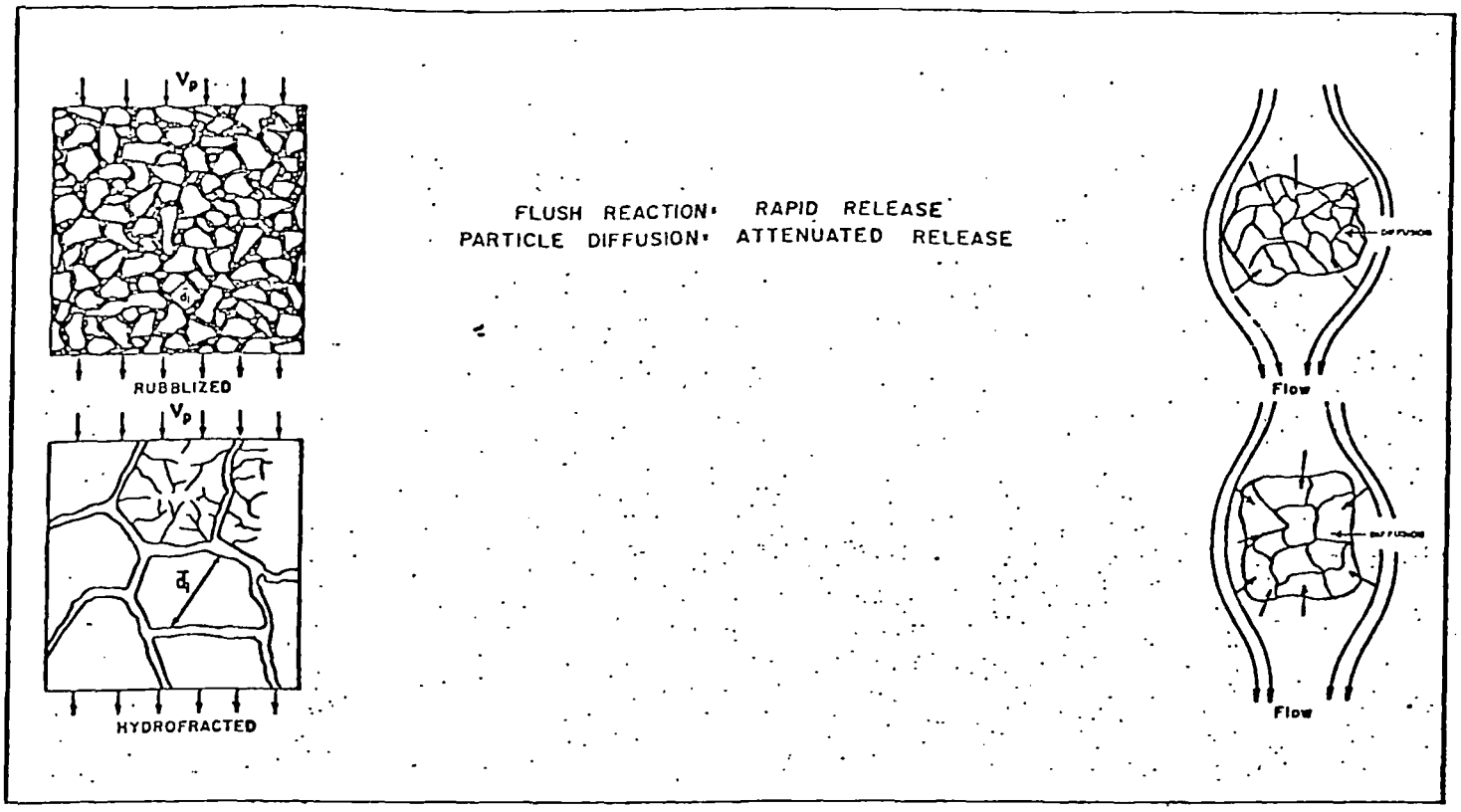

Flow of solution through a volume increment within an ore deposit.

around individual particles or particle domains into which relatively long-range diffusion must occur. Fragment sizes must also be known for successful prediction of leaching results.

Solution flow, solution chemistry, and rate processes for a simple single-phase system, neglecting side diffusion effects, may be represented by the following equations, which are applied to some jth volume increment within the deposit.

$$\left(\frac{\partial c}{\partial t}\right)_L = \frac{V_p}{\epsilon'}\frac{\partial c}{q} + \dot{R}^L \qquad (5)$$

$$\dot{R}^L = \sum_i A_{i_0} C_i (f K_r + K_{ii}) + \left(\frac{\partial c}{\partial t}\right) \qquad (6)$$

$$\epsilon\left(\frac{\partial c}{\partial t}\right) = \dot{R}^p + D^L_{eff}\nabla^2 C \qquad (7)$$

$$\dot{R}^p = \sum_m G_m C f(m) \qquad (8)$$

where V_p is solution velocity, ϵ' is the void space between ore fragments or particles, and q is the coordinate in the direction of flow. The term R^L represents all reactions in the jth volume causing a change in concentration of lixiviant C. Equation (6) includes surface flush reactions involving gange and mineral constituents for each ith ore fragment size where A is the area and K_r and K_{ii} are rate constants for the surface flush reaction and f is the fraction of the surface exposed to mineral capable of releasing the desired metal value. The flush reaction may or may not be needed depending upon whether fracture zones follow mineralized zones preferentially. The right hand term of Eq. (6) represents reaction by particle penetration; Eq. (7) couples diffusion and chemical reaction within an ore fragment where ϵ is the ore fragment porosity D^L_{ff} is the effective diffusivity of lixiviant and $\dot{R}^p$ includes the heterogeneous rate processes for all mineral types m present as indicated in Eq. (8). The term G_m is the geometric term related to particle shape and extent of reaction and $f(m)$ is the intrinsic rate constant. An additional set of equations may be written for each metal value released. The solution chemistry including pH, concentration, and E_h will predict saturation levels and the onset of precipitation. Clearly the coupling of all of these effects presents a challenge of major proportion to the process engineer. Reliable predictability will require intensive scale-up and testing from laboratory to field testing before reliable results may be predicted for a major remote ore body. □

References

[1] Pourbaix, M., 1966, *Atlas of Electrochemical Equilibria in Aqueous Solutions*, Pergamon Press, New York.

[2] Garrels, R. M., and Christ, C. L., 1965, *Solution, Minerals and Equilibria*, Harper and Row, New York.

[3] Forrester, J. D., 1946, *Principles of Field and Mining Geology*, pp. 136-137, John Wiley & Sons, New York.

[4] Bateman, A. M., 1951, *The Formation of Mineral Deposits*, pp. 229-230, John Wiley & Sons, New York.

[5] Braun, R. L., Lewis, A. E., and Wadsworth, M. E., 1974, "In-Place Leaching of Primary Sulfide Ores: Laboratory Leaching Data and Kinetics Model," Met. Trans., Vol. 5, pp. 1717-1726.

[6] Sohn, H. J., 1977, "Primary and Secondary Reactions Important in Copper Hydrometallurgy," Ph.D. thesis, in preparation, University of Utah.

[7] White, L., 1975, "In-Situ Leaching Opens New Uranium Reserves in Texas," *E & MJ*, Vol. 176, No. 7, pp. 73-81.

Milton E. Wadsworth is associate dean of the College of Mines and Mineral Industries, as well as a professor of metallurgy in the Department of Metallurgy and Metallurgical Engineering, University of Utah (209 W. C. Browning Bldg., Salt Lake City, Utah 84112). He received a B.S. degree in metallurgical engineering (1948) and Ph.D. degree in metallurgy (1951) from the University of Utah and has been teaching for 26 years. Dr. Wadsworth is the author of over 75 technical papers in the field of metallurgy, where his major interest is surface chemistry of mineral systems in both mineral dressing and extractive metallurgical processes.

INDUSTRIAL USE OF HYDROMETALLURGY TO PROCESS GOLD-ANTIMONY CONCENTRATES

UDC 669.213:622.775

P. P. Baiborodov, A. B. Ezhkov, and V. I. Zhuravlev

Gold-antimony ores and concentrates are a high-quality raw material. Analysis of the substance composition of these ores showed that the ore minerals comprise up to 50% antimonite, 2% antimony oxides, and gold nuggets. The non-ore minerals include 45% and more quartz, 0.5% feldspars, and up to 1% magnesium aluminosilicate.

Up to 70 g/t of gold nuggets and 5 g/t of silver are noted in antimonite. The content of arsenic and of heavy non-ferrous metals is also characteristic.

Hydrometallurgical treatment of such raw material will provide for a high antimony recovery, since all of its forms -- apart from pentoxide -- pass into solution.

Leaching conditions, developed by the "Sredazniprotsvetmet" Institute [1, 2], are close to those used in industry. The considerable fluctuations in the amount of antimony in the original raw material did not worsen indices on the passage of antimony to a sulfide-alkaline solution, containing up to 100 g/l sodium sulfide and 20-30 g/l caustic soda.

Sulfides and oxides of Pb, Z, Fe, Cu, Cd, Ni, Co, Bi, and Mo pass into solution in amounts no greater than $0.18 \cdot 10^{-5}$ - $5.54 \cdot 10^{-4}$ g/ion/l [3]. This will provide for a sufficiently high purity of the antimony solutions so that they would not require any additional purification.

The literature contains extremely contradictory data on the chemism of dissolving antimony compounds in sulfide-alkaline solutions [4-8]. In order to determine the most probable reactions occurring when antimony compounds are leached with sulfide-alkaline solutions [9], thermodynamic calculations were conducted[1], the results of which are given in the Table.

Standard Isobar Potentials for the Interaction of Antimony Compounds with Sodium Sulfide and Caustic Soda

No.	Reactions	ΔZ_T°, kcal	Possibility of reaction occurring
1	$Sb_2O_3+Na_2S=2NaSbS_2$	−0,5	Possible
2	$Sb_2S_3+2Na_2S=Na_4Sb_2S_6$	−14,3	Occurs
3	$Sb_2S_3+3Na_2S=2Na_3SbS_3$	−26,5	Occurs readily
4	$Sb_2S_3+2NaOH=NaSbS_2+NaSbSO+H_2O$	+31,09	Does not occur
5	$Sb_2S_3+4NaOH=NaSbO_2+Na_3SbS_3+2H_2O$	−17,2	Occurs
6	$Sb_2S_3+6NaOH=Na_3SbO_3+Na_3SbS_3+3H_2O$	+170,6	Does not occur
7	$Sb_2O_3+2Na_2S+H_2O=NaSbS_2+NaSbO_2+2NaOH$	−2,8	Possible
8	$Sb_2O_3+3Na_2S=Na_3SbS_3+Na_3SbO_3$	+120,0	Does not occur
9	$Sb_2O_3+5Na_2S+3H_2O=Na_4Sb_2S_5+6NaOH$	−26,8	Occurs readily
10	$Sb_2O_3+6Na_2S+3H_2O=2Na_3SbS_3+6NaOH$	−31,5	" "
11	$Sb_2O_3+2NaOH=2NaSbO_2+H_2O$	−1,4	Possible
12	$Sb_2O_3+4NaOH=Na_3SbO_3+NaSbO_2+2H_2O$	+7,2	Does not occur
13	$Sb_2O_3+6NaOH=2Na_3SbO_3+3H_2O$	+335,6	" " "
14	$Sb_2O_4+7Na_2S+4H_2O=Na_3SbS_3+Na_3SbS_4+8NaOH$	−60,0	Occurs readily

Reactions 4, 6, 8, 12, and 13 lead to the formation of antimony compunds which are not readily soluble in water [10], and are thermodynamically impossible. Reaction No. 1 can occur as intermediate since when there is a surplus of sodium sulfide, the following reaction occurs:

$$NaSbS_2 + Na_2S = Na_3SbS_3.$$

Dissolving antimony trioxide in an aqueous solution of alkali is thermodynamically possible only when producing sodium metaantimonite.

In accordance with earlier research [1, 2] and calculations, leaching of gold-antimony raw material under industrial conditions was conducted with a surplus (250-300%) of sodium sulfide. The antimony concentration in the solution was about 40 g/l, with a free sodium sulfide content of 50-70 g/l.

Following medium crushing of coarse-lump ore (25-100 mm), it was subjected to wet grinding in a ball mill operating in a closed cycle with a classifier and yielding a grist of -0.5 mm. For every ton of ore to be treated, the mill was supplied with 4 m^3 of solution containing 20-25 g/l antimony 90-100 g/l sodium sulfide, and 20-30 g/l caustic soda.

Pulp with a solid-to-liquid ratio of 5 was leached for 2 hours at 96-97°C, using two series connected reactors, each with a 10 m^3 capacity. The reactors were heated

[1] V. N. Chazov. Determining the Iosbar Potentials of Antimony Thiocompounds and Thermodynamic Research on the Behavior of Antimony When it is Being Produced Hydrometallurgically. Abstract of a Candidate's Dissertation, Tashkent, 1968.

with live steam and equipped with impeller mixers (operating at 150 rpm).

Frame filter presses were used to filter the pulp and the cake was washed with water and steamed. A similar flowsheet made it possible to completely dissolve the sulfide antimony and provide for its total extraction to solution (95%).

The cakes contained an average of 1.6% Sb, including 0.58% trioxide, 0.05% tetroxide, 0.41% pentoxide, and 0.67% water-soluble.

There were several distinctive features related to the behavior of gold [11] under industrial conditions.

It is well known [12] that gold can dissolve in sulfide-alkaline solutions. Only a small amount (0.2-0.3 mg/l) will pass into solution during hydrometallurgical treatment of gold-sulfide raw material; this leads to the content of about 2 g/t Au in the cathode metal. In addition, 90% is extracted to cake.

Analysis from the aspect of the electrochemical possibility of of various oxidation -reduction conditions shows that in the leaching process first of all one will find that the sulfur compounds dissolve, followed by the antimony compounds, and then the gold. Moreover, the concentration of other solution components is much higher than of gold; this tends to reduce still further any possibilities for the latter to oxidize and dissolve in sulfide-alkaline solutions which have a high reducibility.

In the industrial treatment of gold-antimony raw material, the largest gold particles are readily beaten and deposit in the mill, repulper, and reactor. This leads to a drop in the gold content of the cakes in the filter presses and calls for cleaning of the equipment.

The total gold extraction in the cakes was 93.42%. With respect to their chemical composition, they are a high-silicon product, containing over 90% SiO_2, and are suitable for use as quartz flux in lead plants.

Thus, hydrometallurgical treatment of gold-antimony concentrates with subsequent treatment of the cakes at lead plants makes it possible to extract antimony to an electrolytic metal, including 98-99% recycled, and 88-90% gold to a final product.

The higher grades antimony (SuO, SuOO) or cathodic antimony will be produced as an antimony product.

REFERENCES

1. P. P. Baiborodov and A. B. Ezhkov. Scientific Works (Sredazniprotsvetmet). Collection No. 6. Metallurgy of Antimony, Mercury, and Bismuth. Tashkent, 1972, pp. 54-64.
2. P. P. Baiborodov, R. L. Popov, A. B. Ezhkov, et al. Tsvetnaya Metallurgiya. (Byul. In-ta Tsvetmetinformatsiya), 1972, No. 24, pp. 29-31.
3. I. R. Polyvyanny and N. A. Milyutina.Scientific Works (In-t Metallurgii i Obogashcheniya AN KazSSR), 1967, vol. 21, pp. 3-13.
4. V. S. Shestitkcv, A. I. Levin, and V. N. Dmitriev. Scientific Works (UPI im. S. M. Kirova), No. 170. Sverdlovsk, Kinetics and Formation Mechanism - Solid Phase, 1968, pp. 15-21.
5. V. S. Tvertsyn. Uchenye Zapiski, No. 5, Izhevsk, 1960, 92 pp.
6. O. M. Tleukulov, A. G. Shiyanov, and I. R. Polyvyanny. Tsvetnye Metally, 1964, No. 8, pp. 38-41.
7. N. D. Biryukov. ZhPKh, 1963, vol. 36, No. 10, pp. 2167-2179.
8. A. I. Levin, N. V. Ishchenko, L. M. Gryaznukhina, et al. Tsvetnye Metally, 1972, No. 8, pp. 23-26.
9. V. M. Latimer. Oxidation States of Elements and their Potentials in Aqueous Solutions. Moscow, IL, 1954, 400 pp.; ill.
10. N. I. Anan', I. R. Polyvyanny, and I. G. Dem'yanikov. Scientific Works (In-t Metallurgiya i Obogashcheniya AN Kaz SSR), 1967, vol. 21, pp. 35-49.
11. N. I. Tugov, S. Ishankhodzhaev, and P. P. Baiborodov. DAN Uzb SSR, 1972, No. 7, pp. 29-31.
12. V. V. Lodeishchkov. Extraction of Gold from Refractory Ores and Concentrates. Moscow, Nedra, 1968, 203 pp.; ill.

report as they propagated. Thus, it may be inferred that when a joint forms and spreads it releases energy which makes itself manifest in the form of a shock wave. One may envisage, for example, a shock wave generated by a joint developing in one bed and leaving a trail of hackle-marks (see Plate 2), triggering-off failure in adjacent beds which had already begun to fail, possibly in fatigue, as evidenced by the rib-marks.

Joints which develop in one bed may also propagate upward or downward into adjacent rock units as a result of frictional drag along the bedding planes between the units. It has been suggested that this is one of the mechanisms which may give rise to jointing in incompetent material.

In a sedimentary series containing rocks with different physical properties and varying amounts of strain energy, it is clear that rocks in different rock units may develop at different times. It is distinctly possible that the elastic properties, etc., of the various rock types are so different that the development of joints in the various rock units may be separated by a very considerable period. In the time which elapses following the formation of joints in one rock unit and before the joints form in adjacent rock units, it is possible that the stress system in the unjointed rocks may undergo a slight reorientation. As a result of this, the joints which subsequently develop will have an orientation which is different from those which developed earlier in adjacent competent units. In addition, of course, variations in the orientation of shear joints from one rock unit to another, may also be attributed to differences in the coefficient of friction, in the various rock types, which will affect the angle of shear.

JOINTING IN IGNEOUS ROCKS

The development of primary structures in igneous rock, which have been widely studied by Hans Cloos† and his co-workers, can sometimes be related to the mode of emplacement of an intrusive mass.

† An excellent summary of the ideas and conclusions of Cloos *et al.* has been given by Balk.

Cooling and hence crystallization of an igneous melt first takes place at the walls and roof of the intrusive mass. Continued movement and intrusion of the still liquid core gives rise to the development of primary fractures in the solid, but often still plastic, outer shell of the intrusion.

Four main types of primary fractures are recognized and defined with respect to *flow-lines*, *flow-planes* and *Schlieren* which develop during the movement of the viscous liquid melt during the process of intrusion. These are *cross "joints"* (*or Q "joints"*), *longitudinal "joints"* (*or S "joints"*), *diagonal "joints"* and *flat-lying "joints"*. The orientation of these fractures with respect to flow-lines, etc., is represented in Fig. 56.

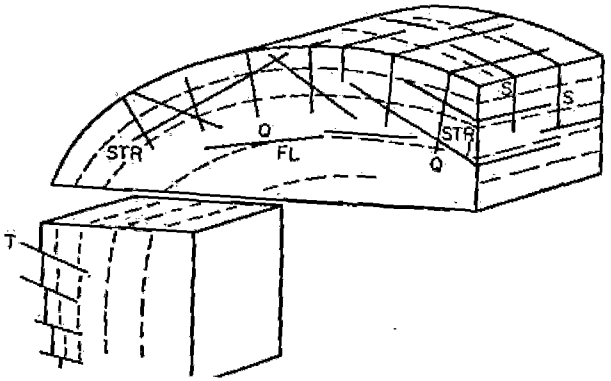

FIG. 56. Orientation of primary joints relative to surface of intrusion and internal structures (after Cloos).

Cross "joints" are among the earliest of fractures to develop in the cooling mass. Typically, they form perpendicular to the flow-lines. In fact, in areas of an intrusion where flow-lines are absent, cross "joints" cannot be identified with certainty; for such "joints" can only be tentatively correlated with cross "joints" which develop elsewhere in the intrusion where flow-lines are present. These fractures are frequently occupied by aplite, or else are almost invariably coated with hydrothermal minerals. The fracture surfaces commonly exhibit slickensiding.

Cross "joints" are regarded as tension fractures which formed when the outer portion of the intrusion had consolidated, as a result of differential movement and drag of the liquid core against the walls and roof; and, possibly, as the result of continued expansion of the intrusion.

Diagonal "joints" form at 45°, or more, to the trend of the flow-lines. Displacement along the fractures indicates that they are shear phenomena which resulted from compression normal to, and extension in the direction of, flow-lines. These fractures are also commonly filled with aplite or hydrothermal minerals.

Primary flat-lying "joints", according to Balk, tend to develop where the apex, or dome, of an intrusion is flat, or in flat sheets and laccoliths. It is difficult to see how these structures can be interpreted on dynamic grounds. It has, however, been suggested that they form when the centre of an intrusion shrinks due to cooling. These structures are also filled with hydrothermal minerals, and have been referred to as primary flat-lying "joints" so that they may be distinguished from barren joints with a similar orientation, which are frequently found in igneous masses and which are dealt with later in this chapter.

Longitudinal "joints" are steep planes which strike parallel to flow-lines. The orientation of these fractures is little affected by variations in pitch of the flow-lines. However, variations in trend of the flow-lines are faithfully followed by changes in the strike of the longitudinal joints. This type of joint is rarely filled with aplite or "dyke" material, and the minerals are usually different from those found in the other forms of primary fractures. Moreover, differential movement of the joint surfaces is rarely observed.

It is suggested that these characteristics indicate that longitudinal joints tend to form later than the other primary fractures. It seems probable that these joints developed in response to tensile stresses which were generated by cooling of the igneous mass, coupled with uplift and lateral stretching.

It will be noted that, with the possible exception of longitudinal joints, primary fractures frequently exhibit evidence of considerable shear movement. Moreover, it appears that the rock mass was in the

plastic state when these structures developed. Consequently, it would probably be better to classify these structures as faults and dykes rather than joints. It is for this reason that the present author has used inverted commas when describing these primary structures, to differentiate them from true joints.

However, the stress systems which gave rise to the primary structures may have influenced the development of joints which formed during a later phase, when the intrusion was cooler, brittle, and possibly undergoing slight lateral extension as a result of uplift. Such joints are likely to be barren, but may have an orientation which is closely related to the primary structures.

In addition to primary structures and cooling joints, igneous rocks are almost certain to contain joints which result from regional tectonic compression. Such joints are best identified when they can be related to major faults and shear zones which cut through the igneous mass (Blyth and Firman).

As with the primary structures, it is inferred that in many of the areas described, shearing has taken place while the igneous mass and the country rock have been in the plastic state. The shears and related structures have consequently been related, and likened, to those formed during the classic experiments on wet clay conducted by Reidel, rather than to the dynamic processes of brittle failure.

COLUMNAR JOINTS

The formation of primary structures may, in part, be attributed to cooling of the igneous rock mass. However, *columnar "joints"*, which are such common features of sills and some dykes, are wholly related to the shrinkage of the rock mass during cooling. Typically, the columns are hexagonal in section (although individual columns may be bounded by four, five, seven or even eight joint planes) and have their long axes orientated perpendicular to the upper and lower surfaces of the rock unit.

It will be noted that a regular hexagonal prism is the geometrical form with the greatest number of surfaces which may be placed in juxtaposition with similar hexagonal prisms, so that there are no

gaping voids between any of the adjacent columns. The other prisms which are capable of such close packing are rectangular and triangular in section. Thus, it is conceivable that the tensile stresses generated by cooling (which will be equally developed in all directions parallel to the rock unit) could be released by two orthogonal sets of joints, giving rise to rectangular columns, or by three intersecting sets of joints, giving rise to columns with a triangular section.

Other things being equal, it is clear that the quantity of strain energy released from a single column by the development of the joints will be related to its cross-sectional area. A simple calculation will show that the total areas of the joint faces bounding columns with square and equilateral triangular sections are respectively 10 and 20 per cent greater than the area of joint surface enclosing a hexagonal column of comparable cross-sectional area. Hence, it appears that the approximately regular pattern of joints delimiting the columns observed in the field is a manifestation of the principle of least work. That is, the maximum amount of strain energy is dissipated at the cost of the least amount of work utilized in the formation and propagation of fracture planes.

It may be noted in passing that a similar mechanism will control the development of shrinkage cracks in mud, which are also commonly hexagonal. In this instance, shrinkage is, of course, due to drying out of the sediments and not a result of cooling.

SHEET JOINTS

It has been noted that in addition to the primary flat-lying joint structures may subsequently develop which have a similar orientation and result in a well developed *sheeting* of the intrusion. When such *sheet joints* are closely spaced they are sometimes termed *mud joints*. A feature of sheeting is that in areas of pronounced topography, the sheet joints tend to develop parallel, or sub-parallel to the surface.

Chapman and Rioux carried out a survey of the joint systems in Arcadia National Park on Mount Desert Island off the coast

Maine. They found that, in general, sheeting was well developed throughout the area in which hornblende granite was exposed. They observed that the frequency of sheet jointing was related to the depth of cover. On the steep slopes of the U-shaped, glaciated valleys, only one or two thick sheeting layers could be seen. On the higher slopes and mountain tops, however, thin sheeting layers were abundant. A typical relationship between the frequency of sheeting, and also the orientation of the sheeting planes with respect to topography, is indicated in Fig. 57. It is suggested that the relationship represented in this figure indicates that sheeting is largely related to pre-glacial topography. In a few localities, however, sheeting has formed parallel to ice-cut surfaces and in these instances are glacial, or post-glacial, in age.

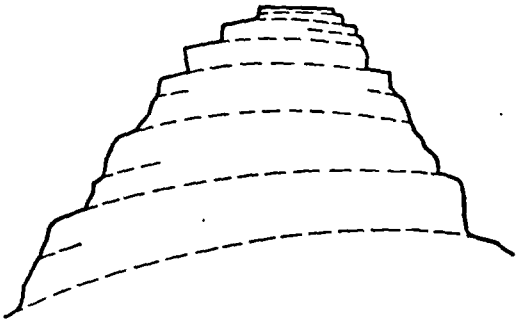

FIG. 57. Sheet joints, their orientation and intensity in relation to topography (after Chapman and Rioux).

Hill suggests that where the sheeting reflects topography, it is probably caused by a combination of factors, such as expansion of the feldspars and ferromagnesian minerals on weathering, removal of the load of superincumbent rock by erosion, and seasonal variations in temperature affecting the rock near the surface.

It has already been noted that such joints sometimes develop during quarrying and that they form suddenly, emitting a low pitched report. Dale presents other evidence that some granites may contain considerable residual strain energy. In areas of marked

formed as a result of downhill sliding of the sheets in response to the forces of gravity. The reason for the development of the diagonal joints is not readily understood, but it is tentatively suggested that they may represent the opening of strongly impressed incipient joint sets which are readily formed. Or, it is suggested, they may be the result of uneven downhill sliding of the sheets due to some local obstructions.

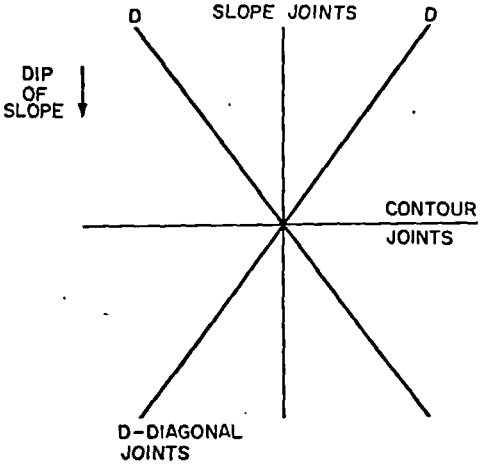

FIG. 58. Typical orientation of Dip, Diagonal and Contour joints (after Chapman and Rioux).

It may be noted that contour joints are not restricted to igneous rocks, for such structures have been reported in sedimentary rocks by Harris *et al.*

JOINTS—BRITTLE FRACTURES

In geological literature the word "joint" is frequently treated as an omnibus term and has been used to describe structures which vary widely in character and which, in many instances, could better be described as extension gashes, fissures, veins, dykes, minor faults or even cleavage. As a result, the reader is often left in considerable doubt as to the precise type of structure being described when it is merely classified as an "unqualified" joint.

As we have seen, this difficulty is not completely obviated even if one adheres to the definition that systematic joints are fracture planes, normal and parallel to which, movement has been negligibly small. Consequently, it is suggested that genetic criterion be included in the definition of a joint; namely that the term joint be restricted to structures which are the result of brittle fracture.

It is appreciated that the introduction of such a genetic criterion into the classification of geological structures is always fraught with danger. However, genetic criteria have already been introduced by classifying joints on dynamic grounds as shear or tensile fractures. Moreover, the possible errors incurred by the incorrect use of such a genetic criterion can be minimized, for if there is any doubt in the field as to whether a fracture is in fact the result of brittle failure, this doubt can be noted and recorded.

Price, N. J., 1966 Fault and Joint development in brittle and semi-brittle rock: London, Pergamon Press, 176 p.

20. Warekois, E. P., M. C. Lavine, A. N. Mariano and H. C. Gatos, *J. Appl. Phys.*, 33, 690 (1962).
21. Pauling, L., "The Nature of the Chemical Bond," p. 98, Cornell Univ. Press, Ithaca, N.Y. (1960).
22. Wells, A. F., "Structural Inorganic Chemistry," Chapter XI, Oxford Press (1945).

Kinetics of the Carbon Catalyzed Air Oxidation of Ferrous Ion in Sulphuric Acid Solutions*

G. THOMAS† and T. R. INGRAHAM‡

Abstract

Air oxidation of acidic ferrous sulphate solutions is catalyzed by activated carbon. The oxidation rate during most of the reaction can be expressed by:

$$-d[Fe^{++}]/dt = k\cdot[O_2]\cdot[C]\cdot f[H_2SO_4]\cdot[Fe^{++}]/[Fe^{++} + Fe^{+++}]$$

For molar concentrations of each of the variables, the rate of oxidation ranges from 0.07 to 1.3 moles of ferrous ion oxidized per litre of solution per minute, for various types of 100-by-150-mesh activated carbon. The rate increases with increasing fineness of the carbon; it also increases almost linearly with increasing sulphuric acid concentration up to 2*M*, but thereafter decreases almost linearly to 10*M* H_2SO_4. The results are consistent with the hypothesis that the carbon surface is sparsely covered with adsorbed oxygen, ferrous ions, and ferric ions. The activation energy estimated for the process is 6 kilocalories per mole in the temperature range 1 to 24°C. At higher temperatures the activation energy is negligibly small. The activated carbon can be used repeatedly, with little loss in efficiency. Two types of apparatus were tested and found suitable for the continuous oxidation of flowing solutions.

INTRODUCTION

Many uranium ores processed by acid leaching require oxidation before their tetravalent uranium can be extracted. This is generally done by ferric ions and the resulting ferrous ions can be reused after reoxidation. For continued leaching, the concentration of ferric ion must be maintained.

In industry, oxidation of ferrous ion for leaching may be done with chemical oxidants such as sodium chlorate or manganese

* Contribution from the Extraction Metallurgy Division, Mines Branch, Department of Mines and Technical Surveys, Ottawa, Canada.
† Senior Scientific Officer.
‡ Head, Research Section.

dioxide.[1–3] However, most of the oxidation is done by oxygen from dissolved air:

$$4\,Fe^{++} + O_2 + 4\,H^+ \rightleftharpoons 4\,Fe^{+++} + 2\,H_2O \qquad (1)$$

Oxidation can be accelerated in autoclaves with elevated temperature and air pressure.[4] More rapid oxidation can also be obtained by the use of a soluble catalyst such as the cupric ion,[5,6] or a solid catalyst such as activated carbon.[5,7] At the Mines Branch, preliminary tests have shown that the rate of oxidation of ferrous ion in 0.5 molar sulphuric acid is increased 14-fold by the use of copper sulphate, or 2400-fold by the use of activated carbon.

In this paper, a description will be given of work done to resolve the effects of different variables on the rate of carbon-catalyzed air oxidation of ferrous ion in sulphuric acid solutions. Commercially-available activated carbons were used in most experiments. To eliminate the effects of extraneous impurities on the oxidation rate, synthetic leach liquors prepared from reagent-grade chemicals were used.

APPARATUS AND PROCEDURE

The apparatus used for most of the oxidation experiments is shown in Figure 1.

The Pyrex-glass reaction cylinder was 5.5 cm in diameter and 60 cm in height. A 2-cm-diameter, porous Pyrex-glass frit was sealed into the tapered base of the reaction cylinder to support the carbon slurry and to disperse the air as fine bubbles. An air stream velocity of 200 ml/min was suitable for suspending the carbon and maintaining oxygen at its maximum solubility. To prevent plugging of the frit by the precipitation of salts, the incoming air was saturated with water. For experiments at temperatures other than ambient room temperature, an ice bath or a heating coil was used to regulate the temperature in the reaction cylinder. A water-cooled condenser was used to prevent losses of solution by evaporation.

In the continuous oxidation experiments, the Pyrex reaction cylinder was used with the settling tube attached. Solution was admitted continuously either at the top or, with inlet air, at the bottom of the reaction cylinder. The apparatus was tilted slightly to prevent air bubbles from entering the settling tube. When baffles were used to eliminate convection currents, and when the solution flow rate in the settling tube was less than the settling velocity of the carbon, the

oxidized effluent was clear. For the batch experiments, the settling tube was removed.

A second type of apparatus used for some batch experiments consisted of a flat hollow stainless steel disc, 28 cm in diameter and 1 cm

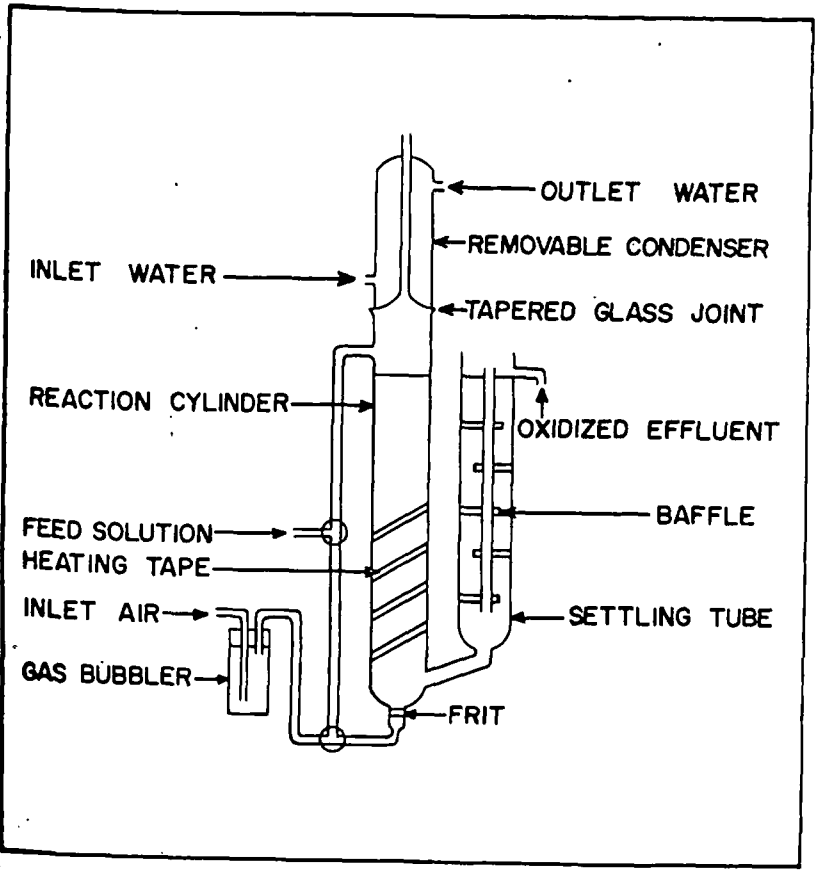

Fig. 1. Oxidation apparatus.

thick at its centre. 60-mesh screen was used to construct the disc, which contained 100 g of 28-by-48-mesh activated carbon. It was rotated vertically with about 40 per cent of its surface immersed in a narrow rectangular lucite box containing the solution.

A coarse-tipped pipet was used to withdraw samples of slurries which were filtered rapidly to separate the carbon and thus quench

the oxidation. The extent of oxidation was determined by titration to the diphenylamine sulphonate end-point with a standard dichromate solution.

RESULTS

In the first group of batch experiments done at room temperature with aerated 0.5*M* sulphuric acid solutions, carbon samples from different sources and with different histories of activation were used to oxidize samples which were 0.018*M* in total iron and 1.1*M* in carbon.

TABLE I

Effect of Type of Carbon on Relative Rate of Oxidation
(1.1*M* carbon, 0.018*M* total iron, 0.5*M* acid, room temperature)

Type of carbon	Relative reaction rate
Household wood charcoal	1.0
Activated wood carbon, brand A	1.0
Activated coconut carbon, brand B	4.4
Activated sugar carbon[a]	6.9
Activated lignite carbon, brand A	8.4
Activated pecan carbon, brand C, grade 1	10.4
Activated coconut carbon, brand C	19.5
Activated pecan carbon, brand C, grade 2	19.7

[a] Prepared from sugar, $FeCl_3$ and urea.[7]

The results in Table I show that the carbon samples have a wide range of activity and that both the source material and the history of activation are important in selecting the most effective catalyst.

TABLE II

Effect of Particle Size of Carbon on Rate of Oxidation
(1.1*M* carbon, 0.018*M* total iron, 0.5*M* acid, room temperature)

Mesh size	14-by-28	28-by-48	60-by-80	115-by-170
Relative particle size	8	4	2	1
Relative external area	1	2	4	8
Relative reaction rate	1.0	1.5	2.3	2.8

In Table II, the results of experiments using different sizes of carbon particles show that the rate of oxidation increases with the state of subdivision of the carbon but is not directly proportional to the screen size of the particles. This lack of direct proportionality is probably

caused by the large internal surface area of the carbon, much of which is available for adsorption.

The next group of batch experiments was done using 750 ml of 0.5*M* sulphuric acid containing carbon and iron in a variety of ratios.

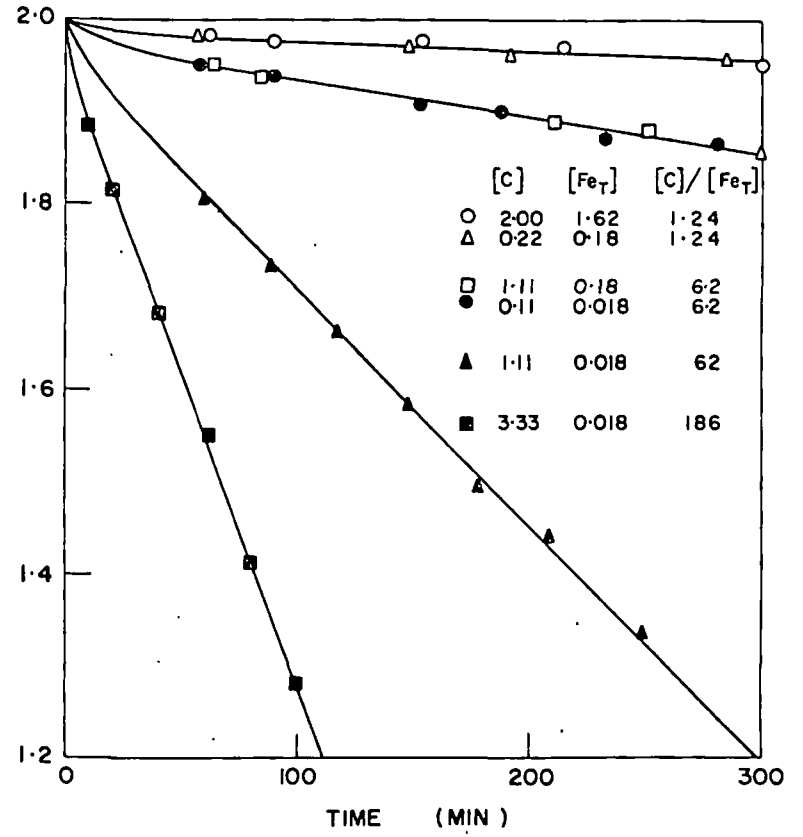

Fig. 2. Effect of carbon/iron ratio on reaction rate.

The results in Fig. 2 show that except for a brief initial period, the reaction is first order with respect to ferrous ion concentration and the rate is determined by the ratio of the concentrations of carbon to total iron, rather than by either concentration alone. The first order reaction rate constant, k_{exp}, was calculated by multiplying the slope of the linear portion of the curves by −2.303.

In the next group of experiments, the rate of oxidation was studied

as a function of acidity. The samples were 0.018 molar in total iron and 1.1 molar in carbon. The results are shown in Fig. 3 in which an adjusted reaction rate constant is plotted against the concentration of

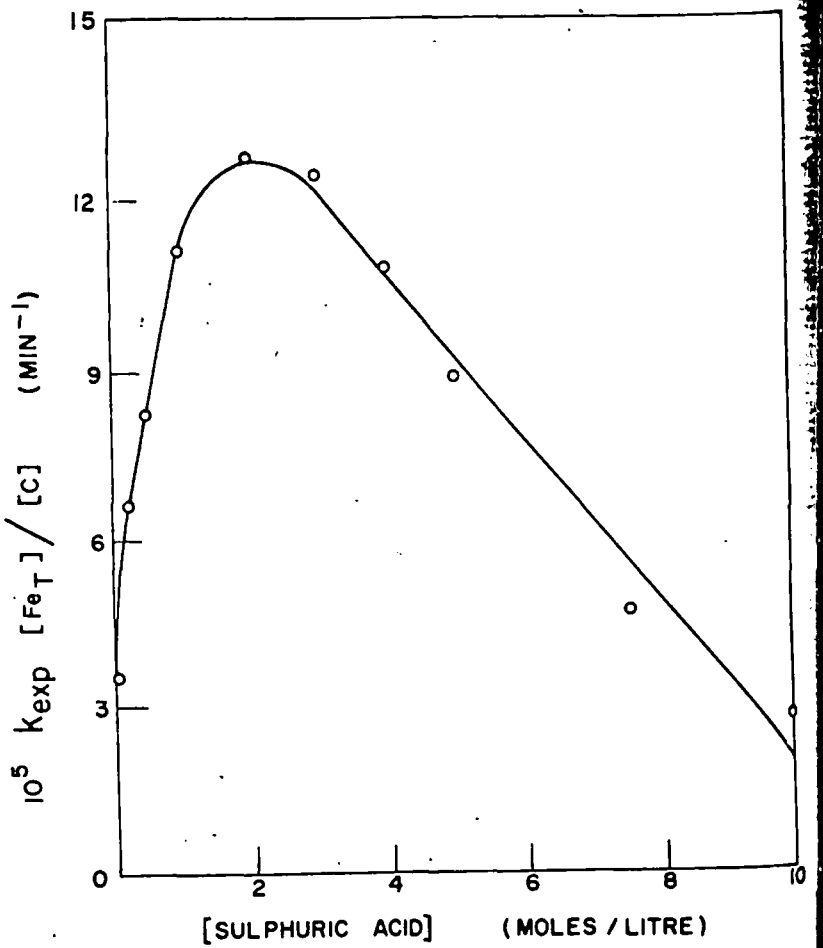

Fig. 3. Effect of acid concentration on reaction rate adjusted to 1 molar carbon and 1 molar total iron.

sulphuric acid. The adjusted rate constant, $k_{exp}[Fe_T]/[C]$, was calculated to express the first order rate constant, k_{exp}, on the basis of one mole of total iron and one mole of carbon per litre of solution. It is evident from Fig. 3 that the adjusted reaction rate increases almost

linearly with increasing acidity in the range 0.1 to 1 molar. The oxidation rate reaches a maximum at about 2 molar, and then decreases almost linearly from 3 to 10 molar acid.

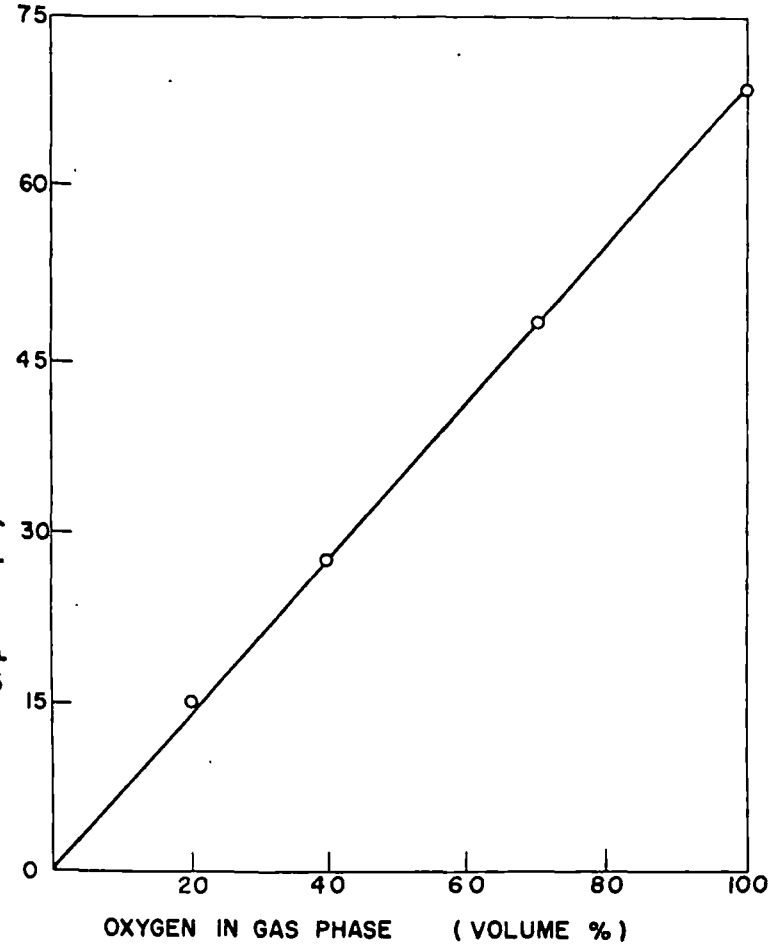

Fig. 4. Effect of oxygen concentration on reaction rate adjusted to 1 molar carbon and 1 molar total iron.

In the next group of batch experiments, samples 0.9M in total iron and 1.1M in carbon were oxidized at room temperature using a 200 ml/min flow of oxygen-enriched air. Figure 4 shows that the rate of oxidation is directly proportional to the volume percentage of oxygen in the gas phase. Since, at constant temperature, oxygen solubility is

proportional to its partial pressure in the gas phase, it follows that the rate of oxidation is directly proportional to the amount of oxygen dissolved in the solution.

In another group of experiments, the rate of oxidation reaction was studied as a function of solution temperature, using samples

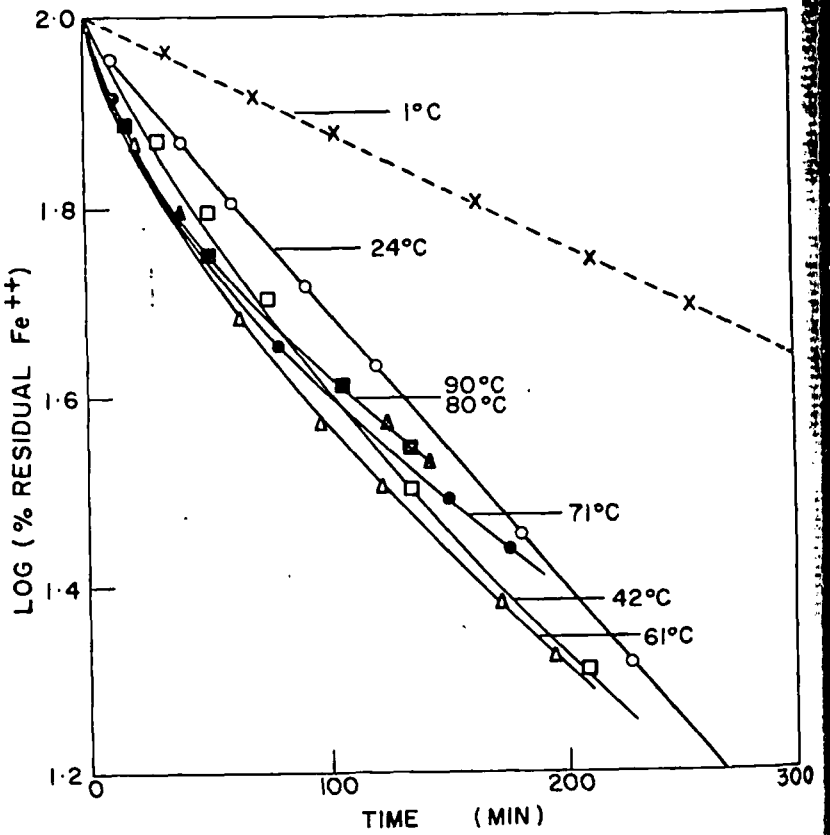

Fig. 5. Effect of temperature on reaction rate.

0.018M in total iron and 1.1M in carbon, with 200 ml/min of air. Using the oxygen solubility versus temperature data of Seidell,[8] the reaction rates were normalized to correspond with air-saturation at 24°C. The results in Fig. 5 show that the rate increases with increasing temperature. The rate of increase is greatest at the lower temperatures, for which an activation energy of about 6 kilocalories per mole was estimated between 1 and 24°C. At temperatures above 60°C, there is

no detectable increase in rate with additional increases in temperature.

Experiments done with a variety of anions and cations as contaminants have shown that the ferric, thiocyanate and chloride ions reduced the rate of oxidation. The sodium, calcium, magnesium, manganous, cupric, aluminum, uranyl and silicate ions did not influence the rate.

In the next group of experiments, a 2-gram sample of activated carbon was used repeatedly, over a 6-week period, to oxidize successive samples of solution containing one mole per litre of total iron. The efficiency of the carbon as a catalyst for oxidation was ascertained at the end of each test by determining the rate at which it was capable of oxidizing fresh 150-ml samples of solution 0.018 molar in total iron. The decrease in activity of the carbon is shown in Fig. 6, in which the rate is plotted against the time in days. It is evident, that although the rate of deterioration of the catalyst is quite rapid for the first few days, after about five days the rate of decrease is very slow. The decrease in activity tends to a logarithmic form, so it would seem reasonable to predict that, after use for one year, the carbon would still have about fifty per cent of its original activity.

Continuous oxidation tests were done with a 200-gram sample of activated carbon which was aerated in a reaction cylinder containing 750 ml of solution. Feed solution was pumped into the reaction cylinder continuously, and clear oxidized solution was collected from the settling tube. Changes were made successively in the iron concentration, in the flow rate, and in the temperature of the solution. The results of these tests are given in Table III.

TABLE III

Continuous Oxidation of Acidic Ferrous Sulphate Solutions
(22 molar carbon, varying iron concentrations)

Test conditions	Test number (1)	(2)	(3)	(4)
Feed solution, Fe^{++}, (g/l.)	25.5	8.64	25.6	19.9
Feed solution flow rate, (ml/hr)	152	151	52.7	44.4
Reaction temperature, (°C)	25	25	25	63
Test duration, (days)	4	3	5	6
Reaction cylinder residence time, (hr)	4.17	4.20	12.0	14.3
Oxidized overflow, Fe^{++}, (g/l.)	14.2	1.59	5.95	2.37
Fe^{++} oxidation, (%)	44.4	81.6	76.8	88.1
Fe^{++} oxidation, (g/hr)	1.7	1.1	1.0	0.8
$10^5\, k_{exp}[Fe_T]/[C]$, (min^{-1})	4.7	4.6	4.1	4.0

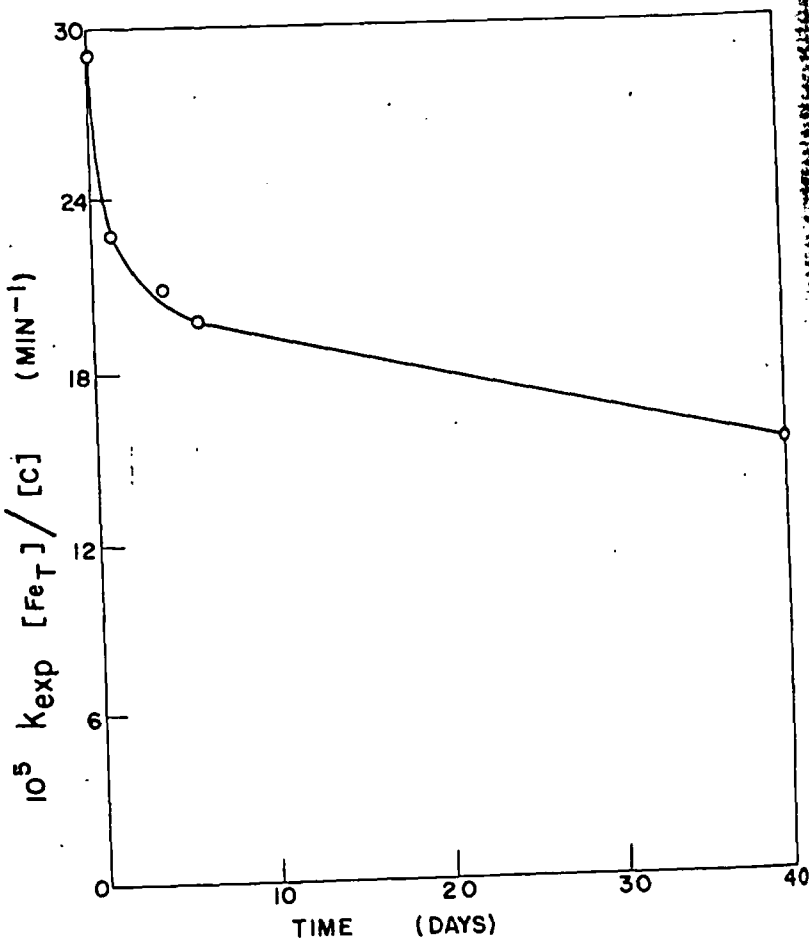

Fig. 6. Effect of continuous use of carbon on reaction rate adjusted to 1 molar carbon and 1 molar total iron.

From Table III it is evident that high percentage oxidations were obtained by using slow flow rates or dilute feed solutions, whereas, on a weight basis, more iron was oxidized when a faster solution flow rate was used. The rate constant for 1 molar concentrations of carbon and total iron, was similar for all tests.

To determine whether the results of batch experiments could be used to predict the results of continuous experiments, a batch experiment was done with amounts of carbon and solution comparable with

those used in test 2 in Table III. The time for 82 per cent oxidation was 3.6 hours in the batch test versus 4.2 hours in the continuous oxidation test. This agreement showed that batch tests should be useful in predicting the amount of oxidation obtainable in a continuous experiment.

To determine the effectiveness of a simple apparatus design which would be applicable to large-scale, multi-unit equipment, batch experiments were done with a stainless steel mesh disc containing granular activated carbon. The disc was partly immersed in solutions of 0.018 molar total iron and was rotated at various speeds for 30-minute

TABLE IV

Effect of Disc Rotation Speed on Oxidation Rate
(12.7 molar carbon, 0.018 molar total iron, 0.5*M* acid, room temperature)

Disc rotation speed, (rpm)	1.6	40	21	30	53
Per cent of Fe^{++} oxidized/30 min	36	70	78	78	52
$10^3 k_{exp}[Fe_T]/[C]$, (min^{-1})	2.1	5.6	7.1	7.1	3.4

periods. The rates of oxidation for various speeds are given in Table IV which shows that there is a wide range of rotation speeds at which a high degree of oxidation can be achieved. This type of apparatus would be suitable for on-stream continuous oxidation of acidic ferrous sulphate solutions

DISCUSSION AND CONCLUSIONS

The foregoing experiments have shown that the rate of oxidation of ferrous ion in sulphuric acid solutions varies directly with the concentration of dissolved oxygen, the amount, fineness and activity of carbon catalyst and the concentration of ferrous ion, and inversely with the sum of the concentrations of ferrous and ferric ions. At acidities between 0.1 and 1 molar, the reaction rate changes almost linearly with changes in acidity. However in the range of acidity from 3 to 10 molar, the rate decreases almost linearly with additional increases in acidity. The rate of oxidation has a small temperature coefficient in the range 1 to 24°C. At temperatures between 40 and 90°C, the rate is almost unaffected by temperature changes.

Neglecting this small but complex influence of changes in temperature, the rate of disappearance of ferrous ion by oxidation may be

expressed by the equation:

$$\frac{-d[Fe^{++}]}{dt} = \frac{k\cdot[O_2]\cdot[C]\cdot f[H_2SO_4]\cdot[Fe^{++}]}{[Fe^{++} + Fe^{+++}]} \quad \ldots \quad (2)$$

Except for a difference in the acid dependency of the reaction rate, this equation is identical with the one postulated by Posner[7] for the catalytic oxidation of ferrous ion in aqueous hydrochloric acid solutions in the presence of activated sugar charcoal.

Except for a brief initial reaction period, the experimental results are consistent with the expected behaviour for a surface reaction in which the surface is sparsely covered with oxygen, acid, and ferrous and ferric ions.[9] It is assumed that ferrous ions are adsorbed in small amounts on selected sites for which ferric ions compete equally. The extent of ferrous ion adsorption is controlled by the fraction of total dissolved iron in the ferrous state. Hydrogen ions are adsorbed also, but more strongly than the other reactants. It is reasonable to expect that when the concentration of sulphuric acid exceeds some critical value, the increased adsorption of acid decreases the adsorption of the other reactants and, consequently, decreases the rate of oxidation.

The activity of the carbon as a catalyst is retained for long periods. None of the substances occurring normally in uranium leach liquors acts as poison to the carbon activity. Oxygen, which is adsorbed in amounts proportional to the amount in solution, probably reacts as a diradical —O—O—,[10] in conjunction with hydrogen ions, to extract electrons from the adsorbed ferrous ions. Because carbon is a good electrical conductor, it is probably not essential that the electron exchange occur at adjacent adsorption sites.

Acknowledgement

The authors wish to express appreciation to J. W. MacNaught for his contribution to the experimental work.

References

1. R. P. Ehrlich, A. G. Roach, and K. D. Hester. *J. Metals* **11**, 628 (1959).
2. W. A. Gow, H. W. Smith, and R. Simard. *Can. Mining Met. Bull.* 539, 128; *Trans. Can. Inst. Mining Met.* 60, 70 (1957).
3. W. Q. Hull and E. T. Pinkney. *Ind. Eng. Chem.* 49, 1 (1957).
4. G. Thomas and B. J. P. Whalley. *Can. J. Chem. Eng.* 36, 37 (1958). *Can. Dept. Mines and Tech. Surveys, Mines Branch, Research Rept.* R3 (1958).

5. A. B. Lamb and L. W. Elder, Jr. *J. Am. Chem. Soc.* 53, 137 (1931).
6. R. E. Huffman and N. Davidson. *J. Am. Chem. Soc.* 78, 4836 (1956).
7. A. M. Posner. *Trans. Faraday Soc.* 49, 389 (1953).
8. A. Seidell. "Solubilities of Inorganic and Metal Organic Compounds." Vol. 1, 3rd ed., D. Van Nostrand Co. New York, p. 1019 (1953).
9. K. J. Laidler. "Chemical Kinetics" McGraw-Hill Book Co. Inc., New York, p. 316 (1950).
10. K. J. Laidler. "Catalysis," Vol. 1, P. H. Emmett, ed., Reinhold Publishing Corp. New York, p. 152 (1954).

Discussion

I. H. Warren:* Have the authors considered the possible role of residual quinoid structures, remaining or present in the various carbon samples, in the oxidation process?

G. Thomas and T. R. Ingraham: According to the literature, the surface of activated carbon has a variety of organic functional groups containing oxygen and hydrogen. The activated carbon has been described as a disordered agglomerate of layers of large polynuclear benzenoid hydrocarbons. It is also known that hydroquinone-type compounds are useful in the production of hydrogen peroxide, which, in turn, can oxidize ferrous ion. Consequently, hydroquinone was added in concentrations from 0.01 to 1 g/l. to aerated acidic ferrous sulphate solutions. Hydroquinone by itself was of little use as a catalyst and it was found to interfere with the catalytic action of activated carbon. Further experiments to identify the exact functional groups which may be responsible for the catalytic action of activated carbon were considered to be outside the scope of the main investigation.

* I. H. Warren, University of British Columbia, Canada.

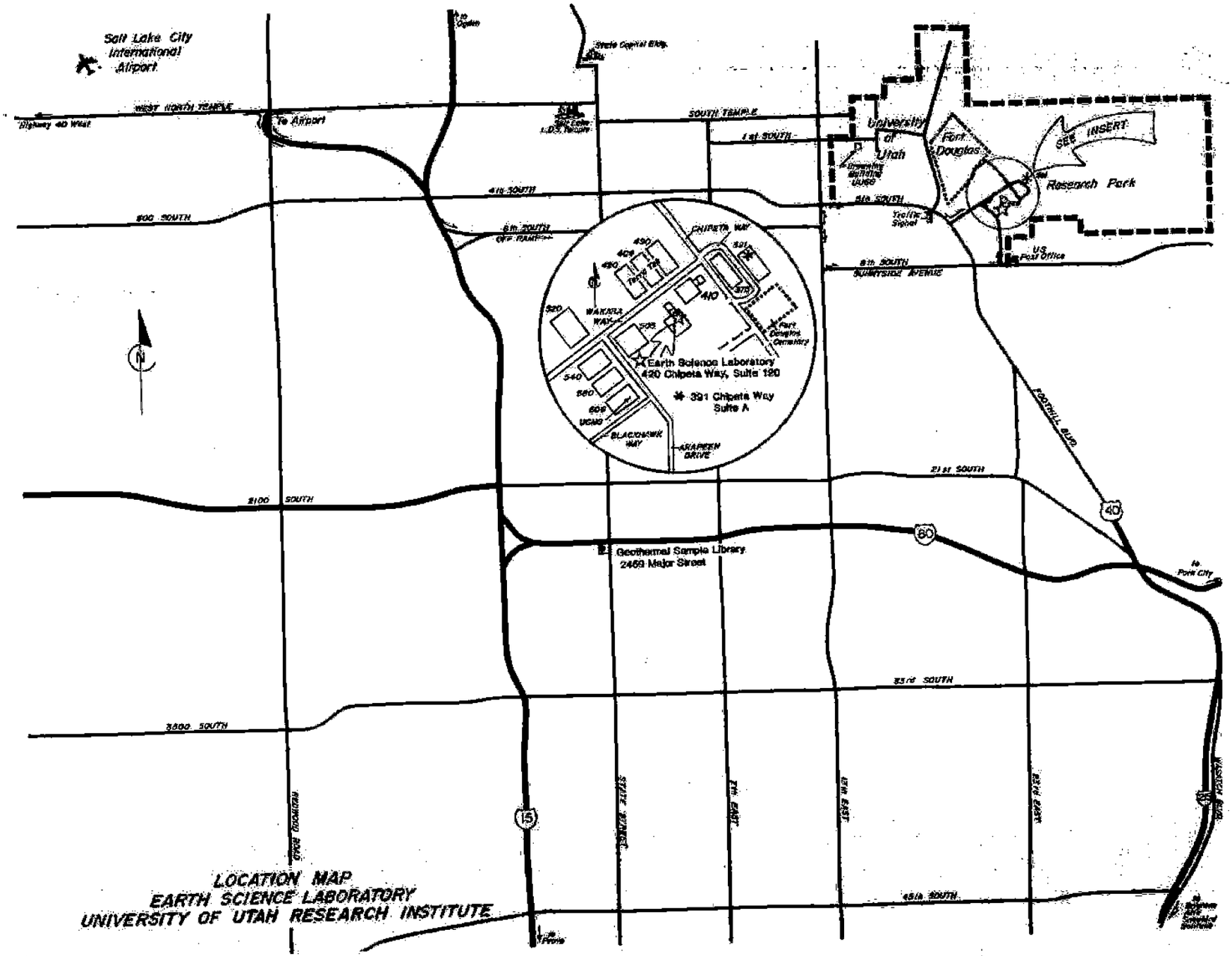

LOCATION MAP
EARTH SCIENCE LABORATORY
UNIVERSITY OF UTAH RESEARCH INSTITUTE

KINETICS OF DECOMPOSING ALUMINATE SOLUTIONS IN INCREASED CONCENTRATIONS

UDC 669.712.1

S. I. Kuznetsov and R. A. Abanin

In recent years, some alumina plants have increased the concentration of solutions directed to decomposition by 10-13%: at the UAZ, from 130 to 140 g/l Al_2O_3 (α_c = 1.67--1.72); at the BAZ, from 125 to 135 g/l (α_c = 1.70-1.75). Corresponding increases were made in the concentration of mother liquors, while the amount of steam used to vaporize the mother liquors was reduced by about 10%. Simultaneously with the increase in aluminate-solution concentration there was a reduction in the degree of their decomposition, a reduction in the caustic modulus of the mother and consequently of the circulation solutions, and a resulting deterioration in the technological indices of the bauxite-leaching indices. If one examines the positive and negative factors of increasing the concentration of aluminate solutions being directed to decomposition, then one would have to recognize that these measures are economically profitable.

Any further increase in concentration will offer greater steam economies; however, it will also strongly reduce the rate and degree of decomposition for solutions and the yield of alumina during leaching. Overall, this approach would be unprofitable.

One approach which we believe has potential is to simultaneously increase the concentration of solutions being directed to decomposition and increase their rate and degree of decomposition or else keep them at the same level used when decomposing less concentrated solutions.

An earlier work [1] showed for kinetic decomposition curves of aluminate solutions containing 124-130 g/l Al_2O_3 (α_c = 1.55-1.6) with varying temperatures and seed ratios there will always be an induction period which will decrease sharply after heating and after an increase in the seed ratio. Consequently, the decomposition rate increases from zero to some maximum, and then drops. The progressive increase in rate during the initial period indicates that the reaction products tends to accelerate the decomposition process. Consequently, decomposition of the aluminate solution is first autocatalytic, where the separated hydroxide serves as the catalyst. Similar, clearly manifesting autocatalytic processes also occur in the kinetic system. According to an earlier work [2], the decomposition rate for aluminate solutions of about the same concentrations is only slightly affected by the mixing velocity, which also confirms the occurrence of the process in a kinetic system.

With respect to the solutions of increased concentrations, containing over 160 g/l Na_2O_0, there has been little research done on the kinetics of their decomposition. According to [1, 3], the viscosity of aluminate solutions containing up to 160 g/l Na_2O at 30°C is similar to the viscosity of caustic soda solutions of the same concentration. At higher temperatures, the viscosity is lower. When the solution concentration is over 160 g/l Na_2O, the viscosity increases several fold. This suggests that when the concentration of solutions being directed to decomposition is raised to over 160 g/l Na_2O that the kinetic system of the process can be shifted to a diffusion system.

In order to verify the data we examined the influence of mixing intensity on the rate of aluminate-solution decomposition.

The starting solutions had the following composition, g/l (see Fig.):

	a	b	c
Na_2O_0	149.5	168.1	181.5
Al_2O_3	124.95	138.12	144.5
α_c	1.97	2.0	2.01
α_k	1.74	1.77	1.77

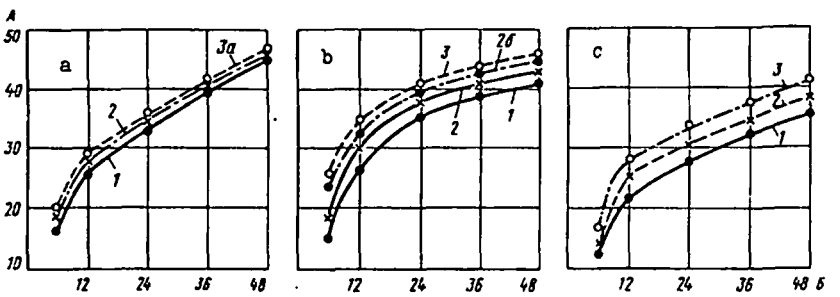

Kinetic decomposition curves for aluminate solutions, containing the following amounts of Na_2O_0 (in g/l): a - 149.55; b - 168.14; c - 181.35, at varying mixing rates (rpm):
1 - 22; 2 - 46; 2b - 54; 3 - 80; 3a - 90; A - decomposition of aluminate solution, %; B - mixing period, in hours.

Test conditions are as follows: seed ratio (ratio of Al_2O_3 in the seed to the Al_2O_3 in the solution) was constant (2.0); solutions with the seed were mixed for 48 hours at 50°C, and samples were selected after 6, 12, 24, 36, and 48 hours.

Solution decomposition was performed in steel vessels, equipped with mechanical mixers. Mixing rates were 22, 46, 54, 80, and 90 rpm's.

It is evident from the Figure that the mixing rate has only a slight effect on the decomposition kinetics of weak solutions (Fig. 1a). When decomposing more concentrated solutions (Fig. 1b), there is an increase in the mixing rate from 22 to 46 rpm and an increase of 3.5% in the decomposition rate in 12 hours, and of 2% in 47 hours.

When the mixing rate is increased to 80 rpm, the degree of solution decomposition increases by 8% after 12 hours, while it increases by 6% after 48 hours -- as compared with a mixing rate of 22 rpm.

Approximately the same picture is noted when decomposing more concentrated solutions (Fig. 1c).

Thus, when the concentration of aluminate solutions is increased to over 160 g/l Na_2O_0 one finds that their decomposition rate begins to be affected by the mixing rate which is determined by the diffusion rate.

In order to verify the accuracy of this conclusion, we examined the decomposition rate of aluminate solutions containing the following amounts of Na_2O (in g/l): 143--146, 155.3-157.8, 165.3-167.2, 182.6-185.3, and 201.3-203.1 with a constant caustic modulus of 1.75. The seed ratio was also constant, equal to 2 at constant temperatures of 30, 40, 50, 60, and 70°C. Solutions were sampled for analysis after 6, 12, 24, and 48 hours.

Using the obtained data, equations were drawn up describing the process rate at its initial stage. For the process overall, we were not able to obtain an equation for the process rate which could more or less satisfactorily describe the complex inluence of the varying conditions. The constants for the rates at which the initial stages of the process occurred (to 24 hr), determined from these equations, were almost fixed. Knowing these values and using the well-known Arrhenius equation, it is possible to determine the activation energy values of a process.

Calculation results showed that when decomposing solutions containing less than 150--160 g/l Na_2O_0 the activation energy of the process is about 8.1 kcal/mol (which conforms to the data of Herrmann and Stipetic [4]); when decomposing solutions, containing over 160 g/l Na_2O_0, the value of activation energy for the decomposition process is much lower and does not exceed 3.5 kcal/mole.

The considerable drop in activation energy for the decomposition process occurring when the original solution concentration increases to over 160 g/l Na_2O_0 also indicates that when solutions of increased concentration are decomposed a decisive role is played by diffusion.

It follows from this that the concentration of aluminate solutions can be increased still further than has been done at the UAZ and the BAZ with increases in the mixing rate. This makes it possible to reduce steam consumption when vaporizing solutions and to maintain a high degree of solution decomposition.

It is evident from comparisons of Fig. 1a and b that when solutions containing 168.1 g/l Na_2O_0 are decomposed, where there has been an increased mixing rate of 46 rpm after 48 hours one will attain the very same Al_2O_3 extraction as is obtained from solutions with 149.55 g/l Na_2O_0 at a mixing rate of 22 rpm. When the mixing rate is increased to 80 rpm, the degree of decomposition for more concentrated solutions is higher than for the less concentrated solutions.

According to data given in the Figure, it is possible to increase the concentration of the starting solution to 165-170 g/l Na_2O_0; it is undesireable to increase the concentration any further, since the degree of solution decomposition will be lowered even at high mixing rates.

When there is an increase in the mixing rate it is possible to effect mechanical mixing of the aluminum hydroxide, though in this work we have not noted this grinding even at such high mixing rates as 80 and 90 rpm.

To some extent mechanical grinding can be useful, since it would contribute to an increase in the seeding activity of the hydroxide. However, a strong grinding of the hydroxide is not desireable since it can lead to increased losses of hydrate pulp with thickener discharges. Therefore, one has to establish the optimum mixing rate for enlarged-laboratory or pilot cyclical tests.

Increases in the mixing rate when decomposing solutions of increased concentrations should be linked with some increase in the decomposition temperature. According to experimental data obtained at the UAZ under production conditions, decomposition of aluminate solutions with increased concentrations is more rapid and more thorough when the starting and final process temperatures are higher. Thus, when the concentration of the starting solution is increased from 145-147 to 155-161 g/l Na_2O_0 and there is a simultaneous increase in the starting temperature from 54-55 to 59-60°C and in the final temperature from 44-45 to 49-50°C, after 65-71.5 hours the degree of solution decomposition will not change, remaining at 50.8-51%. When decomposing the same solution, but maintaining the starting and final process temperatures, the degree of decomposition was 0.8-1% lower.

Increasing the temperature of the decomposition process contributes to reductions in the solution viscosity and consequently to increases in the diffusion rate. Therefore, an increase in the starting and final temperatures increasesthe degree of decomposition for solutions of increased concentration.

When decomposing concentrated solutions, containing 165-170 g/l Na_2O_o, evidently one requires even higher starting and final temperatures for the process. An optimum temperature schedule was not established for solutions of the indicated concentration.

As the concentration of the starting solution is increased to 165-170 g/l Na_2O_o there is a deterioration in the precipitation and filtration of the aluminum hydroxide, due to increases in the viscosity of the mother liquor. However, since the starting and final temperatures of the pulp would be higher, the increased viscosity for the mother liquor would be comparatively low. It is possible that in order to improve precipitation and filtration of aluminum hydroxide one has to shift to adding small amounts of flocculants, as for example polyacrylamide [5] or use other methods. This question needs further study.

CONCLUSIONS

1. As solution concentrations increase to 160 g/l Na_2O_o and higher, the kinetic system of the decomposition process shifts to a diffusion system

2. The possibility was shown of increasing the concentration of solutions directed to decomposition to 165-170 g/l Na_2O_o, while simultaneously increasing the mixing rate, thus affording large steam savings.

REFERENCES

1. S. I. Kuznetsov and V. A. Derevyankin. Physical Chemistry of Alumina Production by the Bayer Process. Moscow, Metallurgizdat, 1964, 352 pp., ill.
2. F. F. Vol'f. The Bayer Method as Used for Ural Bauxites. Moscow, ONTI, NKTP, 1935, 114 pp., ill.
3. S. I, Kuznetsov, L. N. Antipin. I. T. Sryvalin, et al. Metallurgy of Light Metals. Collection No. 58, UPI, Sverdlovsk, 1957, pp. 36-50.
4. E. Herrmann and J. Stipetic. Z. Anorg. Allgem. Chem., 1950, vol. 262, pp. 258-287.
5. O. V. Serebrennikova, S. I. Kuznetsov, and I. A. Kakovskii. Promyshlenno-Ekonomicheskii Byulleten' Sverdlovskogo Sovnakkhoza, 1960, No. 2, pp. 5-8.

UDC 541.123.3+546.87.131

The liquidus diagram of the $BiCl_3$ - $CaCl_2$ - KCl system

B G Korshunov, Yu G Podzolko, V Ya Kerzner and S A Krishtul (Moscow Institute of Steel and Alloys, Department of General Chemistry).

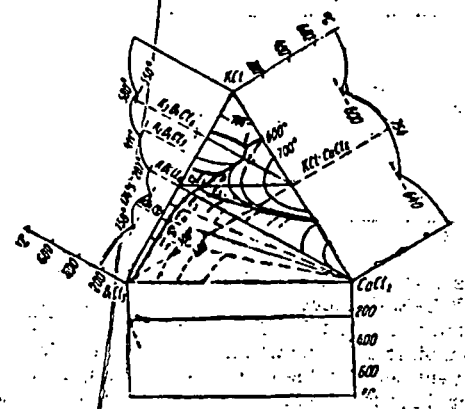

Liquidus diagram of the $BiCl_3$-$CaCl_2$-KCl system.

Summary

The melting of the $BiCl_3$-$CaCl_2$ system was investigated in connection with the use of chloride fuming in the treatment of oxidized and oxysulphide bismuth-containing ores. Nine polythermic sections were studied, and their directions were determined by the position of the nonvariant points on the binary side diagrams (fig.). The results from thermal analysis are given in the figure and in the table.

The results from the sections investigated of the system indicate the existence of crystallisation fields for KCl, K_2BiCl_5, KCl·$CaCl_2$, $KBiCl_4$, $CaCl_2$, $BiCl_3$, K_2BiCl_5, and KBi_2Cl_7 on the liquids surface. Mixtures with figurative points adjacent to the KCl corner have the highest melting points, and those adjacent to the $BiCl_3$ corner have the lowest. The non-variant points of the system are given in the table.

Points of the invariant equilibria in the $BiCl_3$-$CaCl_2$-KCl system

Character of points	Content - mole %				Coexisting phases
	°C	$BiCl_3$	$CaCl_2$	KCl	
Published data [3, 5]					
Eutectic	158	76.0	-	24.0	$L \rightleftarrows BiCl_3 + S_1$
Dystectic	174.5	66.7	-	33.3	$L \rightleftarrows S_1$
Eutectic	158	59.2	-	40.8	$L \rightleftarrows S_1 + S_2$
Dystectic	207	50.0	-	50.0	$L \rightleftarrows S_2$
Transitional	411	38.0	-	62.0	$L + S_4 \rightleftarrows S_3$
Dystectic	580	25.0	-	75.0	$L \rightleftarrows S_4$
Eutectic	550	23.0	-	77.0	$L \rightleftarrows S_4 + KCl$
Published data [6]					
Eutectic	640	-	69.6	30.4	$L \rightleftarrows CaCl_2 + S_5$
Dystectic	754	-	50.0	50.0	$L \rightleftarrows S_5$
Eutectic	600	-	24.0	76.0	$L \rightleftarrows S_5 + KCl$
Experimental data					
Eutectic E_1	369	10.0	19.0	71.0	$L \rightleftarrows KCl + S_4$
E_2	150	41.1	7.9	51.0	$L \rightleftarrows S_2 + S_3$
E_3	160	43.7	6.8	49.5	$L \rightleftarrows S_2 + S_5$
E_4	145	58.0	1.9	40.1	$L \rightleftarrows S_1 + CaCl$
E_5	125	73.1	1.9	25.0	$L \rightleftarrows S_1 + CaCl_2 + BiCl_3$
Eutectic-Van Rein-point					
e_1	555	16.1	19.2	64.7	$L \rightleftarrows S_5$
e_2	160	43.5	6.5	50.0	$L \rightleftarrows S_5$
e_3	166	5.0	47.4	47.6	$L \rightleftarrows S_2 + CaCl_2$
e_4	174	69.3	1.7	29.0	$L \rightleftarrows S_1 + CaCl_2$
Peritectic P	369	11.7	32.3	56.0	$S_4 + L \rightleftarrows S_3 + S_5$

The investigations make it possible to determine the most favourable temperatures and concentration characteristics for the process. The low-temperature bismuth-containing compositions are of interest for the pyro-electrometallurgy of the element.

800. Non-Ff
1975. v. 3 N5

UDC 669.33

Kinetics of the dissolution of copper oxides in hydrochloric acid solutions

M L Episkoposyan, R G Shakhnazaryan, A A Babadzhan, B S Grigoryan and G M Grigoryan (Armenian Scientific-Research and Design Institute of Non-Ferrous Metals.

In spite of the common knowledge of the leaching of copper oxides, there are no published data on investigation of the kinetics of their dissolution in hydrochloric acid solutions. The present article sets out the results from investigations into the kinetics of the dissolution of cupric oxide and cuprous oxide in hydrochloric acid solutions by the rotating disc method [1]. The use of this method secures the production of reproducible results and makes it possible to carry out experiments under the hydrodynamic conditions of the agitation of the solution amenable to calculation and, which is particularly important, makes it possible to compare the experimental data with the theoretical data and also to calculate the absolute values of the reaction rate constants. A detailed description of the apparatus used for the investigations is given in the literature [2-4].

The specific rate of dissolution was calculated from the amount of copper passing into solution from 1 cm^2 of the disc surface in 1 sec. To define the order and character of the process a series of experiments was set up with HCl concentrations of 0.5, 1.0, and 1.5 mole/dm^3 in the solution under the following conditions: disc surface area, 3.14 cm^2; volume of solution, 1 dm^3; disc rotation rate, 15, 16 rps; temperature of solution, 50°C; length of experiment, 15, 30, 45, and 60 min.

The linear character of the curves in fig. a and b and the constancy of the v/[HCl] ratios (where v is the specific dissolution rate, mole/cm) show that both reactions are of the first order. To determine the character of the dependence of the dissolution rate of cupric oxide and cuprous oxide in hydrochloric acid solutions on the disc rotation rate experiments were set up under the following conditions: HCl concentration 0.5 mole/dm^3; temperature of solution 40°C; disc rotation rates 6, 8, 10, 12, and 14 rps. The rate of both reactions (table) increases with increase in the disc rotation rate, i.e., in proportion to $n^{1/2}$, where n is the disc rotation rate, rps.

This relationship is consistent with diffusion theory of the rotation of a disc. The average values of the reaction rate constants at 30°C with an HCl concentration of 0.5 mole/dm^3, calculated by means of the equation:

$$K = \frac{Q}{S\pi n^{1/2}[HCl]} \quad dm^3 \cdot cm^{-2} sec^{-1/2} rev^{-1/2}$$

223, 224 are absent

From the results from determination of the equilibrium concentrations of indium in the resin phase and in the solution phase a relation was plotted between the capacity of the resin and the extraction of indium and the ratio of the equilibrium concentration to the initial (fig. 1). The intersection of the curves corresponds to the ratio of the volume of the solution to the volume of the resin where the greatest capacity of the resin with the greatest extraction of indium from the solution under equilibrium conditions is obtained. This ratio amounts to 40:1. The kinetics of the sorption of indium from the solution with this ratio were studied.

UDC 621.762:546.821

Possibility of using electrolytic powders of titanium and its alloys for the production of thin-walled sintered blanks

S S Kiparisov, O A Nikiforov and V P Luk'yanov (Moscow Institute of Steel and Alloys - Department of Rare and Radioactive Metals and Powder Metallurgy).

Summary

The mechanical characterisitics obtained after the sintering of compacted blanks and the possibility of making thin-walled blanks from electrolytic powders of titanium and its alloys with 1.6 wt.% Al were investigated. The electrolytic powders of titanium and the alloy are quite satisfactory for the production of thin-walled blanks by the most widely used technique of powder metallurgy, consisting of compaction of the initial powder in a steel mould followed by vacuum sintering.

For thin-walled blanks the wall thickness should not be less than 3-4mm.

UDC 658.51:519.2

Planning (Aluminium Smelter) plant running costs on the basis of mathematical-statistical methods

S I Tsetsarkina (Urals Polytechnic Institute - Department of Economics and Organisation of Non-Ferrous Metallurgical Plants.

At the present time the planning of plant running costs, like other costs, is realised from the attained level of the previous year with allowance for the introduction of organisation and technical measures directed towards the reduction of these costs. An increase in the degree of scientific soundness of the plans can be obtained with the use of mathematical-statistical methods. Thus, for planning the plant operating costs it is possible to use the method of integration of the correlation relationship between the above-mentioned costs and the volume of production with allowance for its variation with time.

Let us illustrate this calculation for the case of one of the aluminium plants. From the plant data, using the method of least squares, we determined the laws governing the variation of the plant operating costs as a function of the increase in the volume of production and the dynamics of this increase for 1971-1973 [1-3]. The relationships for the variation in the volume of production with time, expressed in the form of regression equations, are shown in Table 1.

The high values for the correlation coefficient and Student criterion indicate a close and reliable relationship, since the Student criterion considerably exceeds the tabular values [4].

The dynamics of the variation in the production of alumina are given by the equation: $x = 215662.8 + 2014.2t$. The output of alumina in 1974 amounted to:

$$\Sigma x = \int_{12}^{16} (215662.8 + 2014.2\,t)\,dt = 975446 \text{ tons,}$$

and the output in 1975 amounted to 1 008 000 tons.

The dependence of the variation in the plant operating costs on the growth in the volume of production is shown in Table 2. The plant operating costs show a stable and fairly close relationship with the growth in output, since the Student criterion is greater than 2.58 (i.e., this relationship is significant with 99% probability); and the correlation coefficient varies within the limits of 0.6-0.8.

Table 1: Variation of the production volume by quarters in 1971-1973

Form of product	Regression equation	Student's criterion	Correlation coefficient
Alumina t	$x = 215662.8 + 2014.2t$	130.87	0.9868
Electrode mass t	a) $\lg x = 4.433 + 0.036 \lg t$	61.66	0.9723
	b) $x = 27123.4 + 2418.6 \lg t$	57.79	0.9704
Silicon t	$x = 5758.5 + 96.9t$	16.26	0.8991
Ingots t	$x = 1907.5 + 682.6t$	6.36	0.8019

Table 2: Variation of the plant operating costs with the product output

Form of product	Regression equation	Student criterion	Correlation coefficient
Alumina t	a) $y = -109.94 + 0.007x$	6.83	0.7779
	b) $y = -2.54 + 1.075 \lg x$	7.08	0.7847
Electrode mass t	$y = 1.524 + 0.002x$	4.49	0.6859
Silicon t	$y = -54.91 + 0.011x$	3.31	0.6056
Marketable Production, 000's Roubles	$y = -0.258 + 0.68 \lg x$	2.92	0.6268

The Kinetics of the Dissolution of Crystalline Quartz in Water at High Temperatures and High Pressures

H. SIEBERT*, W. V. YOUDELIS†, J. LEJA‡ and E. O. LILGE§

Department of Mining and Metallurgy
University of Alberta,
Edmonton, Alberta, December 1, 1962

Abstract

Dissolution of quartz discs (cut parallel to basal (0001) face) in distilled water, at 205°C–345°C and 3,000 psi, was found to proceed as a zero order reaction, involving an activation energy of 18.8 kcal/mole; i.e. of the same magnitude as for the dissolution of quartz in alkaline media. The molybdate determinations of dissolved silica suggest that monomeric form of silicic acid is formed in solution, $SiO_{2(quartz)} + 2\,H_2O_{(l)} = Si(OH)_{4(solution)}$.

INTRODUCTION

The decreased market value of uranium concentrates has necessitated re-evaluation of the carbonate leaching process in order to reduce the cost of their production. Material balance of the carbonate leaching circuits in the Eldorado-Beaverlodge mill has revealed that a consumption of 3 to 5 pounds of reagents per ton of ore cannot be accounted for.[1] Since the bulk of the ore is made up of silica and silicates, it was thought that part of the loss could be attributed to dissolution of these non-metallics. A research program has been started to examine the variables affecting the solubility and dissolution rates of silica and silicates in alkaline leach liquors.[2,3]

* Research Associate.
† Assistant Professor.
‡ Associate Professor.
§ Professor and Head, all of Dept. of Mining and Metallurgy, University of Alberta, Edmonton, Alberta.

The kinetics of the quartz-water system has been investigated since it forms a basis for a study of the quartz-sodium hydroxide[4] system and quartz-sodium carbonate and sodium-bicarbonate system.

REVIEW OF LITERATURE

Although there are abundant thermodynamic data for the quartz-water system,[5–9] very few kinetic data exist for this system.[10–12] The work of Hooley[11] is mainly concerned with dissolution of silica glass and quartz by hydroxides of Group I at temperatures below 100°C, while that of Greenberg and O'Connor[12] is primarily concerned with amorphous silica in water at temperatures below 100°C. Kitahara[10] has carried out some rate studies on pure crystalline quartz under supercritical conditions (i.e. 400–480°C and specific volumes of water varying from 1.6 to 3.0 ml/g) and found diffusion to be the rate controlling step in his experiments.

(i) The Mechanism of Quartz Dissolution

Hooley[11] proposes that the dissolution of quartz in hydroxide solutions is a two step mechanism:

$$(SiO_2)_{solid} + 2\,H_2O = SiO_2{\cdot}2\,H_2O_{(s)} \quad (1)$$

$$SiO_2{\cdot}2\,H_2O_{(s)} + 2\,OH^- = Si(OH)_6^{-2} \text{ in solution} \quad (2)$$

The first step is an adsorption of water followed by reaction with the hydroxyl ion to produce soluble products. Hooley states that if only water (and no additional hydroxyl ion) is present, as in NaCl solutions, no attack of crystalline quartz will take place. Iler[13] considers that the dissolution of solid silica in water involves a simultaneous hydration and depolymerization:

$$(SiO_2)_n + 2n(H_2O) = n\,Si(OH)_4$$

When silica passes into solution, there must be a chemical reaction on the surface of the solid phase with water, whereby the surface layer of SiO_2 is hydrated; then, as each silicon atom with its surrounding oxygen atoms is detached from the surface, further reaction with the water occurs and soluble monosilicic acid is formed.

According to Franck,[15] the solution of quartz in pure water may be represented by the reaction $Q + n{\cdot}H_2O = SiO_2{\cdot}nH_2O$ where Q represents solid, crystalline quartz. In a thermodynamic treatment of the

solubility data of Kennedy,[9] Mosebach[15] and Franck[16] have both deduced the association value n as equal to 2.

Finally, experiments on freezing point lowering show that silica dissolves predominantly in the form of monosilicic acid, probably H_4SiO_4.

(ii) The Effect of Surface Treatments on Crystalline Quartz

The existence of a high solubility layer on the surface of ground quartz particles has been firmly established by various workers,[18-23] though the nature of this layer is still in doubt. This layer is thought to be either a Beilby-type layer consisting only of mechanically "disturbed" amorphous silica, or an incomplete monolayer or multilayer of silicic acid. Evidence of Holt and King[24] and infrared spectroscopy studies on retention of H_2O and OH groups at high temperature indicate that the second supposition is correct.

(iii) The Effect of Crystallographic Orientation on the Rate of Dissolution

Work by Laudise[25] shows that in quartz crystallization the order of growth rates is under all conditions arranged in the following sequence: basal (0001) face > $(01\bar{1}1)$ face > $(10\bar{1}1)$ face ≫ prism $(10\bar{1}0)$ face. The order of the dissolution rates is also the same and, according to data referred to by Kennedy[9] is nearly 100 times greater for basal (0001) face.

EXPERIMENTAL

(A) Equipment

An electrically heated autoclave of 1 litre capacity manufactured by Autoclave Engineers, Inc. was used for the series of experiments. A "Sym-ply-trol" controller (Assembly Products Inc.) was used to control the temperature of the solution within the autoclave to ±2°C. The pressure was maintained at the desired value by a gas compression pump (Model HG-30). Some modifications to the autoclave were made, viz:

(a) The balanced oil lubrication system was removed and lubrication of the stirring shaft was effected by periodically coating the teflon-asbestos packing with molybdenum disulfide grease.

(b) A 6″ pencil thermocouple was installed immediately below the threads on the autoclave beaker and was bent into an inverted L-shape inside the beaker so that the temperature of the liquid was measured at the point 2 inches above the bottom of the stirring shaft. A Honeywell Brown Electronik recorder was used in conjunction with this thermocouple to continuously record temperature during an experiment.

(c) Measurements of pressure were made on a 4½ ″Bourdon-Type Ashcroft laboratory test gauge (7,500 psi range) attached to the autoclave by an isolation valve. The Bourdon tube of the gauge and the adjoining pressure tubing were vacuum filled with distilled water to eliminate trapped air bubbles, and the isolation valve closed before attachment to the rest of the assembly. The compressibility of water in the Bourbon tube was considered negligible under the test conditions.

(B) The Solution Used

The dissolution tests were carried out in doubly distilled water, the second distillation being from a very dilute potassium permanganate solution. To remove any dissolved carbon dioxide or oxygen, nitrogen was bubbled through the water for one hour immediately before its use in a dissolution test.

(C) Preparation and Mounting of the Quartz Sample

The quartz plates used in this experiment were cut from large crystals obtained from the Murray-American Corporation. These crystals were optically clear and very pure and were sufficiently large to yield plates 3 inches in diameter from any crystallographic plane.

The steps used in the preparation of a sample were as follows:

(1) A 6 mm thick plate was cut perpendicularly to the c-axis to yield a plate whose surface was parallel to the (0001) basal plane.
(2) The plate was then rounded to a disc of 2.550 inches in diameter.
(3) The surfaces of the disc were ground flat and polished using 600 R.A. size of silicon tetracarbide grinding powder.
(4) After thorough rinsing the disc was treated with hot 50% HCl solution for one hour to remove any iron and was again rinsed with distilled water.

(5) The acid-treated disc was then held at 400°C in a furnace for one-half hour to remove any adsorbed organic matter and water, cooled in a desiccator and weighed.

Steps (4) and (5) were repeated on the disc following the completion of a reaction (traces of iron oxide were deposited from the stainless steel holder onto the disc, presumably due to galvanic action of Pt-stainless steel).

In order to study the rate of dissolution of a single crystallographic plane at a time and in order to avoid the high surface free energies of edges, a special stainless steel holder (Fig. 1) was constructed to hold

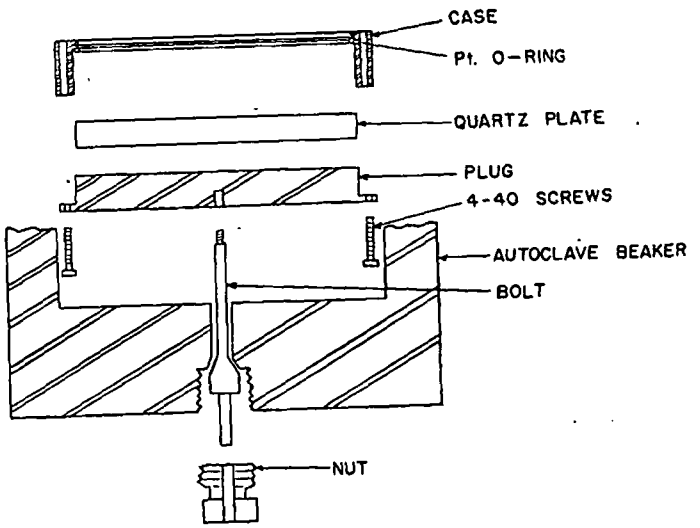

Fig. 1. Exploded view of the stainless steel holder and its disposition in the autoclave.

the prepared plate. The quartz disc mounted in its holder was placed directly beneath the autoclave stirrer and was fastened to the bottom of the autoclave beaker by means of a bolt through the bottom of the autoclave.

(D) Preparation of the Autoclave for an Experiment

Once the sample was placed in the autoclave and the autoclave assembled, the whole system was flushed with nitrogen and subsequently evacuated with a vacuum pump. The flushing and evacuation were

repeated three times with evacuation as the final step. Distilled water previously purged from CO_2 was then siphoned into the autoclave through the sampling assembly, and the pressure within the autoclave increased to 500–900 psi using N_2. The autoclave heaters were then turned on and upon reaching equilibrium conditions at the desired working temperature, the pressure was brought up to 3,000 psi using the gas compression pump, the required overpressure being supplied by compressed nitrogen gas. Following the removal of each sample, the pressure was readjusted to 3,000 psi. On completion of an experiment the autoclave was quenched from working temperature to room temperature in a bucket of water, the time for quenching being of the order of twenty minutes.

(E) Sampling Procedure

A sampling apparatus (Fig. 2) was designed so that liquid samples could be taken from the interior of the autoclave at working temperatures of 205–344°C and quenched to room temperature for determinations of volume and silica content. A capillary tube (a) which extended well below the liquid level in the autoclave was connected to a three-way valve (b) on the exterior of the autoclave. To take a sample, beaker (c), quenched in liquid nitrogen, was screwed to the 3-way valve at (d) and evacuated with a vacuum pump through (e). After the beaker had been evacuated, valve (f) was closed and valve (g) opened to admit a sample, then closed after the beaker had filled. Valve (f) was then opened and the sample was forced out by the residual pressure into a flask for weighing and analysis. Two samples of five millilitres each were taken, the first one being a blank sample to draw off the stagnant liquid from the tubing of the sampling system.

Validity of this method was checked three times by removal and analysis of two consecutive samples after discarding a blank. Concentrations of SiO_2 on these were found to agree within 1%.

(F) Analytical Technique

Three methods of analysis were used in this work:

(a) Weight loss of quartz disc.
(b) The molybdate colorimetric method for silica determination.
(c) The evaporation of the sample, after treatment with a sodium hydroxide solution, followed by fusion and redissolution of the melt in doubly distilled water. This sample was then analysed by the colorimetric method.

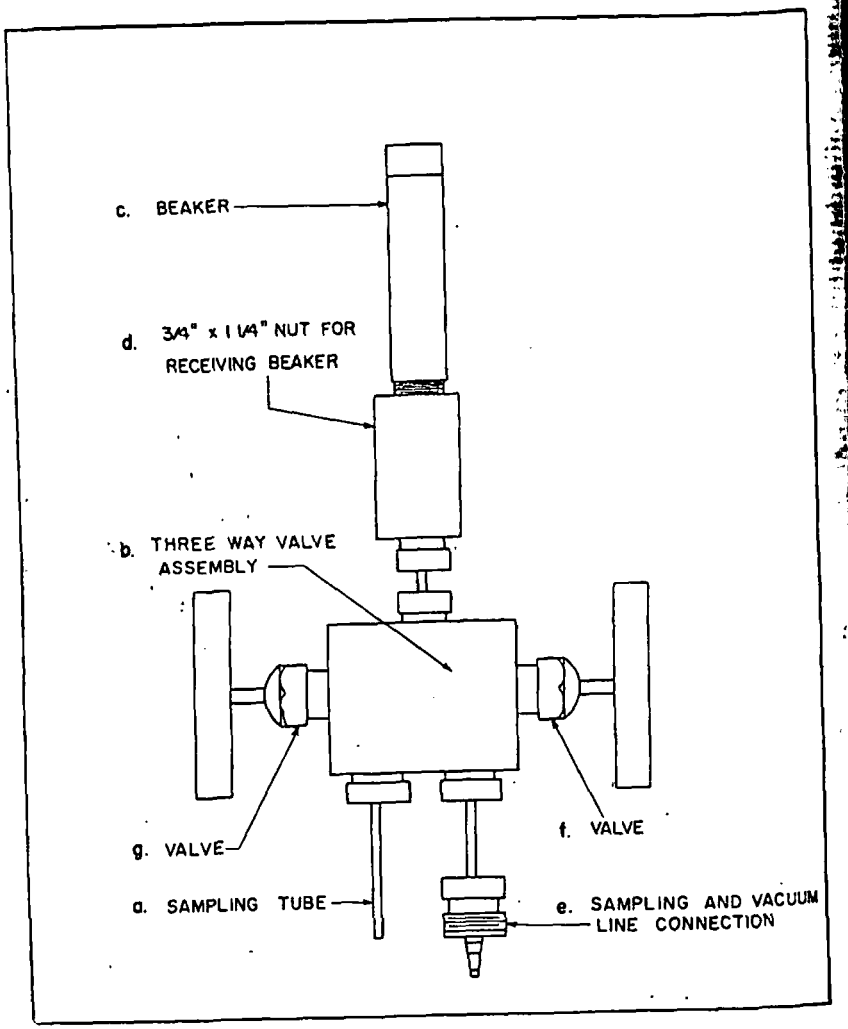

Fig. 2. Sampling apparatus.

The colorimetric method, outlined by Alexander, Heston and Iler[28] is useful for determining the monomeric dissolved silicic acid and the amounts of monosilicate and disilicate ions in solution. Alexander[27] has reported that monosilicic acid forms a yellow silicomolybdate complex with molybdic acid within 75 seconds (at 20°C) while disilicic acid requires 10 minutes.

The colorimetric method is based on the reaction of silica with ammonium molybdate at a pH of 1.5[28] to form the yellow silicomolybdic acid. The ratio of molybdic acid to silica should be such that an optical density not greater than 0.5 is obtained. If the ratio is smaller then insufficient molybdic acid is present to react with all of the silica.

The color intensity of the silicomolybdate complex was measured with Bausch and Lomb Spectronic 20 colorimeter at 400 mμ. The readings were taken two, five and ten minutes after the sample aliquot had been added to the molybdate reagent.

Method (b) outlined above is useful for determining the concentrations of monosilicic acid disilicic acid while method (c) is useful for determining any polymerized and colloidal silica as well after conversion to a sodium monosilicate.

Deviations between methods (a) and (b) were found to be less than ±7%.

EXPERIMENTAL RESULTS

The temperatures and the pressure for this series of experiments, 205–344°C and 3,000 psi, were chosen so that neither the critical conditions for water nor the maximum solubility of quartz in water were exceeded.[9] All parameters other than temperature and stirring rate were kept constant.

It was of interest to know the effect of stirring on the rate of dissolution. Too high a speed would have created a vortex thus reducing the surface area of quartz/solution interface and creating quartz/vapor interface, while too low a stirring speed might allow diffusion from the bulk of the solution to become rate controlling, thus masking the kinetics of the surface reactions. Fig. 3 shows the effect of 3 stirring speeds: 247 rpm, 512 rpm, and 666 rpm, for 3,000 psi pressure and 248–250°C. The concentration versus time curves remain straight lines for all three stirring speeds, the small variation in slope being mainly due to slight differences in temperature for the reactions.

Figure 4 illustrates the effect of temperature on the rate of dissolution of crystalline quartz in water. The data were obtained at the temperatures of 250°, 247°, 269°, 291°, 315° and 332° Centigrade, 3,000 psi, 247 rpm stirring speed for all but one test.

Table I shows the results of the two analytical techniques F (b) and F (c) used on identical samples; i.e. the reaction of molybdic acid with silicic acid in solution and the reaction of molybdic acid with converted sodium monosilicate. Although the comparison appears to be quite satisfactory, indicating absence of polymerized and colloidal silica in

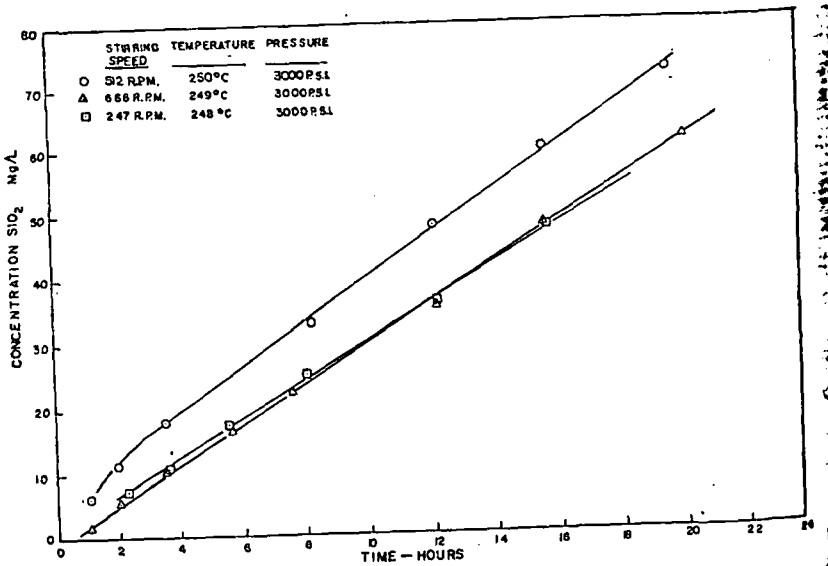

Fig. 3. The effect of stirring on the rate of dissolution.

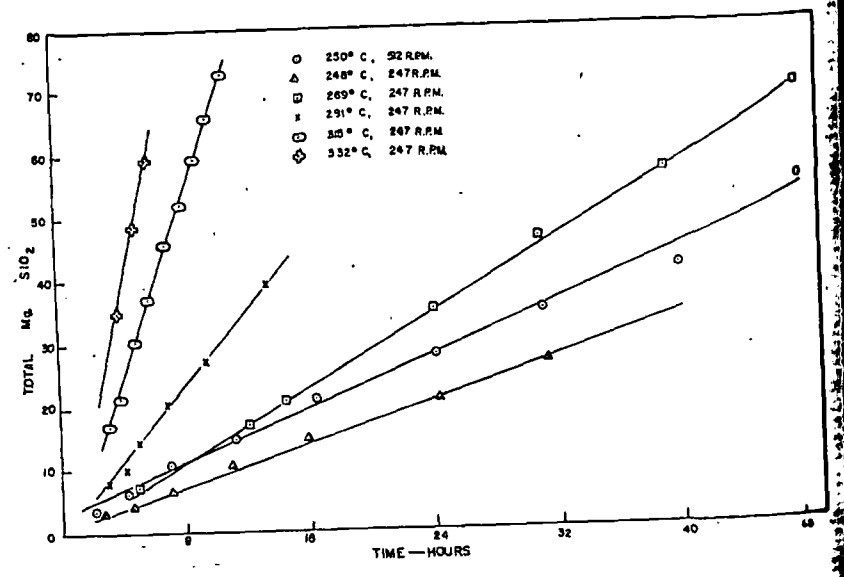

Fig. 4. The effect of temperature on the rate of dissolution.

solutions, the method F (c) probably involves larger errors due to its complicated treatment procedure.

Silicic acid is known to adsorb quite strongly on practically anything and it was expected that considerably more SiO_2 would adsorb on the walls of the autoclave than actually did. The amount of silica adsorbed

TABLE I

Sample	mg/l SiO_2 Method F (b)	mg/l SiO_2 Method F (c)
1	149	154
2	181	186
3	186	188
4	169	166
5	148	139
6	47.6	43.3

on the stainless steel of the autoclave was determined by desorbing it in two consecutive runs with $10^{-2}M$ NaOH after the completion of each experiment. Care had to be taken to keep the temperature below 100°C in these two desorption tests, because above this temperature NaOH

TABLE II

Run #	SiO_2 deposited on the walls mg	Total SiO_2 in solution mg	Temp. °C	Length of Run hrs	Deposited SiO_2 % total
1	2.2	70.5	250 ± 1.5	72.0	3.1
3	1.3	70.4	269 ± 1.5	48.6	1.8
4	0.9	40.0	291 ± 1.0	13.5	2.3
7	2.5	92.5	290 ± 1.5	24.0	2.7
5	1.0	77.0	315 ± 2.5	12.0	1.3
6	1.6	64.8	332 ± 2.5	7.0	2.5

vigorously attacked the stainless steel itself. Following these two desorption runs a third blank run with pure water had to be carried out to remove all traces of hydroxide; this also served as a final desorption to remove any traces of silica. Generally, no silica was detected in the water from the third run.

Table II tabulates the amounts of adsorbed silica for all the runs.

A constant check was kept on the amount of iron in solution. Table III gives a compilation of the analyses of iron for each run.

TABLE III

Run #	Dissolved Fe mg/l	Temp. °C	Length of Run hrs
1	0.40	250	72.0
3	0.17	269	48.3
4	2.38	291	13.5
5	0.15	315	12.0
6	Nil	332	7.0

Microscopic examination of the disc surfaces before and after dissolution tests brought out rather startling differences in their appearance, Figs. 5 (a), (b) and (c). The heavily fissured surface Fig. 5 (c) was obtained on two occasions, while all other specimens showed the surface to be etched nonuniformly as seen in Fig. 5 (b) but without any evidence of fissures. The dissolution rates appeared to be not affected by the appearance of fissures—the results falling in line with those when no fissures were formed.

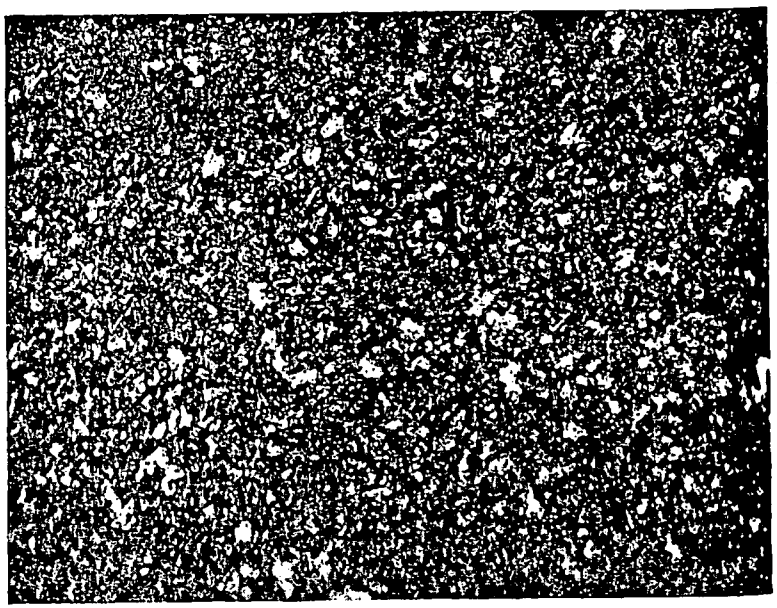

Fig. 5(a). Quartz surface after polishing, before dissolution. 380×

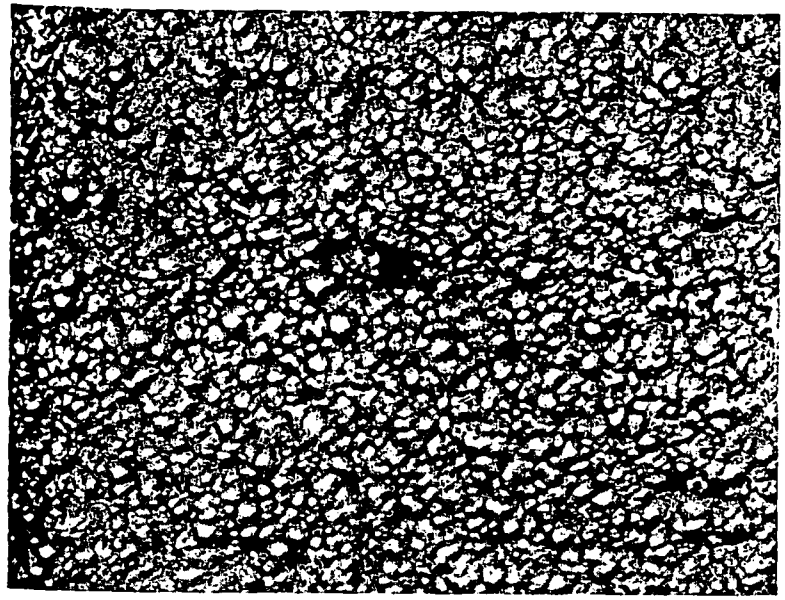

Fig. 5(b). Quartz surface after dissolution at 315°C. 380×

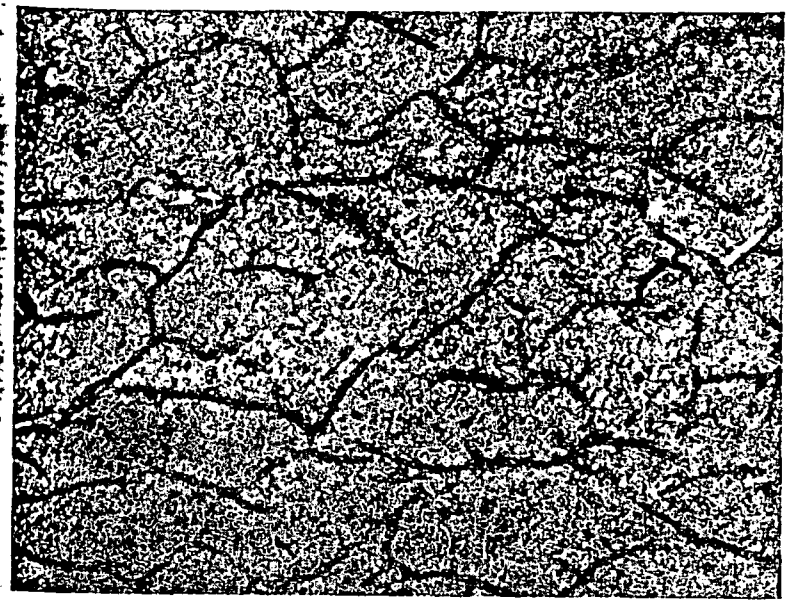

Fig. 5(c). Quartz surface after dissolution at 219°C. 137×

DISCUSSION

Although the quartz-water system appears to be a simple one, many uncertainties exist as to the mechanism involved in dissolution and the state of dissolved species. Frederickson and Cox[29] consider that the dissolution of quartz involves disintegration of mosaic elements (cemented together by weaker O—O bonds than Si—O bonds within the mosaic) to give a suspension of colloidal particles, the average size of which they calculate to be of the order of 800 Å. They argue that the dissolved species exists as a large polyelectrolyte (and not as a simple ion) which titrates with molybdate ions stoichiometrically, in good agreement with gravimetric determinations of SiO_2. Work by O'Connor[30] confirms that polysilicic acids develop full color with molybdic acid in less than 5 minutes if the polysilicic acids are noncyclic. The fact that after 2 minutes no increase in optical density was noted during determinations of solutions obtained in this series of tests would suggest that monosilicic acid was the only species. Yet, despite the apparent confirmation of the determination results by the semigravimetric method (Table I) there is no assurance that the polyelectrolyte species is definitely not present. It would be necessary to carry out light scattering determinations on the dissolution samples in order to establish whether the nature of the dissolved species is colloidal polyelectrolyte or monomeric silicic acid.

The curves of rate of dissolution versus time, for all temperatures investigated, are represented by straight lines (Figs. 3 and 4) suggesting a zero order reaction between quartz and water:

$$\text{Dissolution rate} = \frac{dc}{dt} = k$$

during the initial time period before equilibrium and saturation of water with SiO_2 is reached.

A plot of $\log k$ vs $1/T$ (Fig. 6) gives the activation energy $E_a = 18.8$ kcal/mole, the magnitude of which suggests a surface reaction as the controlling step in the dissolution:

$$(SiO_2)_{(\text{quartz})} + 2\,H_2O = Si(OH)_{4(\text{in solution})}$$

although diffusion through a polymerized layer of silicic acid at the surface of quartz cannot be excluded.

Comparison with activation energies obtained by other investigators on dissolution of quartz in alkali media, Table IV, seems to imply that

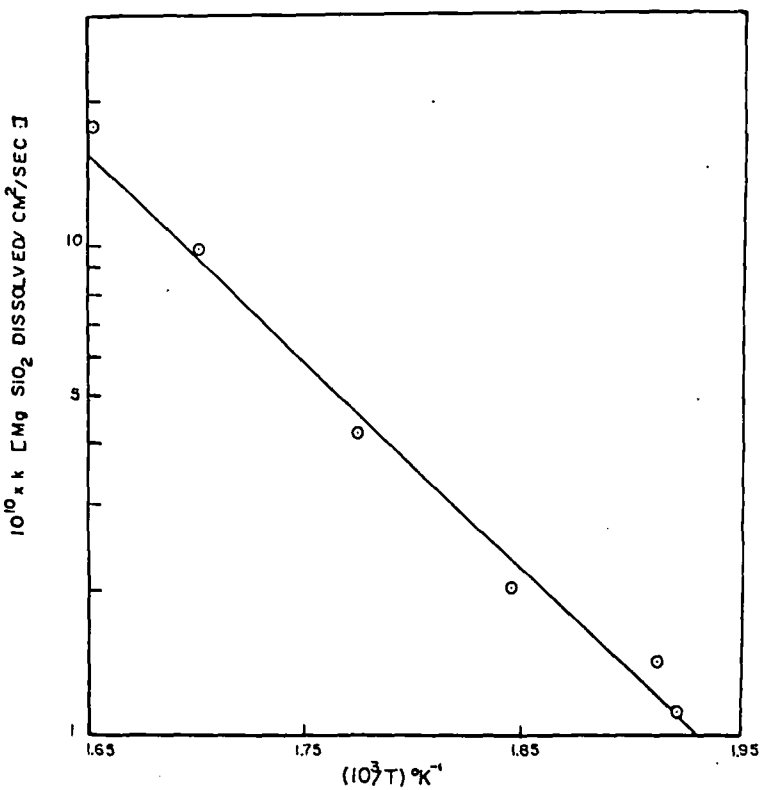

Fig. 6. Arrhenius plot for activation energy.

in all cases a surface reaction is the rate controlling step, although the actual rates of dissolution are very much higher in alkali media.

In solutions of high pH the dissolution reaction involves OH^- ions and the formation of some ionized species like SiO_4^{4-} or $Si(OH)_6^{2-}$.

TABLE IV

Temp.	Solvent	SiO_2 Species	$E_{(\text{activation})}$	Reference
205–344°C	Water	Crystalline Quartz	18.8 kcal/mole	
150–170°C	1.0*N* NaOH	Quartz Sand	17.5 kcal/mole	(4)
125–160°C	7.5*N* NaOH	Quartz Sand	22.6 kcal/mole	(4)
70–90°C	2.73–10.3*N* NaOH	Quartz Cubes	18–25 kcal/mole	(11)
30–60°C	Dilute Alkali	Sp. Bulky Silica	21 kcal/mole	(12)

Additional work is required to find out whether $Si(OH)_4$ species produced in distilled water is monomeric or polymerized, and ionized or unionized.

Acknowledgement

Grants from Eldorado Mining and Refining Co., which enabled this and related work to be carried out, are gratefully acknowledged.

References

1. Woodward, J., Internal report on the solution balances of Eldorado-Beaverlodge mill. (Presented at the Conference of Metallurgists, Hamilton, September, 1962.)
2. Johnson, H. E., Leja, J., Lilge, E. O., Dissolution of Non-Metallic Minerals in Alkaline Leach Liquors, Progress Report #1. Dept. Mining and Metallurgy, University of Alberta, August 1961.
3. Schulz, K. F., Siebert, H., Meimaroglou, H., Leja, J., Lilge, E. O., Progress Report #2, Dept. Mining and Metallurgy, University of Alberta, February, 1962.
4. Burkin, A. R., Proceedings of the International Mineral Processing Congress, 6–9 April, 1960, Ins. Min. & Metallurgy.
5. Kitahara, S., *Rev. Phys. Chem. Japan*, **30**, 122 (1960).
6. Ibid., **30**, 109 (1960).
7. Laudise, R. A., *J. Phys. Chem.*, **65**, 1396 (1961).
8. Wood, J. A., Jr., *Am. J. Sci.*, **256**, 40 (1958).
9. Kennedy, G. C., *Econom. Geol.*, **45**, 629 (1950).
10. Kitahara, S., *Rev. Phys. Chem. Japan*, **30**, 122 (1960).
11. Hooley, J. G., *Can. J. Chem.*, **39**, 1221 (1961).
12. Greenberg, S. A., **62**, 1195 (1958).
13. Iler, R. K., The Colloid Chemistry of Silica and Silicates, pp. 13–14, Cornell University Press, 1955.
14. Kitahara, S., *Rev. Phys. Chem., Japan*, **30**, 115 (1960).
15. Mosebach, R., *Neues Jahrbuch Mineralog. Abb.*, **87**, 351 (1955).
16. Franck, E. U., *Z. Physik, Chem.*, **6**, 345 (1956).
17. Brintzinger, H., *Z. Anorg. allgem Chem.*, **196**, 44 (1931).
18. Kitto, P. H., and Patterson, H. S., *J. Ind. Hyg. Toxicol*, **24**, 59 (1942).
19. Dempster, P. B., and Ritchie, P. D., *J. Appl. Chem.*, **3**, 182 (1953).
20. Dempster, P. B., and Ritchie, P. D., *Nature*, **169**, 538 (1952).
21. Clelland, D. W., Cumming, W. W., and Ritchie, P. D., *J. Appl. Chem.*, **2**, 31 (1952).
22. Clelland, D. W. and Ritchie, P. D., *J. Appl. Chem.*, **2**, 42 (1952).
23. Gibb, J. G., Ritchie, P. D., and Sharpe, J. W., *J. Appl. Chem.*, **3**, 213 (1953).
24. Holt, P. F., and King, D. T., *J. Chem. Soc.*, 733 (1955).
25. Laudise, R. A., *J. Am. Chem. Soc.*, **81**, 562 (1959).
26. Alexander, G. B., Heston, W. M., and Iler, R. K., *J. Phys. Chem.*, **58**, 453 (1954).

27. Alexander, G. B., *J. Am. Chem. Soc.*, **75**, 5655 (1953).
28. Govett, G. J. S., *Anal. Chim. Acta*, **25**, 69 (1961).
29. Frederickson, A. F., Cox, J. E., *American Mineralogist*, **39**, 886 (1954).
30. O'Connor, T. L., *J. Phys. Chem.*, **65**, 1 (1961).

Discussion

L. T. Romankiw:* Have any corrections been made to the data recorded in Figs. 4 and 5 for the decrease in aqueous solution volume arising from depletion of the solution through sampling?

In order to obtain a more meaningful rate constant than that derived by the authors, I think a rate equation of the form

$$\frac{V}{S}\left(\frac{dc}{dt}\right) = k$$

should be used. This would imply the heterogeneity of the reaction and at the same time facilitate the necessary corrections due to volume and surface area changes.

The surface appearance of the leached solid samples deserve some remarks. This might in part be the result of different modes of attack on various parts of the surface as a result of stresses and strains or even phase transformations to high temperature phases, i.e. tridymite, on the surface, arising from the cutting operation during preparation of the specimen.

E. O. Lilge, J. Leja, H. Siebert, and W. V. Youdelis: The data recorded in Fig. 3 have not been corrected for the changes in volume due to sampling, since only the effect of stirring was being tested and it appeared not necessary to do so. However, the data in Fig. 4 have been corrected, the curves having been plotted for the total SiO_2 dissolved, which includes that SiO_2 removed through sampling.

We agree with Dr. Romankiw that the rate equation should involve variables; volume, V, and surface area, S. We chose, however, not to include them explicitly in the rate equation since the surface area remained substantially constant and the variations of the volume have been taken care of by the manner of plotting the results.

A. R. Burkin:† The reaction rates were studied under experimental conditions where the surface area of quartz remained substantially constant. Thus there is no evidence as to the order of the reaction with respect to solid surface area. Therefore, the statement that the order is zero seems dubious.

E. O. Lilge, J. Leja, H. Siebert, and W. V. Youdelis: We stand corrected by Dr. Burkin that the order of the reaction with respect to the solid surface area is not zero but more likely first order reaction.

* L. T. Romankiw, Thomas J. Watson Research Center of I.B.M., New York City, New York.
† A. R. Burkin, Royal School of Mines, London, England.

KINETICS OF DISSOLUTION OF INDIUM SULFIDE IN A FERRISULFATE SOLUTION

UDC 669.872

G. E. Avakyan, I. F. Khudyakov, and E. I. Eliseev

The kinetic characteristics of indium sulfide dissolution have been investigated by the rotating disc method, to study the behavior of indium sulfide during the salt leaching of zinc-bearing sulfide materials.

A massive specimen of sulfide was prepared by the earlier described method [1], by dissolving metallic indium in hydrochloric acid, precipitating the sulfide with arsenic-free hydrogen sulfide, pressing the vacuum-dried residue to form tablets 25 mm in diameter, and firing these in a vacuum at 350°C. The product had the following composition (%): 70.4 In, 29.2 S (theoretical composition: 70.47% In and 29.53% S).

The method described in [2] was used for the experiments. The sulfide disk was glued to a plastic rod with epoxy resin. The working surface of the specimen was ground and polished with felt before each experiment. The rod and the disk (except for the working surface) were covered with chemically stable lacquer.

Ferrisulfate solution with an iron concentration ranging from 4-22 g/liter was used as the solvent. The temperature of the solution in the experiments varied within 60-90°C, and the mixing speed 3-16 rps; the experiment lasted for three hours. The zero sample was taken when the prescribed temperature had been reached, subsequent samples being taken every 15 min during the first hour and then after one hour. The solution samples were analyzed for indium photometrically, with determination of indium in the form of rhodamine bromindate, and for bivalent iron by the volumetric bichormate method.

The initial speed of dissolution was calculated by the formula:

$$v_0 = \frac{Q}{AS}\left(\frac{dC}{d\tau}\right)_{\tau=0},$$

where Q is the initial volume of the solution, dm^2; A - the atomic weight of the element; S - the specimen surface, cm^2; C - the concentration of indium, g/dm^3; and τ - the time, sec.

The value of $\left(\frac{dC}{d\tau}\right)_{\tau=0}$ was obtained by graphical differentiation (see Fig. a).

It was established that the ratio of bivalent iron concentration in the solution to the indium concentration fluctuated within 1.57-1.43 in all of the experiments; this corresponds fairly well to the stoichiometric ratio of these elements in the reaction products (1.46):

$$In_2S_3 + 3Fe_2(SO_4)_3 \rightarrow 6FeSO_4 + In_2(SO_4)_3 + 3S_0.$$

A film of elemental sulfur was observed on the disk surfaces after the experiment was over.

It follows from Fig. b that the amount of dissolved indium is proportion to the leaching time in the degree of 1/2, which is the principal characteristic of a process in the internal diffusion region. However, the Pilling-Bedworth ratio in this case is $K = 3M_S/d_S : M_{In_2S_3}/d_{In_2S_3} = 0.7$, i.e., less than unity; this indicates formation of a loose, porous shell of solid reaction product, and this provided the opportunity for finding the kinetic characteristics of indium sulfide dissolution by the rotating disk method.

The process rate is governed by the kinetics of interaction between the react-

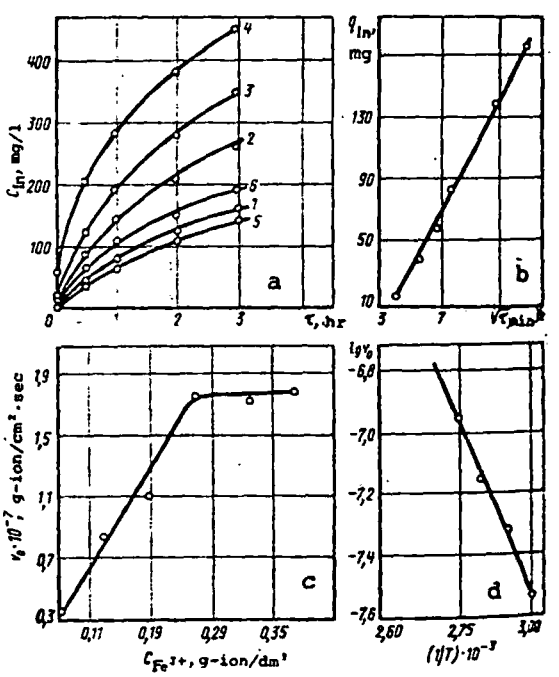

Relationships:
a - indium concentration in solution to leaching time; 1-4 - at t = 90°C and $[Fe^{3+}]$ concentration of 0.8, 0.125, 0.19, and 0.25 g-ion/dm^3, respectively; 5, 6 - t = 60 and 70°C and $[Fe^{3+}]$ = = 0.19 g-ion/dm^3; b - ditto (t = 90°C, $[Fe^{3+}]$ = 0.125 g-ion/dm^3, n = 11 rps); c - initial rate of In_2S_3 dissolution to Fe^{3+} concentration (t = 90°C, n = 11 rps); d - its logarithm to reciprocal temperature ($[Fe^{3+}]$ = 0.19 g-ion/dm^3, n = 11 rps).

ing substances only during the initial period of the experiment; subsequently, the process makes the transition to a diffusion routine, due to formation of elemental sulfur.

Test results showed that the initial speed of dissolution was independent of the rate of solution mixing.

The trivalent iron concentration affects the rate of indium sulfide dissolution only up to a value of 0.5 g-ion/dm^3 (see Fig., c). This is apparently due to saturation of the double diffusion layer by ferri-ions when the concentration of the latter in the solution is greater than 0.25 g-ion/dm^3.

Analagous data on the effect of the trivalent iron concentration upon dissolution speed were obtained by A. S. Yaroslavtsev for zinc sulfide [3] and by the authors of [4] for chalcopyrite.

The time and concentration orders of the reaction (n_τ = 2.2, n_C = 0.75) were found by the Van't Hoff method for the concentration regions Fe^{3+} < 0.25 g-ion/dm^3. It follows from the relationship $n_\tau > n_C$ that certain reaction products retard the process. Obviously, elemental sulfur is such a product.

The average speed constant of the reaction of In_2S_3 dissolution in ferrisulfate solution for the range of Fe^{3+} concentrations from 0.08 to 0.25 g-ion/dm^3 was calculated; it is 1.95 x 10^{-6} dm^3/cm^2·sec. Thus, the amount of the dissolved element can be computed from the equation $q = 1.95 \times 10^{-6} S C_{To}$.

The results of experiments on the effect of temperature upon the dissolution rate are shown in Fig. α in the form of the Arrhenius graph. An apparent activation energy of 10.5 kcal/mole was obtained for the reaction of indium sulfide dissolution in ferrisulfate. In terms of apparent activation energy, indium sulfide is intermediate between sphalerite (E = 7.5 kcal/mole [3]) and chalcopyrite (E = 17+3 kcal/mole [4]).

The following reaction speed-temperature equation was obtained:

$$\lg v = -\frac{10500}{4,575T} - 6,27.$$

Indium behaves like zinc sulfide in leaching with ferrisulfate solution. This conclusion is of practical importance because indium is extracted mostly from zinc concentrates, in which it is present in the form of an isomorphic impurity in sphalerite, sometimes in chalcopyte [5]. A comparison of the activation energies for the reactions of sphalerite and indium sulfide dissolution by ferrisulfate solutions leads to the assumption that the presence of indium as an isomorphic impurity in sphalerite should not prevent indium extraction into the solution.

REFERENCES

1. N. A. Khvorostukhina, Proceedings of the Irkutsk Polytechnical Institute (Metallurgical Series), Irkutsk, Polytechnical Institute, 1963, No. 13, pp. 145-155.
2. I. A. Kakovskii and Yu. M. Potashnikov, Kinetics of Dissolution Processes, Moscow, Metallurgiya, 1975, 219 pp., ill.
3. A. S. Yaroslavtsev and V. M. Piskuniv, New Developments in Mining and Processing Lead-Zinc Materials, Alma-Ata, Nauka, 1975 (VNIItsvetmet, No. 25), pp. 255-259.
4. I. E. Dutrizac, R. I. C. MacDonald, and T. R. Ingraham, Trans. Met. Soc. AIME, 1968, 245, No. 5, 955-959.
5. S. V. Bleshinskii and V. F. Abramova, The Chemistry of Indium, Frunze, Izd. Akad. Nauk Kirgiz SSR, 1958, 372 pp., ill.

UDC 541.11+661.424

Thermodynamic characteristics of the ternary system of sodium, potassium and magnesium chlorides

G Yu Sandler and A Kh Ratner (All-Union Aluminium and Magnesium Institute)

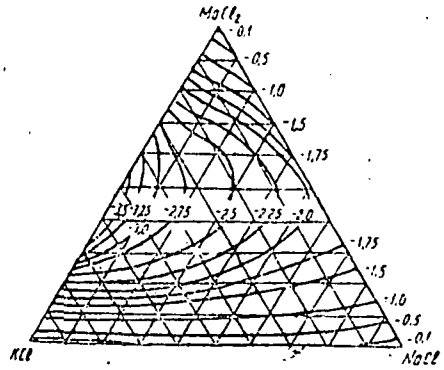

Isolines for the molar enthalpy of mixing (kcal/mole) at 1073°K for binary chlorides of sodium, potassium and magnesium.

Summary

Accurate thermal calculations on new technological processes and operations in the production of magnesium from the chlorides requires a knowledge of the thermodynamic characteristics of the interaction of the components in the sodium, potassium and magnesium chloride ternary system. The standard enthalpies of formation of the binary and ternary alloys of the chlorides were determined for various compositions in the system. The results were used to calculate the isolines of the enthalpies of mixing for the binary chlorides in the whole composition triangle of the system, given in the figure.

The enthalpies of mixing were also calculated analytically and the calculated data were compared with the experimental. The agreement between the calculated and experimental data is considered satisfactory in the light of the experimental errors.

UDC 669.273'283+549.512+532.73

Kinetics of the dissolution of molybdenum and tungsten trioxides in ammonia solution

V V Stetsik, M V Mokhosoev, O I Kovalevskii and A A Kosogov (Donetsk State University - Department of Inorganic Chemistry)

For the hydrometallurgy and technology of the production of pure compounds of molybdenum and tungsten it is of considerable interest to study the kinetics of the dissolution of MoO_3 and WO_3 in alkaline solutions. The kinetics of the dissolution of molybdenum calcine, the main component of which is molybdic anhydride, in ammonia solution were studied in [1]; the kinetics of the dissolution of tungstic anhydride mostly in alkaline solutions were studied in [2,3]. The purpose of the present work was to study the kinetics of the dissolution of pure molybdenum and tungsten trioxides in ammonia solutions. The dissolution kinetics were investigated experimentally by the rotating disc method. The apparatus and the experimental details were similar to those used in [2,3]. Samples as nonporous as possible are required for investigation of the kinetics of dissolution by the method of an equally accessible surface.

Compact samples of WO_3 were prepared by compression of the powder followed by sintering, the optimum conditions for which were determined by special tests. The initial WO_3 powder (of chemical purity for luminophors) was compressed at a pressure of 4.8 ton/cm² with 5% of a binder and roasted in tablets at 1000°C for 3 h. These tablets were thoroughly ground by a dry method, compressed at 4.8 ton/cm² with 3.0-3.2% of binder (an 8% solution of polyvinyl alcohol in water), and sintered at 1200°C for 3.5 h. The open (2.5%) and total (5%) porosity were determined by measuring the absorption of water and by hydrostatic weighing[4].

An attempt to obtain compact samples of MoO_3 by compression followed by sintering did not give satisfactory results. Contractions were not observed during sintering of the compact. During sintering of molybdenum trioxide migration of the substance through the gas phase is evidently realised on account of its high volatility. It is known[5] that contraction does not occur during sintering in such cases. The initial samples were prepared by cutting up polycrystalline bars of MoO_3 (analytical grade), obtained in quartz tubes at normal air pressure by directional crystallisation. The temperature in the zone was 930-960°C, and the rate of movement owas 0.28 mm/min. At crystallisation temperatures above that which we used the obtained samples were dark, which indicates partial decomposition of the MoO_3, and at low temperatures the porosity increased. The open porosity of the sample amounted to 2.5-3%, and the total porosity was 5-6%. The reaction surface was the surface of the melt which had been machined on a lathe and polished.

During the experiment four samples were taken the molybdenum was determined by photometry with pyrocatechol, and the tungsten was determined by the thiocyanate method. The kinetic curves had strictly linear character, and the dissolution rate was determined by graphical differentiation.

Effect of the ammonia concentration. The effect of the concentration of ammonia on the dissolution rate was investigated in the region of 0.01-14.2 M for MoO_3 and $1.7 \cdot 10^{-4}$ 3.2 M for WO_3 (fig.1). It is seen that with an ammonium concentration up to approximately 0.01 M (WO_3) and 0.02 M (MoO_3) the reaction is of first order in ammonia, but with increase in the concentration the observed order in both cases becomes zero. The rate constants for the dissolution of molybdenum trioxide are $1.04 \cdot 10^{-6}$ (25°C) and $4.46 \cdot 10^{-7}$ l/cm² · sec (10°C) in the region of first order (k) and $2.67 \cdot 10^{-7}$ (25°C) and $1.17 \cdot 10^{-7}$ g-ion/cm² · sec (10°C) in the region of zero order (k'). For tungsten trioxide at 25°C the rate constant is $1.58 \cdot 10^{-8}$ in the region of first order and $3.10 \cdot 10^{-10}$ in the region of zero order. The errors in the determination of the dissolution rate constants from four isoparametric experiments (at 25°C, 3 rps, ammonia concentrations 0.1 M for MoO_3 and 0.01 M for WO_3) were 9 and 12% respectively with reliability 0.95. We note that dissolution in water can in this case be neglected, since the rate of dissolution of MoO_3 in water at 25°C is $5.6 \cdot 10^{-10}$ and that of WO_3 is 1.10^{-12} g-ion/cm² · sec; the error in the determination of these rates amounts to about 20%.

Effect of temperature. The effect of temperature in the range of 10-65°C on the dissolution rate of MoO_3 was investigated with ammonia concentrations of 0.016 M (the region of first order) and 10 M (the region of zero order) with disc rotation rates between 1.2 and 7.4 rps (fig.2). At

low temperatures the rate constant is practically independent of the intensity of agitation with n>1.2 rps (the common part of the curve) and can be calculated by means of the equation

$$\lg k = 0.47 - \frac{1920}{T}$$

and the experimental activation energy for these conditions (0.016 M) is 8.8 kcal/mole. With increase in temperature the activation energy (for n = 1.2, 3.0, and 7.4 rps) decreases to approximately the same value of 4 kcal/mole. It can be supposed that the regime changes substantially with temperature.

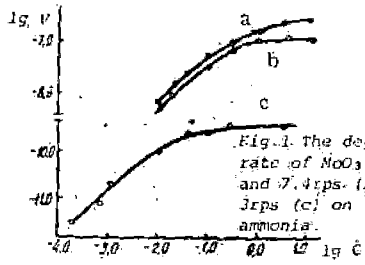

Fig. 1. The dependence of the dissolution rate of MoO_3 at 25°C and 3 rps (a), 10°C and 7.4 rps (b), and of WO_3 at 25°C and 3 rps (c) on the molar concentration of ammonia.

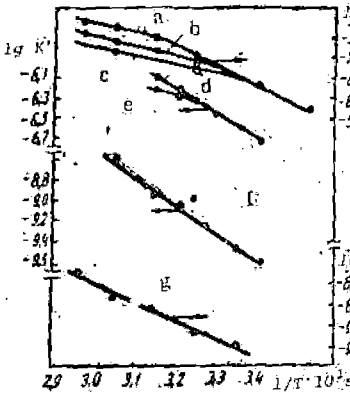

Fig. 2. Dependence of the logarithms of the rate and rate constants of dissolution on the reciprocal temperature for MoO_3 (in): 0.016 (a, b, c); 10 (d, e); for WO_3 (K): 0.3 (f); for MoO_3 in H_2O (g); and on the disc rotation rate (rps): 7.4 (a, d); 3 (b, f, g); 1.2 (c, e).

With a high concentration of ammonia (10 M) in the region of low temperatures the rate constant is also independent of the intensity of agitation for n>1.2 rps (the common part of the curve) and can be calculated by means of the equation

$$\lg k' = 1.41 - \frac{2370}{T}$$

and the experimental activation energy is 10.8 kcal/mole. With increase in temperature, as at the lower concentration, the constant begins to depend on the intensity of agitation, and the activation energy decreases. (It is difficult to study the process at higher temperatures on account of the decrease in the solubility of ammonia).

Somer difference in the values of the activation energy at low and high concentrations of ammonia (8.8 and 10.8 kcal/mole) can be explained by the fact that at low concentrations under the above-mentioned conditions there is an intermediate regime approaching a kinetic regime. Under purely kinetic conditions the process is characterised by an activation energy of 10.8 kcal/mole.

For the WO_3 dissolution process in the range of temperatures 20-55°C (0.3 M, 3 rps) the dependence of the rate constant on temperature is described by the equation

$$\lg k' = -0.64 - \frac{2630}{T}$$

and the experimental activation energy is 12 kcal/mole. For the dissolution of MoO_3 in water the dependence of the dissolution rate (g-ion/cm²·sec) on temperature for 3 rps is determined by the equation

$$\lg v = -3.46 - \frac{1720}{T}$$

Effect of the disc rotation rate. The effect of the disc rotation rate in the range of 0.42-28 rps on the dissolution of MoO_3 was investigated at concentrations of 0.016 and 10 M and at temperatures between 25 and 55°C (fig. 3). At both ammonia concentrations the dependence of the dissolution rate on the disc rotation rate becomes appreciably stronger with increase in temperature. At 55°C (0.016 M) the dissolution rate depends on the rotation rate raised to a power of 0.30, and at 35°C to a power of 0.17. Under identical conditions in the case of the high concentration the dissolution rate depends on the rotation rate to a lesser degree.

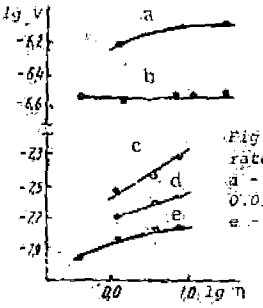

Fig. 3. Dependence of the dissolution rate of MoO_3 on the disc rotation rate: a - 10 M, 45°C; b - 10 M, 25°C; c - 0.016 M, 55°C; d - 0.016 M, 35°C; e - 0.016 M, 25°C.

During dissolution of WO_3 in ammonia the rate does not depend on the intensity of agitation (n>1.2 rps, 0.3 M, 25°C). The rate of dissolution of MoO_3 in water at 25°C with n>1.2 rps also does not depend on the intensity of agitation. The dependence of the dissolution rate of WO_3 in water on the intensity of agitation was not investigated experimentally, but the absence of such a dependence is not subject to doubt on account of the very small dissolution rate, incomparable with the rates of diffusion in the solution.

The results obtained make it possible to reach conclusions about the regime of the dissolution processes. The dissolution of tungstic anhydride in water and ammonia solutions under the conditions investigated takes place under kinetic control. This is shown by the non-dependence of the dissolution rate in ammonia on the intensity of agitation and is confirmed by the high value of the activation energy (12.0 kcal/mole), and the low value of the dissolution rate in water ($1.10^{-1.8}$ g-ion/cm²·cm) makes it possible to reach a conclusion about kinetic control without further investigations. The dissolution of MoO_3 in water also takes place under kinetic control. (The dissolution rate does not depend on the intensity of agitation, and the activation energy is 7.4 kcal/mole and does not vary with temperature).

The regime of the dissolution of molybdic anhydride in ammonia solution varies depending on the conditions. At a temperature not higher than 25°C and with agitation at not less than 7.4 rps the process approximates to kinetic control over the whole range of concentrations, but at high concentrations there is pure kinetic control. At low concentrations of ammonia the process approximates to diffusion control with increase in temperature, and this is demonstrated by the considerable dependence of the dissolution rate on the disc rotation rate (the exponent at the rotation rate reaches a value of 0.30), and is confirmed by the low value (4.0 kcal/mole) of the activation energy at high temperature. A high concentration of ammonia promotes transition to kinetic control over the whole range of agitation intensities and temperatures.

The dependence of the dissolution rate of MoO_3 and WO_3 on the ammonia concentration in the kinetic region (fig. 1b, c) in accordance with the concepts of Langmuir kinetics makes it possible to suppose that the slowest stage at the surface of the solid phase in both cases is a reaction having first order in the surface concentration of the dissolved substance.

In [3] for the dissolution of WO_3 in a solution of sodium hydroxide it was shown that the constant ($1.75 \cdot 10^{-3}$) obtained in the first-order region (in NaOH) can to a first approxi-

mation be related to the concentration of hydroxide ions. On the supposition that the dissolution of WO_3 in a dilute solution of ammonia only takes place on account of hydroxide ions the dissolution rates were calculated for 25°C and ammonia concentrations of 1.10^{-4} - 1.10^{-2} M. The calculated rates were found to be an order of magnitude lower than the experimental values, from which it follows that dissolution takes place predominantly on account of ammonium hydroxide molecules. This conclusion also holds for the dissolution of MoO_3.

It can be imagined that during the dissolution of molybdenum and tungsten trioxides over the whole range of ammonia concentrations slow rate-controlling processes take place at the surface:

$$MO_3 + OH^- = HMO_4^-$$

$$MO_3 + NH_4OH = HMO_4^- + NH_4^+$$

and then rapid processes occur:

$$HMO_4^- + OH^- = MO_4^{2-} + H_2O$$

$$HMO_4^- + NH_4OH = MO_4^{2-} + NH_4^+ + H_2O$$

At each successive transformation the bonds between M (Mo or W) and the crystal lattice are broken, and the process at the surface is concluded by desorption of MO_4^{2-} ions into solution.

The data on the dissolution of MoO_3 and WO_3 obtained under kinetic control give reason to propose similar mechanisms for the dissolution of these compounds in ammoniacal solutions with the difference that molybdenum trioxide has greater reactivity. A similar mechanism was proposed earlier for the dissolution of WO_3 in sodium hydroxide solution [3]. We note also that the saturation concentrations in the dissolution of WO_3 in ammonia and sodium hydroxide solutions [3] coincide, while the concentration for the dissolution of MoO_3 in ammonia solution is an order of magnitude higher.

Conclusions

1. The dissolution of tungsten trioxide in water and alkaline solutions and of molybdenum trioxide in water takes place under kinetic control. The regime for the dissolution of molybdenum trioxide in ammonia solution under the investigated conditions varies from kinetic to diffusion control, and the departure from kinetic control is realised more easily at low concentrations of ammonia.

2. Mechanisms of the same type can be proposed for the dissolution processes of molybdenum and tungsten trioxides in ammonia and of tungsten trioxide in sodium hydroxide.

References

1) A N Zelikman et alia: In: Hydrometallurgical and chlorine processes in the technology of rare metals. Metallurgiya, Moscow, 1972, 15.
2) Yu M Potashnikov et alia: In: Chemistry and technology of molybdenum and tungsten. Nal'chik 1971, 1, 213.
3) V V Stetsik et alia: In: Chemistry and technology of molybdenum and tungsten. Nal'chik 1974, 2, 175.
4) D N Poluboyarinov and R Ya Popil'skii (editors): Practical course in the technology of ceramics and refractories. Stroiizdat, Moscow, 1972, 106.
5) Ya E Geguzin: Physics of sintering. Nauka, Moscow 1967, 90

UDC 669.296

Decomposition of limestone-zircon sinter by mineral acids

A I Ismailov, I F Poletaev and M A Kolenkova (Moscow Institute of Steel and Alloys - Department of Rare and Radio-active metals and powder Metallurgy)

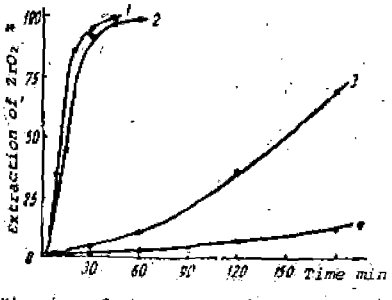

Fig.1 Kinetics of the decomposition of synthetic calcium zirconate (1,2) and the sinter (3,4) at 90°C in nitric acid %: 1 and 3 - 40; 2 and 4 - 30.

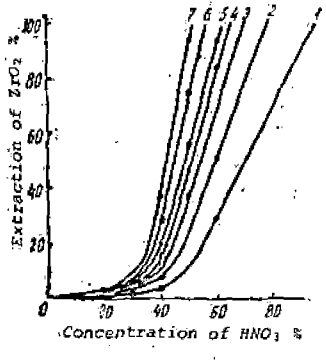

Fig.2 Kinetics of the decomposition of the zircon sinter with nitric acid at 90°C. Reaction time: 1 - 30; 2 - 45; 3 - 60; 4 - 70; 5 - 80; 6 - 100; 7 - 120 min.

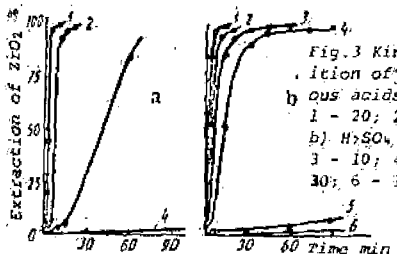

Fig.3 Kinetics of the decomposition of zircon sinter by various acids at 90°C: a) HCl %: 1 - 20; 2 - 15; 3 - 10; 4 - 5; b) H_2SO_4 %: 1 - 30; 2 - 20; 3 - 10; 4 - 5; $HClO_4$ %: 5 - 30; 6 - 10.

Summary

The sintering of zircon with calcium carbonate in the presence of calcium chloride gives complex zirconosilicates in addition to calcium zirconate and silicate. The behaviour of the zirconium during dissolution of the calcium zirconate on subsequent leaching is complicated by the presence of the calcium zirconosilicates and various impurities. The effect of the nature of the mineral acid on the decomposition of the sinter was investigated on material obtained by sintering zircon with calcium carbonate in a revolving furnace at 1100-1200°C and also on synthetic calcium zirconate.

The kinetics of the decomposition of the sinter and the calcium zirconate are illustrated in the figures. The decomposition rate of the zircon sinter is determined not only by the hydrogen ion concentration in the system and the temperature but also by the nature of the acid groups. The decomposition rate is highest in acids where the anion tends to form complexes with zirconium.

Kinetics of the dissolution of antimony in polysulphide solution

V S Shestitko, A S Titova and A I Levin (Krasnoyarsk Institute of Non-Ferrous Metals - Department of the Metallurgy of Light Metals and Alumina Production)

The behaviour of antimony in aqueous solutions of sodium polysulphide has been studied extremely inadequately. It is known only[1]) that Na_2S_2 possesses the highest corrosion activity (of all the components of the sulphide-alkali electrolyte) in relation to electrodeposited antimony. It seemed of interest to investigate the kinetics of the dissolution of antimony in an aqueous solution of Na_2S_2, since the occurrence of this process under industrial conditions may have an effect on the current efficiency.

The experiments were carried out on special apparatus with a rotating disc electrode. At the centre of an ebonite disc (14mm in diameter) an opening was drilled to a depth of 7mm with a diameter of 10mm under an antimony (Su000) disc, which was attached by BF-2 adhesive. The free end surface of the sample was taken as the surface area of the rotating disc. The samples were thoroughly cleaned and weighed on an AVD-200 analytical balance with an accuracy of $\pm$0.1mg.

The rotation rate was varied by means of pulleys. The supply voltage was stabilised; the disc rotation rate was determined by means of an ST-5 stroboscopic tachometer. The sodium sulphide was first recrystallised. Sodium polysulphide was obtained by dissolving the calculated amount of elemental sulphur of chemical purity in a solution of Na_2S with heat. The reaction vessel with a working capacity of 1 litre was thermostated.

The rate of dissolution from unit surface area was calculated from the difference in the weight of the sample dissolved before the experiment and after rotation in the solution for time τ. Having fixed a Reynolds number ($Re = \omega r^2/\nu$) equal to 10^4 for r = 0.7cm and a kinematic viscosity of 0.015St, we determined the maximum disc rotation rate. It was found to be equal to 2920rpm.

To determine the controlling stage of the investigated process we investigated the effect of the disc rotation on the dissolution rate of antimony. From the experimental data it was concluded that the reaction rate hardly depends on the disc rotation rate at all. The kinetic relationship has the form of a straight line (fig. 1) passing through the origin of the co-ordinates. The dissolution rate (the tangent of the gradient of the straight line) remains constant. The reproducibility of the dissolution rate for various reaction times is satisfactory; the points deviate little from the straight line. The non-dependence of the dissolution rate of antimony in Na_2S_2 on the time and the rotation rate of the disc is a characteristic feature of a process occurring under kinetic control.

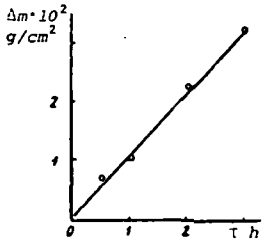

Fig.1 The effect of the reaction time on the specific change in the weight of the disc. n = 735rpm, $C_{Na_2S_2}$ = 100g/l, t = 25°C.

By investigating the effect of the sodium polysulphide concentration on the dissolution rate it was possible to determine the reaction order. The dependence of the dissolution

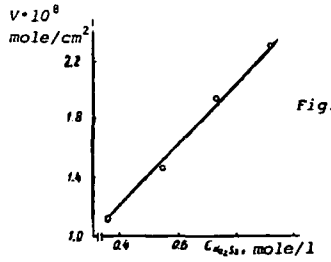

Fig.2 The effect of the sodium polysulphide concentration on the dissolution rate. n = 400rpm, t = 25°C, τ = 1 h.

rate on the Na_2S_2 concentration (fig. 2) is close to linear, i.e. the process takes place according to the laws of a second-order reaction. In this case the amount of dissolved metal can be calculated by means of the following equation[2]):

$$V = kc = \frac{\Delta m}{S\tau}$$

A check on the applicability of this equation to the case being investigated showed (table) that the rate constant remained constant for various concentrations. The constancy of the rate constant of a heterogeneous reaction with variation in the concentration of the main reagent is a characteristic feature of a first-order reaction[3]).

The effect of temperature on the rate of chemical reactions is one of the main problems in chemical kinetics. Temperature must be regarded as the most important factor for the intensification of chemical processes. In order to establish an analytical relationship between the reaction rate constant and temperature experiments were carried out with the following parameters: n = 700rpm; $C_{Na_2S_2}$ = 100g/l; t = 20-50°C. The modified Arrhenius equation is usually employed for determination of the controlling stage of the reaction. As follows from the experimental data (fig. 3), against the co-ordinates of this equation we obtained a straight line, the gradient of which to the abscissa axis made it possible to determine the effective activation energy:

$$E_{eff} = -2.3RT\,tg\alpha = 9.15\text{kcal/mole}$$

The value of E_{eff} provides additional evidence for the fact that the investigated process takes place under kinetic control. From the Arrhenius graph we obtained an equation for the relation between the logarithm of the rate constant and the temperature:

$$\lg K = -1.03 - \frac{2000}{T}$$

Intermediate products formed as a result of reaction between the ions of the reagent of the surface of the solid phase play an important part in heterogeneous reactions. As a rule, such intermediate products arise as the result of activated adsorption of the ions (e.g. S_2^{2-}) at the interface. Thermodynamic evaluation of the probability of direct occurrence of the reaction:

$$Sb + Sb_2^{2-} \rightarrow SbS_2^-$$

gives a ΔG value of -20.85kcal/mole. From this it follows that the dissolution reaction must take place relatively readily and irreversibly. Nevertheless, the experimental data indicate the presence of kinetic limitations.

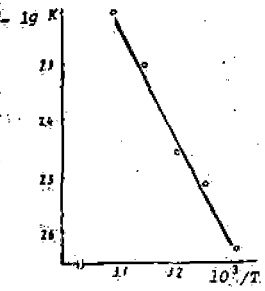

Fig. 3 The effect of temperature on the dissolution rate. $C_{Na_2S_2}$ = 100g/l, n = 700 rpm, τ = 1h.

Table: The dependence of the specific rate and of the rate constant of the reaction on the sodium polysulphide concentration

$C_{Na_2S_2}$ mole/litre	$V \cdot 10^6$ mole/cm² · sec	$K \cdot 10^7$ litre/cm² · sec
0.364	1.07	0.29
0.546	1.48	0.27
0.727	1.77	0.25
0.910	2.33	0.25

The following mechanism for the investigated process is proposed as a working hypothesis:

1. Activated adsorption with the formation of an activated complex:

$$Sb + nS_2^{2-} \rightarrow Sb\left[S_2^{2-}\right]^n_{ads} \rightarrow \left[Sb\begin{matrix}S\\|\\S\end{matrix}\right]_n$$

2. Decomposition of the activated complex with the formation of hydrated complex ions and the formation of a sulphide film on the surface of the antimony:

$$\left[Sb\begin{matrix}S\\|\\S\end{matrix}\right]_n + Sb_2S_{3\,solid\,ph.} + SbS_2^- \cdot mH_2O$$

It can be supposed that the formation of such a film has a significant effect on the rate of the dissolution reaction. We note that a passive oxide film is not formed on the surface of antimony in solutions with pH > 7.84[2].

3. The sulphide ions formed as a result of disproportionation:

$$[-S-S-] \rightleftarrows S^{2-} + S$$

give rise (with increase in their concentration) to accelerated dissolution of the film:

$$Sb_2S_3 + S^{2-} \rightarrow 2SbS_2^-$$

4. In solutions of sodium polysulphide the most characteristic valency of antimony is +5:

$$SbS_2^- + S_2^{2-} \rightarrow SbS_4^{3-}$$

This reaction always takes place in sulphide-alkali electrolyts.

Conclusions

1. The kinetics of the dissolution of antimony in sodium polysulphide solution were investigated.
2. It was established that the process takes place with kinetic control according to the relationships characteristic of first-order reactions.
3. The effective activation energy was determined.
4. An opinion is expressed about the mechanism of the process.

References

1) N V Ishchenko et alia: Zashchita Metallov 1967, (4), 502.
2) I A Kakovskii and Yu M Potashnikov: Kinetics of dissolution processes: Metallurgiya, Moscow 1975, p. 24.
3) N M Knorre and D G Emanuel': Course of chemical kinetics: Vysshaya Shkola, Moscow 1969.
4) Z A Solov'eva and L N Solodkova: Advances of Science and Technology: Electrochemistry: Vol. 8, 1972, p. 222.

time, the activation energy for the 'relay' mechanism must be higher than that for the normal mechanism. Since the proportion of reaction (2) increases with increase in temperature[2]), the role of the 'relay' mechanism of diffusion increases and the activation energy increases.

Table 2: The dependence of the diffusion coefficient on the concentration of alumina. Cryolite ratio 3.2; t = 1060°C

Al_2O_3 wt. %	$C_c \cdot 10^4$ g-eq cm^3	$(i\tau^{1/2})$ A·cm^{-2} sec$^{1/2}$	$D \cdot 10^4$ cm^2/sec
1	2.927	0.867	11.95
2	2.906	0.847	11.64
4	2.850	0.831	11.75
6	2.713	0.790	11.50
8	2.661	0.716	10.000
9	2.620	0.576	6.68
11	2.581	0.348	2.51

The investigations of the effect of the alumina content of the melt on the diffusion coefficients are given in table 2. From the data in table 2 it follows that the diffusion coefficient varies little up to an alumina content of 6.0 wt. %. The diffusion coefficient then decreases significantly with increase in the alumina content. At the same time, increase in the alumina concentration in the melt with an unchanged cryolite ratio and unchanged temperature leads to a decrease in the concentration of Na^+ ions in the melt and, consequently, to a decrease in their activity. The decrease in the activity of sodium ions in the melt leads to a decrease in the proportion of reaction (2) and the proportion of the 'relay' mechanism of diffusion. At the same time, the viscosity of the melt increases with increase in the alumina content, and this leads to a decrease in the proportion of the translational mechanism of transfer of the reaction products.

The results from determination of the overall concentration of aluminium and sodium subions in the height of the melt are shown in fig. 2.

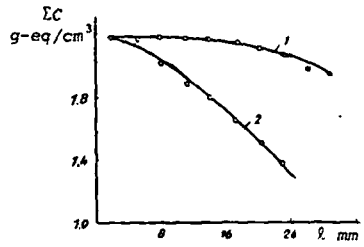

Fig.2 The dependence of the overall concentration of aluminium and sodium subions on the distance to the surface of the molten aluminium. Cryolite ratio 3.2; [Al2O3] = 5 wt.%; t = 1060°C, in an atmosphere of argon (1) and carbon dioxide (2).

The distance from the indicator electrode to the surface of the molten aluminium was varied between 2 and 23-28mm with the total height of the melt at 30mm. When the experiments were carried out in an atmosphere of argon, the variations in the concentration of the subions along the height were insignificant (fig. 2, curve 1) and were due to the preferential evaporation of aluminium and sodium subfluorides. In an atmosphere of carbon dioxide the concentration of the subions decreases sharply, and this is due to their oxidation by the carbon dioxide dissolved in the electrolyte.

The chronopotentiometric method can be used to study the distribution of the metal in the depth of the electrolyte in industrial electrolytic reduction cells. This is important for establishing the mechanism of the losses of the metal.

References

1) M M Vetyukov and B S Dyblin: Elektrokhimiya 1969, 5, 362.
2) M M Vetyukov and V B Vinokurov: Physical chemistry and electrochemistry of molten salts and slags: Nauk. Dumka, Kiev 1969, Part 1, 367.
3) E A Ukshe and N G Bukun: Uspekhi Khim. 1961, 30, 3, 243.

UDC 669.712.1:518.61

Kinetics of the desiliconising of aluminate solutions in continuously operating reactors

L P Ni, I G Grinman, B B Buribaev and L V Olenina (Institute of Metallurgy and Concentration - Academy of Sciences of the Kazkh SSR)

It is known that the reaction of silica with aluminate solutions is complex[1]). The desiliconising process is regarded as a combination of several elementary stages with the formation of intermediate products[2]), for the description of which a set of differential equations is employed. To describe a continuous technological scheme it is more convenient to express the kinetics in explicit form, which makes it possible with a sufficient degree of accuracy to establish the relation between the desired functions and the measured and controlled parameters, required for the formulation of an algorithm for automatic control.

Desiliconising of aluminate solutions occurs in series-connected reactors, in which reliable agitation is provided. As a result of agitation the aluminate solution has a uniform composition, and the reactor can be considered an ideal mixer. The average time for which the particles are present is often used in calculations for an ideal mixer. However, it is difficult to obtain a real picture of chemical transformations from the average residence time on account of the complexity of the processes occurring in continuously operating reactors. It is therefore necessary to consider the distribution function of the residence time in a continuous cascade of reactors.

For n series-connected reactors the distribution function of the residence time for identical volumes V_p and consumption rate P is described by the equation [3]):

$$\theta(t) = \frac{P^n}{n-1!V_p^n} t^{n-1} \exp\left(-\frac{P}{V_p} t\right) \quad (1)$$

With a known dependence of the concentration of a substance on time C(t) the concentration of the substance C_0 at the outlet from the reactor will be given by:

$$C_0 = \int_0^\infty \theta(t) C(t) dt \quad (2)$$

To determine the function C(t) we used a series of 14 pairs of parallel experiments, representing the periodic process of the digestion of bauxite in a closed system, in an isothermal gradient-free reactor. Here a portion of ground bauxite was flooded with a specific volume of the alkali-aluminate solution, the agitator was placed in a

thermostat at the specified temperature, it was heated for some time, and the mechanical stirrer was then switched on, realising intense agitation. The moment when the stirrer was started was taken as the beginning of the experiment. After specific intervals of time samples were taken. The pulp was filtered to separate the liquid phase from the solid. The liquid phase was analysed for sodium hydroaluminosilicate (SHAS), the concentration of which is an indicator of the occurrence of the process.

After analysis of the experimental results we proposed the following semi-empirical equation describing the concentration of silica at any moment of time:

$$C(t) = \frac{qK_1}{V(K_2 - K_1)}\left[\exp(-K_1 t^{1/2}) - \exp(-K_2 t^{1/2})\right] \qquad (3)$$

where: $K_1 = a(T - 65)(1 + 0.2\alpha_c)$;

$$K_2 = \frac{bq(T - 65)}{VC_a}$$

q is the amount of SiO_2 in the bauxites; V is the volume of the alkali-aluminate solution; T is temperature °C; α_c is the caustic ratio of the solution; C_a is the concentration of Al_2O_3 in the solution; t is time; a and b are constants.

Equation (3) satisfactorily describes all the laboratory experiments (196 measurements); the constants a and b were determined on a Mir-2 computer, and it was found that a = 0.003 and b = 0.08. These values can be used in the transition to continuous processes by means of the equation (2), since they were determined in the range of temperatures, caustic ratios and Al_2O_3 concentrations in the solution corresponding to the industrial desiliconising regime with T = 70-105°C, α_c = 2.4-4.4 and C_a = 90/195g/l. The index t in equation (3) makes it possible to see that the desiliconising reaction can be assigned approximately to second-order reactions.

Table: The results from treatment of the experiment on the determination of the SiO_2 concentration for the following parameters: q = 3.3g; V = 0.05 litre; C_a = 92.8g/l; T = 105°C; α_c = 2.4

t min	C_1 g/l	C_2 g/l	C_c g/l	D_e	D_c
5	1.2	1.2	1.659	0	0.459
10	1.25	1.0	1.944	0.25	0.819
15	1.85	1.15	2.061	0.7	0.561
30	1.75	2.10	2.107	-0.35	0.182
60	1.55	1.70	1.885	-0.15	0.260
120	1.15	1.30	1.399	-0.15	0.174
180	1.0	1.10	1.048	-0.10	-0.001

A typical experiment is given as an example in the table, which contains the results from parallel measurements of C_1 and C_2, the values of the SiO_2 concentration calculated by means of equation (3), C_c, and the differences in concentration between parallel measurements $D_e = C_1 - C_2$ and between C_c and the average value of the parallel data $D_c = C_c - (C_1 + C_2)/2$. The mean-square errors from D_e and D_c are respectively equal to $\delta_e = (1/7)\left(\sum_{i=1}^{7} D_{ei}^2\right)^{1/2}$ and $\delta_c = (1/7)\left(\sum_{i=1}^{7} D_{ci}^2\right)^{1/2}$; for the case given in the table $\delta_e = 0.122$ and $\delta_c = 0.164$.

To determine the accuracy the mean-square errors were also determined for all 14 experiments:

$$\delta_{tr} = \frac{\frac{1}{14}\sum_{i=1}^{14}\delta_{ei}}{\sqrt{2}} = \frac{0.154}{\sqrt{2}} = 0.11$$

The mean-square error of the theoretical curve according to equation (3) will be:

$$\delta = \sqrt{\delta_p^2 - \delta_{tr}^2} = 0.18$$

We will now determine the concentration at the outlet from successive reactors by means of equation (2) and the distribution function of the residence time.

In the case of a continuous technological scheme the concentration of silica in unit volume of the reactor C_{sv} is used in equation (3) instead of the ratio q/V:

$$C_0 = \int_0^\infty \frac{C_{sv}K_2}{K_2 - K_1}\left[\exp(-K_1 t^{1/2}) - \exp(-K_2 t^{1/2})\right] \frac{p^n t^{n-1}}{n-1!V_p^n}\exp\left(-\frac{Pt}{V_p}\right)dt \qquad (4)$$

The integral in equation (4) cannot be evaluated analytically and integration was therefore performed by a numerical method on a Mir-2 computer.

In the figure the numbers of the series-connected reactors are given on the abscissa axis, and the concentrations of silica C_0 at the outlets are given on the ordinate axis. For convenience the points corresponding to the concentrations at the outlet for identical conditions are connected by dotted lines. A diagram of the series-connected reactors is given at the top right corner of the figure.

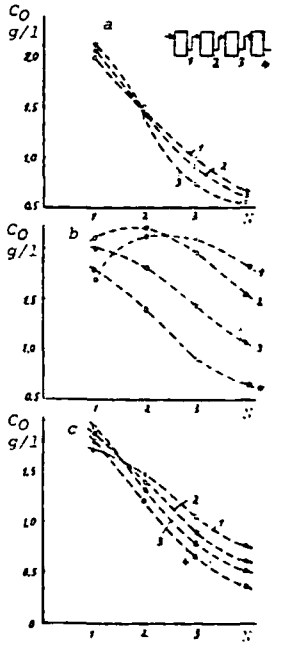

The variation of the concentration of silica at the outlets from series-connected reactors: a) for C_a = 100g/l, T = 105°C, C_{sv} = 16g/l and various α_c values: 1 - 2.5, 2 - 3.5, 3 - 4.5; b) for C_a = 90g/l, C_{sv} = 10g/l, α_c = 2.5 and various T °C: 1 - 75, 2 - 85, 3 - 95, 4 - 105; c) for C_a = 90g/l, T = 105°C, α_c = 4, and various concentrations of SiO_2 in unit volume of the reactor C_{sv} g/l: 1 - 6, 2 - 10, 3 - 14, 4 - 18.

The curves in fig. a correspond to various caustic ratios α_c, those in fig. b correspond to the temperatures T, and those in fig. c correspond to the concentrations of SiO_2 in unit volume of the reactor C_{sv}.

The SiO_2 concentration decreases with increase in α_c, and the higher the temperature the better the bauxite dissolves and the more effective the desiliconising process.

Conclusion

The described method of modelling by means of the dis-

tribution function of the residence time makes it possible to plan the desiliconising process and can be used for the automation of continuously operating technological schemes.

References

1) L P Ni and L G Romanov: Physical chemistry of hydroalkaline methods for the production of alumina: Alma-Ata, Nauka 1975, p. 103.
2) N F Pecherskaya et alia: Collection: Rational utilisation of aluminium, vanadium and phosphorus containing raw material: Alma-Ata, Nauka 1975, p. 91.
3) E M Vigdorchik and A B Sheinin: Mathematical modelling of continuous dissolution processes: Khimiya, Leningrad 1971, p. 22.

UDC 669.712:66.065.51

Formation and growth of aluminium hydroxide particles during mass crystallisation in a cascade of mixing units

R L Dubrovinskii and V V Zhukovetskii (North-Caucasian Mining-Metallurgical Institute - Department of Light, Noble, and Rare Metals)

Mass crystallisation from solutions is characteristic of many industrial separating processes. The questions of crystallisation theory are touched upon in numerous articles from the standpoints of thermodynamic[1]), molecular-kinetic[2]), and kinetic theory. However, the proposed methods of calculation are specific and in some cases start from indefinite ideas about the metastable zone[3]).

In the kinetic method examined below the following assumptions are made:

1. The quantity determining the formation rate of the particles ν' (particles/g·h) and the linear growth rate V (cm/h) is the given removal rate Π (g/l·h) or the rate of transfer of the crystallising substance from the solution into the solid phase under the given hydrodynamic conditions.
2. The formation and growth of the particles occur with any non-zero removal rate.
3. Particles which can be detected quantitatively by the normal methods of dispersion analysis (sedimentation and crystal-optical, i.e., greater than 1μ) are considered. For this reason the terms "nucleus" and "nucleation" are not used.
4. The form of the growing particles is spherical on account of the isotropicity of the concentration field around them; the mass transfer is intensive and levels out the difference in the growth rates of the crystal faces.

Initial data. A specific removal rate, to which the v_i and v_i' values correspond, is maintained in each of the cascade units having equal volume (decrease or increase in temperature, salting out, evaporation, dilution, neutralisation). The length of the process in the unit is τ; the mass of the released substance is m. In each unit the crystallised substance separates in two ways, i.e., on previously formed particles $m_{i,s}$ and in the form of new growth parparticles $m_{i,1}$ (the result from homogeneous and heterogeneous nucleations - as a consequence of point 2 above). If there is no seed in the first unit, the substance which crystallises in it separates with the formation of new particles ($m_{i,1}$). The number of particles formed in a given unit N' is determined by the length of the process τ_1 and by the formation rate of the particles v_i'.

$$N_i' = v_i' \cdot \tau_i$$

Each particle which forms grows during the time from the moment of its appearance to the moment of its release from the unit. Particles with various ages and, consequently, sizes are present in the unit. Since the number of particles and the frequency of their appearance in a given unit are determined by the removal rate Π maintained in it, a whole set of n_0 particles at the outlet from the unit corresponds to each first particle formed from the solution at the moment of its entry into the mixing unit. The particle of greatest size in the set has the diameter[4]):

$$\rho = 2V \cdot \tau \qquad (2)$$

The smallest size is determined by the procedural possibilities, and they are close to 1μ[5]). The distribution function of the masses of the particles according to size in the set may differ and for the general case is taken in the following form:

$$dm/d\rho = f(\rho) \qquad (3)$$

The mass of one set m_0 will be determined by the sum of the masses of all the particles entering it, i.e.,

$$m_0 = \int_1^{2V\tau} f(\rho)\,d\rho \qquad (4)$$

The number of sets formed in the unit is equal to

$$N = N'/n_0 = \nu_i' \cdot \tau / n_0 \qquad (5)$$

or

$$N = \nu \cdot \tau \qquad (6)$$

where $\nu = \nu'/n_0$ is the formation rate of the set of particles.

The mass of precipitate released in the first unit of the cascade (without a seed) is equal to

$$m_{1,1} = m_0 \cdot N_1 = \nu_1 \cdot \tau_1 \int_0^{2V_1\tau} f(\rho)\,d\rho \qquad (7)$$

For convenience of calculation the lower limit of integration (unity) is replaced by zero.

In the cascade units from 0 to i we have:

1. $m_1 = m_{1,1}$;
2. $m_2 = m_{2,s} + m_{2,1}$; $m_1 + m_2 = m_{1,1} + m_{2,s} + m_2$,
3. $m_3 = m_{3,s} + m_{3,1}$; $m_1 + m_2 + m_3 = m_{1,1} + m_{2,s} + m_{2,1} + m^{3,s} + m_{3,1}$;

i. $m_i = m_{i,s} + m_{i,1}$; $\sum m_i = m_{i,1} + \sum_1^2 m_{i,s} + \sum_1^2 m_{i,1}$.

The amount of substance separated on the solid phase in the second unit will be determined by the distribution function of the seed (the output of the first unit) and by the linear growth rate V_2, determined by the value of the removal rate Π_2

$$m_{2,s} = V_1 \cdot \tau \int_{2V_2\tau}^{2\tau(V_1+V_2)} f(\rho)d\rho - m_{1,1} \qquad (8)$$

In Eq.(8) the integration limits are determined by the minimum and maximum sizes of the particles in the set.

The amount of precipitate which separates on account of the formation of new particles at Π_2 will amount to:

$$m_{2,1} = \nu_2 \cdot \tau \int_0^{2V_2\tau} f(\rho)\,d\rho \qquad (9)$$

In all, the amount of solid phase which separates in the second unit [Eqs. (7), (8) and (9)] is:

current density. (This conclusion must not be extended in any way to the statistical-mean dimensions of the bubbles situated over the whole area of the bottom of the anode).

It can be supposed that the dimensions of the gaseous inclusions emerging from the edge of the horizontal and downward facing anode are determined by the conditions for coalescence of the bubbles and by their dynamic interaction with each other. At the present time the mechanism of these processes has not been investigated.

Conclusions

It was established that the frequency of the ejection of bubbles in electrolysis with horizontal electrodes is proportional to the current density. The range of bubble sizes becomes narrower with increase in the anodic current density.

2. It was shown that the dimensions of the gaseous inclusions emerging from the edge of the anode during electrolysis with horizontal electrodes do not depend on the current density.

References

1) V V Burnakin et alia: Izv VUZ Tsvetnaya Metallurgiya 1973, (3), 56.
2) A I Begunov et alia: Izv VUZ Tsvetnaya Metallurgiya 1973, (2), 28.
3) A I Begunov et alia: Izv VUZ Tsvetnaya Metallurgiya 1975, (2).

UDC 669.753.053.4

Kinetics of the dissolution of Sb_2S_3 and sodium antimonate in an aqueous solution of Na_2S

V S Shestitko, A S Titova, A M Sedova and A I Levin (Krasnoyarsk Institute of Non-ferrous Metals - Urals Polytechnical Institute

In industrial production practice the leaching of antimony ore material, represented mainly by Sb_2S_3[1]), and the intermediate product sodium antimonate[2,3]) is realised with solutions of sodium sulphide. Determination of the reaction mechanism and of the factors which accelerate the dissolution process helps to intensify the production process. We note that the dissolution rate of the pure thiosalt of Na_3SbO_4 in aqueous solutions of sodium sulphide has been investigated[4]), but there are no data on the kinetics of the dissolution of the intermediate product sodium antimonate. As far as Sb_2S_3 is concerned there is only one paper devoted to this problem[5]). By the rotating disc method it was established that the dissolution of Sb_2S_3 in Na_2S is controlled by diffusion.

During investigation of the solubility of Sb_2S_3 in Na_2S it was shown[6-8]) that it is determined by the concentration of Na_2S in the solution. However, we note that data on the equilibrium constants of the dissolution reactions are somewhat contradictory: 8.0[6]); 5.0[7]); $1.0 \cdot 10^{-3}$[8]). This is evidently due to differences in the stoichiometry of the reaction and in the views concerning the nature of the obtained complexes SbS_2^-[6]), $Sb_4S_7^{2-}$[7]), and SbS_3^{3-}[8]).

The dissolution of Sb_2S_3 in solutions of NaOH and KOH has also been investigated[9,10]). However, as was demonstrated earlier[6]), the solubility of antimony (III) sulphide in sodium hydroxide solutions is much lower than the solubility in sodium sulphide solutions. In addition, sodium hydroxide is not a primary industrial solvent.

The method of investigation corresponded to that described in the literature[11]). The antimony content of the solution was determined by a volumetric bromate method[12]). Recrystallised sodium sulphide and antimony sulphide of chemically pure grades were used to prepare the solutions. Before the experiment the sodium antimonate (49.5%Sb) was ground to a uniform fractional composition.

The solubility of Sb_2S_3 in water is extremely small, $2 \cdot 10^{-5}$% [13]). The solubility of the oxygen compounds Na_3SbO_3 and $NaSbO_3$ (in the form of which the antimony is present in sodium antimonate) in water is also small[14]). The process of their dissolution in Na_2S involves replacement of the oxygen in the SbO_3^{3-} and SbO_2^- ions by sulphur from the sodium sulphide to form water-soluble compounds according to the reactions:

$$Na_3SbO_3 + 3Na_2S + 3H_2O \rightarrow Na_3SbS_3 + 6NaOH$$

$$NaSbO_3 + 3Na_2S + 3H_2O \rightarrow NaSbS_3 + 6NaOH$$

The passage of antimony into solution from Sb_2S_3 is determined by a chemical reaction with the S^{2-} ions and is accompanied by the formation of complexes:

$$Sb_2S_3 + mS^{2-} \rightleftarrows 2SbS_{(3+m)/2}^{3-} \qquad (1)$$

It is clear that both the reaction rate and the magnitude of the equilibrium concentration of antimony in the solution must be determined largely by the initial concentration of sodium sulphide.

As follows from the kinetic curves (fig.1), the antimony content of the solution is determined unambiguously by the initial concentration and by the time. The equilibrium concentration of antimony, attained after 10, 15, and 30 min respectively for Sb_2S_3 and sodium antimonate, does not change for 24 h and increased with increase in the Na_2S concentration (fig.2).

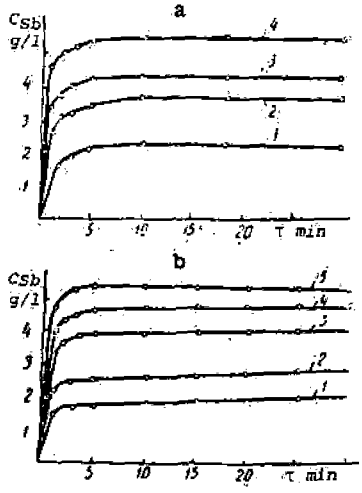

Fig.1 Kinetic curves for the dissolution of Sb_2S_3 (a) and sodium antimonate (b) in Na_2S at 25°C with Na_2S concentrations (g/l): 1 - 5, 2 - 10, 3 - 15, 4 - 20, 5 - 25.

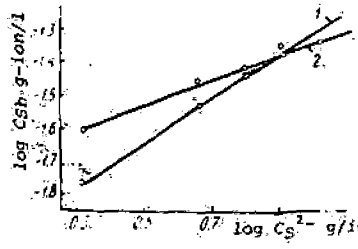

Fig.2 Dependence of the equilibrium concentration of antimony in the solution on the concentration of S^{2-} ions for Sb_2S_3 (1) and sodium antimonate (2) at 25°C.

It is known[18] that for the initial stage of the isothermal dissolution of a solid the dissolution rate can be expressed in terms of the equation:

$$V_{in} = K \frac{S}{V} C^{\alpha} \qquad (2)$$

where C is the initial concentration of the solvent, K is the rate constant, S is the magnitude of the reacting surface, V is the volume of the solution, and α is the reaction order. Taking logarithms of Eq.(2), we obtain the equation

$$\lg V_{in} = \lg K + \alpha \lg C$$

from which it follows that with a linear relation between log V_{in} and the logarithm of the concentration of S^{2-} ions it becomes possible to determine the order of the reaction:

$$\frac{d \lg V_{in}}{d \lg C_{S^{2-}}} = \operatorname{tg} \beta = \alpha$$

The initial rates of the dissolution process were determined by drawing tangents to the beginning of the kinetic curves. In accordance with the foregoing, the reaction rate increases in direct proportion to the Na_2S concentration. The relations between log V_{in} and log $C_{S^{2-}}$ fit satisfactorily onto straight lines (fig.3). The experimental orders of the reactions were found to be close to unity: $\alpha = 1.18$ (Sb_2S_3); $\alpha = 0.98$ (sodium antimonate). This fact[16] and also the strong effect of the hydrodynamic conditions on the process rate (fig.4) give reason to suppose that the dissolution process in both products is controlled by diffusion limitations.

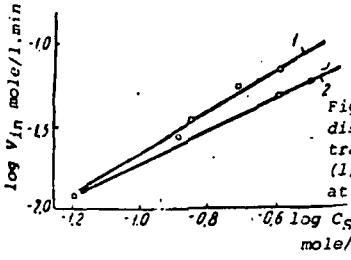

Fig.3 Dependence of the initial dissolution rate on the concentration of S^{2-} ions for Sb_2S_3 (1) and sodium antimonate (2) at 25°C.

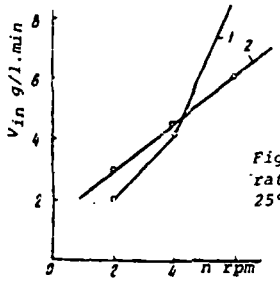

Fig.4 Dependence of the dissolution rate on the stirrer rotation rate at 25°C: 1 - Sb_2S_3; 2- sodium antimonate

On the basis of the possibility of the formation of mononuclear complexes during dissolution of Sb_2S_3 in Na_2S[9,17,19] by means of Eq.(1) we determine the coordination number of the complex which predominates under equilibrium conditions. We write the equilibrium constant of reaction (1) as follows

$$K = \frac{[SbS^{-}_{(3+m)/a}]^2}{[Sb_2S_3][S^{2-}]^m}$$

Since Sb_2S_3 is present in the form of the bottom phase, the concentration of Sb_2S_3 in the solution is constant. Assuming that practically all the antimony present in the solution is combined into a complex[20], we can consider that $SbS^{-}_{(3+m)/a}$ is equal to the concentration of antimony C_{Sb}. Then,

$$C_{Sb} = \text{const}\,[S^{2-}]^{m/a}$$

The equilibrium concentration of antimony in the solution is proportional to the concentration of S^{2-} ions raised to the power of m/2. If a graph is plotted against the coordinates of the equation

$$\lg C_{Sb} = \lg \text{const} + \frac{m}{2} \lg C_{S^{2-}}$$

the desired value of tan β can be obtained from the gradient of the straight line (fig.2).

$$\frac{d \lg C_{Sb}}{d \lg C_{S^{2-}}} = \operatorname{tg} \beta = \frac{m}{2}$$

The tan β value was found to be 0.7, and m = 1.4. In such a case it can be supposed that a complex ion with a coordination of 2 (SbS_2^-) predominates in the solution.

The effect of temperature on the solubilities of the two products shows up to a lesser degree than the effect of the Na_2S concentration. Thus, with increase of 10° in the temperature (for Sb_2S_3) the equilibrium concentration of antimony increases by only 0.4 g/l. The effective activation energy was determined from the graphical relationship against the coordinates of the Arrhenius equation (fig.5). It amounted to 4 kcal/mole (for Sb_2S_3) and 3.3 kcal/mole (for sodium antimonate). The temperature coefficient of the reaction rate for Sb_2S_3 and sodium antimonate amounted to 1.15 and 1.32 respectively. The presented values confirm conclusively that the dissolution of both products in Na_2S takes place in the diffusion region.

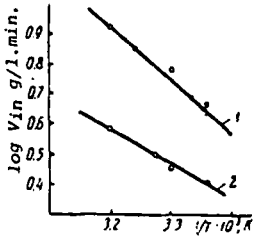

Fig.5 Temperature dependence of the dissolution rate against the co-ordinates of the Arrhenius equation: 1 - Sb_2S_3; 2 - sodium antimonate.

Conclusion

The kinetics of the dissolution of the intermediate product (sodium antimonate) and of Sb_2S_3 in aqueous solutions of Na_2S were investigated. It was established that the process takes place in the diffusion region. The order of the reaction, the temperature coefficient of the reaction rate, and the effective activation energy were determined.

References

1) A G Shiyanov: Production of antimony. Metallurgizdat, Moscow 1961.
2) N V Ishchenko et alia: Izv. Vuz Tsvetnaya Metallurgiya 1968, (2), 82.
3) I R Polyvyannyi and N I Anan'ev: Akad. Nauk KazSSR 1963, 6, 138.
4) A L Tseft et alia: Vestn. Akad. Nauk KazSSR 1965, (11), 55.
5) R A Sarkisyan et alia: Uch. Sap. Erevansk. Gos. Univ. 1969, (3), 67.
6) A K Babko and G S Lisetskaya: Zh. Neorgan. Khim. 1965, (5), 969.
7) R H Arntson et alia: Science 1966, 153, 1673.
8) N A Milyutina et alia: Tr. Inst. Metallurgii i Obogashcheniya Akad. Nauk KazSSR 1967, 21, 14.
9) R A Sarkisyan and M L Episkoposyan: Uch. Zap. Erevansk. Gos. Univ., 1970, (3), 78.
10) S K Afanas'ev and V F Smachnaya: Zap. LGI 1970, 50, (3), 38.
11) V S Shestitko et alia: Izv. Vuz Tsvetnaya Metallurgiya 1974, (5), 70.
12) E V Alekseevskii et alia: Quantitative analysis. Goskhimizdat 1955, p.372.
13) A N Kirgintsev et alia: Solubility of inorganic materials. Khimiya, Moscow 1972.
14) V S Lovchikov: Alkaline refining of lead. Metallurgiya Moscow 1964.
15) V V Dolivo-Dobrovol'skii: Zap. Leningr. Gorn. Inst. 1963, 42, (3), 3.
16) R T Marchenko: Physical and colloid chemistry, Vysshaya Shkola, Moscow 1965.
17) G L Shlefer: Complex formation in solutions. Khimiya Moscow-Leningrd 1964, p.37.
18) N Kanopik and R Fiala: Monatsh. Chem. 1950, 81, 497,

504.
19) V S Shestitko and O P Demina: Zh. Neorgan. Khim., 1971, (11), 3167.
20) V S Tvetsin: Theory and practice in the electro-deposition of antimony during the treatment of sulphide ores. Izhevsk, Udmurskoe KN. Izd., 1960, p.5.

UDC 669.721:66.096.5

Dehydration of magnesium chloride dihydrate in a mixture with potassium and sodium chlorides in a fluidized bed

A I Orekhova, E I Savinkova and R P Lelekova (Urals Polytechnical Institute - Department of the Technology of Inorganic Materials).

Summary

The possibility of the reaction of crystalline potassium and sodium chlorides with magnesium chloride dihydrate in a fluidized bed to form carnallite and solid solutions of sodium chloride in carnallite and magnesium chloride was demonstrated.

During the dehydration of magnesium chloride dihydrate in the mixture with spent electrolyte carnallite and solid solutions of sodium chloride in carnallite and magnesium chloride are formed simultaneously. The degree of dehydration and hydrolysis of synthetic carnallite is approximately identical with the degree of dehydration and hydrolysis of artificial carnallite obtained by recrystallisation of natural carnallite.

UDC 661.424.05

Rate of reaction of steam with hydrolyzed molten carnallite

E I Savinkova, R P Lelekova, V A Rudakov and L G Sarapul'tseva (Urals Polytechnical Institute and Kalush Chemical-Metallurgical Combine).

Summary

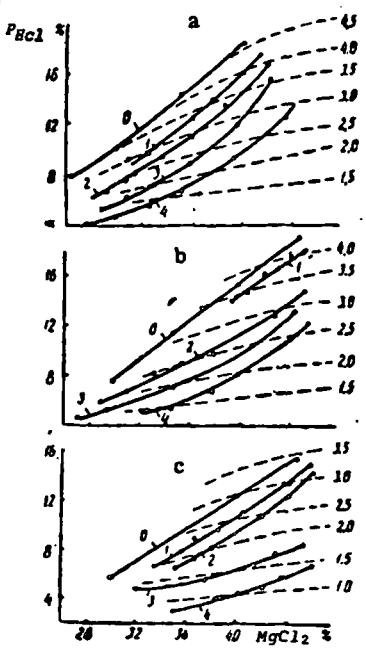

Dependence of the partial pressure of HCl in the gas phase on the concentration of $MgCl_2$ in the melt at temperatures °C a) 540; b) 500; c) 460. Steam flow rates -/min: 0 - equilibrium; 1 - 1.69- 2 - 3.44, 3 - 5.40, 4 - 7.75. The dotted line represents the degree of hydrolysis of $MgCl_2$ %.

Table

Steam flow rate l/min	$p^{eq}_{H_2O}$ %	$p^{curr}_{H_2O}$ %	Difference $p^{curr}_{H_2O} - p^{eq}_{H_2O}$	Amount of HCL formed g/min
1.69	84.6	85.5	0.9	0.500
3.44	84.6	89.0	4.4	0.580
5.40	84.6	89.6	5.0	0.855
7.75	84.6	91.2	6.6	1.110

The aim of the work was to study the effect of the rate of passage of steam through molten carnallite on the degree of its hydrolysis at temperature close to the melting point of carnallite. The results were used to plot the dependence of the partial pressures of hydrogen chloride in the gas phase on the magnesium chloride content of the melt and on the rate of passage of the steam at 460, 500, and 540°C. The figure shows the variation in the degree of hydrolysis of magnesium chloride in the melt, calculated according to the equation for the hydrolysis reaction.

By reducing the difference between the current and equilibrium values for the partial pressure of H_2O, e.g., by the introduction of hydrogen chloride into the gas phase, it is possible to reduce the hydrolysis of magnesium chloride during the dehydration of carnallite.

UDC 669.2

Investigation of conditions for extraction of germanium from sublimates by simplex design of experiments

E Bekyarova, V Angelova and St Stoynov (Peoples Republic of Bulgaria)

The fine dusts obtained during the combustion of germanium-containing coals are rich in germanium and are used for its extraction. It has been established that the germanium passing into the gas phase is distribution in the form of GeO, GeO_2, germanates, silicogermanates and solid solutions of GeO_2 in SiO_2 in various ratios, depending on the combustion conditions and on the composition of the fuel[1]). The sublimates containing relatively high concentrations of germanium are treated with HCl, with a mixture of HCl and H_3PO_4, and with H_2SO_4 or are decomposed with a solution of alkali in autoclaves[1-3]). When poorly soluble germanium compounds are present, pyrometallurgical methods are employed.

UDC 669.536.22

Kinetics of the dissolution of zinc oxide in aqueous solutions of sulphuric acid

I A Kakovskii and B D Khalezov (Urals Polytechnical Institute. Department of the Metallurgy of Noble Metals)

Since this reaction is of great interest for practical purposes, it has been studied by a series of authors[1-3]. In [3] the rotating disc method was used and it was concluded that the reaction takes place under diffusion control. In[4], however, the authors came to the conclusion that it takes place according to mixed kinetics. Let us consider the problem of the methods of establishing the reaction regime in greater detail. The following criteria have been proposed[5] for this purpose: a) The dependence of the dissolution rate on the intensity of agitation of the solution (the number of revolutions of the disc); b) the numerical value of the activation energy of the reaction; c) the presence of characteristic etch figures on the surface of the disc; d) comparison of the experimental dissolution reaction rate constant with the theoretical value. It should be noted that not all the criteria give an unambiguous solution to the problem during the investigation of reactions in which films of intermediate products are formed on the surface of the disc. Cases are known where the experimental activation energies of reactions taking place under diffusion and kinetic control are practically identical[6] (p.111, 196); the reason for the appearance of etch figures on an equally accessible surface is not quite clear[6] (p.48); during the formation of films on the reaction surface (additional diffusion resistance) the experimental reaction rate constant is often less than the theoretical value. There consequently remains one most reliable criterion for the character of the process, i.e., the dependence of the individual reduced reaction rate ($\nu' = Q/S\tau C$) on the intensity of agitation of the solution (according to theory, on the number of revolutions of the disc raised to the power of 1/2), i.e., the construction of graphs for the function $\nu' = f(n^{1/2})$. Here the following functional relationships are possible (fig.1, curves a-f). The relationship characteristic

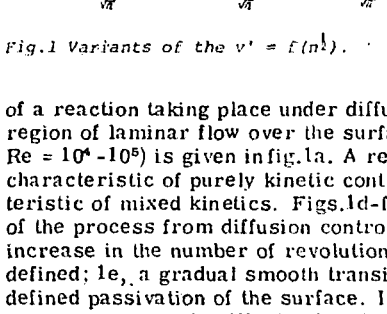

Fig.1 Variants of the $\nu' = f(n^{1/2})$.

of a reaction taking place under diffusion control in the whole region of laminar flow over the surface of the disc (up to $Re = 10^4 - 10^5$) is given in fig.1a. A relationship of type 1b is characteristic of purely kinetic control, and type 1c is characteristic of mixed kinetics. Figs.1d-f correspond to transitions of the process from diffusion control to kinetic control with increase in the number of revolutions of the disc: 1d, clearly defined; 1e, a gradual smooth transition; 1f with strongly defined passivation of the surface. In the literature there are very many examples illustrating these relationships. We will only give some of the most characteristic relationships: 1b, dissolution of mercury in cyanide solutions[7]; 1c, reduction of chlorine[8]; 1d, ionisation of hydrogen[9]; 1f, dissolution of gold in cyanide solutions with oxygen blown through them [5] (p.45). The relationship of type 1a (a purely diffusion process) can be illustrated by numerous examples[6] and in papers by a series of other authors.

We now turn to the reaction we investigated. (The experimental conditions were set out in detail elsewhere[10]), and some of the data have been supplemented and recalculated). Fig.2 shows the dependence of the specific dissolution rate of discs of zinc oxide on the square root of the number of revolutions of the disc per second at 25°C. As follows from these data, the required relationship is observed for both sulphuric acid concentrations, i.e., according to theory the process takes place under diffusion control. For a weakly

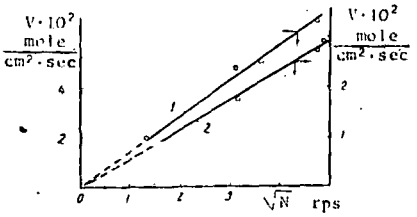

Fig.2 Dependence of the dissolution rate of zinc oxide on the square root of the number of revolutions of the disc per second. Curves 1-5, g/l H_2SO_4; curve 2, 100 g/l H_2SO_4.

acidic solution (5 g/l) this is additionally confirmed by the agreement of the experimental reaction rate constant (see below) and the theoretical value. Our opinion about the character of the process differs somewhat from the conclusions in[5]. The reason for this is the fact that in[3,4] the reaction rate was studied over a comparatively narrow range of sulphuric acid concentrations (from 14.5 to 41 g/l), while the dissolution of zinc oxide in acids is characterised by one feature which is of specific theoretical interst; the diffusion coefficients of the reagent-solvent and the reaction product (sulphuric acid and zinc sulphate) differ greatly. In infinitely dilute solutions at 25°C they are 2.65 and $0.78 \cdot 10^{-5}$ cm²/sec[10]). This is the reason for one of the complications in the process investigated.

Using the diffusion coefficient of sulphuric acid, we obtain the numerical value of the reaction rate constant (ref.[6]) (p.52):

$$k = \frac{6.18 \cdot 10^{-4} (2\pi)^{1/2} (2.65 \cdot 10^{-5})^{2/3}}{(0.893 \cdot 10^{-2})^{1/6}} = 3.0 \cdot 10^{-5} \left(1/cm^2 \cdot sec^{1/2} \cdot rev^{1/2}\right)$$

We studied the dissolution rate of zinc oxide discs over a wide range of sulphuric acid concentrations (from 0.5 to 805 g/l) at 25°C and 10 rps, and this made it possible to detect the complex character of the reaction (fig.3). From the data of

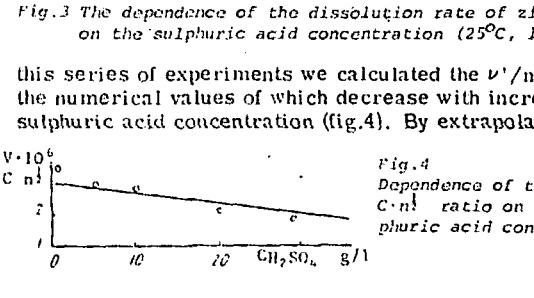

Fig.3 The dependence of the dissolution rate of zinc oxide on the sulphuric acid concentration (25°C, 10 rps).

this series of experiments we calculated the $\nu'/n^{1/2}$ ratios, the numerical values of which decrease with increase in the sulphuric acid concentration (fig.4). By extrapolation to C=0

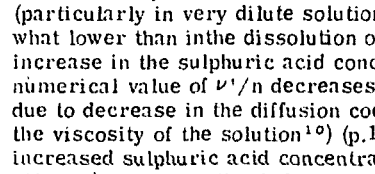

Fig.4 Dependence of the $\nu/C \cdot n^{1/2}$ ratio on the sulphuric acid concentration.

we obtain the reaction rate constant for its occurrence without complications, which is also approximately equal to $3.0 \cdot 10^{-5}$ in view of the fact that the reproducibility of the experimental data in experiments on the dissolution of zinc oxide discs (particularly in very dilute solutions of the acid) is somewhat lower than in the dissolution of metallic discs. With increase in the sulphuric acid concentration to 30 g/l the numerical value of ν'/n decreases, but this is not merely due to decrease in the diffusion coefficient and increase in the viscosity of the solution[10]) (p.186). In the region of increased sulphuric acid concentrations a second factor (the difference between the diffusion coefficient and the concentration gradients of sulphuric acid and zinc sulphate) begins to have an effect. This shows up particularly clearly in the region of sulphuric acid concentrations between 30-40 and

200 g/l, in which the dissolution rate is practically independent of the acid concentration (fig.3). Such a relationship is typical of processes controlled by diffusion of the reaction products (zinc sulphate in the present case). The diffusion character of this process is confirmed by the proportions relationship between the rate of passage of zinc into solution and the square root of the number of revolutions of the disc (fig.2, curve 2). Attention must be paid to one further complication: since more sulphuric acid approaches the surface of the disc than zinc sulphate passes into solution [10] (p.188), a film of zinc sulphate naturally forms on the surface of the disc, and this can be regarded as an additional diffusion resistance. In the steady state this film reaches a thickness where a dynamic equilibrium is established between the amount of zinc sulphate passing into solution and the amount of sulphuric acid interacting with the surface of the disc. As a result of this the flow of solution from the surface of the disc carries not only the zinc sulphate but also unreacted sulphuric acid. Here equality is established between the flows:

$$C_s \cdot D_1^{2/3} = (C_o - C_n) D_2^{2/3}$$

where C_s = the concentration of the saturated solution of zinc sulphate at the surface of the disc

C_o and C_n = the concentrations of sulphuric acid in the volume of the solution and at the surface of the disc

D_1 and D_2 = the diffusion coefficients of zinc sulphate and sulphuric acid in this solution.

With a knowledge of the rate of passage of zinc into solution and of the amount of sulphuric acid approaching the surface of the disc it is possible to calculate the degree of its utilisation in the reaction. (An example of such a calculation was given in the literature (ref. [10]) (p.188). The zinc sulphate films have an effect in the region of sulphuric acid concentrations up to 30 g/l, since the transition from control in sulphuric acid to control in zinc sulphate takes place gradually as the films on the reaction surface form and become thicker. These films gradually increase the zinc sulphate concentration gradient and reduce that for sulphuric acid, as a result of which the reaction rate decreases to the value at which it is determined only by the diffusion of zinc sulphate (in acid concentrations higher than 30 g/l). However, it is not possible to attribute all these complications to mixed kinetics. They do not change the character of the process occurring under diffusion control both in the region of sulphuric acid concentrations from 0 to 30 g/l and in the region from 30 to 200 g/l. The difference is only in its slow stage: in the first region of concentrations it is determined by the diffusion of sulphuric acid to the surface of the disc and in the second by the diffusion of zinc sulphate from the surface of the disc into the volume of the solution.

The decrease in the dissolution rate in the region of more concentrated solutions (above 200 g/l sulphuric acid) is explained by the large decrease in the solubility of zinc sulphate in the solutions (ref. [13]) (p.150) and, consequently, by the decrease in the zinc sulphate concentration gradient. In this connection it is interesting to discuss the numerical values of the activation energies which we obtained (3.0 for 5 g/l sulphuric acid and 7.7 kcal/mole for 100 g/l). Whereas the first glance not quite typical of a diffusion process. However, this is explained by the fact that with a sulphuric acid concentration of 100 g/l the slow link is the diffusion of zinc sulphate, the diffusion coefficient of which in these solutions is small and therefore, according to the Egolm coefficient (ref. [13]) (p.950), the temperature coefficient (1.45) and activation energy of diffusion (6.5 kcal/mole) are large. In addition, the solubility of zinc sulphate and, consequently, its concentration gradient increase with increase in temperature. Both these factors secure a sufficiently high activation energy for the overall process. If we calculate the diffusion coefficient of zinc sulphate from the reaction rate constant for this region of sulphuric acid concentrations ($5.8 \cdot 10^{-7}$ mole/cm^3·sec$^{1/2}$·rev$^{1/2}$) with allowance for the viscosity of the solution (ref. [5]) (p.201), we obtain a value of $0.24 \cdot 10^{-5}$ cm^2/sec, which agrees well with published data [11]).

The decrease of the dissolution rate in more concentrated solutions (above 200 g/l sulphuric acid) is explained by a large decrease in the solubility of zinc sulphate in these solutions (ref. [10]) (p.190) and, consequently, by a decrease in the zinc sulphate concentration gradient. For this region the kinetic equation has the following form:

$$\nu = \frac{Q}{S\tau} = k\,(C_s - C)\,n^{1/2}$$

but it is better to use the logarithmic equation (ref. [5] (p.25):

$$\lg \frac{C_s}{C_s - C} = p\tau, \text{ where } p = \frac{kSn^{1/2}}{2.303V}$$

The dissolution rate of the zinc oxide disc at 25°C can be calculated from the following equations: a) in the region of sulphuric acid concentrations between 0 and 30 g/l, $\nu = (3.0 - 3.4C) \cdot 10^{-6} \cdot C \cdot n^{1/2}$ (with allowance for the decrease in the dissolution rate with increase in the sulphuric acid concentration); b) in the region between 30 and 200 g/l, $\nu = 0.58 \cdot 10^{-6} \cdot N^{1/2}$. In these equations the sulphuric acid concentration is expressed in moles/litre, and the rate is expressed in mole/cm^2·sec. For other temperatures the dissolution rate can be calculated by using the activation energies given in the article (ref. [5]) (p.77). In the region of sulphuric acid concentrations between 30 and 200 g/l, which is of most interest for the hydrometallurgy of zinc, the dissolution rate of zinc oxide is practically independent of the acidity of the initial solution, and it is consequently possible to intensify the process mainly through intensive agitation of the pulp and to some degree through increase in temperature (in contrast to more dilute solutions). In conclusion it should be noted that it has been possible to investigate the unique character of the reaction between zinc oxide and aqueous solutions of sulphuric acid by investigating it on a fully accessible surface and by using the proposed criterion of $\nu' = f(n^{1/2})$ for the process conditions.

Conclusions

1. By use of the relationship $\nu' = f(n^{1/2})$ as a criterion of the process condition it was possible to establish that the reaction between zinc oxide and sulphuric acid solutions takes place according to the laws of diffusion kinetics at all the acid concentrations.

2. Investigation of the reaction rate over a wide range of sulphuric acid concentrations showed that the character of the slow link in the process depends on the concentration of the solvent (sulphuric acid); in the region of more dilute solutions it is diffusion of the acid to the reaction surface, and in the region of more concentrated solutions it is diffusion of the reaction products (zinc sulphate) from the surface into the volume of the solution. The unique character of the process is due to the sharply differing diffusion rates of these two compounds.

References

1) A N Krestovnikov et alia: Zh. Fiz. Khim., 1936, 8, (1), p.77.
2) E M Sergievskaya et alia: Sb. Tr. Moskovskogo In-ta. Tsvetnykh Metallov i Zolota 1957, (26), 265.
3) I A Vishnyakov et alia: Izv. Vuz. Tsvetnaya Metallurgiya 1972, (3), 56; (4), 22.
4) A D Fogorelyi et alia: Izv. Vuz. Tsvetnaya Metallurgiya 1973, (5), 21.
5) I A Kakovskii et alia: Kinetics of dissolution processes. Metallurgiya 1975.
6) Yu V Pleskov et alia: The rotating disc electrode. Nauka, Moscow 1972.
7) I A Kakovskii et alia: Dokl. Akad. Nauk SSSR 1966, 169, (5).
8) A N Frumkin et alia: Dokl. Akad. Nauk SSSR 1958, 118, (3).
9) A N Frumkin et alia: Dokl. Akad. Nauk SSSR 1955, 100, (2).
10) B D Khalezov et alia: Sb. tr. Inta, Unipromed' (18), Sverdlovsk 1975.
11) J G Albright et alia: J. Solut. Chem., 1975, 4, (9), 809.
12) H S Taylor: Physical Chemistry. ONTI, Leningrad 1936, 2.

There has to be a discharge velocity at least equal to the settling velocity of the biggest particle and the coarsest particles in the vertical channel in order for them not to accumulate in the bottom of the tank.

An air lift is one way to achieve some additional suspension action in this vertical channel.

Kinetics of Dissolution of Zinc Sulfide in Aqueous Sulfuric Acid

L. T. ROMANKIW* and P. L. DE BRUYN†

Abstract

The rate of reaction of crystalline zinc sulfide with aqueous sulfuric acid was studied in the concentration range 0.25*N* to 17.5*N* and over a temperature range of 0.6°C to 65°C. The progress of the reaction was followed by a continuous recording of the pressure increase due to H_2S evolution. If care is taken to eliminate diffusion control of the reaction, the overall dissolution rate in the concentration range 1*N* to 10*N* H_2SO_4 may be expressed by the relation

$$\frac{d[Zn^{++}]}{dt} = A_0(k_F[H^+] - k_R[Zn^{++}]^{1/2} p_{H_2S}^{1/2})$$

An activation energy of 11.1 ± 1 Kcal is determined for the dissolution reaction and of 7.8 ± 1 Kcal for the reverse reaction. A qualitative picture of the reaction mechanism is presented based on rate studies and etching tests with single crystals. Studies with natural sphalerite containing iron substituted for zinc in the lattice show an increasing dissolution rate and the presence of elemental sulfur as a reaction product.

INTRODUCTION

During the last thirty years considerable attention has been given to the leaching of sulfide ores by aqueous sulfuric acid at elevated temperatures and oxygen pressures. In the published literature eight separate investigations of the dissolution of zinc sulfide by aqueous sulfuric acid have been reported.[1-8] With the exception of the study by Tronev and Bondin[2] zinc ores or concentrates constituted the solid phase in these investigations. In view of the chemical complexity of

* L. T. Romankiw, formerly graduate student at Massachusetts Institute of Technology, is presently associated with Thomas J. Watson Research Center, I.B.M., Yorktown Heights, New York.

† P. L. de Bruyn is Professor of Metallurgy, M.I.T., Cambridge, Massachusetts.

these systems and the emphasis placed on the engineering aspects of the leaching problem no attempts were made to unravel the kinetics of the dissolution process.

The main conclusion to be drawn from these studies is that in the treatment of ZnS with sulfuric acid at temperatures varying from 25°C to 200°C, the sulfide sulfur may be converted to H_2S gas, elemental sulfur, or sulfate. The oxidation state of the converted sulfur as well as the rate at which the reaction proceeds depends in a complex way on the oxidizing conditions, concentration of sulfuric acid, and chemical impurities such as Cd, Mn, and Fe in the solid zinc sulfide. These qualitative observations are also in agreement with similar studies on sulfuric acid leaching of other metallic sulfides.[9-14]

In the absence of oxidizing conditions the dissolution of ZnS by sulfuric acid may be represented by the stoichiometric reaction

$$ZnS(s) + H_2SO_4(aq) \rightleftharpoons ZnSO_4(aq) + H_2S(g) \quad (1)$$

The reaction products are Zn^{++} and H_2S. Since zinc exists in solution in only one oxidation state, its concentration can readily be determined. If the reaction is carried out in a closed system its progress may also be followed by recording the increase in total pressure due to evolution of H_2S. Furthermore, since it is known that concentrated H_2SO_4 (36.5*N*) will oxidize H_2S[15] according to the reaction

$$H_2SO_4 + H_2S(g) \rightleftharpoons H_2SO_3 + H_2O + S \quad (2)$$

the oxidizing nature of strong aqueous solutions of sulfuric acid should not be overlooked. This paper deals with a kinetic study of the dissolution reaction (1) and reports on the effect of the degree of agitation, sulfuric acid concentration, temperature, surface area, impurities (iron and manganese), and mechanical deformation of ZnS on the dissolution rate.

MATERIALS

Zinc Sulfide

A coarsened zinc sulfide precipitate was used in the majority of the experiments. This pigment-grade material, designated as Cryptone ZS-800, was obtained through the courtesy of the New Jersey Zinc Company. It is prepared by precipitation from a slightly basic zinc sulfate solution with hydrogen sulfide gas. The precipitate is then filtered, washed, dried and coarsened at 800°C in an inert atmosphere. A chemical analysis of the final product is given in Table I. X-ray

analyses of the powder showed it to be crystalline and to contain approximately 75% of the cubic variety (sphalerite) and 25% of the hexagonal variety (wurtzite). The presence of wurtzite may be explained by the coarsening treatment at 800°C since it is the stable form above 750°C. Both crystal modifications consist of a regular tetrahedral arrangement of zinc and sulfur atoms; differences in structure show up when the second nearest neighbors are considered. Based on seven independent BET Krypton adsorption measurements, the average specific surface of this material is 5.54 m^2/g. Electron micrographs of the powder indicate that the particle size lies in the range 0.1 to 0.3 micron with a root mean square diameter of 0.18 micron.

In addition to ZS-800, three different samples of natural sphalerite were used in the investigation of the role of chemical impurities on the dissolution rate. Chemical analyses of these materials are given in

TABLE I

Chemical Analyses of ZnS Samples Used in Rate Studies

Sample	Analysis (weight per cent)							
	Zn	S	Fe	Mn	Cd	Ca	Cl	Insol
ZS-800	66.45	32.3	0.006	<0.002	<0.0001	0.13		
Natural sphalerite (1)	63.83	31.28	0.38	<0.01	<0.005	—		2.28
(2)	64.71	32.24	0.78	<0.01	<0.005	—		1.31
(3)	52.07	32.84	9.69	1.82	<0.005	—		1.53
Single crystals	67.0	32.8	—	—	—	—	0.02	
Theoretical	67.2	32.8						

Table I. Fine powders of these mineral samples were prepared by grinding for 24 hours in methyl alcohol to prevent oxidation of the surface and caking during drying in an inert atmosphere.

Single crystals of artificially grown cubic zinc sulfide were kindly supplied by Dr. H. Samelson of General Telephone and Electronics Laboratories, Bayside, New York. These crystals were used in etching studies and a chemical analysis is included in Table I.

Reagents

Distilled, de-ionized water of average specific conductivity 6.5×10^{-7} mho/cm was used in all experiments. Sulfuric acid solutions of desired concentration were prepared by dilution of acculute standard

volumetric solutions. Prepurified nitrogen gas was used in deoxygenating solutions and purging of the reactors. All other chemical reagents were of analytical grade.

EXPERIMENTAL METHODS

Dissolution Rate Study

The reactor consisted of a 200 ml volumetric flask fitted with a rubber stopper through which a connection was made with surgical tygon tubing to a 2 mm glass manometer. Depending on the anticipated pressure either a water or mercury-under-water manometer was used. Four flasks were mounted on the arm of a Burrel Wrist-Action Shaker, the bulbs of these flasks were completely immersed in a constant temperature bath with the temperature controlled to within 0.1°C at 25°C and 0.3°C at 65°C by a Merc-to-Merc mercury control element. Agitation was accomplished by a rapid up-and-down motion. By turning a dial the speed of the motion could be adjusted to give a maximum agitation of about 300 cpm and an amplitude of about 2 cm.

Exactly 50 ml of aqueous sulfuric acid of desired concentration was added to two of the four flasks, the other two flasks serving as additional agitators for the constant temperature bath. This acid solution was then deaerated by passing prepurified nitrogen gas for at least one hour through it, then 3 grams of zinc sulfide was added to one of the two reactors. The second flask acted as a dummy and was connected to a water manometer which registered the pressure changes due to variation in barometric pressure. The reaction was allowed to proceed for 60 minutes to ensure attainment of equilibrium while pressure readings were taken at set time intervals. In most experiments no changes occurred after 10 to 20 minutes. At completion of the reaction the solids were filtered on a fine glass-frit and the solution was analyzed for zinc and sulfate.

Etching of Single Crystals of Sphalerite

In an attempt to understand the mechanism of the dissolution reaction, single crystals of sphalerite were etched under conditions similar to those used in the leaching tests. A single crystal was mounted in paraffin at the end of a glass rod which was then inserted in a glass

cell filled with the desired solution. Prior to mounting, the crystals were treated by different methods; some were used as grown from the vapor phase, others were polished, scratched or strained by heating in a nitrogen atmosphere at 450°C and quenched in liquid nitrogen. After several hours of etching, the crystals were washed with water to remove sulfuric acid and with petroleum ether to remove paraffin. The extent of the chemical attack was evaluated by microscopic observation.

Analytical Methods

The concentration of zinc in solution was determined by titration with sodium ethylene diamine tetra-acetate[16] and eriochrome black T as indicator. The pH of the solution was adjusted between 8–10 by addition of an ammonium chloride—ammonium hydroxide buffer. This analytical technique gave accurate and highly reproducible results for zinc in the concentration range 10^{-4} to 1 mole per liter. Iron, if present, did not interfere with the analysis.

An analysis for both ferrous and ferric iron was obtained by direct titration with ethylene diamine tetra-acetic acid at pH 2 in the presence of sodium salicilate, as indicator. The ferric iron was titrated at pH 2 in the presence of sodium salicilate, upon reaching the end point the ferrous iron was oxidized by addition of ammonium persulfate and the titration was continued. The presence of zinc did not interfere with the titration since zinc does not form complexes with ethylene diamine tetra-acetate until the pH is raised to about eight.

Two methods were used for sulfate analysis. The standard barium sulfate precipitation technique[17] was used and gave excellent results if care was taken to eliminate co-precipitation of zinc. In the second method, an ion exchange technique,[18] a dilute sample of the sulfate solution was passed through a column of a cation exchange resin in the hydrogen form. The metallic cations in solution were exchanged for hydrogen ions on the resin, the free sulfuric acid thus formed in solution was then titrated with sodium hydroxide.

The presence of elemental sulfur in the leach residue was detected by extraction with carbon disulfide.[17] The sulfur analysis was carried out in a Soxhlet Extractor and it was possible to detect as little as 3×10^{-4} gram of elemental sulfur in two to three grams of residue. Sulfur amounts in excess of a milligram could be determined with high accuracy and reproducibility.

EXPERIMENTAL RESULTS

A major part of this study is concerned with the evaluation of the variables, temperature and sulfuric acid concentration, on the rate of dissolution of zinc sulfide. Most experiments were done in duplicate, and a large number of tests were repeated many times. Since a continuous recording of H_2S pressure during the progress of the reaction could be readily obtained, pressure measurements were relied upon to

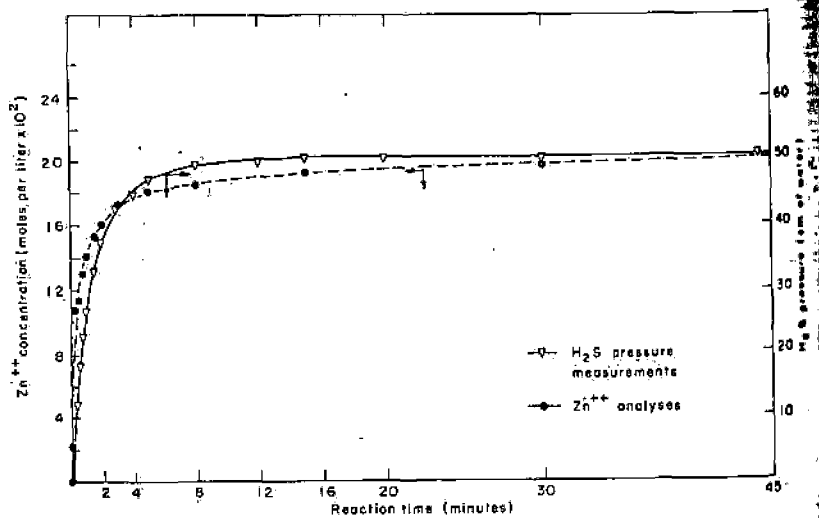

Fig. 1. Comparison of rate of dissolution of ZnS as measured by zinc analyses with rate of H_2S gas evolution in $1N$ H_2SO_4 and at 25°C.

furnish kinetic data. Zinc analyses were made at completion of the test. A series of tests was made in which the progress of the reaction was followed by analyzing the solution for zinc at predetermined time intervals. In Fig. 1 the kinetic results of this series are compared with similar data obtained from H_2S pressure measurements. The ordinate axis on the left hand side of this figure gives the concentration of Zn^{++} in solution at time t and the ordinate axis on the right gives the H_2S pressure at time t.

Conversion from zinc ion concentration to H_2S pressure and reverse is obtained as follows. Assuming ideal behavior of H_2S gas and utilizing the distribution coefficient for H_2S between the solution and vapor phase

$$K_D = p_{H_2S}/[H_2S]_{aq} \quad \text{(atmosphere-liters per mole)},$$

a material balance on the products of reaction shows that per liter of solution,

$$[Zn^{++}] = p_{H_2S}\left(\frac{1}{K_D} + \frac{V^1}{RT}\right) = p_{H_2S}C_0 \qquad (3)$$

where C_0 is a constant of dimensions, moles per liter-atmosphere, and V^1 is the ratio of the volume of gas to volume of solution at the specified temperature. The major assumption made in the application of Equation 3 to this kinetic study is that the equilibrium distribution of H_2S between the gas and liquid phase is obtained at all times. This assumption appears to be well substantiated in this investigation. The distribution constant K_D was obtained experimentally at different sulfuric acid concentrations.[19]

The agreement between the two rate curves is very good especially since the analysis of zinc must be preceded by a filtration step which normally consumes about two minutes.

Effect of Agitation

In the absence of agitation the dissolution reaction proceeds very slowly and appears to be controlled by diffusion. A series of tests run at different dial settings showed that as soon as the solids were suspended in the liquid the rate of dissolution increased markedly and with increasing agitation reached a steady state. To eliminate diffusion as a variable, all experiments were run at maximum setting (amplitude of vibration 2 cm). Under these conditions of agitation equilibrium was reached within approximately eight minutes at 25°C. At higher temperatures equilibrium was reached within 2 to 5 minutes.

Dependence of Rate of Dissolution on Surface Area

The dependence of the rate of reaction on the amount of total surface was evaluated at two sulfuric acid concentrations ($1N$ and $3N$). Changes in total surface area were obtained by increasing the weight per cent of solids in the reactor. The exact dependence of the initial reaction rate on surface area was determined by plotting the logarithm of the initial slopes of the rate curves against the logarithm of the initial surface area (or log weight of ZnS). These plots showed that the initial reaction rate at constant sulfuric acid concentration is proportional to the first power of the total surface area.

Effect of Sulfuric Acid Concentration and Temperature

At 25°C the concentration of sulfuric acid was varied from 0.1*N* to 17.5*N*; at 35°C, 45°C and 65°C the concentrations of H_2SO_4 investigated were 0.25*N*, 0.5*N*, 1*N*, 2*N*, 3*N*, 5*N*, and 10*N*. Table II

TABLE II

Equilibrium Pressure and Zinc Ion Concentration at 25°C

Sulfuric Acid Concentration (moles/liter)	$[Zn^{++}]$ (moles/liter)	Partial Pressure of H_2S (atmospheres)	$t_{1/2}$ (minutes)
0.375	0.017	0.036	0 .61
0.5	0.021	0.051	0.84
0.75	0.030	0.079	0.90
0.875	0.035	0.094	0.88
1.0	0.040	0.109	0.84
1.25	0.048	0.137	0.92
1.5	0.057	0.173	0.98
1.78	0.066	0.204	0.95
2.0	0.073	0.236	0.87
2.5	0.091	0.318	0.91
4.0	0.139	0.509	0.86
5.0	0.170	0.650	0.86

gives the equilibrium H_2S pressure and zinc concentration attained for twelve sulfuric acid solutions at 25°C. In addition, the time in minutes for which one half of the equilibrium pressure was reached is also included in Table II. It is interesting to note that at constant temperature the time ($t_{1/2}$), at which the reaction is 50 per cent completed is nearly constant for all initial sulfuric acid concentrations except for concentrations below 0.5*M*. This observation suggests that the reaction is first order with respect to the sulfuric acid concentration.

A logarithmic plot of the initial slopes of the rate curves against the initial hydrogen ion concentration, $[H_0^+]$, in moles per liter is given in Fig. 2. An analysis of thermodynamic data of aqueous sulfuric acid solutions[19] reveals that in the acid concentration range covered by these tests the following relation exists between the concentration of sulfuric acid and hydrogen ion,

$$[H_2SO_4] = 0.8[H^+] \tag{4}$$

Within a hydrogen ion concentration range of 0.65 to 12.5*M* (1*N* to 20*N* sulfuric acid) the slope of the straight line in Fig. 2 is equal to 1.23. If the partial pressure of H_2S is converted to Zn^{++} concentration by means of Equation 3, and if the logarithm of the initial change in

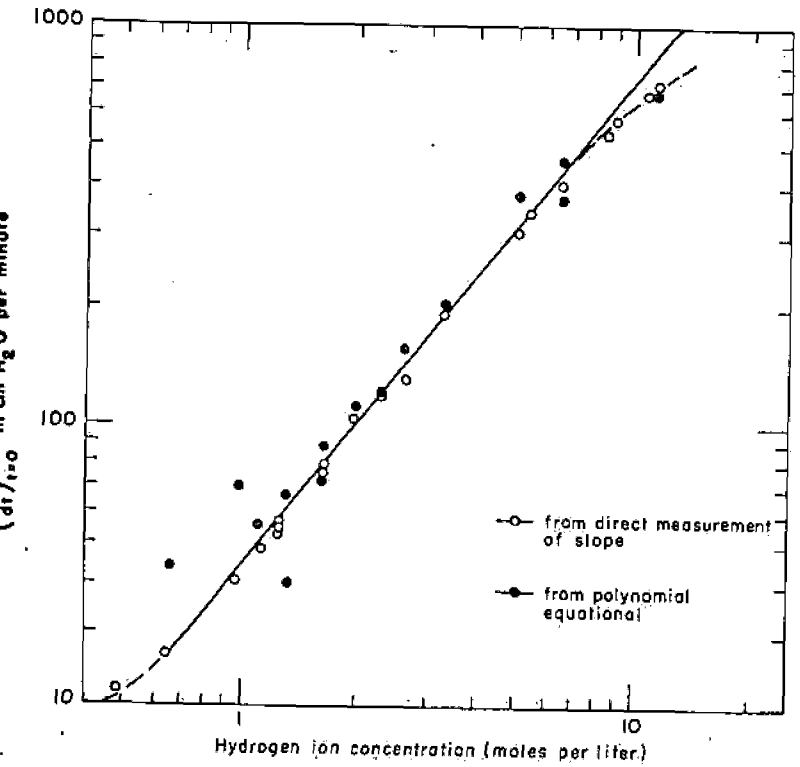

Fig. 2. Effect of acid concentration on the initial reaction rate.

zinc ion concentration is plotted against log $[H^+]$, a straight line with slope of unity is obtained in the same concentration range. Such plots at temperatures 25°C, 45°C and 65°C are shown in Fig. 3 and it its seen that for all three temperatures the initial reaction rate is first order with respect to acid and free hydrogen ion concentration.

Accurate measurements of the initial slope of the rate curves are not easily obtained. In some tests the reaction was as much as 30% completed before it was possible to take the first pressure reading. This

was especially true at sulfuric acid concentrations below 1*N* and also at higher temperatures. At concentrations below 1*N* the reverse reaction already occurred at a finite rate within five seconds of the

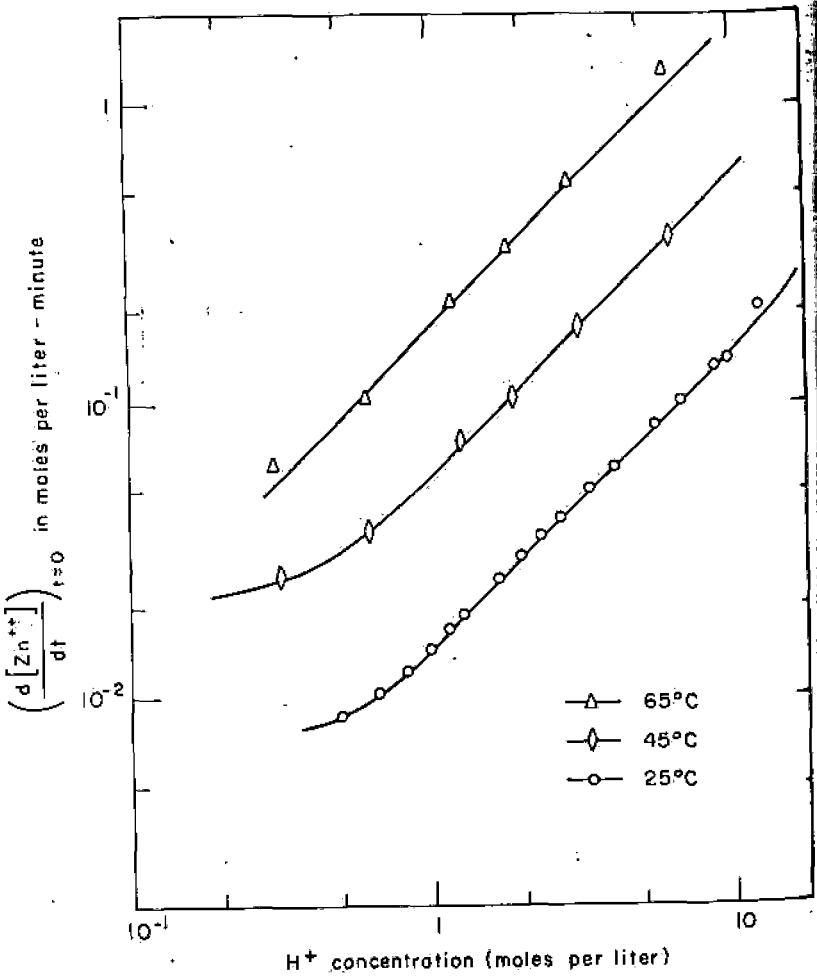

Fig. 3. Effect of acid concentration on initial rate of dissolution at 25°, 45°, and 65°C.

initiation of the reaction. To obtain the straight lines shown in Figs. 2 and 3, the initial slopes of the rate curves were measured directly and were evaluated also by first fitting the experimental rate data to a

polynomial expression of the form

$$p_{H_2S} = a + bt + ct^2 + dt^3 + \ldots$$

where the constant b determines the initial slope.

At high concentrations, the deviation from the straight line shown in Fig. 2 is probably due to formation of elemental sulfur according to Equation 2. At sulfuric acid concentrations of 17.5*N* and higher the presence of elemental sulfur in the leach residues has been positively detected. Under such oxidizing conditions the H_2S pressure no longer measures the total dissolution rate of sphalerite nor will it be related to the zinc ion concentration by Equation 3.

Effect of Impurities in ZnS on Its Dissolution Rate

The results of a series of leaching tests with ZS-800 and three different samples of sphalerite containing varying amounts of Fe and Mn

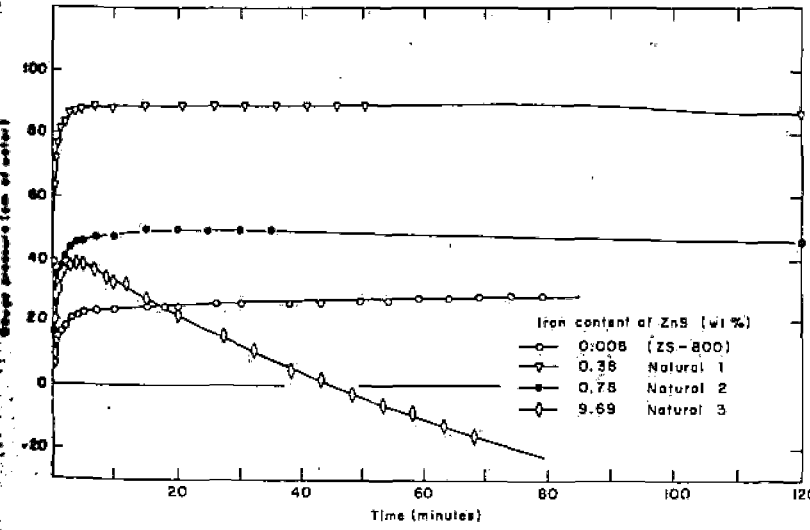

Fig. 4. Dissolution rate as a function of chemical impurities in sphalerite.

(see Table I) are summarized in Fig. 4 and in Table III. These tests were carried out in 0.75*N* H_2SO_4 solutions at 25°C. In all tests the initial surface area was the same.

A comparison of the leaching curves of the two materials lowest in iron (ZS-800 and natural sphalerite sample 1) shows that an increase

in iron content leads to an increasing dissolution rate and a higher equilibrium Zn^{++} concentration. The rate curves obtained with natural samples (2) and (3) cannot be compared directly with the former two curves because of the presence of elemental sulfur as one of the reaction products. In the two latter curves the variation in

TABLE III

Analyses of Reaction Products Formed by Leaching ZnS of Different Amounts of Chemical Impurities

Material	Impurities (wt. %)		Reaction Products (moles/liter)				
	Fe	Mn	Zn	Fe	Mn	H_2S (total)	S
ZS-800	0.006	<0.001	0.016			0.017	
Natural ZnS (1)	0.38	<0.01	0.040	0.01		0.041	0.002
Natural ZnS (2)	0.78	<0.01	0.052	0.01		0.029	0.008
Natural ZnS (3)	9.69	1.82	0.49	0.02	0.02	0.047	0.047

H_2S pressure is no longer a measure of the rate of dissolution of the ZnS, but represents in a complex way the rate of formation of H_2S and its oxidation to elemental sulfur. The oxidation of hydrogen sulfide to sulfur starts early in the dissolution reaction and appears to be directly related to the presence of Fe and Mn. The negative pressures obtained with the natural sphalerite sample (3) cannot be readily explained.

Results of Etching Studies in Absence of Oxidizing Agents

The single crystals of ZnS used in these tests had well developed {III} faces which are characterized atomically by the presence of only one kind of atom, either Zn or S. To identify the polarity of these crystal faces, a special etching method developed by Warekois, Lavine, Marino and Gatos[20] was followed. Later on it was possible to identify the polarity of the crystals without subjecting them to a special chemical treatment. It was noted that the crystals were grown in such a way that the zinc-bearing {III} face tended to exterminate itself.

Etching tests were carried out in 4*N* and 10*N* sulfuric acid solutions at 40°C. The crystals that were strained either by polishing or by heat treatment followed by quenching in liquid nitrogen were observed to

etch more rapidly than the untreated crystals. To produce noticeable changes on the untreated crystals, the etching treatment had to be continued for two to three weeks while the effects of chemical attack were observed after one or two days on the strained crystal surfaces.

On zinc {III} faces the surface scratches etched into long narrow troughs bounded by relatively unattacked surfaces whereas the sulfur faces etched more uniformly. In general the chemical attack may be described as a pitting rather than a uniform attack of exposed surfaces.

DISCUSSION

In the absence of oxidizing conditions the dissolution reaction, Equation 1, may also be represented by the heterogeneous chemical reaction

$$ZnS(s) + 2\,H^+(aq) = Zn^{++}(aq) + H_2S(g) \qquad (5)$$

The equilibrium constant for this reaction is expressed by the relation

$$K = \frac{[Zn^{++}]p_{H_2S}}{[H^+]^2} \cdot \frac{f_{(Zn^{++})}}{f^2_{(H^+)}} = K_c\Phi \qquad (6)$$

where

$[Zn^{++}]$, $[H^+]$ = molar concentrations of Zn^{++} and H^+ in solution

p = partial pressure of H_2S vapor

$f_{(Zn^{++})}, f_{(H^+)}$ = activity coefficients of Zn^{++}, H^+ which may be related to the mean ionic activity coefficients of the electrolytes, $ZnSO_4$ and H_2SO_4

K_c = mass action constant

Values of K_c were determined experimentally as a function of temperature and sulfuric acid concentrations for precipitated ZnS(ZS-800). The best value for the equilibrium constant was obtained by plotting K_c as a function of ionic strength and extrapolating to zero ionic strength. The results of this extrapolation at 25°, 45° and 65°C are given in Table IV together with the values obtained by calculation from standard free energy data at 25°C.

Since the dissolution of ZnS proceeded at constant volume, the reaction rate per unit volume may be written as

$$\frac{d[Zn^{++}]}{dt} = [A_0]^m(k_F[H^+]^n - k_R[Zn^{++}]^q p^r) \qquad (7)$$

where

$[A_0]$ = initial surface area of solids per liter of solution
k_F, k_R = forward and reverse reaction rate constants
m, n, q, r = empirical constants.

In arriving at Equation 7 the following assumptions were made:

(a) the dissolution of ZnS is not diffusion-controlled,
(b) the surface area of the solids remains essentially constant during the reaction,
(c) the rate with which equilibrium is established between H_2S in solution and in the gaseous phase is rapid,
(d) both the forward and the reverse reaction are surface reactions.

Assumptions (a) and (b) have been verified experimentally. Although no direct experimental justification of assumption (c) was possible it is believed that this postulate is in agreement with the observed results. Regarding assumption (d), experimental results showed that the forward reaction is a surface reaction but no direct evidence was obtained to prove that a surface reaction also describes the reverse process. However, as will be shown from an analysis of the kinetic data and a comparison with the observed equilibrium constants, this assumption is consistent with all experimental and derived results. It should be noted that the reverse step in the dissolution reaction may not necessarily be equated to a crystal growth reaction for which the dependence on surface area may not hold or may be of a complicated nature.

From the experimental results it was established that the dissolution rate in the sulfuric acid concentration range, $1N$ to $10N$, is directly proportional to the initial surface area and to the hydrogen ion concentration. Equation 7 may, therefore, be replaced by the expression

$$\frac{d[Zn^{++}]}{dt} = k_F^1[H^+] - k_R^1[Zn^{++}]^q p^r \tag{8}$$

where

$$\left.\begin{aligned} k_F^1 &= k_F A_0 \\ k_R^1 &= k_R A_0 \end{aligned}\right\} \tag{9}$$

In writing Equation 7 the activity coefficients of the ionic species were included in the rate constants, these quantities are, therefore, functions of temperature and concentration. If we may assume that k_F and k_R or the modified constants, k_F^1 and k_R^1, are independent of concentration then it follows that

$$\frac{k_F}{k_R} = \frac{k_F^1}{k_R^1} = K^n \tag{10}$$

where n is a positive quantity and is numerically equal to one-half in view of the first power dependence of the dissolution rate on the hydrogen ion concentration.

Since the progress of the dissolution process was followed by recording changes in H_2S pressure whereas H^+ and Zn^{++} concentrations were only known at zero time and at equilibrium, it is desirable to express the reaction rate in terms of the partial pressure of H_2S. This transformation is readily made with the aid of Equation 3 and Equation 8 now assumes the form

$$C_0 \frac{dp}{dt} = k_F^1(H_0^+ - 2C_0 p) - k_R^1 \sqrt{C_0}\, p \tag{11}$$

where H_0^+ is the initial hydrogen ion concentration.

At equilibrium Equation 11 reduces to the relation

$$\frac{H_0^+ - 2C_0 p_{eq}}{C_0} = \frac{k_R}{k_F} p_{eq} \tag{12}$$

If k_R and k_F are independent of concentration then a plot of the logarithm of the term on the left hand-side of Equation 12 against $\log p_{eq}$ should give a straight line with unit slope. Excellent straight lines with unit slope are obtained if the experimental data at 25°, 45° and 65°C in the concentration range $1N$ to $10N$ are plotted as suggested. This observation suggests that the activity coefficient quotient Φ of Equation 6 is approximately constant in this concentration range.

The magnitudes of k_F^1 and k_R^1 may be evaluated by noting that according to Equation 11

$$k_F^1 = \frac{C_0}{H_0^+}\left(\frac{dp}{dt}\right)_{t=0} \tag{13}$$

By combining Equations 12 and 13 the value of k_R^1 (also k_R) may be obtained. If Equation 11 is differentiated with respect to pressure then

$$\frac{d(dp/dt)}{dp} = -\left(2k_F^1 + \frac{k_R^1}{\sqrt{C_0}}\right) \tag{14}$$

At fixed sulfuric acid concentration and temperature, a plot of dp/dt against p should give a straight line with slope equal to the right hand side of Equation 14. In combination with Equation 12, Equation 14 may be used instead of Equation 13 to solve for k_F^1 and k_R^1. Table

TABLE IV
Calculated Values of k_F^1 and k_R^1.

Temp. (°C)	k_F^1 (min^{-1}) From Equation 13			k_R^1 (moles)$^{1/2}$(liter)$^{-1/2}$ (atm)$^{-1/2}$(min^{-1}) From Equations 12 and 14			$\left(\frac{k_F^1}{k_R^1}\right)^2$	K by Extrapolation
	1N	Average*	1N	3N	1N	3N		
0.6	1.9×10^{-5}				5.1×10^{-4}			
8.9	2.6×10^{-5}		2.1×10^{-5}		6.6×10^{-4}			
15	3.0×10^{-5}		3.1×10^{-5}					
25	5.0×10^{-5}	4.7×10^{-5}	5.9×10^{-5}	7.2×10^{-5}	1.2×10^{-3}	1.3×10^{-3}	2.0×10^{-3}	1.13×10^{-3}
								4.67×10^{-4}†
								1.36×10^{-1}‡
35	9.9×10^{-5}	9.7×10^{-5}	1.1×10^{-4}	1.1×10^{-4}	1.8×10^{-3}	1.7×10^{-3}	4.0×10^{-3}	
45	1.9×10^{-4}	1.8×10^{-4}	1.7×10^{-4}	1.9×10^{-4}	2.2×10^{-3}	2.5×10^{-3}	5.8×10^{-3}	1.75×10^{-3}
65	5.2×10^{-4}	5.6×10^{-4}	5.2×10^{-4}	5.0×10^{-4}	5.6×10^{-3}	4.9×10^{-3}	10^{-3}	2.70×10^{-3}

* This average includes 1N, 2N, 3N, 5N, and 10N sulfuric acid solutions.
† Sphalerite from standard free energy data.
‡ Wurtzite from standard free energy data.

IV summarizes the values calculated from different combinations of Equation 12, 13, and 14.

This Table also compares the extrapolated values for the equilibrium constant as obtained from equilibrium data alone with the values

Fig. 5. Dependence of reaction rate constants on temperature. For the reverse reaction the experimental constants are actually k_R^1/A_0.

obtained by taking the square of the quotient, k_F^1/k_R^1. If the reverse reaction were not a surface reaction then the magnitude of the corresponding rate constant would be equal to k_R, and the equilibrium constant will be determined by the relation

$$\left(\frac{k_F A_0}{k_R}\right)^2 = K$$

However, according to Table IV the ratio $(k_F^1/k_R^1)^2$ agrees with the observed values of K. It is this agreement between K and the quotient $(k_F^1/k_R^1)^2$ that may be cited as evidence that the reverse reaction is also a surface reaction and that the overall dissolution rate may be expressed by Equation 7.

Figure 5 gives Arrhenius plots of the kinetic data included in Table IV. For the reverse reaction the values plotted in this figure are actually the modified constant k_F^1 divided by the constant A_0 (333 m^2/liter). This does not effect the slope of the Arrhenius plot. The activation energies of the forward and reverse reactions as determined from Fig. 5 are 11.1 ± 1 Kcal/mole and 7.8 ± 1 Kcal/mole respectively. Usually the activation energies for diffusion range between 3 Kcal and 6 Kcal, therefore, the observed values, especially for the forward reaction may be regarded as additional proof that the dissolution process is not diffusion controlled.

For this system the heat of reaction (ΔH) is approximately related to the difference in activation energies (ΔE_a) by the relation,

$$\Delta H \simeq \frac{\Delta E_a}{n} = 6.6 \text{ Kcal/mole}$$

For sphalerite as the solid phase a heat of reaction of 7.3 Kcal/mole is calculated from enthalpy data at 25°C.

PROPOSED MECHANISM OF REACTION

The analysis of the available experimental data suggests that the dissolution process may be looked upon primarily as a chemical reaction at the interface between zinc sulfide and the solution. Transfer of reacting species to the interface and of reaction products from the interface does not appear to control the rate of the process if sufficient agitation is provided. Although it is not possible to give quantitative discussion of the mechanism by which the dissolution is affected a few qualitative comments and observations may be made.

Both the zinc blende and wurtzite structures of crystalline ZnS have the same short range order which is characterized by the four fold coordination of the zinc and sulfur atoms. This coordination is the result of the directional and predominantly covalent bond formed between the zinc and sulfur atom. The density of atoms exposed at the solid surface and the number of broken bonds per surface atom

will depend on the crystallographic orientation of the surface plane. Structural considerations, therefore, suggest that the chemical reactivity and thus the rate of dissolution of zinc blende should decrease with orientation of the surface planes in the following order;

$$\{100\} > \{110\} > \{111\}$$

Both {110} and {111} surfaces show crystallographic polarity with one broken bond per atom. A surface atom in a {100} face has two broken bonds.

The actual dissolution process for ZnS may be represented by the reactions

$$Zn^{++}(s) \rightarrow Zn^{++}(aq)$$

$$S^{=}(s) \rightarrow S^{=}(aq)$$

The zinc dissolution reaction includes the effects due to hydration and the sulfide dissolution is, of course, complicated by the formation of H_2S. According to these reactions the dissolution process proper must be preceded by rupture of the covalent bond and a transfer of electrons to yield the ions, Zn^{++} and $S^{=}$. Although predominantly covalent in character, the Zn-S bond has some ionic character because of the difference in electronegativity of the zinc and sulfur atoms. A rough calculation based on the Pauling approach[21] suggests that the Zn-S bond is about 20% ionic in character. The more ionic in nature the bond is, the more soluble the solid should be. The observed increasing rate of dissolution of natural sphalerite may be explained qualitatively by the substitution of Fe and Mn for Zn in the lattice. Iron is more electropositive than Zn thus the more ionic character of the Fe-S bond should aid the dissolution; MnS is an example of an essentially ionic sulfide.[22]

Increasing dissolution rates also result from defects other than those due to chemical substitution. The etching studies showed that dislocations and strain effects also lead to faster chemical attack. At constant total surface (but not constant particle size) the dissolution reaction rate constant, k_F, therefore, may be expressed as the product of two terms,

$$k_F = Yk_F^*$$

where k_F^* represents the intrinsic rate constant for the "perfect crystal" and the variable factor Y measures the number of reactive sites per unit area and reflects the nature of the imperfections present.

Although it is not possible to present a quantitative analysis of the various steps by which the dissolution of ZnS is effected, the experimental results suggest that one or more of the steps involved in the process of transferring sulfur from the solid to the solution phase may be rate controlling. This suggestion is substantiated by the observation that on etching the single crystals the {111} sulfur-bearing surfaces are more strongly attacked than the corresponding zinc surfaces. By dissolving the bond between zinc and sulfur in the solid through an attack on the *sulfur* atom, the solid eventually passes in solution. Since the sulfide ion concentration in solution under the conditions of experimentation is extremely small ($10^{-24}M$ to $10^{-15}M$), no accumulation of $S^=$ in the solution is expected during the reaction and it is more than likely that the slow kinetic step takes place at the interface.

SUMMARY AND CONCLUSIONS

The rates of dissolution of crystalline zinc sulfide in aqueous sulfuric acid solutions were studied in the concentration range of $0.125M$ to $8.75M$ H_2SO_4 and in the temperature range 0.6 to 65°C. The reaction products were H_2S and dissolved zinc. Additional studies were made on natural sphalerite to determine the effect of chemical impurities on the dissolution process. Etching studies were also made on single crystals of vapor-grown cubic zinc sulfide subjected to strain. The following conclusions may be drawn from this investigation.

1. The dissolution reaction in the absence of oxidizing conditions and under conditions of vigorous agitation to eliminate diffusion control of the reaction is a function of:
   (a) hydrogen ion (or sulfuric acid) concentration
   (b) the initial surface area
   (c) temperature
   (d) crystal imperfections (chemical and physical defects)
2. In the sulfuric acid concentration range, $1N$ to $10N$, the net dissolution rate of ZnS varies directly with the initial surface area, with the first power of the hydrogen ion concentration and with the square root of Zn^{++} and H_2S concentration in solution.
3. The forward and reverse reaction rate constants have been evaluated and from the temperature dependence of these an activation energy of 11.1 Kcal for the dissolution process is indicated and an activation energy of about 7.8 Kcal for the reverse process is calculated.
4. The presence of substituted iron and manganese in the crystal lattice of zinc blende increases the rate of solution and in presence of large quantities of iron (>0.1% by weight) elemental sulfur appears as one of the reaction products.
5. Etching studies on single crystals at 40°C in $4N$ and $10N$ H_2SO_4 solutions reveal that the dissolution reaction depends on the degree of deformation and physical defects imposed on the crystal. The {111} sulfur faces are more strongly attacked than the {111} zinc faces.

Acknowledgements

This investigation was sponsored by the United States Atomic Energy Commission under Contract No. AT(30-1)-956. The authors wish to acknowledge the interest shown by Dr. A. M. Gaudin in this study and the helpful suggestions made by Drs. T. B. King and A. Witt in the interpretation of the experimental data.

References

1. Bosch, W., Farbenindustrie, Aug., 30 (1927), April, 16 (1931).
2. Tronev, V. G., and S. M. Bondin, *C. R. Acad. Sci. USSR*, **23**, 541 (1939).
3. Neuhaus, H. and F. Pawlek, *Z. Erzbergbau u. Metal Hüttenwesen*, **6**, 41 (1953).
4. Bjorling, G., *Metall. Wirtsch. Wiss. Tech.*, **8**, 781 (1954).
5. Pawlek, F. and H. Pietsch, *Z. Erzbergbau u. Metal Hüttenwesen*, **10**, 373 (1957).
6. Forward, F. A. and H. Veltman, International Symposium on the Physical Chemistry of Process Metallurgy, Pittsburgh, Penn., April, 30 (1958).
7. Stanczyk, M. H. and C. Rampacek, U.S. Bureau of Mines; R. I. 5848 (1961).
8. McKay, D. R. and J. Halpern, *Trans. A.I.M.E.*, **212**, 301 (1958).
9. Gray, P. M. J., *Rev. Pure and Applied Chem.*, **5**, 194 (1955).
10. Forward, F. A. and J. Halpern, *Trans. Inst. of Min. and Met.*, **66**, 191 (1956).
11. Gray , P. M. J., *Research, London*, **7**, 432 (1954).
12. E. Von Discher and F. Pawlek, *Z. Erzbergbau u. Metal Hüttenwesen*, **10**, 158 (1957).
13. Downes, K. W. and R. W. Bruce, *Trans. Can. Inst. of Min. and Met.*, **58**, 77 (1955).
14. Warren, I. H., *Australian J. Appl. Science*, **7**, 346, (1956).
15. Holleman, A. F. and E. Wiberg, "Lehrbuch der Chemie" Erster Teil, Anorganische Chemie, p. 188, Walter de Gruyter and Co., Berlin (1945).
16. Welcher, F. J., "The Analytical Uses of Ethylenediamine Tetracetic Acid," pp 149, 224, Van Nostrand Co. Inc., Princeton, N.J. (1957).
17. Scott, W. and H. N. Furman, "Standard Methods of Chemical Analyses," p. 931, D. Van Nostrand Co. Inc., 5th Ed. (1939).
18. Samelson, O., "Ion Exchange in Analytical Chemistry," John Wiley and Sons, N.Y. (1953).
19. Romankiw, L. T., *S. M. Thesis, M.I.T.* (1962).

UDC 661.183.12:546.161

The behaviour of the ions of alkali metals, copper (II) and silver (I) during sorption by granulated iron hydroxide from solutions of ammonium fluoride

V S Pakholkov and V F Markov (Urals Polytechnical Institute, Department of the Metallurgy of Rare Metals)

Summary

The sorption of lithium, sodium, potassium, rubidium, copper (II), and silver (I) ions from solutions of their fluoride containing ammonium fluoride, by iron hydroxide granulated by freezing the gel was investigated under dynamic conditions. It was established that the sorbability of the ions decreases in the order $Cu^{2+} > Ag^{+} > Li^{+} > Na^{+} > K^{+} > Rb^{+}$. This corresponds to the pK values for the formation of the corresponding hydroxy complexes formed in the reaction between the cation and the hydroxyl group of the hydroxide. The relationships obtained are explained in terms of a coordination copolymerisation process.

The formation of a copper hydroxyfluoride [illegible] position CuOHF in the ion-exchange phase was confirmed by IR spectroscopy and by chemical and X-ray [illegible]

Kinetics of the electrochemical reduction of thiourea complexes of metals.

G N Shivrin and E M Shivrina (Krasnovarsk Institute of Nonferrous Metals)

In nonferrous metallurgy thiourea solutions are used for the elution of noble metals from ion-exchange resins[1]. Acidic solutions of thiourea can also be used as a solvent for gold and silver ores [2, 3]. Electrolysis is an effective method for the treatment of thiourea solutions of noble metals.

In this connection the kinetics of the electro-chemical reduction of thiourea complexes of metals at a cathode during the electrolysis of thiourea solutions are of theoretical and practical interest.

In accordance with the series of normal dissociation potentials of the thiourea complexes of metals (table), the noble metals are reduced at the cathode preferentially compared with the accompanying nonferrous metals (lead, zinc, cadmium, copper, etc). Silver is less easily reduced than gold.

Normal dissociation potentials and pK_D values for thiourea complexes of some metals

Complex ions	pK	E m/m(Thio)$_n^{m+}$ B
$Au(Thio)_2^+$	21.96	+0.380 [9]
$Ag(Thio)_3^+$	13.10	+0.023 [3]
$Cu(Thio)_5^{2+}$	15.39 [10]	-0.119
$Cd(ThiO)_4^{2+}$	8.60 [11]	-0.657
$Pb(Thio)_3^{2+}$	8.23 [12]	-0.647
$Zn(ThiO)_2^{2+}$	1.77 0.73 [14]	-0.650 -0.785

Investigation of the electrochemical reduction of the thiourea complex of silver was carried out on apparatus with a rotating disc electrode, described in the literature[4]. The reduction of the thiourea complexes of gold and copper was studied in a cell with vertical electrodes.

When silver is present in the thiourea solution, four polarisation waves are observed on the curve for the relationship between current density and cathode potential.

As shown in [4], the first wave is due to the reduction of electrochemically active impurities (mostly dissolved oxygen) at the cathode. This process takes place under diffusion control and is characterised by the presence of a limiting current.

The second and third polarisation curves are due to the electrochemical decomposition of the thiourea complex of silver, which is accompanied by the release of metallic silver at the cathode. The second wave is due to the discharge of silver ions. The third wave, as will be shown subsequently, is due to electrochemical reduction of thiourea molecules contained in the thiourea silver complex at the cathode. Both waves are characterised by the existence of a limiting current, which demonstrates the diffusion control of the reduction of the silver ions.

The fourth wave is due to electrochemical reduction of hydrogen ions, which takes place under kinetic control and is described by a Tafel equation (5).

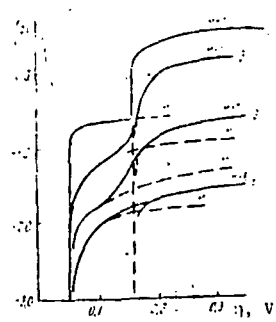

Fig.1
The effect of the silver concentration in the thiourea solution on the dependence of i_d and $i_{d,r}$ (1-4) on the potential. Concentration of $Ag(Thio)_3^+$, m-ion/dm^3: 1 - 0.92 and 1.85; 2 - 8.4; 3 - 27.7; 4 - 37.0.

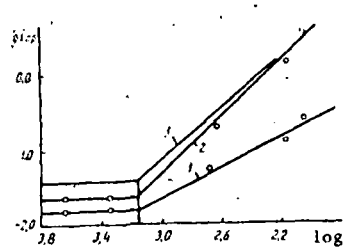

Fig.2
Dependence of the limiting current on the activity of silver ions in a 0.5M solution of thiourea in 0.5M sulphuric acid: 1 - i_{Ag}; 2 - i_{H^+}; 3 - i_{H_2}

The discharge current of the silver ions becomes appreciable with an overpotential of 0.05V, and then with increase in the overpotential it increases sharply and passes into the limiting current (fig.1). The magnitude of the limiting current is proportional to the activity of silver ions in the solution (fig.2):

$$(i_{Ag})_{lim} = k_1 \cdot a \qquad (1)$$

and is proportional to the square root of the disc rotation rate in strict accordance with the theory of the disc electrode. This confirms the diffusion character of the silver

reduction process.

The inflection points on the curves in fig.2 correspond to a silver concentration $C_{Ag} = 2.75 \cdot 10^{-3}$ g-ion/dm³ in the layer adjacent to the electrode in a thiourea solution (0.52 mole/dm³ of thiourea and 0.5 mole/dm³ of sulphuric acid in the absence of current.

A sharp increase in the cathodic current is observed with an overpotential greater than 0.16V (fig.1). The current rapidly reaches a limiting value, which was found to bear a power relation to the activity of the silver ions in the solution within the silver concentration limits[6,2]):

$$(i_T)_{lim} = k_2 \cdot a^2_{Ag} \qquad (2)$$

In spite of the fact that the current i_T is a function of the activity of silver ions in the solution, it cannot be due to discharge of Ag^+ ions, since calculation of the activity of silver ions in the solution required to secure the current i_T leads to values 1.5-20 times greater than the actual activity. Nevertheless, the current i_T is due to discharge of the thiourea silver complex $Ag(Thio)_3^+$, since it is only observed in the presence of an appreciable amount of silver in the solution and depends on the concentration of silver in accordance with Eq.(2).

Thiourea molecules present in the solution but not combined into the complex are reduced at the silver cathode at a negligible rate. However, thiourea molecules entering into the composition of the thiourea silver complex are present in a transition state at the moment of decomposition of the complex during the reduction of $Ag(Thio)_3^+$, and their reduction at the cathode becomes more likely. As a result there is a sharp increase in the cathodic current. During the reduction of thiourea molecules in accordance with the equation (6):

$$(NH_2)_2CS + 8H^+ + 6e \longrightarrow H_2S + CH_3NH_3^+ + NH_4^+ \qquad (3)$$

the current i_T can reach 18 i_{Ag}, which agrees with the experimental data.

Direct measurements of the consumption of thiourea during the electrolysis of silver, due mainly to its decomposition at the cathode, showed that 2.85 moles of thiourea are consumed in the reduction of 1 g-ion of silver[7]). Thus, the cathodic reduction of thiourea silver complex is the main source of the losses of the thiourea, if decomposition of the thiourea molecules at the anode is prevented by separation of the cathode and anode compartments by a conducting membrane.

In the region of overpotentials of 0.16-0.40 V, where the discharge currents of dissolved oxygen and the reduction current of hydrogen ions are relatively small in value, the main reason for the decrease in the current yield during the electrolysis of silver is the discharge current of the thiourea complex i_T.

If the overall cathodic current due to the occurrence of the silver and thiourea reduction processes is plotted in fig.2 as a function of the activity of silver ions in the thiourea solution (curve 3), an empirical relationship is obtained which can be approximated as the power function

$$(i_{M+T})_{lim} = k_3 \cdot a^m_{M} \qquad (4)$$

where $m = 1.68$.

Simultaneous solution of Eqs.(1) and (4) leads to the equation:

$$i_H = k_4 (i_{M+T})^{0.60} \qquad (5)$$

The general relationships governing the electrochemical reduction, as established for silver, also hold for other metals.

Thus, if the electrolysis of a metal from a thiourea solution is realised under conditions where the electrochemical reduction of oxygen and hydrogen can be neglected, the ratio of the discharge current of the metal i_M and the total cathodic current i_{tot} must be described by a relationship of the type in Eq.(5). In fact, as seen from the data obtained during the electrolysis of silver and gold in a cell with vertical electrodes (fig.3), for $i_{tot} < 0.1$ A/dm² when $i_H + i_T \gg i_H$, the dependence on i_{tot} is described by an equation similar to Eq.(5):

$$\lg i_{Ag} = 0.62 \lg i_{tot} - 1.08 \qquad (6)$$

$$\lg i_{Au} = 0.62 \lg i_{tot} - 1.18 \qquad (7)$$

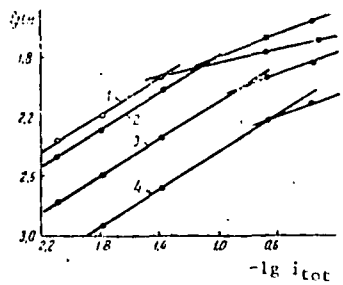

Fig.3
The dependence of the reduction current of the metal ions (1-i_{Ag}; 2 - 4 - i_{Au}) on the total cathodic current density in the cell with vertical electrodes without special agitation. C_{Ag}, mg-ion/dm³: 1 - 4.4; C_{Au}, mg/ion/dm³: 2 - 4.4; 3 - 2.41; 4 - 1.24.

The coefficient before log i_{tot} is the same for gold and silver and is a consequence of the fact that in both cases electrochemical reduction of thiourea molecules released during decomposition of the thiourea metal complex occurs. The practicallycomplete agreement of this coefficient in Eqs.(6) and (7), obtained during investigations in a cell with vertical electrodes and without special agitation, with the power index in Eq.(5) which was derived during investigation of the reduction at a rotating disc electrode shows that the relation (5) is universal and does not depend on the conditions under which the electrolysis of the thiourea solution is realised.

With $i_{tot} > 0.1$ A/dm² the discharge current of the silver ions reached a limiting value, and the discharge of the hydrogen ions increased sharply. The amount of released hydrogen is proportional to the density of the hydrogen ion reduction current i_H. The more hydrogen is released, the more intense the agitation in the layer of electrolyte near the electrode, and as a result the magnitude of the current which is limiting for a given metal concentration gradually increases. In this region, when $i_H > i_M + i_T$, the metal discharge current is related to the total current in the cell by the equation (fig.3):

$$\lg i_{Ag} = 0.23 \lg i_{tot} - 1.62 \qquad (8)$$

$$\lg i_{Au} = 0.37 \lg i_{tot} - 1.44 \qquad (9)$$

where $i_{tot} = i_H + i_M + i_T$.

From comparison of the normal dissociation potentials of the thiourea complexes of various metals (table) with the cathodic potential at which hydrogen release becomes predominant (from -0.55 to -0.70 V) it follows that only gold, silver, and possibly copper can be reduced from the thiourea solution at normal rates. The thiourea complexes of such metals as lead, zinc, and cadmium can hardly be reduced at all at the cathode. Noble metals can be isolated selectively from the thiourea solution by electrolysis, since at the cathode potential when the reduction current of gold and silver reaches the limiting value the reduction rate of copper and other nonferrous metals is still too low.

Investigation of the joint deposition of silver and copper from a thiourea solution containing 0.5 mole/dm³ of thiourea, 1.0 mole/dm³ of sulphuric acid, 4.17 mg-ion/dm³ of silver, and 7.03 mg-ion/dm³ of copper was undertaken in a cell with vertical electrodes. With current density $i_{tot} = 3.79$ A/m² the silver discharge current amounted to

i_{Ag} = 0.225 A/m² and the copper discharge current i_{Cu} = 0.008 A/m². Increase in the cathode potential leads to an increase in the reduction rate of the copper ions, and here the release of hydrogen increases and the current yield of copper decreases.

From the experimental data presented the diffusion coefficient of the $Ag(Thio)_3^+$ ion was calculated. Its value for 293°K ($D_{Ag} = 0.47 \cdot 10^{-5}$ cm²/sec) agrees well with published data [9].

Simultaneous solution of Eqs. (6) and (7) leads to the following result:

$$\frac{(i_{Ag})_{lim}}{(i_{Au})_{lim}} = 1.26$$

With all other conditions equal the difference in the limiting currents for the reduction of gold and silver from thiourea solutions is due to the difference in the diffusion coefficients of the respective ions. Consequently, the diffusion coefficient of the $Au(Thio)_2^+$ ion at 293°K is:

$$D_{Au} = 0.33 \cdot 10^{-5} \text{ cm}^2/\text{sec}$$

References

1) I N Maslenitskii et alia: Metallurgy of noble metals. Metallurgiya, Moscow 1972, 212.
2) I N Plaksin: Metallurgy of noble metals. Metallurgizdat, Moscow 1958, 319.
3) V V Lodeishchikov et alia: Izv Vuz Tsvetnaya Metallurgiya 1975, (2), 77.
4) G N Shivrin et alia: Izv Vuz Tsvetnaya Metallurgiya 1970, (6), 22.
5) G N Shivrin et alia: Izv. Vuz Tsvetnaya Metallurgiya 1971, (1), 47.
6) B B Damaskin et alia: Absorption of organic compounds at electrodes. Nauka, Moscow 1968.
7) G N Shivrin et alia: Development of hydrometallurgical processes and extension of the regions of application of extraction, sorption, and ion exchange in nonferrous metallurgy Part 3. Tsiintsvetmet, Moscow 1968, 27.
8) R Yu Bek et alia: Izv SO Akad Nauk SSSR, Khimiya 1970, (7), 47.
9) V P Kazakov et alia: Zh Neorgan Khim 1964, 9, (5), 1299.
10) E J Onstott et alia: Amer. Chem. Soc., 1950, 72, 4724.
11) P K Migal' et alia: Zh. Neorgan. Khim. 1963, 8, (3), 629.
12) T J Lane et alia J. Amer. Chem. Soc. 1958, 80, 315.
13) O S Fedorova: Collection of articles on general chemistry. Izd. Akad. Nauk SSSR, Moscow 1953, 1, 206.
14) T V Kramareva et alia: Izv. SO Akad. Nauk SSSR, Khimiya 1961, (8), 68.

UDC 541.123.3

Investigation of the reaction of higher germanium, silicon, tellurium and molybdenum chlorides

V V Safonov, Zh K Fes'kova, N M Grigor'eva and V I Ksenzenko (Moscow Institute of Fine Chemical Technology and the Technology of Halurgical Products)

In the literature there are mentions of the use of the chloride method for the treatment of various waste products from the radiotechnical industry [1,2]. The present report gives the results from physicochemical investigations into the solubility of tellurium tetrachloride in liquid germanium and silicon tetrachlorides and of the phase equilibria in the $GeCl_4$-$MoCl_5$-$SiCl_4$, $GeCl_4$-$MoCl_5$-$TeCl_4$, and $MoCl_5$-$SiCl_4$-$TeCl_4$ systems.

The industrial germanium and silicon tetrachlorides required for the work were freed from possible hydrolysis products by vacuum distillation. Tellurium (IV) and molybdenum (V) chlorides were obtained by chlorination of the respective metals [3]. The results from chemical analysis and the melting points of the chlorides obtained agreed well with calculated and published data.

The solubility and fusibility were investigated by isothermal saturation [4]) and by differential-thermal analysis. The time-temperature curves were recorded on a pyrometer of the PK-59 type.

The solubility of tellurium tetrachloride in germanium tetrachloride and silicon tetrachloride at 40-110°C is shown in table 1. The data obtained and the data from thermographic investigations of the $GeCl_4$-$TeCl_4$ [5]), $SiCl_4$-$TeCl_4$ [6]), and $GeCl_4$-$SiCl_4$-$TeCl_4$ [7]) systems indicate the possibility of the separation of the greater part of the tellurium tetrachloride by low-temperature crystallisation of the mixture.

The above-mentioned ternary systems are limited by the concentration tetrahedron of the $GeCl_4$-$MoCl_5$-$SiCl_4$-$TeCl_4$ quaternary system. The phase diagrams of the binary systems bounding the ternary systems have been investigated by ourselves or have been described in the literature. The phase relations in the binary systems are shown in table 2.

The crystallisation surfaces of the phase diagrams of the ternary systems $GeCl_4$-$MoCl_5$-$SiCl_4$, $GeCl_4$-$MoCl_5$-$TeCl_4$ and $MoCl_5$-$SiCl_4$-$TeCl_4$ were constructed on the basis of investigation of the polythermal sections, the direction of which was determined by the position of the invariant points in the binary systems. The phase diagrams of the ternary systems are presented as the developed surface of the tetrahedron for the $GeCl_4$-$MoCl_5$-$SiCl_4$-$TeCl_4$ system (fig.).

Table 1: Solubility of $TeCl_4$ in $MeCl_4$ mole %

Temperature °C	$GeCl_4$	$SiCl_4$
40	0.0451	-
50	0.0675	0.0116
60	0.0820	0.0126
70	0.0990	0.0157
80	-	0.0189
90	-	0.026
100	0.1400	0.033
110	0.1530	-

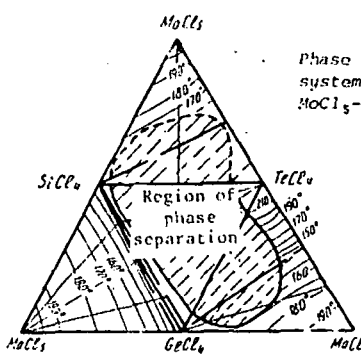

Phase diagrams of the ternary systems defining the $GeCl_4$-$MoCl_5$-$SiCl_4$-$TeCl_4$ system.

TsIINTsvetmet, Moscow 1970.
5) G N Shivrin et alia: Isv. Vuz Tsvetnaya Metallurgiya 1970, (6), 22.
6) A I Stabrovskii: Zh. Fiz. Khim. 1952, 26, 949.
7) M Oudinet et alia: Compt. Rend. 1953, 377.
8) V S Bagotskii et alia: Uspekhi Khimii
9) K J Vetter: Electrochemical kinetics. New York 1967.
10) G N Shivrin et alia: Izv. Vuz Tsvetnaya 1971, (1), 47.

Tsvetnye Metally, 1974

UDC 669.3-404.5:547.491:541.135.2

Kinetics of the electrochemical reduction of copper from cyanide-thiocyanate solutions

G N Shivrin, E M Shivrina and V S Klimchenko Krasnoyarsk Institute of Nonferrous Metals - Department of the Metallurgy of Heavy and Noble Metals)

Electrolytic recovery of metals from cyanide solutions and pulps finds use in the technology of the treatment of gold-containing ores[1]). Electrolysis of thiocyanate eluates [1, 2]) and re-extracts [3]) is used for the production of the pure metals. The insufficient degree of investigation of the electrode processes and kinetics of electrochemical reduction of metals in cyanide-thiocyanate solutions substantially retards the application of the electrolysis of cyanide-thiocyanate solutions in non-ferrous metallurgy.

The kinetics of electrochemical reduction from cyanide-thiocyanate solutions were investigated on apparatus with a rotating disc electrode[4]) and also in a cell with vertical electrodes. In an aqueous solution of $Na_2Cu(CN)_3$ the dependence of the cathode current density on the cathode potential has several polarisation waves. Dissolved oxygen is first reduced at the cathode. Reduction of $Cu(CN)_3^{2-}$ ions begins at a cathode potential of about -0.30 V. The rate of the process increases rapidly with polarisation of the cathode, but a limiting current (fig.1) exactly corresponding to the reduction current of singly charged copper is established at an over-potential higher than 0.15-0.20V.

The reduction of the CN^- ligands entering into the composition of the complex $Cu(CN)_3^{2-}$ ion begins at a cathode potential of about -0.5 V. At a $Cu(CN)_3^{2-}$ ion concentration above 0.06 g-ion/dm³ the reduction of the CN^- ligands passes into the diffusion region, as shown by the appearance of a limiting current onthe polarogram (fig.1, curve 4).

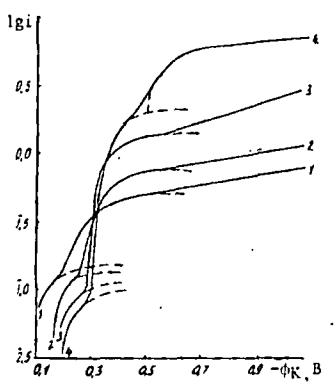

Fig.1 The dependence of the current density on the potential of a rotating copper disc cathode in solutions with various concentrations of $Na_2Cu(CN)_3$ (mole/dm³): 1 - 0.0078; 2 - 0.0281; 3 - 0.0608; 4 - 0.125.

The limiting current for the reduction of CN^- is approximately three times higher than the limiting current for the reduction of singly charged copper:

$$(i_{CN})_{lim} = 3(i_{Cu})_{lim} \quad (1)$$

Consequently, one electron is used for each CN^- ligand entering into the composition of the complex $Cu(CN)_3^{2-}$ ion. The reduction of the CN^- ligands can be represented by the following reaction:

$$CN^- + 3H_2O + 1e \longrightarrow NH_3 + CO_3^{2-} + 1.5H_2 \quad (2)$$

It should be noted that free CN^- ions not entering into the composition of the $Cu(CN)_3^{2-}$ complex are not reduced at the cathode under these conditions. The reduction of ligands which are electrochemically inert inthe free state is clearly a phenomenon characteristic of the reduction of the complex ion at the cathode.

The fourth polarisation wave on the log i-φ_c diagram in an aqueous solution of $Na_2Cu(CN)_3$ is due to the reduction of hydrogen (not shown in the figure). Increase in the concentration of $Cu(CN)_3^{2-}$ ions in the solution leads to a decrease in the hydrogen overpotential, and this is due to a decrease in the negative ζ potential at the cathode.

Increase in the concentration of NaNCS in the solution leads to a shift of the decomposition potential of $Cu(CN)_3^{2-}$ towards the negative side and to a decrease in the limited current density for the reduction of the copper. However, calculations showed that the decrease in the limiting current density for the reduction of copper is not due to a change in the composition of the copper complex or to specific adsorption of NCS^- ions at the cathode but is brought about by a change in the activity of the $Cu(CN)_3^{2-}$ ions as a result of a change in the ionic strength of the solution.

The effect of the concentration of sodium cyanide on the reduction of copper from the cyanide- thiocyanate solution was studied in a cell with vertical electrodes without special agitation of the electrolyte. Electrolysis was carried out with a constant cathodic current density. The copper reduction rate was monitored by weighing the cathode at half hour intervals. The change in the concentration of copper in the electrolyte during electrolysis was calculated from the increase in the weight of the cathode. At the end of the experiment a control analysis of the electrolyte was undertaken for copper content, and this made it possible to draw up a balance in respect of the copper in the cell. The electrolyte temperature was 20°C.

The reduction of copper under these conditions takes place in the diffusion region, and the limiting current for the reduction of copper is determined by the activity of the $Cu(CN)_3^{2-}$ ions (a_{Cu}):

$$(i_{Cu})_{lim} = n \cdot F \cdot k \cdot a_{Cu} \quad (3)$$

where k is the rate constant of the electrochemical reaction, which is independent of the activity of $Cu(CN)_3^{2-}$ ions in the solution. Experimentally it was established that k also does not depend on the activity of NCS^- ions in the solution but depends on the activity of CN^- ions in the solution (fig.2). The dependence of k on the activity of CN^- ions can be expressed in terms of a power function of the following type:

$$k = k_1 \cdot a_{CN}^{-m} \quad (4)$$

The experimental value of m is 0.33.

The overall cathode current density in the electrolytic recovery of copper from cyanide-thiocyanate solutions is composed of several components:

$$i_{ove} = i_{O_2} + i_{NCS} + i_{CN} + i_{Cu} + i_H \quad (5)$$

The only useful current is i_{Cu}. The currents i_{O_2} and i_{NCS} are comparatively small and can be practically disregarded during electrolysis in a cell with vertical electrodes.

If the overall cathode current density is kept within limits corresponding to a cathode potential less than φ_c for the beginning of intensive reduction of hydrogen, the overall cathode current density will be determined by the sum of the current density for the reduction of copper i_{Cu} and the cur-

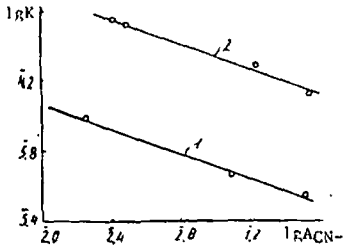

Fig.2 The dependence of the rate constant for the reduction of $Cu(CN)_3^{2-}$ from a thiocyanate solution (0.617 mole/dm³ NaNCS) on the activity of CN^- ions with cathodic current densities of 0.1 [1]) and 2.0 A/dm² [2]).

rent density for the reduction of the ligand i_{CN}. Under optimum conditions there is a power relationship between the current densities (fig.3):

$$(i_{Cu})_{lim} = k_3 \cdot a_{Cu} \cdot (i_{ove}) \qquad (6)$$

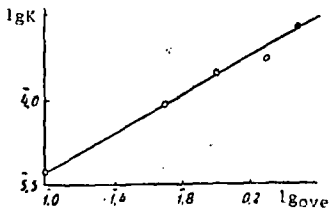

Fig.3 The dependence of the rate constant for the reduction of copper from the cyanide-thiocyanate solution on the cathode current density.

In a cell with vertical electrodes and with an electrolyte containing 0.305 g-ion/dm³ of $Cu(CN)_3^{2-}$, 0.617 g-ion/dm³ of NCS^-, and 1.53 g-ion/dm³ of CN^- at 20°C we obtained n = 0.56.

The effect of the electrolyte temperature on the reduction rate of copper from the cyanide-thiocyanate solution was investigated by means of the polarisation relationship at a rotating disc cathode and also by means of the increase in the weight of copper at the cathode in a cell with vertical electrodes and without special agitation of the electrolyte. The temperature was kept constant within ±0.5°C by means of a thermostat.

At the disc cathode with increase in the electrolyte temperature from 24 to 60°C there was a negative shift of the reduction potential for dissolved oxygen, copper, and the CN^- ligand. However, the log i-φ_c relationship for the hydrogen reduction process remained alsmost unchanged in the investigated range of temperatures.

The limiting current for the reduction of copper increased with increase in temperature. The experimental value for the activation energy of the electrochemical reduction of the $Cn(CN)_3^{2-}$ ion at the disc electrode was E = 4120 cal/g-ion.

During electrolysis of copper from the cyanide-thiocyanate solution in a cell with vertical electrodes and without special agitation the range of investigated temperatures was somewhat wider (15-60°C). In this case the activation energy of the copper reduction process within the limits of 30-60°C amounted to E = 4570 cal/g-ion, which is extremely close to the activation energy at the disc electrode.

The low value of the activation energy is consistent with the diffusion character of the electrochemical reduction of copper from the cyanide-thiocyanate solution at temperatures above 20-24°C and under hydrodynamic conditions characterised by Re ≤ 1200. At temperatures below 20-24°C and under hydrodynamic conditions characterised by Re ≤ 1200. At temperatures below 20-24°C there is an abrupt change in the form of the dependence of k on temperature (fig.4).

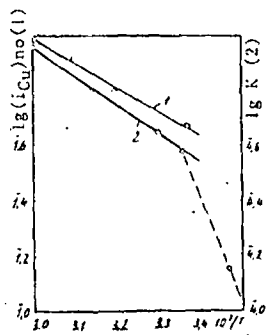

Fig.4 The limiting current for the reduction of copper at the rotating disc cathode [1]) and the rate constant for the reduction of copper at the vertical cathode [2]) as functions of the electrolyte temperature.

The activation energy of the process increases abruptly to E ≥ 16.9 kcal/g-ion, which indicates a transition to the kinetic region. The dependence of the copper reduction rate on the concentration at an electrolyte temperature of 15°C leads to the same conclusion:

$$i_{Cu} = n \cdot F \cdot k \cdot C_{Cu}^3 \qquad (7)$$

In the diffusion region of the process the dependence of the current density for the reduction of copper on temperature can be expressed by the equation:

$$(i_{Cu})_{lim} = k_3 \cdot 10^{-\frac{E}{2.3RT}} \cong k_3 \cdot 10^{-\frac{10^3}{T}} \qquad (8)$$

Not only the rate of the copper reduction process but also the current efficiency increase with increase in temperature. Thus, at 50-60°C, even without special agitation of the electrolyte the current efficiency amounts to 46%.

Combining the obtained equations (1), (4), (6), and (8), we express the copper reduction rate in terms of the electrolysis conditions:

$$(i_{Cu})_{lim} = 10^{-\frac{10^3}{T}} \cdot (i_{ove})^{0.68} (a_{CN})^{-0.33} \cdot a_{Cu} \cdot f \qquad (9)$$

where f is a coefficient which depends on the design of the electrolysis cell and the intensity of the agitation of the electrolyte.

References

1) The gold-extracting industry of capitalist countries. TsIINTsvetmet, Moscow 1963.
2) I N Plaksin et alia: Hydrometallurgy with the use of ion exchangers. Metallurgiya, Moscow 1964.
3) G N Shivrin: Technology of the extraction of valuable components from the effluents of concentration plants. TsIINTsvetmet, Moscow 1970.
4) G N Shivrin et alia: Izv. Vuz Tsvetnaya Metallurgiya 1970, (6), 22.

UDC 621.762.274

Maintaining a constant electrolyte composition in the electrolytic production of copper powder

A V Pomosov, A A Yun', and L P Tabatchikova (Urals Polytechnical Institute - Department of the Technology of Electrochemical Processes)

The stability of the physical and technological characteristics of electrolytic copper powder depends on the strict observance of the electrolysis conditions, among which the electrolyte composition is of considerable importance. However, the electrolyte composition is subject to rapid variation on account of the inequality of the cathode (B_{ic} = 85-94%) and anode (B_{ia} ≈ 100%) current yields; the copper sulphate concentration increases, and the sulphuric acid concentration decereases. Moreover, on the average 1.5% of the copper passes from the dissolving anode into the solution on account of chemical dissolution of the copper anodes.

The currently employed method of maintaining a constant

can be inventoried. But in addition to these reserves, there are known, low grade deposits not profitable to mine deposits of reserve quality that ically inferred but are as yet ed, and even new types of de-

posits not yet recognized."

"Our total resources in 1975 are vast," the report concludes, "but they cannot be mined, much less used, until they have been identified, appraised, and finally moved into the category of reserves. We must begin now, in both industry and government, to inform the public about the real nature of our minerals problem, and to stimulate the research that will make our mineral resources available." □

...rson mine tunnel holed through by Amax after 4½ years' work

FOUR AND ONE-HALF YEARS of around-the-clock tunneling ended with a dynamite blast on July 15, when miners "holed through" the 9.6-mi ore haulage tunnel for the Henderson mine. The mine, 50 mi west of Denver, is under construction by Amax Inc.

The 15-ft-high, 16.5-ft-wide tunnel is one of several major engineering feats at the largest privately financed project in the history of Colorado. Before molybdenum production begins in the third quarter of 1976, Amax will have spent close to $400 million on the Henderson project.

The tunnel will serve ore trains hauling molybdenum ore from the mine on the east side of the Continental Divide to an ore processing plant on the west side, in the Williams Fork Valley. After emerging from the tunnel, the trains will travel another 4.8 mi to the ore crushing and milling facility. (For additional details on the underground transport system, see discussion of the Henderson mine in the feature section of this issue.)

Work on the tunnel began Jan. 10, 1971. It was driven on a 3% downgrade from the western portal 9,000-ft elevation to connect with the train-loading level of the mine, a 7,500-ft elevation. Complex engineering and survey work was required as eastbound crews of Dravo Corp. and westbound Amax crews worked toward each other in holing through the tunnel. Because of its nearly 10-mi length, corrections had to be made to allow for the curvature of the earth. A laser guidance system was used for working control, and at the time of hole-through, the two tunnel headings were within 5 in. of being exactly on line and within 1 in. of being on grade.

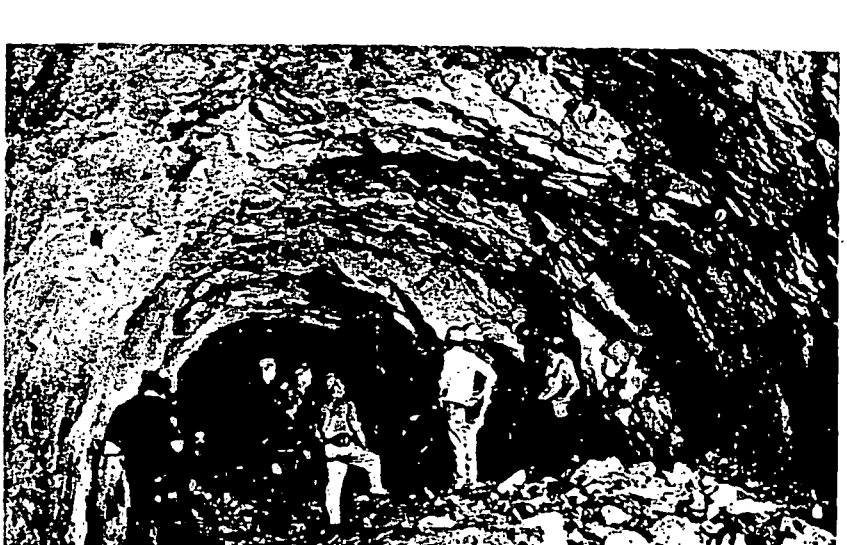

Amax officials atop muck pile inspect holethrough of the Henderson haulage tunnel.

At least an additional year of work will be required on the mine, mill, and tunnel before the project goes onstream.

Ultimate planned production of 50 million lb of molybdenum annually from the Henderson mine will nearly double Amax's current annual production capacity of approximately 60 million lb of molybdenum. The Henderson project now employs about 2,100 Amax and contractor employees, and when the facility goes onstream the permanent work force is expected to number 1,100.

Henderson has been cited as an outstanding example of industrial development with emphasis on environmental concern. During early planning of the project, a committee of Amax managers and representatives from Colorado environmental groups met regularly to study methods of minimizing the environmental impact of the operation. As a result, the Henderson mine was selected by the US as the subject for a case history presentation in an international symposium on "Environmental Accomplishments to date—A Reason for Hope," held in conjunction with the Expo 74 World's Fair in Spokane, Wash. □

Kennecott investigates solution mining potential of deep Cu deposit

KENNECOTT COPPER CORP. has been experimenting with a solution mining process at its Safford area copper deposit, 124 mi northeast of Tucson and about 9 mi north of Safford, in the Gila mountains. Solution mining of deep copper ores has attracted growing industry interest in recent years as an environmentally compatible, industrially safe, and potentially economic means of recovering copper from deep-seated deposits without resorting to expensive underground development.

A Kennecott research and development team is considering a $5 million program of at least five injection and solution recovery holes. Leach solutions would be forced several thousand feet deep under high pressure in the injection bores to soak copper-bearing rock and attack copper minerals. The recovery wells in the leach area would establish a circulation system returning to the surface, similar to oilfield hydrofracturing techniques.

The wells at Safford could go as deep as 5,000 ft, and if the system is successful, low grade ores may be recovered that would not be economically accessible by conventional open pit or underground methods.

Previously, Kennecott had considered a possible non-vented subsurface nuclear explosive experiment jointly with the AEC, to break a small portion of a 2-billion-ton copper deposit lying at great depth near Safford. The blast was to be designed to create a glassy, slag-walled chimney typical of underground nuclear explosions. The concept—long since abandoned—would have involved drilling of solution injection and recovery wells to leach copper from the rubble, along with a complex monitoring system of additional boreholes to check radiation levels.

Current testing by Kennecott is directed at completion of two holes. The company's Ledgemont Laboratory at Lexington, Mass., is conducting the experiments and is seeking funds to expand to a five-hole pattern. Solution would be pumped into a single injection

(Continued on p 41)

hole and out of the remaining withdrawal holes. Hole diameters are reported to be about 10 in.

Leach liquor would be pumped under pressures of more than 1,000 psi into the injection wells to penetrate the formation through cracks, fissures, and faults. Acting as a wedge, the high pressure solution is expected to pry through fractures, cracking them while loosening and dissolving grains of copper along the way. Assuming that an effective injection and recovery well circulation system could be established in which the copper concentration builds to suitable levels, the pregnant solution returning to the surface would be processed for recovery of copper before it is returned to the injection bore.

It is anticipated that the technique could be used on sulphide as well as oxide ores. Success of such a system would substantially increase Arizona copper reserves, now estimated at about 9 billion tons of ore.

Kennecott has not permanently shelved the possibility of using a nuclear explosion to establish an underground leaching cavity. A contract signed with the AEC in 1973 called for a joint study of such a technique. However, this study focused not on the Safford deposit but on a theoretical orebody having the characteristics of several Kennecott copper deposits. The study has been completed and is being reviewed.

The solution mining technique is attractive in that it would not pollute the air and would create relatively little surface disturbance. How the method would affect underground water supply has not been determined, but the Arizona Department of Mines feels that any water problems could be solved to assure the public of a safe water supply. □

Tennessee's proposed minerals tax creates storm of opposition

TENNESSEE GOVERNOR RAY BLANTON, confronted with a continuing financial pinch, is expected to ask the 1976 legislature in January to approve a severance tax on state-owned minerals that would most affect the coal and zinc mining industries. According to mining interests, the tax—which would raise an estimated $22 million—could put some zinc operations out of business.

Most of the opposition to the governor's mineral tax bill—which failed to win approval earlier this year—comes from the mountainous east Tennessee area, where the state's mining operations are concentrated. Concern about revival of the tax issue is so great that a meeting was scheduled for August in Knoxville to organize an association of mining interests to fight the bill.

In an attempt to solve a deficit budget

(Continued on p 44)

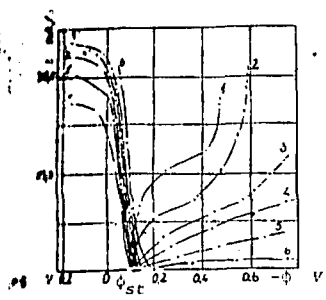

Fig.1 The effect of the concentration of copper on the polarisation of copper electrodes. Cathodic polarisation with copper concentrations mole/l: 1 - 0.683; 2 - 0.449; 3 - 0.243; 4 - 0.136; 5 - 0.090; 6 - 0.010. Anodic polarisation at the same concentrations (1'-6').

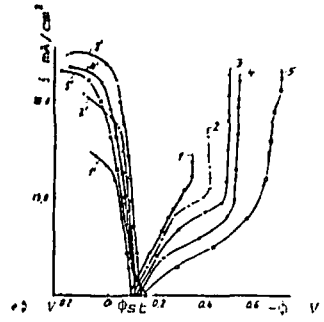

Fig.2 The effect of the ammonium sulphate concentration on the polarisation of copper electrodes. Cathodic polarisation with ammonium sulphate concentration mole/l: 1 - 0.1; 2 - 0.25; 3 - 0.5; 4 - 0.75; 5 - 1.5. Anodic polarisation at the same concentrations (1'-5').

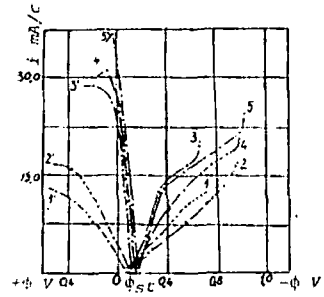

Fig.3 The effect of the concentration of free ammonia on the polarisation of copper electrodes. Cathodic polarisation with concentrations of free ammonia mole/l: 1 - 0.324; 2 - 0.586; 3 - 0.892; 4 - 1.149; 5 - 1.387. Anodic polarisation at the same concentrations (1'-5').

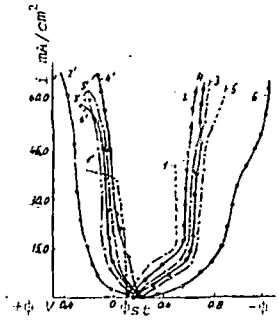

Fig.4 The effect of the concentration of zinc on the polarisation of copper electrodes. Cathodic polarisation with the following molar ratios of copper to zinc in the solution: 1 - 1:0; 2 - 1:1; 3 - 1:2; 4 - 1:3; 5 - 1:4; 6 - 1:5. C_{Cu} = 0.25mole/l. Anodic polarisation with the same molar ratios (1'-6').

experiments

Soo. Non-Fe metals Research
v.6 N6, 1978

UDC 669.334.22: 669.243.822

yes

Kinetics of the leaching of pyrrhotite with ferric chloride solutions

A L Krestan and G N Dobrokhotov (Leningrad Mining Institute. Department of the Metallurgy of Heavy and Noble Metals)

Known schemes for the concentration of copper-nickel sulphide ores usually include the operation of selective isolation of a pyrrhotite concentrate. Its subsequent metallurgical treatment makes it possible to obtain the principal components of the concentrate (iron and sulphur) comparatively simply in commercial form and partly to extract the accompanying copper and nickel. However, the possible treatment schemes are greatly complicated when there is a large content of nonferrous and noble metals. One of the variants permitting the complete extraction of the main components of the concentrate may be a scheme of leaching with concentrated ferric chloride solutions[1]. In this process the first stage of the overall treatment (assuming arbitrarily that the composition of pyrrhotite corresponds to the formula FeS)

$$FeS + 2FeCl_3 = 3FeCl_2 + S^0$$

terminates in the production of a solution of $FeCl_2$, elemental sulphur, and a small amount of an insoluble residue. The bulk of the nonferrous and noble metals concentrate in the latter. The second stage of the process, involving oxidative hydrolysis,

$$3FeCl_2 + 0.75O_2 = 2FeCl_3 + 0.5Fe_2O_3$$

makes it possible to regenerate the reagent and to isolate the iron of the pyrrhotite as an independent product. The overall equation of all the operations

$$FeS + 0.75O_2 = 0.5Fe_2O_3 + S^0$$

shows that the process can be realised in closed technological schemes and does not involve the release of any chemically harmful substances to the environment. At the same time, separate realisation of the stages makes it possible to reduce the possible losses of nonferrous and noble metals with the iron hydroxide precipitate, while the choice of concentrated solutions of ferric chloride secures the attainment of acceptable rates for the operations even at comparatively high temperatures[2]. The present report sets out the results from investigations into the kinetic features of the first stage of the overall treatment.

The experiments were carried out with a sample of flotation concentrate containing 46.2%Fe, 28.6%S, 3.62%Ni, 1.62%Cu, 12.4%SiO_2, 1.9%CaO, and 4.4%Al_2O_3. The iron of the sample was largely represented by hexagonal and partly monoclinic pyrrhotite and also (in a small amount) by magnetite, nickel-pentlandite, and a partially isomorphous mixture with pyrrhotite, copper-chalcopyrite, and cubanite. The initial solution for leaching with a concentration of 100 g dm^3 of Fe^{3+} in the experiments with a

solid-liquid ratio of 1:10 examined [illegible] approximately stoichiometric consumption of the reagent. It was established that lower concentrations of Fe^{3+} appreciably reduce the oxidation rate of the pyrrhotite, while higher concentrations hardly change it; additions of $FeCl_2$ do not have a significant effect on the kinetics of leaching. In this respect the selected initial concentration of Fe^{3+} can be considered optimum.

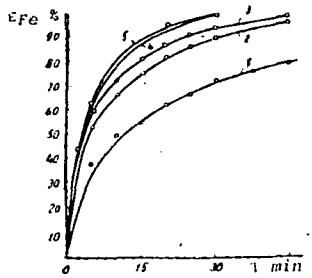

Fig.1 The effect of the intensity of agitation (rpm) on the transfer of iron into solution: 1 - 50; 2 - 100; 3 - 150; 4 - 200; 5 - 250.

The leaching of the concentrate was realised in a glass reactor with a mechanical stirrer and provided with a reflux condenser. The temperature was regulated with an accuracy of $\pm 2^{\circ}C$. During sampling the overall volume of solution (0.5 dm^3) was maintained by constant additions of the initial solution with equal volume. The extraction of the metals into the solution was calculated from the change in the composition of the solution, and the extraction of iron was additionally monitored by analysis of the final residue. It was established that the dissolution rate of the main component of the concentrate (iron sulphide) depends substantially on the intensity of agitation (fig.1). Practically complete transition into the internal diffusion region was achieved with a stirrer rotation rate of about 250 rpm or with the water value of the modified Reynold's criterion:

$$Re_M = \frac{nd_M^2}{\nu} = \frac{250 \cdot 0.04}{60 \cdot 10^{-6}} = 7000$$

(where n is the stirrer rotation rate, γ is the kinematic viscosity, and d_M is the diameter of the stirrer). The low values of Re_M bore witness to the high porosity of the sulphur film which forms, and this was confirmed by direct visual observations. It was also shown that the dissolution rate of the main components of the concentrate (iron, copper, and nickel) in the initial periods of leaching agreed with the empirical equation:

$$\left(1 - \sqrt[3]{1-\varepsilon}\right)^2 = K_1 c_{Fe^{3+}} \tau = K\tau$$

where: ε = the degree of extraction of the component into
$c_{Fe^{3+}}$ = the initial concentration of ferric chloride

This made it possible to express the effect of the various kinetic factors by comparison of the nominal rate constants K. In the range of investigated temperatures (60-98°C) with $c_{Fe^{3+}}$ = 100 g/dm^3, Re_M = 7000, and c_{HCl} = 30g/dm^3 the dissolution rate of the iron in the concentrate was approximately seven times greater than the dissolution rate of nickel and copper (figs.2-4, table). This secured preferential dissolution of iron sulphides compared with copper and nickel sulphides. For instance, at 80°C 98,16, and 18% of the respective metals were extracted into solution with a leaching time of 30 min. The difference in the leaching rates secured the production of comparatively poor final solutions. With an overall iron content of 140-150 g/dm^3 the content of copper and nickel was not usually greater than tenths of a g/dm^3. The production of such poor solutions naturally guarantees the output of comparatively pure iron hydroxide.

By graphical treatment of the experimental results of this series of experiments in the form of the normal Arrhenius curves it was possible to determine the activation energies of dissolution of the components of pyrrhotite. They had the following values, kJ/mole; E_{Fe} = 16.74; E_{Cu} = 60.24; E_{Ni} = 51.64. This showed that the dissolution of iron sulphide takes place under diffusion control and the dissolution of copper and nickel sulphides takes place under kinetic control. However, the selectivity of dissolution decreases somewhat with increase in temperature.

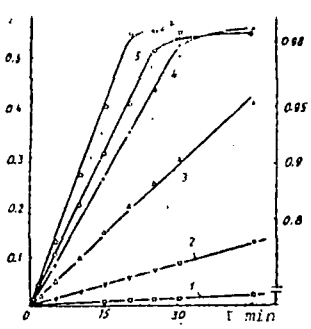

Fig.2 The effect of temperature on the transfer of iron into solution %: 1 - 50; 2 - 60; 3 - 70; 4 - 80; 5 - 90; 6 - 95.

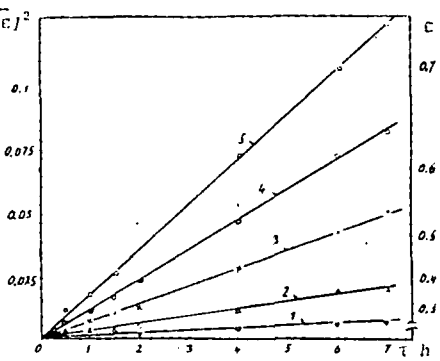

Fig.3 The effect of temperature on the transfer of nickel into solution °C: 1 - 60; 2 - 70; 3 - 80; 4 - 90; 5 - 98.

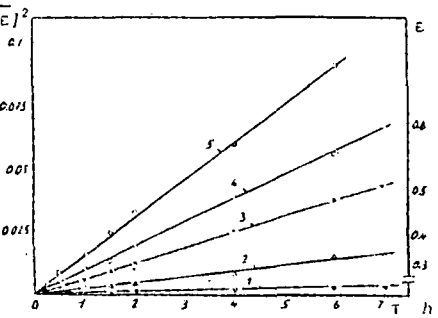

Fig.4 The effect of temperature on the passage of copper into solution. For the notation see fig.3.

The variation of the rate constants for the dissolution of the components of the concentrate with temperature

Rate constant h^{-1}	Temperature °C					
	50	60	70	80	90	98
K_{Fe}	0.0343	0.171	0.596	1.062	1.224	1.653
K_{Cu}	-	$6.75 \cdot 10^{-4}$	$0.23 \cdot 10^{-2}$	$0.62 \cdot 10^{-2}$	$1.04 \cdot 10^{-2}$	$1.56 \cdot 10^{-2}$
K_{Ni}	-	$8.41 \cdot 10^{-4}$	$0.347 \cdot 10^{-2}$	$0.705 \cdot 10^{-2}$	$1.14 \cdot 10^{-2}$	$1.82 \cdot 10^{-2}$
K_{Fe}/K_{Ni}	-	203,33	171,76	150,64	107,37	90,82

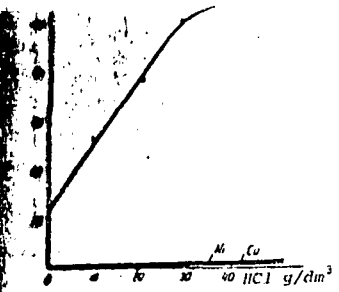

Fig. 1 The effect of additions of HCl on the transfer of iron, nickel and copper into solution.

The addition of acid up to approximately 30 g/dm³ of HCl appreciably accelerated the dissolution of pyrrhotite and had comparatively little effect on the dissolution rate of chalcopyrite and pentlandite (fig.5). From this observation in view of the acidic characteristics of sulphides it can be concluded that the overall dissolution of the sulphides, taking place according to the equation

$$MeS + 2FeCl_3 = MeCl_2 + 2FeCl_2 + S^0$$

is in fact composed of two parallel reactions, i.e., the topochemical oxidation of the sulphides by the ferric ion in the solution

$$MeS + 2Fe^{3+} = Me^{2+} + 2Fe^{2+} + S^0$$

and simple chemical reaction with the acid

$$MeS + 2H^+ = Me^{2+} + H_2S$$

with subsequent oxidation of the hydrogen sulphide which forms in the general mass of the solution (or more accurately, on the outer surface of the diffusion layer) according

$$H_2S + 2Fe^{3+} = 2Fe^{2} + 2H^+ + S^0$$

Of course, the reaction characteristics of the solution could acquire different character at the end of the leaching operation, i.e., with low concentrations of ferric chloride and with adequate rates of formation of hydrogen sulphide. In practice a higher acidity in the final solutions, which is always observed with additions of acid to the initial mixtures, promoted the appearance of free hydrogen sulphide, change in the redox potential of the system, and redeposition of the dissolved copper and nickel.

Conclusions

1. During the treatment of pyrrhotite by concentrated solutions of ferric chloride dissolution of the the accompanying copper and nickel sulphides, which react under kinetic control.
2. With increase in temperature the selectivity of the dissolution of iron and nonferrous metal sulphides decreases.
3. The oxidation of sulphur takes place by topochemical and volume mechanisms. Small additions of acid accelerate the dissolution and, on account of the release of hydrogen sulphide, promote redeposition of the nonferrous metals at the end of leaching.
4. Dissolution of the flotation concentrate at an acceptable rate for industrial purposes (interrupted leaching time 0.5-1 h) takes place at 90-100°C with an initial Fe^{3+} content of about 100 g/dm³.

References

1) A P Serikov, Collection: Physicochemical investigations in the hydrometallurgy of non-ferrous metals. Irkutsk, IPI, 1975, p.3.
2) V E Klets et alia: Collection: Physicochemical investigations inthe hydrometallurgy of nonferrous metals. Irkutsk, IPI, 1975, p.67.

UDC 669.2

Correlation of the parameters of the sinter roasting of lead sulphide ores and concentrates

A I Kalashnikov and I V Aleksanyants (SKF VNIKI TsMA. Elektrotsink Works)

One of the technical measures called upon to secure increased production of lead is the industrial assimilation of progressive technological processes for the preparation of lead sulphide concentrates and other lead-containing materials for smelting in a blast furnace. Improvement in smelting technology makes ever greater demands on the metallurgical quality of the sinter (solidity, porosity, reducibility). The creation of highly effective control systems for the sintering processes facilitates to a considerable degree the solution of the problems involved in the production of a high-grade sinter and improvement in the productivity of sintering machines.

In this connection a passive experiment by the rank correlation method[1]) was undertaken under the conditions of the Elektrotsink lead works. As a result of treatment of the a priori information it was established that in the degree of influence on the main characteristics of the sinter roasting the recycled sinter stands at second place after the physicochemical composition of the sintering charge, and this served as the reason for investigations on an industrial charge and recycled sinter from the Elektrotsink works. The effect of the quantitative content of the recycled sinter in the charge on the characteristics of the sinter roasting process was studied.

In the experiment the charge consisted of a mixture of concentrates, fluxes, granulated slag, lead cake, and lead production dust. The raw charge contained 39%Pb, 13%S_{tot}, 11.9%S_s, 7.5%Zn, 11.5%Fe, 7%CaO, and 8.0%SiO_2. In the recycled sinter 0.67% of S was found. The lead content of the sintering charge was stabilised with pyrite[2]). Charges in which the ratios of the amounts of fresh charge to the recycled sinter were 1:0, 1:1, 1:2, 1:3, 1:4, and 0:1 were tested. On account of the unsatisfactory gas permeability it was not possible to fire the charge in which this ratio amounted to 1:0. Coke with particle size of 1mm was added to the subsequent charges in ever increasing amounts in order to keep the fuel content constant, and the additions were calculated so that the absolute content of S_s + coke amounted to 7.1%, which determined the optimum fuel content for the charge of the Elektrotsink works.

The obtained sinters with various charge-recycle ratios were analysed for magnetic permeability, reducibility, solidity, sulphur content, and softening. Special schemes were developed to analyse the quality of the sinter. The investigations showed that the temperature in the bed increases somewhat with decrease in the charge-recycle ratio, the suction rate increases significantly, and the sintering time is reduced. This is explained by the coarsening of the charge and by the increase in its gas permeability.

With increase in the content of recycled sinter in the sintering charges the softening temperature and the relative magnetic permeability increase, while the sulphur content decreases. Decrease in the charge-recycle ratio to 1:3 significantly increases the reducibility of sinter. By correlation analysis

Table 1: Concentration dependence of the volatility of beryllium chloride from NaCl-$BeCl_2$ melts

In melt mole %	In sublimates mg
35.5	6.42
36.8	9.61
39.7	16.20
42.4	52.47
45.7	79.30
49.9	159.00
54.2	264.36
64.6	559.90
81.1	825.00
100	1025.00

Table 2: Activity (a) and activity coefficient (γ) of beryllium chloride in NaCl-$BeCl_2$ melt at 400°C

$BeCl_2$ in melt mole %	α	$-\lg \alpha$	γ	$-\lg \gamma$
35.5	$7.19 \cdot 10^{-3}$	2.14	$2.02 \cdot 10^{-2}$	1.69
36.8	$1.08 \cdot 10^{-2}$	1.97	$2.43 \cdot 10^{-2}$	1.53
39.7	$1.82 \cdot 10^{-2}$	1.74	$4.58 \cdot 10^{-2}$	1.34
42.4	$5.85 \cdot 10^{-2}$	1.24	$1.38 \cdot 10^{-1}$	0.86
45.7	$8.80 \cdot 10^{-2}$	1.05	$1.92 \cdot 10^{-1}$	0.72
49.9	$1.74 \cdot 10^{-1}$	0.76	$3.49 \cdot 10^{-1}$	0.46
54.2	$2.84 \cdot 10^{-1}$	0.55	$5.24 \cdot 10^{-1}$	0.29
64.6	$5.72 \cdot 10^{-1}$	0.24	$8.85 \cdot 10^{-1}$	0.05
81.1	$8.04 \cdot 10^{-1}$	0.09	$9.90 \cdot 10^{-1}$	0.004
100	1	0	1	0

Sov. Non-Fe.
1980 v. 8 N1

UDC 669.2

Laitfeles

Kinetics of the leaching of polydisperse material

O N Tikhonov (Leningrad Mining Institute - Department of the Concentration of Minerals)

Below we give a quantitative description of the kinetics of the leaching of a polydisperse material, starting from the known (constant or variable) linear velocity ($\nu_1/2$) of the leaching front towards the centre of the grain. With a knowledge of ν_1, it is possible by "geometric" arguments and equations to

predict the change in the granulometric characteristics $\gamma(l, t)$ and weight $m(t)$ of the leached particles of the solid phase in the course of the time t of the periodic process or in the discharge from continuous equipment.

The important initial value of ν_1 can either be measured experimentally or calculated theoretically[1]. For instance, in the case of the known assumption[1] (p. 108) that the decrease in the weight of the dissolving particle in 1 sec is proportional to its surface area S and also to the difference between saturation concentration and the concentration of the dissolved product in the volume of the solution $C_s - C(t)$, we obtain

$$\frac{dl}{dt} = \nu_1 = K[C_s - C(t)] \tag{1}$$

where: K = a proportionality factor
l = the grain size
In the case of the more general assumption about the decrease in the weight m of the solid phase[1] (p. 94)

$$\frac{dm}{dt} = -jS = \rho \frac{\nu_1}{2} S \tag{1a}$$

we obtain a relation between ν_1 and the specific leaching flow $J(kg/m^2 \cdot sec)$ in the form $j = \rho\nu_1/2$. In the general case ν depends on the concentration and on the type of solvent reagent, on the temperature and pressure in the apparatus, on the design of the apparatus and the intensity of the agitation of the pulp, and on the particle size l of the solid particles; below, in problems on periodic and continuous leaching ν_1 is contained (directly or indirectly) in the known factors.

During periodic leaching of a polydisperse material the differential particle size distribution in the soluble part of the solid phase $\gamma(l, 0)$ and its general mass $m(0)$ at the initial time $t_0 = 0$ are known; it is necessary to predict the change in the granular characteristics $\gamma(l, t)$ and the change in the mass $m(t)$ in the subsequent time $t > t_0 = 0$.

We will denote the number of particles of the narrow class $(l, l+dl)$ of the soluble solid phase density ρ) by $\gamma_4(l, t)\, dl = dl\, m(t)\gamma(l, t)/\rho(\pi/6)l^3$. The kinetic equation is then derived on the basic of geometric arguments and is obtained in the following final form:

$$\frac{\partial \gamma_4(l, t)}{\partial t} = \nu_1 \bar{1}(l) \frac{\partial \gamma_4(l, t)}{\partial l}; \quad \bar{1}(l) = \begin{cases} 1 \text{ for } l > 0 \\ 0{,}5 \text{ for } l = 0 \\ 0 \text{ for } l < 0 \end{cases} \tag{2}$$

(In the discussions $\nu_1 = dl/dt$ is the rate of decrease in the diameter l). Its solution for $t > 0$ and for the special case $\nu_1 = \text{const}$ has the following form:

$$\gamma_4(l, t) = \gamma_{4i}[l + \nu_1 \bar{1}(l)t] \tag{3}$$

where $\gamma_{4\,i} = m(0)\gamma(l, 0)/\rho(\pi/6)l^3$ is determined by the initial condition (the granular characteristics of the initial material).

In order to obtain a solution according to (3) it is necessary to substitute the argument l in the known initial function $\gamma_{4\,i}(l)$ for t by the time-displaced argument $l + \nu_i \cdot t$, which corresponds geometrically to displacement of the $\gamma_4(l, t)$ graph to the left at a constant rate as the solid phase is "consumed" by the solvent.

From the obtained $\gamma_4(l, t)$ function we calculated m(t):

$$m(t) = \int_0^{\infty} \rho \frac{\pi}{6} l^3 \gamma_4(l, t)\, dl = \int_{v_1 t}^{l_{max}} \rho \frac{\pi}{6} (l - v_1 t)^3 \gamma_4(l, 0)\, dl \tag{4}$$

We then calculate the mass of dissolved material at time t, i.e., m(0) - m(t). We further calculate the total leaching flow per second, equal to the mass of solid passing into the solution per second at the current time,

$$Q_{leach}(t) = \int_0^{\infty} \frac{v_1}{2} \pi l^2 \rho \gamma_4(l, t)\, dl \tag{4a}$$

where $(\nu_1/2)\pi l^2$ is the loss in weight per second by one solid grain with size l.

The following equation, equivalent to eq. (4), hold:

$$m(t) = m(0) - \int_0^t Q_{leach}(t)\, dt \tag{4b}$$

Example 1. The equilibrium initial distribution $0 < l < l_{max}$ for γ_4 is given by

$$\gamma_{4\,i} = A\,|\bar{\gamma}(l) - \bar{\gamma}(l - l_{max})|; \quad A = m(0)\,\frac{2i}{\pi \rho\, l_{max}^4} = \text{const} \tag{5}$$

where l_{max} is the maximum size of the grain.
The solution according to equ. (3) is:

$$\gamma_4(l, t) = A\,|\bar{\gamma}(l) - \bar{\gamma}(l + v_1 t - l_{max})| \tag{6}$$

According to eq. (4) the change in weight of dissolved material is given by:

$$m(t) = \int_{v_1 t}^{l_{max}} \frac{\rho\pi}{6} (l - v_1 t)^3 A\,|\bar{\gamma}(l) - \bar{\gamma}(l - l_{max})|\, dl = m(0)\left(1 - \frac{v_1 t}{l_{max}}\right)^4 \tag{7}$$

The leaching flow per second according to eq. (4a) is given by

$$Q_{leach}(t) = m(0)\frac{4v_1}{l_{max}}\left(1 - \frac{v_1 t}{l_{max}}\right)^3 \tag{7a}$$

Thus, the graph for the $\gamma_4(l, t)$ function is displaced to the left at rate ν_1, the mass of solid decreases according to the law (7), and full dissolution is complete after time

$t_{fin} = l_{max}/v_1$

Here the leaching flow decreases gradually from the maximum $4m(0)\nu_1/l_{max}$ at $t = 0$ to zero at $5 = 5_{fin}$.

Example 2. The equilium initial distribution for $\gamma(l)$ corresponds to the non-equilibrium distribution for $\gamma_4(l)$:

$$\gamma(l, 0) = \frac{1}{l_{max}}\,|\bar{\gamma}(l) - \bar{\gamma}(l - l_{max})| \tag{8}$$

$$\gamma_4(l, 0) = m(0)\,\gamma(l, 0) \Big/ \left(\rho \frac{\pi}{6} l^3\right) \tag{9}$$

The solution according to eq. (3) is

$$\gamma_4(l, t) = \frac{m(0)}{l_{max}} \left[\bar{\gamma}(l) - \bar{\gamma}(l + v_1 t - l_{max})\right] \Big/ \rho \frac{\pi}{6} (l + v\, t)^3 \tag{10}$$

The change in the mass of solid with time according to eq. (4) is

$$m(t) = \int_0^{\infty} \rho \frac{\pi l^3}{6} \gamma_4(l, t)\, dl = \frac{m(0)}{l_{max}} \int_{v_1 t}^{l_{max}} \frac{(l - v_1 t)^3}{l^3}\, dl \tag{11}$$

In this case the mass of solid also decreases to zero after an analogous time $t_{fin} = l_{max}/\nu_1$, but the law governing this decrease differs from the previous case.

More complicated is the case of continuous leaching with C(t) = const and consequently, $\nu_1 \neq$ const; an example of the apparatus may be a separate autoclave in a chain of autoclaves under steady operating conditions. The main equations for the kinetics of cotinuous leaching then have the following form:

$$\frac{\partial \gamma_4(l, t)}{\partial t} = v_1\, \bar{\gamma}(l)\, \frac{\partial \gamma_4}{\partial l} + Q_{in}\gamma_{in} \Big/ \left(\rho \frac{\pi}{6} l^3\right) - Q_{out}\gamma_{out} \Big/ \left(\rho \frac{\pi}{6} l^3\right) \tag{12}$$

$$M \frac{dC(t)}{dt} = Q_{p\,in} C_{in} - Q_{p\,out} C_{out} + \int_0^{l_{max}} \frac{v_1}{2} \pi l^2 \rho \gamma_4(l, t)\, dl \tag{13}$$

where: $\gamma_4(l, t)dl$ = the number of particles with size $(l, l + dl)$ in the autoclave
$\nu_1 = -K\,C(t) - C_{(sat)}$ = the linear rate of decrease in the size of the particles
$C(t)$ = the concentration of the dissolved component in the pulp in the autoclave
$Q_{in}, Q_{out}, Q_{p\,in}$ and $Q_{p\,out}$ = the ingoing and the outgoing flows of solid (soluble) in the pulp and also of the pulp itself
m = the amount of pulp in the autoclave
$m = \int_0^{\infty} \rho(\pi l^3/6)\gamma_4 dl$ = the amount of solid in the autoclave
C_{in} and C_{out} = the concentrations of material dissolved in the ingoing and outgoing flows

$\gamma_{in}(l, t)$ and $\gamma_{out}(l, t)$ = the granular characteristics in the charge and discharge of the apparatus

Equation (12) is derived from eq. (2) with allowance for the ingoing and outgoing flows of solid particles of the narrow class $(l, l+dl)$; it is an equation of balance in the indicated narrow class for apparatus under nonsteady operating conditions. Equation (13) reflects the balance in the dissolved part of the leached material. Equations (12) and (13) remain in force during a hypothesis differing from $v_1 = K C_{[sat]} - C(t)$. The last integral term in eq. (13) is the leaching flow in the apparatus Q_{leach}.

If the conditions in the apparatus are steady with respect to the material flow, $Q_{p\ in} = Q_{p\ out} = Q_p$ = const and M = const, eq. (13) has the following form:

$$T\frac{dC(t)}{dt} = C_{in}(t) - C_{out}(t) + \frac{Q_{leach}(t)}{Q} \tag{13a}$$

where $T = M/Q_p$ characterises the time spent by the particles in the apparatus. [Under ideal mixing conditions ~63% of any initial particles, or more accurately $(1-e^{-1})\cdot 100\%$, leave the apparatus in time T]. However, even with $Q_{p\ in} = Q_{p\ out}$ = const and M = const nonsteady characteristics can occur with respect to the leached solid ($\partial\gamma_4/\partial t \neq 0$; $\partial C/\partial t \neq 0$) on account of the fluctuations in $Q_{in}(t)$, $\gamma_{in}(l, t)$, and $Q_{out}(t)$. Also useful during investigation of the nonsteady operating conditions may be the equation showing the variation of m(t); in order to obtain it we multiply eq. (12) by $\rho(\pi/6)l^3$ and integrate the equation with respect to l from 0 to l_{max}:

$$\frac{dm(t)}{dt} = \int_0^{l_{max}} v_1 \rho \frac{\pi}{6} l^3 \frac{\partial \gamma_4(l, t)}{\partial l}\, dl + Q_{in}(t) - Q_{out}(t) \tag{14}$$

The integral on the right side of the equation is equal to the leaching flow with opposite sign; this is demonstrated by integration by parts:

$$-Q_{leach}(t) = \int_0^{l_{max}} v_1 \rho \frac{\pi}{6} l^3 \frac{\partial \gamma_4}{\partial l}\, dl = \frac{v_1 \rho \pi}{6} l^3 \gamma_4 \Big|_0^{l_{max}} - \int_0^{l_{max}} \frac{v_1}{2} \pi l^2 \rho \gamma_4(l, t)\, dl. \tag{15}$$

The first term on the right side of the equation is equal to zero, and the second term is equal to Q_{leach}.

For a mathematical solution of eqs. (12)-(13), apart from information on $Q_{in}(t)$ and $\gamma_{in}(l, t)$, we require information (direct or indirect) on the amount $Q_{out}(t)$ and composition $\gamma_{out}(l, t)$ of the outgoing product; here various special cases determined by the character of agitation in the apparatus and by the character of the discharge (solid phase), are possible.

Example 1. Ideal mixing in the leaching zone, controlled flow of solid in the discharge, steady conditions.

With intense agitation in the autoclave it can be assumed that the composition of the outgoing product is equal to its composition in the autoclave, i.e., in the case of ideal mixing in the apparatus:

$$\gamma_{out}(l, t) = \frac{\gamma_4(l, t)}{m}\rho\frac{\pi}{6}l^3,\quad C_{out}(t) = C(t) \tag{16}$$

For operation of the apparatus under steady conditions the seat of eqs. (12)-(14) gives the following equations (C = const, $\partial\gamma_4/\partial t = 0$, $Q_{p\ in} = Q_{p\ out} = Q$):

$$Q_{p\ in} = Q_{p\ out} = Q):$$

$$v_1\frac{\partial\gamma_4(l)}{\partial l} - Q_{out}\frac{\gamma_4}{m} = -Q_{in}\gamma_{in}(l)\Big/\rho\frac{\pi}{6}l^3 \tag{17}$$

$$C_{out} = C = C_{in} + \frac{Q_{leach}}{Q} \tag{18}$$

$$Q_{in} = Q_{leach} + Q_{out} \tag{19}$$

With the possibility of controlling the flow of solid in the discharge we consider the quantities Q_{out} and m to be specified (and constant); then, from eq. (17) it is possible to obtain an analytical solution (2) (p. 440):

$$\gamma_4(l) = \exp\left(\int_{l_{max}}^{l}\frac{Q_{out}\,dl}{mv_1}\right)\left[-\int_{l_{max}}^{l}\frac{Q_{in}\gamma_{in}(l)}{v_1\rho\frac{\pi}{6}l^3}\exp\left(\int_{l_{max}}^{l}\frac{-Q_{out}dl}{mv_1}\right)dl\right] \tag{20}$$

In the special case for $\gamma_{in}(l) = 4l^3/l_{max}^4$ the solution of eq. (20) takes the following form (in the initial stage the equilibrium distribution $\gamma_{4\,in}(l)$ = const):

$$\gamma_4(l) = \frac{Q_{in}}{Q_{out}}\frac{m\cdot 24}{\rho l_{max}^4}\left\{1 - \exp\left[\frac{Q_{out}}{mv_1}(l - l_{max})\right]\right\}$$

$$\gamma_{out}(l) = \frac{4Q}{Q_{out}}\frac{\rho}{l_{max}^4}\left\{1 - \exp\left[\frac{-Q_{out}}{mv_1}(l - l_{max})\right]\right\} \tag{21}$$

Example 2. Displacement apparatus and uniform distribution with respect to the number of particles inthe initial feed,

$$\gamma'_{4in}(l) = \frac{24m'_{in}}{\pi\rho l_{max}^4}\left[\bar{l}(l) - \bar{l}(l - l_{max})\right] \tag{22}$$

where: $\gamma'_{4\,in}\,dl$ = the number of particles with size $(l, l+dl)$ in 1 m^3 of initial pulp $1/m^3$

m'_{in} = the mass of solid in 1 m^3 of the initial pulp kg/m^3

In the determination of the leaching results it is here possible to use the solution obtained above for the periodic process (6) and (7), and assuming that the leaching time in the apparatus is equal to $T = M_p/Q_p$, we obtain:

$$\gamma'_{4out}(l) = \frac{24m'_{in}}{\pi\rho l_{max}^4}\left[\bar{l}(l) - \bar{l}(l + v_1T - l_{max})\right] \tag{23}$$

$$m'_{out} = m'_{in}\left(1 - \frac{v_1T}{l_{max}}\right)^4 \tag{24}$$

$$Q_{leach} = Q_p(m'_{in} - m'_{out}) = Q_p m'_{in}\left[1 - \left(1 - \frac{v_1T}{l_{max}}\right)^4\right] \tag{25}$$

where Q_p and M_p are the flow (m^3/sec) and the reserve (m^3) of pulp in the apparatus.

The examples investigated are comparatively simple and were selected so as to illustrate the analytical solution of the leaching equations. In complex cases it is possible to use computer techniques with numerical methods for solution of the differential equations. Thus, for instance, if the assumption about the possibility of controlling the flow Q_{out} is not made, even for steady operating conditions eq. (17) contains the desired function γ_4 (l) under the integral sign for Q_{out} and m, and this greatly complicates the mathematical solution.

References

1) A N Zelikman et alia: Theory of Hydrometallurgical processes. Metallurgiya, Moscow 1975, p. 504.
2) I N Bronshtein et alia: Handbook of mathematics. GITTL, Moscow 1953, p. 608.

UDC 669.334.1/4

Hydrothermal reaction of pyrite with copper sulphate

S S Naboichenko, V I Neustroev, and I F Khudyakov (Urals Polytechnical Institute - Department of the Metallurgy of Heavy Nonferrous Metals).

Pyrite is one of the main components of copper-containing concentrates. The present article gives the results from investigations into the reaction of pyrite with acidified solutions of copper sulphate at elevated temperatures.

In the investigations we used samples obtained after crushing, grinding, and washing the required class of pyrite A and B with the following compositions, wt.%: 0.12 and 0.01Zn; 0.11 and 0.1Cu; 45.1 and 43.7Fe; 51.2 and 50.0S; 0.48 and 0.59CaO; 0.06 and 0.08MgO; 0.73 and 0.94Al_2O_3; 2.0 and 3.5SiO_2. The experimental procedure has been described before [1]. The contents of copper, iron (II and III), and acid in the solution were determined. The initial and activated samples of pyrite were studied by chemical, mineral-petrographic x-ray crystallographic, derivatographic analysis, and x-ray microanalysis. The degree of transfer of iron into solution and precipitation of copper were used as the criteria of the process.

The parabolic form of the kinetic curves indicated that the diffusion resistances increased on account of the thickening film of reaction products. The initial rates of deposition of copper and dissolution of iron were used for kinetic analysis. Variation in the stirrer rotation rate in the range of 740-2 800rpm (180°C,

0.1 M H_2SO_4, $CuSO_4$:FeS = 1.0) had practically no effect on the characteristics of the process, and we subsequently therefore used n = 1420rpm.

The passage of iron into solution and the precipitation of copper increased with increase in temperature (table 1), but these values were not greater than 9.5 and 20% respectively even at 200°C. The initial rates of dissolution of iron and precipitation of copper were practically identical. The values of the observed activation energy, calculated from the values of the initial process rates, amounted to 44.4 ($CuSO_4$:FeS_2 = 1.0) and 40.2 kJ/mole ($CuSO_4$:FeS_2 = 1.2). Increase in the relative dose of copper sulphate led to a proportionate increase in the process rates and also to a more appreciable increase in the acid content.

With increase in the initial acidity of the medium the rates of dissolution of iron and precipitation of copper increased in proportion, and the fraction of oxidised forms of iron in the residue decreased. Similar behaviour was observed with other "copper sulphate-pyrite" ratios. The decrease in the rates of dissolution of iron and, particularly, of precipitation of copper with H_2SO_4 > 0.2 M indicates direct breakdown of the pyrite by the acid and confirms the relation between the degree of dissolution of iron and precipitation of copper. The results from the investigation show that the kinetic stage plays a determining role in the reaction of pyrite with acidified solutions of copper sulphate.

Attention is drawn to the fact that the amount of precipitated copper is much larger than the amount of dissolved iron; the experimental value of their ratio is >1, whereas in the reaction

$$CuSO_4 + FeS_2 \longrightarrow CuS + FeSO_4 + S^0;\ \Delta G^0 = -48.4 \text{ kJ/mole}$$
$$[Cu_2]:[Fe^{2+}] = 1. \qquad (1)$$

This indicates the development of additional processes which promote the precipitation of copper. The content of elemental sulphur in the residues decreases with increase in temperature. Chalcocite and covellite were found by mineral petrographic analysis (MIM-6, x500-2 000). These sulphides and also α-Fe_2O_3 and Cu_9S_5 were also detected by x-ray crystallographic analysis (URS-60 instrument, Fe-K, RKD camera, asymmetric recording and x-ray microanalysis (Cameca MS-46 instrument). X-ray microanalysis indicated the presence of metallic copper in the residues from experiments carried at t ≥ 180°C. The derivatograms and the microstructures of the initial and treated pyrites differed little. The results from phase analysis of the residues, the character of the dissolution of the iron, the precipitation of the copper, and the accumulation of the acid make it possible to suppose that the following processes are probable in the reaction of pyrite with acidified solutions of copper sulphate in addition to reaction (1):
Disproportionation of the elemental sulphur which forms

$$4S + 4H_2O \longrightarrow 3H_2S + H_2SO_4 \qquad (2)$$

Reaction of hydrogen sulphide formed according to reaction with copper sulphate

Table 1: Conditions and characteristics of the reaction of pyrite A with acidified solutions of copper sulphate (-44 μ fraction* sample weight 12g, V_0 0.6 l, τ = 60 min)

$\frac{[CuSO_4]}{[FeS_2]}$	$C^o_{H_2SO_4}$ mole	°C	Content g/l			Extrac. %		Content in cake %			$V_c \cdot 10^3$ g-ion/m²·min		$\left[\frac{V_{Cu}}{V_{Fe}}\right]_o$	$\left[\frac{Q_{Cu}}{V_{Fe}}\right]_\tau$
			Cu	Fe	H_2SO_4	Cu	Fe	Cu	S	S^o	Cu	Fe		
1.2**	0.1	140	8.65	0.3	10.0	6.0	4.4	1.2	52.0	1.2	-	-	-	1.62
		160	8.44	0.3	10.2	8.4	4.4	1.9	51.3	0.85	1.08	1.12	0.96	2.26
		180	8.38	0.32	10.8	8.6	4.7	2.75	52.2	0.64	1.69	1.56	1.09	2.18
		200	8.3	0.66	11.1	9.3	9.5	5.53	50.4	0.30	2.94	3.03	0.96	1.14
1.0	0.1	140	9.95	0.35	8.2	8.9	3.39	4.6	49.4	0.62	0.47	0.44	1.07	2.4
		160	9.8	0.35	8.9	9.2	3.68	4.4	48.5	0.48	0.86	0.81	1.06	2.5
		180	9.5	0.65	8.2	17.1	6.17	6.1	49.1	0.56	1.41	1.3	1.08	2.49
		200	8.5	0.80	9.3	19.9	7.4	9.3	47.2	0.24	2.80	2.64	1.06	1.90
2.0	0.1	180	19.3	0.8	12.8	10.8	7.70	10.9	50.4	tr.	2.53	2.69	0.94	2.56
1.0	0.05	180	9.6	0.23	1.5	10.8	2.2	5.7	50.2	tr.	1.13	-	-	4.58
	0.2		8.6	0.58	19.6	19.0	4.86	10.4	51.6	tr.	2.22	2.34	0.95	3.11
	0.3		9.3	0.51	23.4	12.0	3.67	6.9	49.6	tr.	1.28	1.5	0.85	2.26

* Specific surface area 0.64 m²/g
** V_c = 0.81

Table 2: The effects of temperature, initial acidity, and reaction time on the reaction of pyrite with copper sulphate solution [-44 μ fraction, pyrite consumption according to reaction (1)]

$C^o_{H_2SO_4}$ mole	t°C	τ min	Extraction %		ΔH_2SO_4 g/l	Precipitation of copper %				Molar ratio		
			S	Fe		Total		By double decomposition	$\frac{Q_e - Q_c}{Q_e}$	$\frac{Cu_S}{H_2SO_4}$	$\frac{Fe^{2+}}{H_2SO_4}$	$\frac{Cu_S}{Fe^{2+}}$
						Q_e	Q_c					
0.1	160	15	1.2	3.1	1.2	7.6	5.0	60.0	33.0	2.75	1.1	2.51
		30	1.5	3.3	1.5	9.9	5.5	59.2	41.3	3.03	1.06	2.87
		60	1.8	3.5	1.8	10.4	6.0	56.2	42.2	2.91	0.96	3.04
		180	2.2	4.3	2.2	11.9	7.7	55.8	35.8	2.62	0.94	2.78
	180	15	3.2	3.3	3.2	11.9	8.2	40.1	31.6	1.78	0.49	3.64
		30	3.6	3.5	3.5	12.8	9.0	39.5	30.4	1.79	0.50	3.59
		60	3.9	3.9	3.8	13.8	9.7	40.3	30.0	1.80	0.50	3.57
		180	4.9	4.7	4.8	16.7	12.0	39.0	28.6	1.73	0.49	3.54
	200	15	4.1	3.3	4.0	14.3	9.4	34.7	34.2	1.75	0.46	4.34
		30	5.5	3.5	5.4	16.4	11.8	29.8	27.7	1.49	0.32	4.56
		60	10.4	4.5	10.2	21.5	20.1	22.5	6.4	1.03	0.22	4.69
		180	18.9	14.2	18.4	42.6	42.4	33.6	0.6	1.13	0.38	3.01
0.25	200	1 0	15.4	12.7	15.1	36.3	35.8	35.5	1.4	1.19	0.42	2.85
0.50			10.2	9.0	10.3	27.4	24.8	36.6	9.6	1.32	0.44	3.04
0.75			7.2	6.5	7.1	20.9	17.2	37.2	17.4	1.45	0.45	3.2
1.00			4.4	4.9	4.3	13.5	11.4	42.8	14.9	1.54	0.55	2.77

$$H_2S + CuSO_4 \longrightarrow CuS + H_2SO_4 \quad (3)$$

The resultant reaction of elemental sulphur with copper sulphate is described by the equation

$$3CuSO_4 + 4S + 4H_2O = 3CuS + 4H_2SO_4 \quad (4)$$

The overall reaction with the formation of covellite (a simple double decomposition reaction) can be written as follows:

$$7CuSO_4 + 4FeS_2 + 4H_2O = 7CuS + 4FeSO_4 + 4H_2SO_4;$$
$$\Delta G^0 = -474.0 \text{ kJ/mole} \quad (5)$$
$$[Cu_s]:[H_2SO_4] = 1.75;\ [Fe^{2+}]:[H_2SO_4] = 1.0;\ [Cu_s]:[Fe^{2+}] = 1.75$$

The chalcocite is probably formed according to the reaction:

$$3CuSO_4 + 5CuS + 4H_2O = 4Cu_2S + 4H_2SO_4;$$
$$\Delta G^0 = -193.1 \text{ kJ/mole} \quad (6)$$

Thus, the reaction of pyrite with an acidified solution of copper sulphate in the general form can be written as follows:

$$2.8CuSO_4 + FeS_2 + 2.4H_2O = 1.4Cu_2S + FeSO_4 + 2.4H_2SO_4;$$
$$\Delta G^0 = -539.5 \text{ kJ/mole} \quad (7)$$
$$[Cu_s]:[H_2SO_4] = 1.17;\ [Fe^{2+}]:[H_2SO_4] = 0.42;\ [Cu_s]:[Fe^{2+}] = 2.8$$

Reactions (5) and (7) were investigated with 0.5 M $CuSO_4$ and pyrite B (table 2). (V K Pinigin took part in the investigation).

A sample of sulphide was taken in relation to its chemical and phase composition, the acid content (0.042 g H_2SO_4/g) and the stoichiometry of the reactions. During treatment of the experimental data it was assumed that all the iron is in the sulphide form; the precipitation of copper by the chalcopyrite (0.29%) and sphalerite (0.012%) which were present was disregarded on account of their low contents. From reaction (5), knowing the content of iron in the solution, we calculated the amount of precipitated copper and the amount of acid formed; the excess acidity [the difference between the experimental data and the acidity according to reaction (5)] was used to calculate the amount of copper precipitated according to reaction (6); at the same time we estimated the fraction of copper in the covellite [reaction (5)] in relation to the total amount of precipitated copper. Although the initial rates of precipitation of copper and dissolution of iron are 3-5 times lower in absolute value than in the kinetic experiments, the character of the positive effect of temperature and the negative role of the acid (with H_2SO_4 $_0 \geq 0.25$ M) on the characteristics of the process (table 2) is preserved. The observed activation energies for the precipitation of copper, dissolution of iron, and oxidation of the sulphide sulphur are comparable and are equal to 52.8, 46.1, and 54.2 kJ/mole respectively. Satisfactory agreement between the experimental and calculated data on the precipitation of copper was only obtained at 200°C with an initial acidity of ≤ 0.25 M

and a reaction time of not less than 60 min. The fact that the amount of precipitated copper according to the experimental data exceeds the calculated amount at t<200°C is explained not only by the role of the sphalerite and chalcopyrite present in the pyrite but also indicates the development of additional processes, leading to the precipitation of copper and not taken into account inthe adopted method of calculation. Since the iron in the pyrite and in the obtained solutions is present in the divalent form, the presence of α-Fe_2O_3 in the solid residue indicates oxidation of ferrous sulphate and hydrolysis of the ferric sulphate according to the following reactions:

$$2FeSO_4 + 2CuSO_4 = Cu_2SO_4 + Fe_2(SO_4)_3,$$
$$Cu_2SO_4 \rightleftarrows Cu + CuSO_4,$$
$$Fe_2(SO_4)_3 + 3H_2O = Fe_2O_3 + 3H_2SO_4,$$
$$2FeSO_4 + CuSO_4 + 3H_2O = Cu + Fe_2O_3 + 3H_2SO_4;$$
$$\Delta G^0 = -15.9 \text{ kJ/mole} \quad (8)$$

With allowance for reaction (7) the overall process is described as follows:

$$3.3CuSO_4 + FeS_2 + 3.9H_2O = 1.4Cu_2S + 0.5Cu + 0.5Fe_2O_3 + 3.9H_2SO_4;$$
$$\Delta G^0 = -45838 \text{ kJ/mole} \quad (9)$$

i.e., the copper ions exhibit oxidising characteristics. The development of reaction (9) reduces the amount of iron in the solution and, as a consequence, increases the $[Cu_{pr}]:[Fe^{a+}]$ ratio and reduces the $[Cu_s]:[H_2SO_4]$ and $[Fe^{a+}]:[H_2SO_4]$ ratios; this agrees with the results from the experiments (tables 1 and 2) carried out under conditions securing the hydrolysis of ferric sulphate ($[H_2SO_4]_c \leq 0.1$ M and $t \geq 180°C$). An increase in acidity retards the development of the hydrolysis of ferric sulphate and at the same time promotes direct breakdown of the pyrite with the formation of hydrogen sulphide, which actively reduces the ferric ions to the ferrous ion according to the reaction

$$H_2S + 4Fe_2(SO_4)_3 + 4H_2O \longrightarrow 8FeSO_4 + 5H_2SO_4;$$
$$\Delta G^0 = -456 \text{ kJ/mole} \quad (10)$$

which excludes the precipitation of copper according to reaction (8) and increases the amount of dissolved iron. The $[Cu_s]:[Fe^{2+}]$ and $[Fe^{a+}]:[H_2SO_4]$ values must be lower and approach the stoichiometry of reaction (7), and this agrees with the experimental data. Similar arguments hold for the disproportionation of the elemental sulphur according to reaction (2), which occurs quantitatively only at $t \geq 200°$, securing the stoichiometry of reaction (7).

Thus, in the reaction of pyrite with an acidified solution of copper sulphate reaction (1) occurs primarily with the formation of a layer of covellite and elemental sulphur on the surface of the pyrite. Using the Pilling-Bedworth criterion as a characteristic of the permeability of the solid film, we can assume that the layer of covellite creates appreciable hindrances ($K_{PB} = 0.87$) for the diffusion of copper ions to the surface of the pyrite. Additional diffusion complications are presented by the viscous layer of molten elemental sulphur, which (to judge from its content in the cake at temperatures above

160°C) hydrolyzes appreciably in the presence of copper sulphate. Therefore, at a temperature of more than 160°C the overall double decomposition reaction leads to an additional increase in the amount of covellite. (According to the stoichiometry of reactions (1) and (5), the molar $CuS:FeS_2$ value increases from 1 to 1.85). This screens the pyrite even more and at the same time creates conditions for effective reaction of the freshly precipitated covellite with copper sulphate solution according to reaction (6), and the overall process is described by reaction (7). The film of lower copper sulphide which forms is less permeable (K_{PB} = 1.66), and this intensifies the hindrances to diffusion of copper sulphate to the pyrite. The amount of chalcocite or covellite is determined by the ratio of the kinetics of reactions (5) and (6). The rate of reaction (6) depends significantly on temperature (E_a = 107.8kJ/mole). Therefore reaction (7) is the main reaction at $t \geq 180°C$; with decrease in temperature the role of reactions (1) and (8) becomes appreciable. The acid content has a significant effect on the characteristics of the reaction of pyrite with copper sulphate solution.

Thus, the rate of the reaction of pyrite with copper sulphate is extremely insignificant under hydrothermal conditions. The inertness of pyrite is due not only to characteristics of the structure of its crystal lattice but also to the impermeable films of copper sulphides which form and also to the formation of elemental sulphur, the complete hydrolysis of which is achieved at temperatures above 200°C. Consequently, during hydrothermal activation of copper, copper-zinc, and other concentrates the breakdown of the pyrite will be insignificant, and this will lead to incomplete extraction of the isomorphous zinc and cadmium sulphides.

References

1) S S Naboichenko et alia: Tsvetnye Metally 1978, (6), 8-11.

UDC 669.536

Kinetics of oxidative roasting of sulphide concentrates in a fluidised bed

L A Danilin, A S Malyugin, and L V Prede (North-Caucasian Mining-Metallurgical Institute - Department of General Metallurgy)

There are published data on the mechanism and kinetics of the oxidation of zinc sulphide concentrates (and of zinc sulphide in particular) and on the behaviour of other substances (iron, silicon dioxide, lead, etc.) and their effect on the quality of the calcine. It is characteristic that the kinetic relationships are represented in the form of the degree or rate of desulphurisation or ferrite formation with time, temperature, particle size, amount of air blast, and oxygen concentration. As a rule, the relationships governing desulphurisation were determined from the amount of sulphur dioxide and sulphur trioxide released after specific intervals of time. Most of the kinetic relationships were obtained for short time intervals, whereas the calcine is present in the industrial furnaces for periods ranging from several minutes to tens of hours. The processes occurring in the solid phase have been insufficiently investigated, and there is little information on the effect of the duration and temperature of roasting on such a quality characteristic as the content of acid-soluble zinc in the calcine during fluidised-bed roasting in the range of 900-1000°C, which corresponds to the working conditions in the majority of foreign plants.

The kinetics of the oxidation of zinc sulphide concentrates were investigated on fluidised-bed apparatus consistent of a fluidised-bed reactor situated in an electric resistance furnace, an air delivery system, and automatic control and regulation systems. The reactor was made of 19Kh20N10T steel. The internal diameter of the working part of the reactor was 50min. The material was unloaded by lowering the bottom part of the reactor with a perforated base. The material from the working part was transferred to a quartz glass test tube in a flask of cold water.

The temperature in the bed was controlled and regulated by means of a system consisting of a CA thermocouple, a KSP-3-2300 potentiometer, and an MKRO-58 magnetic starter. The air consumption rate was controlled by means of an RS-5 rotameter, and the pressure drop in the bed was monitored by means of a differential manometer filled with water. The concentration of sulphur dioxide in the outgoing gases was measured by a gas analyser of the TKG-4Ts type.

Zinc sulphide concentrates of the -200 +125 and -100+80μ fractions were submitted to roasting. They came from three deposits (Sadon, El'brus, and Fiagdon) differing in the contents of zinc, sulphur, iron, and silicon dioxide (table 1). X-ray crystallographic analysis revealed the following minerals in the Sadon concentrate (in decreasing order): Wurzite, sphalerite, pyrrhotite, pyrite, quartz, galena.

The composition of the Sadon concentrate was established by mineralogical analysis %: 75 sphalerite, 15 pyrrhotite, 3 pyrite, 5 chalcopyrite, 0.8 quartz, 0.2 calcite. In the El'brus concentrate the sphalerite constantly contained an emulsion-type impregnation of chalcopyrite and very often galena and pyrite. The composition of the Fiagdon concentrate was as follows%: 70-75 sphalerite, 13-15 pyrite, 3-4 chalcopyrite, 1-1.5 galena, 3-4 quartz.

Roasting was realized at 920, 940, 960, 980, and 1020°C (but only at 980°C for the Fiagdon concentrate). The air consumption rate amounted to 1.0 m^3/h to the reactor, which corresponded to a nominal linear rate of 14 cm/sec, for the -200+125μ fractions, and 0.8 m^3/h (11 cm/sec) for the -100+80μ fractions. It was established that for both fractions change in the air consumption rate from 0.8 to 1.0 m^3/h did not have an appreciable effect on the phase composition of the calcines roasted at 960°C for 5 and 10 min but appreciably affected the dust removal.

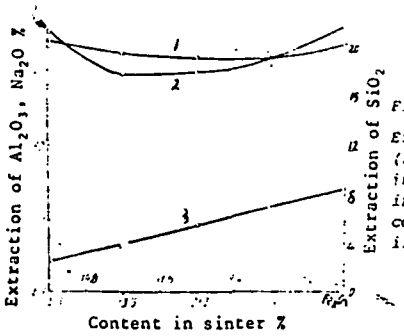

Fig. 3

Extraction of Al_2O_3 (1) Na_2O (2) and SiO_2 (3) from sinters into solution for the sintering of charges with various contents of silica and of iron in the form of haematite.

With further increase of the iron oxide content and simultaneous decrease of the silica content of the charge the extraction of the valuable components increased. At the same time, the extraction of silica into solution increased. The sintering temperature range became wider.

The identical effect of haematite, magnetite and siderite on the sintering process is explained as follows. On heating, siderite decomposes into ferrous oxide and carbon dioxide. The obtained ferrous oxide and also the magnetite are oxidised, being converted into ferric oxide. Moreover, the oxidation is complete before the ferric oxide begins to react with the soda.

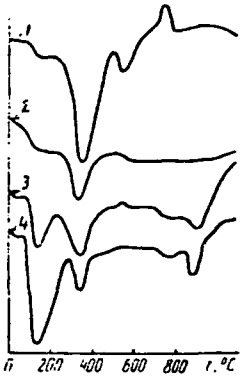

Fig. 4

Thermograms of some of the products: Weakly magnetic siderite (1) strongly magnetic magnetite (2) charges of siderite (3) and magnetite (4) concentration products.

This conclusion is confirmed by the results from differential thermal analysis. The thermograms of the strongly magnetic and weakly magnetic concentration products and of the charges containing these products are given in fig. 4. Siderite and magnetite are converted into ferric oxide when heated to 600°C (exothermic peaks at 575 and 510°C, curves 3-4), whereas the chemical reaction in the charges begins at higher temperatures of 770-890°C (curves 3 and 4).

Curves 1 and 2 in figs. 1-3 have minima, showing that the sinters enriched with silica and ferric oxide contain more alkali and alumina in the insoluble form. It was found that these sinters contain the compounds $2Na_2O \cdot 2CaO \cdot 5SiO_2$ and $4CaO \cdot Al_2O_3 \cdot Fe_2O_3$, which do not decompose during leaching of the sinter[4]. Apart from the above-mentioned compounds, alkaline silicates of iron such as $Na_2O \cdot Fe_2O_3 \cdot 4SiO_2$, which lead to losses of alkali during leaching of the sinter, can form under analogous conditions.

We note that in the oxidation of siderite and magnetite during the heating of the charge a more active ferric oxide is formed in comparison with haematite. The extraction of the valuable components is therefore somewhat lower in the case of the sintering of charges containing siderite, magnetite and iron hydroxides compares with haematite charges.

The results show that a high extraction of the valuable components can be obtained from sinters containing much silica (more than 15%) but little ferric oxide (less than 7%) or, conversely, with a large content of iron oxide (more than 32%) and a small content of silica (less than 3.5%). The sintering temperature range for such charges amounts to 200-250°C. Thus, high-silica but low-iron bauxites and also high-iron and low-silica bauxites can be successfully processed to alumina by the sintering method with good technological characteristics.

References

1) V A Derevyanki et alia: Rational utilisation of low-grade bauxites: Moscow Metallurgizdat 1972.
2) F F Fedyaev et alia: Tsvetmetinformatsiya Tsvetnaya Metallurgiya 1971, (3), 21.
3) F F Fedyaev et alia: Tsvetmetinformatsiya Tsvetnaya Metallurgiya 1973, (22), 28.
4) O I Arakelyan: Legkie Metally Giproalyuminii 1957, (3). 54.

UDC 669.223.421

Kinetics of the dissolution of silver chloride in aqueous solutions containing chloride ions

I A Kakovskii and V V Gubailovskii (Urals Polytechnical Institute. Department of the Metallurgy of Noble Metals)

Previous articles[1,2] gave the results from investigations into the kinetics of the dissolution of AgCl in aqueous solutions of cyanides, thiosulphate, ammonia and thiourea. However, chloride solutions can also be used as a solvent for silver. They can be used both for the extraction of silver from chlorination products and to improve the hydrochlorination of silver-bearing gold[3]. In the reaction of silver chloride with chloride ion in dilute solutions the following reaction occurs:

$$AgCl + Cl^- = AgCl_2^-$$

(according to our data $K^0_{298} = 3.1 \cdot 10^{-5}$), and in the more concentrated solutions having practical significance the following reaction occurs:

$$AgCl + 2Cl^- = AgCl_3^{2-}$$

($K^0_{298} = 5.5 \cdot 10^{-6}$). The equilibrium constants of these reactions are low, and to obtain a sufficiently high silver content in the solutions it is therefore necessary to increase the chloride ion concentration.

The kinetics of the dissolution of silver chloride in solutions of sodium chloride, as the cheaper reagent, were therefore studied in greater detail, and only individual experiments were carried out for comparison with ammonium chloride and hydrochloric acid. The rotating disc method was used[5]. However, the character of the kinetics and the method of the calculations were somewhat different in the present work. The high concentration of the reagent-solvent and the comparatively low concentration of silver in the solution make it possible to suppose that the process rate will be determined not by diffusion of sodium chloride to the surface of the disc, but by the rate of removal of the reaction product (the Na_2AgCl_3 complex). Under diffusion conditions this corresponds to the equation:

$$\frac{dQ}{d\tau} = kS(c_s - c)n^{1/2}$$

and the dissolution rate must decrease with increase in the silver concentration of the solution in proportion to the decrease in the co-factor ($c_s - c$). This can be illustrated by fig. 1, which was plotted from our data (25°C, 500rpm, disc surface area 10.2cm², concentration of chlorides 5.0moles/litre, volume of solution 1 litre).

The curved nature of the kinetic curves complicates the treatment of the experimental data. However, a different

kinetic equation can be used, i.e.

$$\lg \frac{c_s}{c_s - c} = \frac{kSn^{1/2}}{2.303V} \quad \text{or} \quad \lg (c_s - c) = \lg c_s - \frac{kSn^{1/2}}{2.303V}$$

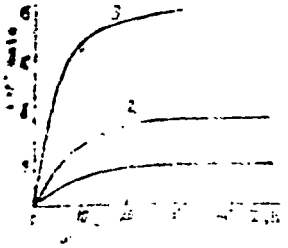

Fig. 1

Dependence of the dissolved [illegible] on the [illegible] HCl [illegible]

The experiments were carried out [illegible] sampling of the solution to determine the silver [illegible] them (by the xanthate method). At the end of the experiment silver chloride pellets were added to the reaction vessel, and the solution was stirred until equilibrium was attained (usually two days), after which the concentration of silver (c_s) and chloride ion was determined (several control tests). Since the equation contains the volume of the solution, and the volume varied as a result of sampling, the equation was modified a little:

$$\lg (c_s - c) = \lg c_s - k' \sum \frac{\tau}{V} \quad (*)$$

We will illustrate the method (table 1) as exemplified by one of the experiments (25°C, 615rpm, sodium chloride concentration 3.38moles/litre, initial volume of solution 1200ml, surface area of disc 4.91cm²).

$$\lg k = -2.746 - \frac{962}{T}$$

The experimental activation energy is 4.0kcal/mole, and the reaction rate constant at 25°C is $1.06 \cdot 10^{-4}$ litre/cm² · sec$^{1/2}$ · rev$^{1/2}$. This value is somewhat higher than in normal reactions taking place under diffusion conditions, and with increase in temperature not only does the diffusion rate increase and the viscosity of the solution decrease but the solubility of silver chloride in the aqueous solutions of sodium chloride increases. An analogous relationship has been observed[1]) in the dissolution of silver chloride in aqueous solutions of sodium thiosulphate (ΔE = 5.03kcal/mole) and ammonia (ΔE = 4.58kcal/mole). It is very important to note that when silver chloride is dissolved in sodium chloride solutions the activation energy does not depend either on the concentration of the reagent-solvent or on the intensity of agitation of the solution.

Let us define the nature of the investigated reaction more precisely. The dependence of the dissolution rate on the square root of the disc rotation rate is most convincing evidence for the fact that the process is controlled by diffusion. From the fact that the reaction rate constant does not depend on the sodium chloride concentration it follows that the slow link in the process is diffusion of the reaction product (the silver chloride complex). However, the sodium chloride concentration, while not affecting the rate constant, has an appreciable effect on the dissolution rate, since

$$\dot{V} = \frac{Q}{S\tau} = k(c_s - c)$$

and the limiting solubility of silver chloride (c_s) increases very strongly with increase in the concentration of sodium chloride in the solution.

By means of the value obtained for the reaction rate it is possible also to obtain a value for the diffusion coefficient

Table 1

Interval between samples h.	Volume of solution ml	Concn. of silver g-ion/l	$\frac{\tau}{V}$	$\sum \frac{\tau}{V}$	$\lg \frac{c_s}{c_s - c}$	k'
1.5	1200	$1.27 \cdot 10^{-4}$	1.25	-	0.0318	0.0254
1.5	1000	2.69	2.69	2.75	0.0703	0.0256
1.0	900	3.67	3.67	3.86	0.0990	0.0256
1.0	800	4.68	4.68	5.11	0.1308	0.0256
1.0	700	5.78	5.78	6.54	0.1681	0.0257
		$c_s = 1.83 \cdot 10^{-3}$				

From the average value of the reaction rate (0.0256litre/h) the rate constant was calculated in normal units:

$$k = \frac{2.303k'}{3.6 \cdot 10^3 Sn^{1/2}} = \frac{2.303 \cdot 0.0256}{3.6 \cdot 10^3 \cdot 4.91 \cdot 3.205} = 1.04 \cdot 10^{-6} \text{ l/cm}^2 \cdot \text{sec}^{1/2} \cdot \text{rev}^{1/2}$$

A series of experiments was set up to determine the effect of the number of revolutions of the disc on the dissolution rate (25°C, sodium chloride concentration from 3.38 to 5.42moles/litre, number of revolutions 295-1815 per minute). The results from part of these experiments are given in fig. 2. The average value of the rate constant is $1.06 \cdot 10^{-6}$ and, which is very important, does not depend on the sodium chloride concentration.

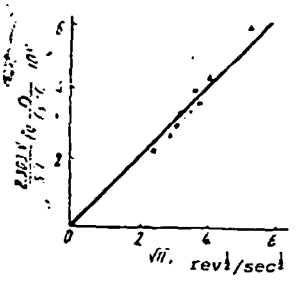

Fig. 2

Dependence of the specific dissolution rate of silver chloride on the square root of the number of revolutions of the disc per second; sodium chloride concentration mole/l ● - 3.38; x - 4.08; ▲ - 4.38; ■ - 4.85.

The effect of temperature was investigated in the range between 15 and 55°C. The dependence of the rate constant on temperature can be expressed in terms of the equation:

of the complex Na_2AgCl_3 at 25°C in concentrated solutions of sodium chloride, since they are related by the following equation:

$$k = \frac{6.18 \cdot 10^{-4} (2\pi)^{1/2} D^{2/3}}{\nu^{1/6}}$$

$$D^{2/3} = \frac{1.06 \cdot 10^{-6} \nu^{1/6}}{6.18 \cdot 10^{-4} (2\pi)^{1/2}} = 6.84 \cdot 10^{-4} \nu^{1/6}$$

For 3.0, 4.0 and 5.0M solutions of sodium chloride the kinematic viscosities are 1.096, 1.228 and $1.385 \cdot 10^{-2}$ cm²/sec, and the diffusion coefficients are 0.58, 0.595 and $0.61 \cdot 10^{-5}$ cm²/sec. These values agree very closely with the data obtained by Berne and Weill[5]) by an independent radiochemical method.

The rate constants for the dissolution of silver chloride in aqueous solutions of hydrochloric acid and ammonium chloride are 1.45 and $1.68 \cdot 10^{-6}$ litre/cm² · sec$^{1/2}$ · rev$^{1/2}$. However, in spite of the large value of the rate constant, the dissolution rate of silver chloride (with identical concentrations of the complexing agent) is lower in hydrochloric acid solutions than in sodium chloride solutions (fig. 1). This is explained by the lower solubility of silver chloride in hydrochloric acid solutions and, consequently, by the lower value of the co-factor ($c_s - c$) in the kinetic equation. In solutions of ammonium chloride, however, the dissolution rate is higher than in solutions of sodium chloride on account of the higher solubility of silver chloride in them. Thus, for example, with the complexing agent at a

concentration of 5.0M the solubility of silver chloride in ammonium chloride, sodium chloride and hydrochloric acid solution is 1.60, 0.70 and $0.38 \cdot 10^{-2}$ mole/litre (at 25°C).

In conclusion we will compare the relative effectiveness of the silver chloride solvent reagents which we investigated using for this purpose the rate constants of the dissolution reactions (table 2) occurring under diffusion conditions.

Table 2

Complexing reagent	Rate constant $k \cdot 10^6$ $l/cm \cdot sec^{1/2} \cdot rev^{1/2}$	Activation energy kcal/mole
Potassium cyanide	0.78	-
Sodium cyanide	0.68	-
Ammonia	0.12	4.58
Sodium thiosulphate	0.52	5.03
Thiourea	0.60	3.45
Sodium chloride	1.06	4.40

From the data presented in table 2 it follows that sodium chloride is not inferior to other complexing agents in its kinetic characteristics and has a series of advantages over them, i.e. non-toxicity, cheapness and availability. When used, it is necessary to pay attention to the choice of optimum concentration, which is determined by the silver content in the material being treated. The results from the investigation can be used for calculations of the sodium chloride concentration required for hydrochlorination of silver-bearing gold[3]).

References

1) I A Kakovskii and V V Gubailovskii: Dokl. Akad. Nauk SSSR 1969, 184, (5), 1157.

2) V V Gubailovskii et alia: Tsvetnye Metally 1972, (5), 32.

3) I N Plaksin: Metallurgy of noble metals: Moscow Metallurgiya 1958, p. 324.

4) I A Kakovskii and O K Shcherbakov: Izv Akad. Nauk SSSR Metally 1967, (5), 76.

5) E Berne and M J Weill: J. Phys. Chem 1960, 64, (2), 258.

UDC 661.183

Investigation of the composition of sorbed molybdenum ions of anion-exchange resins by an IR-spectroscopic method

L V Vasilenko and E I Kazantsev (Urals Polytechnical Institute. Department of the Metallurgy of Rare Metals)

Summary

The IR spectra of macroporous highly basic ion-exchange resins in the Cl form were recorded after contact with a solution of molybdenum. During the sorption process at pH = 9 the spectrum initially contains two absorption bands characteristic of the sorption of molybdenum in the form of the monomeric MoO_4" ions. During sorption a considerable increase in the pH value of the filtrate was observed. This effect can be explained by the formation of a complex polycompound with bridging hydrogen bonds consisting of MoO_4" ions and H_2MoO_4 molecules.

At pH = 5 the IR spectrum indicates complication in the composition of the sorbed molybdenum ions and the formation of tetramolybdate ions $Mo_8O_{26}^{4-}$.

The results confirmed earlier conclusions about the composition of molybdenum ions sorbed on ion-exchange resins.

UDC 669.72.15

Cavitation-resistant aluminium bronze alloyed with nickel, manganese and titanium

M V Stepanova, Yu P Kosikhin, F A Bronin and B A Agranat (Moscow Institute of Steel and Alloys. Department of the Physical Metallurgy of Non-Ferrous, Rare and Radio-active metals)

The present work is a continuation of investigations[1-3]) which are being carried out with a view to increasing the cavitation resistance of aluminium bronzes for use in ultrasonic equipment. The resistance to high-intensity cavitation (excess pressure in chamber 0.4MPa[4])) is being investigated in aluminium bronze BrA12 of eutectoid composition, alloyed with nickel (3-4%), manganese (2-3%) and titanium (0.2-0.3%) to improve the strength and anti-corrosion characteristics.

It is well-known [5]) that the highest grain refinement in aluminium bronzes is obtained with an iron content of 4% and that there is a simultaneous increase in the amount of the X-phase, i.e. in our case, evidently, seats of cleavage, at which brittle fracture of the bronze can occur under powerful ultrasonic influence. The replacement of 3-4% iron by only 0.2-0.3% titanium leads to greater grain refinement and to increased cavitation resistance in aluminium bronzes[1]).

The cavitation resistance of Br.AMtsNT12-3-3-0.25 bronze (Author's Certificate No. 377381, 27 March 1972) was compared with the cavitation resistance of the binary (aluminium) bronze BR.A12, with two standard bronzes Br.AMts9-2 and Br.A10, and with Kh18N10T steel, used for the radiators of ultrasonic devices.

All these bronzes were tested in the hot-rolled and then in the water-quenched (from the β-region) states (heating temperature under quenching 800-850°C for Br.A12 and Br.AMtsNTZ-3-0.25). The structure was a martensitic β'-phase. For Br.AMtsNTZ9-2 and Br.A10 the heating temperature under quenching was 980-1000°C. The structure was excess α phase against a background of martensitic β'phase [1]). The experimental procedure and conditions were described earlier[1]).

The rate of the losses in weight and the weight losses in a 25h test are given in the table. (The rate of the weight losses was determined from the "loss in weight-ultrasonic treatment time" curves during the period of intense increase in the weight losses). From the data in the table it follows that the complex-alloyed bronze Br.AMtsNT12-3-3-0.25, containing the added elements within the limits of 11.8-12.3% Al, 2-3% Mn, 3-4% Ni, 0.2-0.3% Ti surpasses Kh18N10T steel in cavitation resistance by 5 times, standard bronzes Br.A10 and Br.AMts9-2 by two times, and Br.A12 by 1.5 times. In contrast to the materials being compared with it, there were no traces of erosion on the surface of samples of Br.AMts-NT12-3-3-0.25 bronze after 25h ultrasonic cavitation treatment.

The surface hardness of the samples (fig.) changes during ultrasonic cavitation treatment. In relation to its cavitation resistance the material is characterised by the character of the change in hardness together with the weight losses. The greatest increase in hardness is achieved after ultrasonic treatment for 1h. For the cavitation-resistant materials Br.A12 and Br.AMtsNT12-

UDC 669.3.053.

Kinetics of the oxidation of metallic copper by copper ions in ammoniacal sulphate solutions

S E Klyain, S V Karelov, T A Chemezova and A P Doroshkevich (Urals Polytechnical Institute. Department of the Metallurgy of Heavy Nonferrous Metals)

The use of ammoniacal solutions for the treatment of copper-containing materials has a series of advantages compared with other solvents on account of their selectivity, the high dissolution rate of the copper, and the comparative simplicity of the treatment of the obtained solutions. It is known that metallic copper is readily oxidised by divalent copper ammoniates[1]). An extremely limited number of researches have been undertaken for ammoniacal carbonate solutions[2])[3]); there are hardly any such data for ammoniacal sulphate solutions. The aim of the present work was to study the effect of the composition of the ammoniacal sulphate solutions, the temperature, and the intensity of agitation on the dissolution rate of metallic copper by means of a rotating disc. The solutions were prepared from reagents of pure and chemically pure grades with distilled water. The amount of combined ammonia was calculated on the formation of copper tetra-amine. Discs 2cm in diameter were prepared from an annealed rod of copper of grade MOO. The discs were prepared for the experiment by the method described in the literature[2]). The volume of the working solution amounted to 1 l. The cell containing the disc was thermostated, and the temperature was controlled with an accuracy of $\pm 0.2^{\circ}C$.

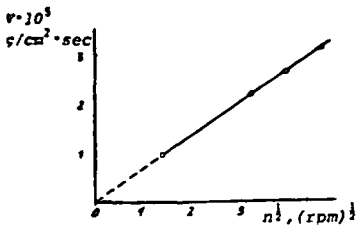

Fig.1 *The dependence of the copper dissolution rate in a solution of 0.2M Cu^{2+} $(NH_4)_2SO_4$ + 2.4M NH_3^{free} on the disc rotation rate.*

In order to prevent oxidation of the copper by oxygen the experiments were carried out in an atmosphere of argon. By preliminary tests it was established that dissolution did not occur when the disc was rotated at 300 rpm for 2h in a solution containing 2.0M NH_3 + 0.5 M $(NH_4)_2SO_4$. The dissolution rate of the copper was determined from the loss in the weight of the disc. The dependence of the dissolution rate of the copper disc (V) on its rotation rate is shown in fig.1. The proportionality of the dissolution rate to the square root of the rotation rate of the disc shows that the process takes place under conditons controlled by mass transfer. Analogous results were obtained with variation of the copper content of the solution between 0.1 and 0.0 M, and of the total ammonia content between 0.5 and 4.0 M.

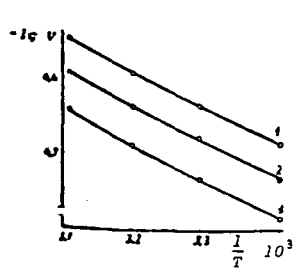

Fig.2 *The dependence of the copper dissolution rate in the same solution on temperature with the following disc rotation rates, rpm: 1 - 670; 2 - 340; 3 - 170.*

The effect of temperature on the copper dissolution rate was studied in the range of 20-48°C. The upper temperature limit was restricted by appreciable losses of ammonia. At 48°C the losses of ammonia in 1h were not greater than 12-15%. All the initial kinetic relationships against the loss in weight of the disc and time gave straight lines. The temperature dependence for various disc rotation rates is shown in fig.2. The calculated activation energy of the copper dissolution process for all disc rotation rates amounted to 6.9 ± 0.3 kcal/mole. With increase in temperature from 20 to 40°C the copper oxidation rate increases by approximately twice. In a solution containing 0.2 M Cu^{2+}, 2.4 M $NH_{3\,free}$, and 0.5 M $(NH_4)_2SO_4$ the copper dissolution rate obeys the relationship:

$$V = 88.76 \cdot 10^3 \exp\left(-\frac{6900}{RT}\right) n^{0.5}$$

where V = the copper dissolution rate, $g/cm^2 \cdot sec$
n = the disc rotation rate, rps.

The theoretical rate constant for the copper dissolution process calculated by means of the equation

$$K = \frac{6.18 \cdot 10^{-4}\, D^{2/3} (2\pi)^{0.5}}{m\nu^{1/6}} \quad (l/cm^2 \cdot sec^{\frac{1}{2}} \cdot rps^{\frac{1}{2}})$$

is equal to $1.07 \cdot 10^{-6}$, which is twice as high as the value obtained experimentally is the same solution ($0.51 \cdot 10^{-6}$). The reason for this is clearly the fact that two ions of monovalent copper are formed for one reacting ion of divalent copper in the process

$$Cu(NH_3)_4^{2+} + Cu^{0} \rightarrow 2Cu(NH_3)_2^{+}$$

i.e., the process is controlled by the rate of removal of the reaction products. The kinematic viscosity of a solution containing 0.2 M Cu^{2+}, 2.4 M $NH_{3\,free}$, and 0.5 M $(NH_4)_2SO_4$ was measured at 21°C and is equal to $11.45 \cdot 10^{-3}$ cm^2/sec; the diffusion coefficient of the Cu^{2+} ion was taken from the literature[3]) and amounts to 6.10^{-6} cm^2/sec; m is a stoichiometric coefficient of the reaction, equal to one. An increase in the content of Cu^{2+} ions in the solution increases the copper dissolution rate (fig.3a); in the range of variation of the copper concentration between 0.2 and 0.8 M it increases in proportion to the copper concentration raised to a power 0.5. For a disc rotation rate of 190 rpm with 0.88 M $NH_{3\,free}$ in the solution the copper dissolution rate is described by the equation

$$V = 3.55 \cdot 10^{-5} C^{0.5} \exp\left(-\frac{E}{RT}\right)$$

The effect of the ammonium sulphate concentration on the viscosity and density of the solution at 30°C

Concentration of $(NH_4)_2SO_4$ mole/l	Dynamic viscosity cP	Density g/cm^3	Kinematic viscosity cm^2/sec
-	0.916	1.049	0.8732
0.25	0.980	1.065	0.9197
0.50	1.041	1.082	0.9621
0.75	1.104	1.098	1.0054
1.00	1.166	1.114	1.0466
1.25	1.228	1.130	1.0862

The effect of free ammonia on the copper dissolution rate was investigated in a solution containing 0.4 M Cu^{2+} + 0.5 M

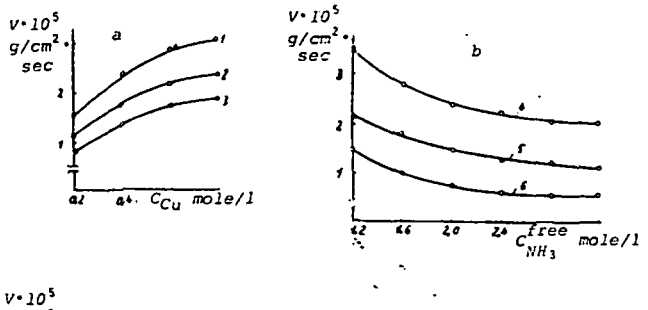

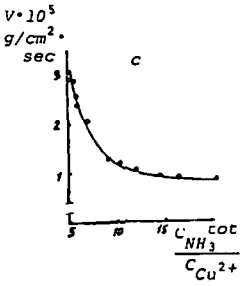

Fig.3 The dependence of the copper dissolution rate on the concentration of Cu^{2+} (a), the concentration of NH_3^{free} (b), and the ratio $C_{NH_3}^{tot}/C_{Cu^{2+}}$ (c). 1 - 0.88M NH_3^{free}; 2 - 1.6M NH_3^{free}; 3 - 2.0M NH_3^{free}; 4 - 40°C; 5 - 30°C; 6 - 22.5°C (190rpm).

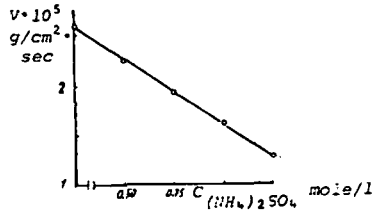

Fig.4 The effect of the ammonium sulphate concentration on the copper dissolution rate in a solution of 0.4M Cu^{2+} + 1.6M NH_3^{free} at 30°C and 190rpm

$(NH_4)_2SO_4$ at various temperatures (fig.3b). The dissolution rate of copper decreases particularly noticeably with increase in the free ammonia content to 2.4 mole l. For the same conditions (190 rpm, 30°C) fig.3c shows the dependence of the copper dissolution rate on the ratio of the concentration of total ammonia to the concentration of copper in the solution. The dissolution rate decreases abruptly at a ratio $C_{NH_3}^{tot}/C_{Cu^{2+}} > 10$: at values above 15 the copper dissolution rate decreases slightly. This relationship is described by the empirical equation

$$V = 270.155\left(\frac{C_{NH_3}^{tot}}{C_{Cu^{2+}}}\right)^{-2.84} - 0.786$$

The effect of ammonium sulphate on the copper dissolution rate was studied in a solution containing 0.4 M Cu^{2+} and 1.6 M $NH_{3\,free}$, where the ratio of the amount of free ammonia to combined ammonia was unity. The concentration of ammonium sulphate in the solution was varied between 0.25 and 1.25 M. This series of experiments was carried out at 30°C with a disc rotation rate of 190 rpm. The obtained experimental data (fig.4) show that the copper dissolution rate decreases linearly with increase in the ammonium-sulphate concentration. Since the dissolution rate of the rotating disc depends both on the kinematic viscosity ($\gamma^{-1/6}$) and on the diffusion coefficient ($D^{2/3}$), which is related to the dynamic viscosity ($D = const/\mu$), experiments were set up to determine the viscosity and density of solutions with various concentrations of ammonium sulphate. The results are given in the table.

With increase in the ammonium sulphate concentration from 0.25 to 1.25 M the copper dissolution rate changes from $2.7 \cdot 10^{-5}$ to $0.26 \cdot 10^{-5}$ g/cm²·sec, i.e., decreases by a factor of 2.14. According to the obtained experimental data the ratio of the copper dissolution rates as a function of the variation in the viscosity and density (e.g., with ammonium sulphate concentrations of 0.25 and 1.25 M) is determined by the expression:

$$\frac{V_1}{V_2} = \left(\frac{\mu_2}{\mu_1}\right)^{5/3}\left(\frac{\rho_1}{\rho_2}\right)^{2/3} = \left(\frac{1.228}{0.980}\right)^{5/3}\left(\frac{1.065}{1.130}\right)^{1/3} = 1.20$$

The calculation shows that the decrease in the copper dissolution rate cannot be attributed solely to diffusion limitations due to the increasing of the solution. The addition of ammonium sulphate evidently increases the concentration of NH_4^+ ions and shifts the equilibrium of the reaction $NH_4^+ + OH^- \rightleftarrows NH_3 + H_2O$ towards an increase in the concentration of free ammonia. The established relations between the copper dissolution rate and the $C_{NH_3}^{tot}/C_{Cu^{2+}}$ ratio and the $(NH_4)_2SO_4$ content are clearly due to the formation of more complex copper amines with increase in the concentration of the ligand and are brought about by statistical factors and by increased steric hindrances (4, pp.181, 182).

Conclusions

1. The oxidation of metallic copper by divalent copper amminiates in an ammoniacal sulphate solution takes place under diffusion control, the intensity of agitation is an important factor in the intensification of the process.
2. In order to obtain high copper dissolution rates in the absence of oxygen it is necessary to have the smallest possible content of free ammonia in the solution.
3. The best kinetic characteristics can be achieved by increasing the temperature of the dissolution process.

References

1) I A Kakovskii et alia: Dokl. Akad. Nauk SSSR 1960, **130**, (4), p.812.
2) K A Smith et alia: International Symposium on Hydrometallurgy, New York 1973, p.262.
3) M I Nicol et alia: Inst. Mining and Met., 1975, (1).
4) F Cotton et alia: Inorganic Chemistry. Mir, Moscow 196

UDC 669.3'24.476

Polarisation of a copper electrode in an ammoniacal electrolyte

V I Rybnikov, S V Karelov, A P Doroshkevich, I F Khudyakov and N V Ishchenko (Urals Polytechnical Institute)

Summary

The effect of the concentrations of copper, zinc, ammonia, and ammonium sulphate in the solutions on the overall polarisation of a copper electrode was studied. It was established that the steady-state potential is shifted towards electronegative values and the polarisation values and the limiting current of the electrodes vary with increase in the concentration of each of the components (except copper). Zinc has an extremely significant effect on the limiting passivation current of the anode, which amounts to i_{lim} = 37.5mA/cm² in the absence of zinc and rises to 67.5 mA/cm² with a Cu:Zn molar ratio of 1:3. To prevent the joint discharge of copper and zinc ions the concentration of zinc in the electrolyte must be limited to a Cu:Zn ratio of 1:2. The optimum in the investigated system is an electrolyte containing 0.2-0.5 mole/l of Cu, 0.5-0.75 mole/l of $(NH_4)_2SO_4$, 1.0-1.2 mole/l of $NH_{3\,free}$ and up to 0.5 mole/l of Zn.

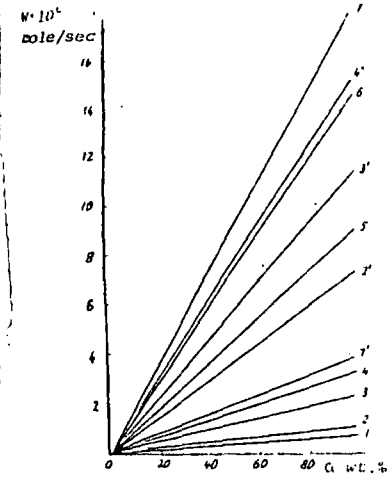

Fig.4 The relation between the rate of the purification process and the degree of conversion. c_i of phenol 12.4mg/l. V_w ml/min: 1 - 0.325; 2 - 0.480; 3 - 1.0; 4 - 1.4; 5 - 4.2; 6 - 6.8; 7 - 8.3. c_i of phenol 42.0mg/l. V_w ml/min: 1' - 0.50; 2' - 0.96; 3' - 1.52; 4' - 2.00.

For any A it is possible to plot a curve for the dependence of the process rate on the degree of conversion. From the obtained calculated data we plotted these relationships for initial phenol concentrations of 12.4 and 42.0mg/l (fig. 4). As seen from the curve, various degrees of conversion of the contaminant can be obtained for the same delivery rate, depending on the volume of the packing.

Conclusions

1. It is possible to use an ozone-containing gas with ozone concentrations of less than 0.01 vol.% for the purification of industrial effluents containing up to 42mg/l of phenol.
2. Columns filled with a porous packing can be used as reaction vessels for the oxidation.
3. The obtained experimental and calculated data make it possible to select the amount and form of packing required for a given degree of purification.

References

1) Bilitzky Laszlo, et alia: Magy. Kem. Lapja 1974, 29, (10), 520.
2) Problems of the contamination of the atmosphere and water arising in ferrous metallurgy: UNO. New York 1970.
3) Kh A Loorits: Author's Abstract of Thesis: Tallin 1968.

yoj Soo. Non-Fe metals v 6, No Research, 1978

UDC 669.2

Kinetics of the leaching of pyrrhotite by ferrous sulphate solutions

A L Krestan and G N Dobrokhotov (Leningrad Mining Institute - Department of the Metallurgy of Heavy and Noble Metals)

In the previous report we set out the kinetic relationships governing the leaching of pyrrhotite concentrates by concentrated solutions of ferric chloride. It is also possible to use ferrous iron in the form of the sulphate as solvent[1)2)]. The main reaction in this process

$$\left[1/(1-x)\right] Fe_{1-x}S + Fe_2(SO_4)_3 = 3FeSO_4 + \left[1/(1-x)\right] S^\circ \quad (1)$$

terminates in the production of a solution of ferrous sulphate, elemental sulphur, and an insoluble precipitate. The solvent can be regenerated by oxidative hydrolysis of the final solution

$$3FeSO_4 + 0.75O_2 = Fe_2(SO_4)_3 + 0.5Fe_2O_3 \quad (2)$$

with the release of the iron from the pyrrhotite into a separate product.

Below we give the results from investigations into the kinetics of the process in sulphate solutions. The experimental procedure was the same as in the previous work[3)]. It was established that the decomposition rate of pyrrhotite depends significantly on the intensity of agitation (fig.1). The full transition to the internal diffusion region was observed with a stirrer rotation rate of 250rpm or with a water value of 7000 for the modified Reynold's number. Subsequent experiments were carried out with this optimum intensity of agitation. For iron, as in the case of chloride systems, the obtained kinetic data were described satisfactorily by the empirical equation

$$\left(1-\sqrt[3]{1-\varepsilon}\right)^2 = K\tau$$

where is the degree of extraction of the component into solution. This made it possible to express the effect of the various kinetic factors by comparison of the nominal rate constants K. For copper and nickel sulphides the obtained kinetic data were treated also by the empirical equation given above, with which they agreed satisfactorily, so that it would be possible to compare them with data on iron sulphide. Such an assumption was possible since this equation described the initial stage of the transfer of the nonferrous metals into solution.

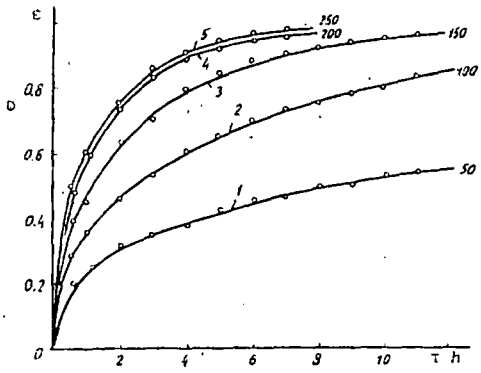

Fig.1 The effect of the intensity of agitation on the transfer of iron into solution. Stirrer rotation rate rpm: 1 - 50; 2 - 100; 3 - 150; 4 - 200; 5 - 250.

Tests with samples of concentrate having various particle sizes with other parameters constant showed that the leaching rate increases in direct proportion to the reacting surface of the particles. The composition of the solution had a significant effect on the intensity of oxidation of iron in the concentrate (fig.2). The character of dissolution remained constant at various temperatures. At low concentrations of the solvent (< 60 g/dm³ of ferric ion) the process was limited by transport of Fe^{3+} to the reacting surface. Since Fick's law $(dc/d\tau) = KC$ held for these conditions, the observed reaction order was first. Trivalent iron concentrations ≥ 100 g/dm³ corresponded to saturation of the boundary layer in ferric ions, the process became nonvariant in Fe^{3+}, and other factors (the amount of Fe^{2+} ions in the

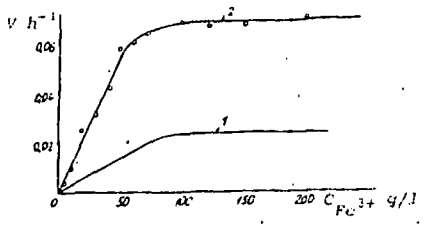

Fig.2 Effect of the Fe^{3+} concentration on the oxidation rate of pyrrhotite at 65 (1) and 75 (2) °C.

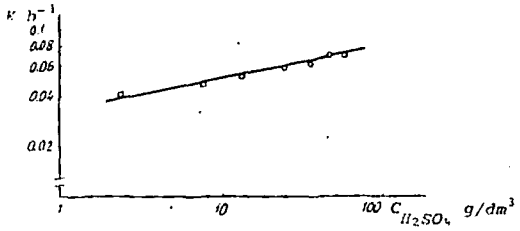

Fig.3 The effect of the H_2SO_4 concentration on the oxidation rate of pyrrhotite.

solution, etc) played a determining role. With increase in the concentration of divalent iron the oxidation rate of pyrrhotite decreased linearly, and the rate of withdrawal of Fe^{2+} from the reacting surface into the mass of the solution was the controlling quantity.

It was found that the experimental determinations were described well by the normal Arrhenius curves in the investigated range of temperatures 50-103°C. This made it possible to calculate the observed activation energies for the dissolution of iron, copper, and nickel sulphides, which were equal to 15.0, 38.9, and 41.4 kJ/mole respectively. These values showed that the dissolution of pyrrhotite occurs under diffusion control, and that of copper and nickel sulphides occurs under kinetic control. The results agreed well with theories about the limitation of dissolution by internal diffusion of ferrous ions.

Additions of sulphuric acid up to a concentration of 30-40 g/dm³ appreciably accelerated the decomposition of pyrrhotite and had little effect on the behaviour of copper and nickel. In view of the acid characteristics of the sulphides, this observation made it possible to consider that, apart from the main reaction (1), their dissolution also occurs on account of simple chemical reaction of the sulphides with the acid

$$MeS + 2H^+ = Me^{2+} + H_2S \qquad (3)$$

with subsequent oxidation of hydrogen sulphide in the general mass of the solution:

$$H_2S + 2Fe^{3+} = 2Fe^{2+} + 2H^+ + S^\circ \qquad (4)$$

It was proposed to describe the effect of acidity by the equation $K = ax^m$, where x is the concentration of free acid (g/dm³), and a and m are coefficients. The logarithmic form of this equation showed that the experimental data in the experiments with additions of sulphuric acid at the rate of 5-50g/dm³ fitted on to a straight line. Extrapolation of the obtained curve to the region where acidification of the initial mixtures was not realised made it possible to determine the amount of free sulphuric acid formed during the hydrolysis of trivalent iron, which always occurs in real solutions. This value was 2.5 g/dm³. The final form of the relationship K = f(x) with allowance for the calculated correction is shown in fig.3. The reaction order in the acid was determined as 0.7. The amorphous sulphur released by reactions (1) and (4) had a porous structure and hindered the transport of the reagents. In time it slowly recrystallised into the rhombic modification. The dissolution rate of the iron from the concentrate exceeded the dissolution rate of copper and nickel sulphides (tables 1 and 2), and this secured its preferential dissolution. Increase in temperature from 50 to 103°C deteriorated the selectivity of the release of iron into solution, and the K_{Fe}/K_{Ni} ratio decreased by a factor of approximately 3. From these observations we determined that under industrial conditions it is most suitable to realise the process at high concentrations of ferric ion and acid securing more intensive decomposition of the pyrrhotite. A high acidity in the final solutions also assists in the appearance of free hydrogen sulphide

Table 1: The rate constants for the oxidation of pyrrhotite in chloride and sulphate systems

Rate constant h^{-1}	Temperature °C					
	50	60	70	80	90	103
K'_{Fe} for $FeCl_3$	0.0343	0.171	0.596	1.062	1.224	1.86
K''_{Fe} for $Fe_2(SO_4)_3$	0.005	0.0160	0.048	0.076	0.087	0.103
$K'_{Fe}:K''_{Fe}$	7	11	12	14	14	18
$K'_{Fe}:K'_{Ni}$	171	203	172	151	107	102
$K''_{Fe}:K''_{Ni}$	38	25	16	16	13	10

Table 2: The rate constants for the oxidation of copper and nickel sulphides in chloride and sulphate systems

Rate constant h^{-1}		Temperature °C					
		50	60	70	80	90	103
For $FeCl_3$	K'_{Cu}	$1.5 \cdot 10^{-4}$	$6.8 \cdot 10^{-4}$	$0.23 \cdot 10^{-2}$	$0.62 \cdot 10^{-2}$	$1.04 \cdot 10^{-2}$	$1.56 \cdot 10^{-2}$
	K'_{Ni}	$2.0 \cdot 10^{-4}$	$8.4 \cdot 10^{-4}$	$0.35 \cdot 10^{-2}$	$0.70 \cdot 10^{-2}$	$1.14 \cdot 10^{-2}$	$1.82 \cdot 10^{-2}$
For $Fe_2(SO_4)_3$	K''_{Cu}	$1.0 \cdot 10^{-4}$	$4.5 \cdot 10^{-4}$	$0.20 \cdot 10^{-2}$	$0.36 \cdot 10^{-2}$	$0.56 \cdot 10^{-2}$	$0.87 \cdot 10^{-2}$
	K''_{Ni}	$1.3 \cdot 10^{-4}$	$6.3 \cdot 10^{-4}$	$0.29 \cdot 10^{-2}$	$0.46 \cdot 10^{-2}$	$0.69 \cdot 10^{-2}$	$1.06 \cdot 10^{-2}$
$K'_{Cu}:K''_{Cu}$		1.5	1.3	1.2	1.5	1.6	1.8
$K'_{Ni}:K''_{Ni}$		1.5	1.5	1.1	1.7	1.8	1.7

and, with low concentrations of the basic oxidizing agent, it promotes the inactivity of copper and nickel sulphides from the pyrrhotite. Comparison of the obtained results on the leaching of the concentrates in ferric sulphate and ferric chloride solutions shows that the qualitative relationships are the same in both systems, but a quantitative evaluation shows the advantage of systems with ferric chloride (table 1). On the average the dissolution rate of pyrrhotite in ferric chloride solution is approximately ten times higher than the dissolution rate in ferric sulphate. This ratio increases with increase in temperature. The difference is probably explained by a difference in the diffusion rates of Fe^{3+} ions. The diffusion rate is considerably lower in the sulphate on account of its lower solubility, which decreases with increase in temperature[4]). Copper and nickel sulphides also react more strongly with ferric chloride, but the difference in the oxidation rates is not so significant and amounts on the average to about 1.5 (table 2). The selectivity of the transfer of iron into solution is higher in the chloride systems (table 1).

The disadvantages of the use of ferric sulphate must also include the need to work with more dilute pulps having a liquid-solid ratio of (12-14):1, due to the lower solubility of ferrous oxide at 70-100°C (about 110 g/dm³). In the case of ferric chloride this ratio os (5-6):1.

Conclusions

1. Dissolution of pyrrhotite in concentrated solutions of ferric sulphate occurs under diffusion control and is more rapid than dissolution of the accompanying copper and nickel sulphides, which react under kinetic control.
2. The composition of the solution has a strong effect on the oxidation rate of the iron from the concentrate. High concentrations of trivalent iron and acid are most favourable.
3. The rate of the process is reduced by an increase in the content of divalent iron in the solution.
4. The selectivity of the dissolution of iron from the pyrrhotite decreases with increase in temperature.
5. The qualitative relationships in the leaching of pyrrhotites by ferric chloride and ferric sulphate are the same, but the oxidation of iron from the concentrate occurs more strongly in chloride solutions.
6. The use of ferric sulphate requires operation with dilute pulps, and this requires a larger volume of equipment.

References

1) K N Subramaian et alia: Can. Met. Quart., 1972, **11**, (2), 387
2) I M Toguri: Can. Met. Quart., 1975, **14**, (4), 323.
3) A L Krestan et alia: Izv. Vuz Tsvetnaya Metallurgiya 1978, 1.
4) Solubility Handbook. Vol.3, Leningrad, 1970.

UDC 669.2

Lead ferrites in lead sinters

A E Guriev, V N Murav'ev, T I Ivankova and A S Malyugian (North-Caucasian Mining-Metallurgical Institute)

For the theory of lead smelting it is important to know the scale to which lead ferrites are present in the sinter. Metallurgists have investigated the compositions and properties of lead ferrites and have discussed their behaviour in the smelt- of lead sinter[1-4]). At the same time, those who have investigated the mineral composition of the sinters have not come to concerted conclusions on the question of the presence of lead ferrites[5-7]). In this connection an attempt was made to supplement the available data by experimental data.

According to the literature, ferrite formation begins at 665°C and takes place vigorously at 725°C. Above 725°C decomposition of ferrites occurs[2,3]). During lead sintering the temperature reached in the bed fluxtuates most often between 1000 and 1150°C, and the lead ferrites which form with increase in temperature must inevitably decomposed. Consequently, the lead sinter can in principle contain only ferrites of secondary formation, formed in the same differential layer with decrease in temperature. On the basis of these considerations samples of lead ferrites were prepared under two different sets of conditions.

The first sample was prepared by calcination of a meta-ferrite mixture at 725°C for 3h. In the obtained sinter 4% of PbO_{free} on the total PbO content of the sinter was determined by leaching with 10% acetic acid solution. The second sample was prepared from an analogous mixture by calcination for 2h at 725°C and then for 1h at 920°C with subsequent slow cooling. In this sample we determined 25.3% PbO_{free}, and the remaining PbO was presumably combined into a ferrite of secondary formation. Samples of industrial sinters, the chemical compositions of which are given in the table, were also investigated.

Table

Sample No.	Plant	Pb	Zn	Cu	Fe	S_{tot}	SiO_2	CaO	MgO	Al_2O_3
1	Chimkent	37.9	10.3	1.92	10.3	1.8	9.22	7.51	2.56	2.56
2	Leninogorsk	41.7	9.9	2.22	7.4	3.2	6.43	11.13	1.07	1.69
3	Elektrosink	40.3	9.9	1.01	12.2	2.1	7.11	10.89	1.74	1.78
4	Ust'-Kamenogorsk	42.5	10.1	2.12	7.8	3.3	6.21	6.21	1.75	2.07

The microscopic investigations were carried out on an MIN-8m and a Neofot-2 microscope. X-ray analysis was performed on a URS-50IM instrument and also on a URS-70 instrument. Investigation of the synthesised samples showed that they have a fine two-phase structure. The boundaries between the phases are soft on account of the small difference in their reflective power and only differ in immersion at large magnifications.

One of the phases is represented by the finest (3-5μ) short-prismatic crystals and grains fairly uniformly distributed in the containing phase (normal magnetite). The phase (lead ferrite) is determined by extremely weak relief, a yellowish-cream tint, and by higher reflective power than magnetite. In addition, the crystal form and the weak anistropy of the phase are characteristic. The described microgrowths are similar to the normal decomposition structures of solid solutions of natural two-component systems (of the magnetite-haematite, magnetite-ilmenite, and other types) which, as known[8,9]), are formed during the cooling of solid solutions with the corresponding compositions.

A homogeneous system, which was subsequently differentiated during cooling of the sinter with the formation of structures from decomposition of the solution, is evidently formed initially with increase in temperature as a result of solid-phase reactions between the components of the charge. Thus, the appearance of lead ferrite detected in the sinters is determined unambiguously by the fact of its participation in the decomposition structures. The presence of lead ferrite and magnetite in the synthesised samples is confirmed by the data from X-ray analysis (fig. 1), which demonstrates the fundamental possibility of the formation of secondary ferrites during the sintering of the lead charge. However, restricted amounts of ferrites are detected in some samples of the ground sinter, and this is easily explained by the presence of contacts between PbO and Fe_2O_3 only in local volumes.

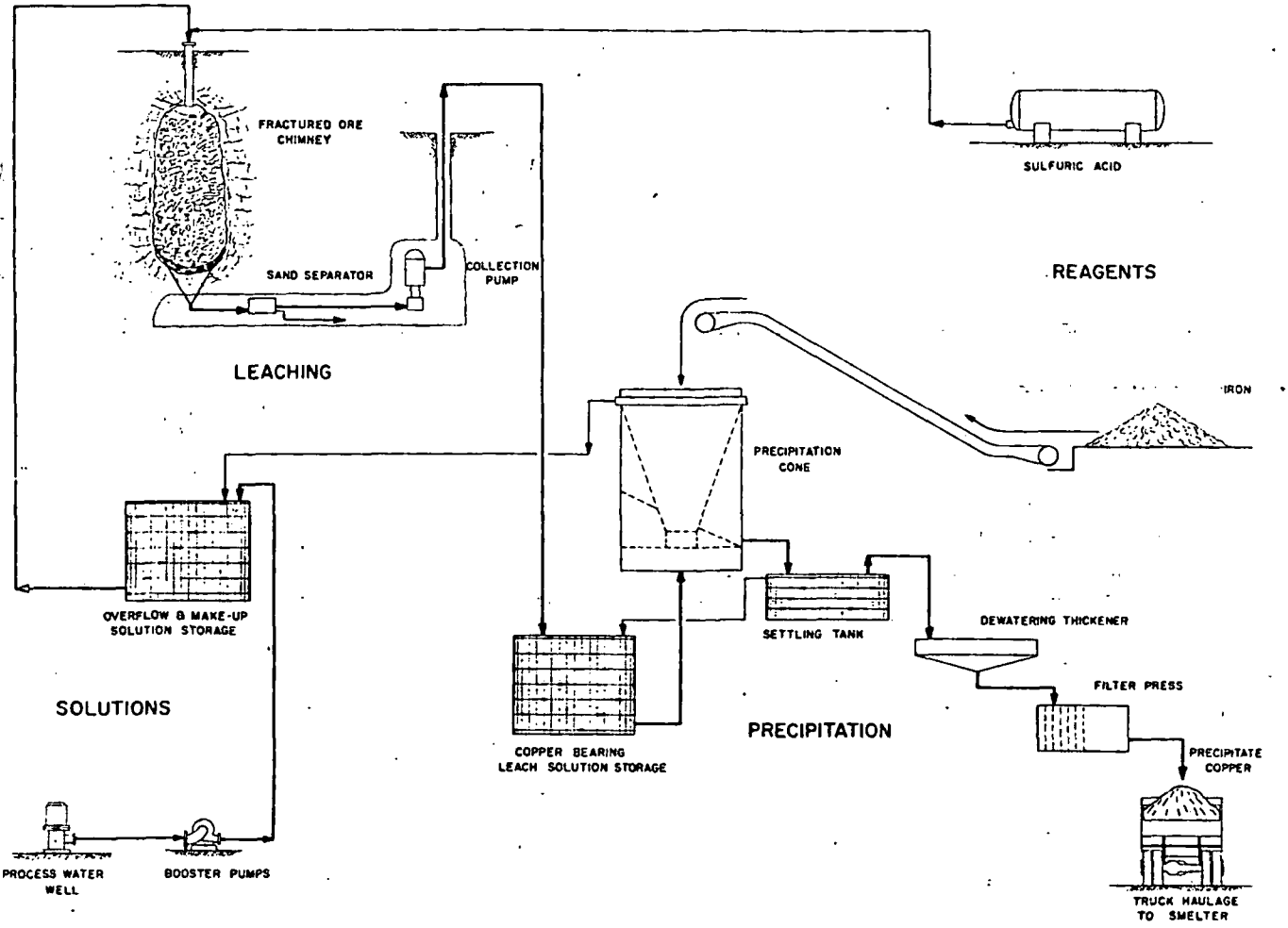

Proposed flowsheet for treatment of 2600 gpm of copper leach solution from in-situ ore broken by a confined nuclear blast.

To make feasible the extraction of metal from deposits uneconomic to mine by conventional methods, Kennecott president Frank R. Milliken told the AEC on October 24, is why . . .

Kennecott Proposes Nuclear Mining Experiments at Safford Deposit

Kennecott Copper Corp. has submitted a proposal to the U. S. Atomic Energy Commission for a joint experiment to determine if a contained underground nuclear explosion can be used to fracture a low-grade copper ore deposit to recover the copper by *in-situ* leaching. If authorized, safety and technical studies in the field would be undertaken to determine whether such an experiment could be conducted with full protection for public health and safety.

The proposed experiment, known as "Sloop," would be part of the AEC's Plowshare Program to develop peaceful uses of nuclear explosives. As now visualized, the project involves the detonation of about a 20-kiloton nuclear explosive at a depth of 1200 ft.

If a nuclear explosive is emplaced deep underground, upon detonation the blast will be fully contained. The energy of the explosion is released in a fraction of a microsecond and vaporizes, melts and crushes the surrounding rock. A cavity forms and expands spherically around the blast center following the outward moving shock wave until the pressure of the gas in the cavity approaches equilibrium with the weight of the overlying rock. The molten rock that initially lines the cavity walls will flow and form a pool on the cavity bottom and as it cools, solidifying into a relatively inert glass, it traps and entrains up to 95% of the radioactive fission products generated by the explosion.

The explosion would be expected to result in a chimney of broken ore about 440 ft high and 200 ft in diameter containing about 1.3 million tons of ore. The chimney material is extremely permeable; in earlier Plowshare experiments, shattered granite has contained about 25% void space. Also, 75% of the fragments have been smaller than 12 in. in size. The force of the

explosion will also fracture rock beyond the chimney, increasing the original rock's permeability for a distance approaching three cavity radii.

The Sloop study proposes an experiment to evaluate the combined nuclear fracturing/*in-situ* leaching technique for recovery of copper from low grade orebodies. The Safford deposit of Kennecott Copper Corp., about nine miles northeast of Safford, Ariz., is suggested as the experimental site. The cost is estimated at more than $13,000,000, including construction of pilot processing plant facilities at the Safford site and its operation for one year. If the proposal is accepted by the AEC, terms of the joint project, including the division of costs between the government and Kennecott, would be negotiated.

It is estimated that 9 months would be required from the authorization date until detonation of the explosive. In an additional 9 months the leaching tests could begin. A minimum of one year of leaching would probably be required to accumulate sufficient data to evaluate the techniques. The overall project time from authorization to evaluation would approximate 30 months.

The plan is to place the nuclear explosive in a 20-in. diam hole drilled from the surface. The hole would then be plugged to prevent venting to the atmosphere and the explosive would be detonated at a depth of 1200 ft.

After the shot, holes would be drilled from the surface into the chimney to define its height, take samples of the atmosphere inside it and measure the void volume. Holes would also be drilled to investigate the extent and radius of fracturing outside the chimney. As soon as the post-shot safety requirements are satisfied, existing underground openings would be rehabilitated and facilities installed for the leaching tests.

For the leaching tests, leach liquid input holes would be drilled to the top of the chimney. An access drift and a system of drill holes would be installed beneath the chimney to collect the pregnant (metal-bearing) leach solutions. The copper would be recovered from the solution by treatment with iron to precipitate a copper powder. A precipitation plant using cone precipitators similar to those now used at Kennecott's western mines would be constructed near the shaft. The plant would be capable of treating a throughput of about 2600 gpm of solution obtained from the collection system, and of recycling the barren (stripped) solutions to the chimney zone.

The operation of the pilot leaching plant should produce a moderate amount of copper that, after suitable treatment, could be made available for ordinary usage. A portion of the copper precipitates would be used for developmental studies to determine the most efficient process for refining the crude copper for marketing on a commercial scale.

The feasibility study concludes that there appears to be no safety problems that cannot be satisfactorily managed and that the project can be conducted at the Safford site without hazard or serious inconvenience to the population of the area. Radioactivity in the leaching solutions should be at low enough levels that shielding for personnel protection would not be required. Any residual contaminants in the raw copper product would be removable by refining processes so that the finished copper would be virtually free of any radioactive material.

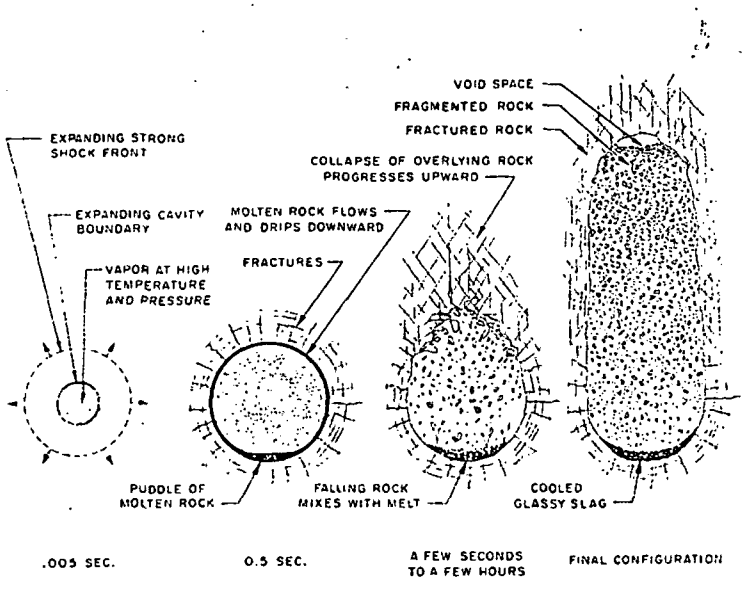

Sequence of cavity—chimney formation by a nuclear blast.

Project Sloop would be a joint effort of the U.S. Government and Kennecott Copper Corp., with the AEC providing the nuclear explosive and conducting the operation and program for the protection of public health and safety. Kennecott would be responsible for the leaching and copper recovery phase of the experiment. The U. S. Bureau of Mines would participate in all phases of the experiment, evaluating results, estimating applicability of the technique to other potential orebodies and cooperating with the other participants in reporting the results of the experiment.

At the present time the AEC is not authorized to supply explosives and the required support services on a commercial basis. The AEC can, however, under the Atomic Energy Act of 1954, utilize nuclear explosives in cooperative research and development arrangements with industry, including demonstrations of particular applications.

In order to assist industry in evaluating possible future uses, the AEC has published projected charges for nuclear explosives for use as a guide in evaluating Plowshare excavation applications.

Projected Costs for Thermonuclear Explosives

Yield, Kilotons	Approx. Charge
10	$350,000
50	425,000
100	460,000
350	500,000
500	535,000
1,000	570,000
2,000	600,000

The AEC believes that the projected charges are sufficiently representative of the future situation to warrant their use in feasibility studies.

These charges cover nuclear materials, fabrication and assembly, and arming and firing services. Significant related services which are not covered by these projected charges are safety studies, site preparation including construction of emplacement holes, transportation and emplacement of the explosives and support of the operations in the field. The charges would be produced in quantity for routine commercial utilization and it is possible that reductions in these costs could occur as a result of future technological developments.

The nuclear fracturing and "solution mining" concept, if successful, could greatly increase the mineable copper reserves in the United States by permitting development of low grade deposits which cannot be mined economically by conventional methods. In addition, it would keep disturbance of the natural landscape at a minimum.

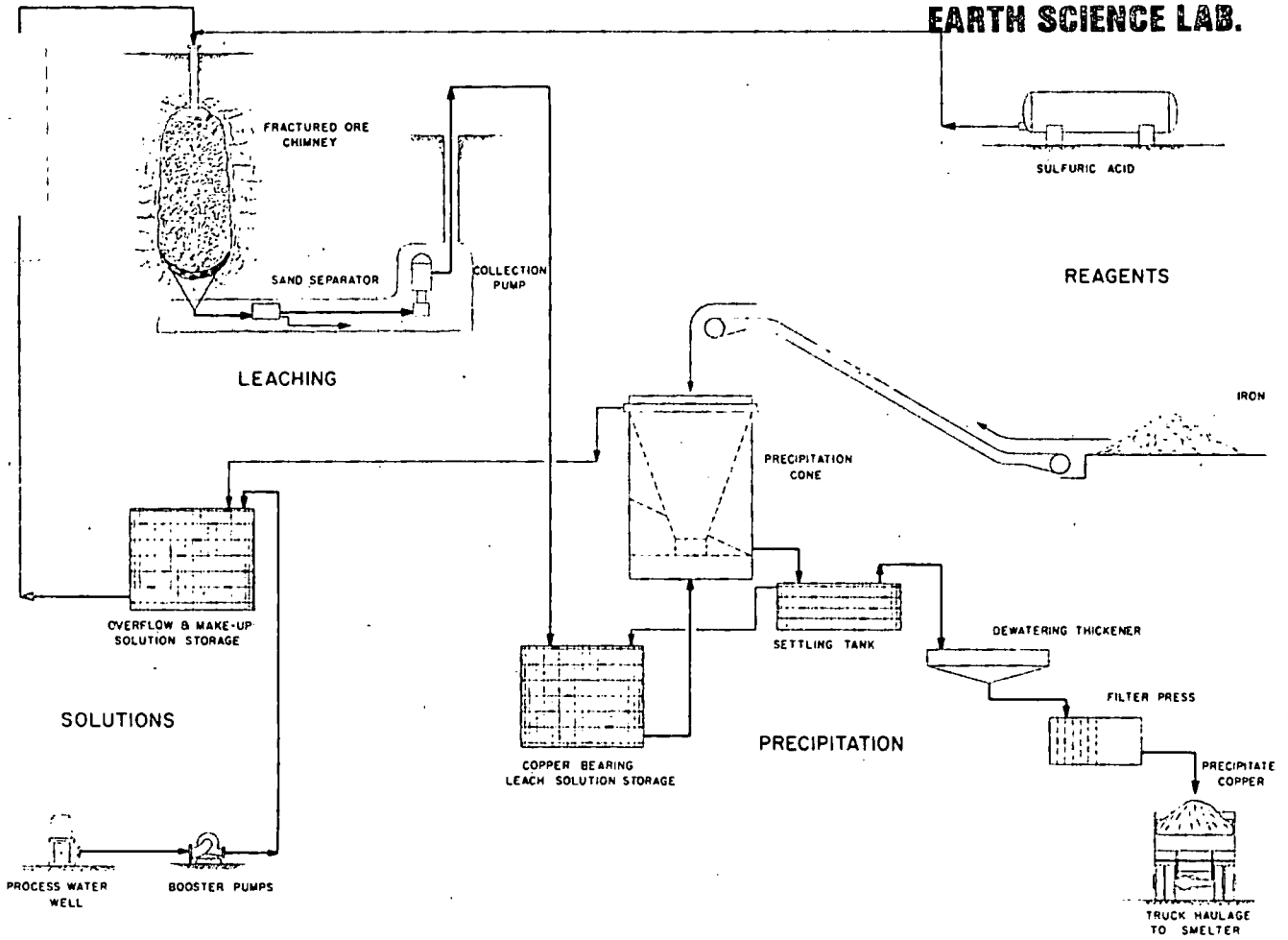

Proposed flowsheet for treatment of 2600 gpm of copper leach solution from in-situ ore broken by a confined nuclear blast.

To make feasible the extraction of metal from deposits uneconomic to mine by conventional methods, Kennecott president Frank R. Milliken told the AEC on October 24, is why . . .

Kennecott Proposes Nuclear Mining Experiments at Safford Deposit

Kennecott Copper Corp. has submitted a proposal to the U. S. Atomic Energy Commission for a joint experiment to determine if a contained underground nuclear explosion can be used to fracture a low-grade copper ore deposit to recover the copper by *in-situ* leaching. If authorized, safety and technical studies in the field would be undertaken to determine whether such an experiment could be conducted with full protection for public health and safety.

The proposed experiment, known as "Sloop," would be part of the AEC's Plowshare Program to develop peaceful uses of nuclear explosives. As now visualized, the project involves the detonation of about a 20-kiloton nuclear explosive at a depth of 1200 ft.

If a nuclear explosive is emplaced deep underground, upon detonation the blast will be fully contained. The energy of the explosion is released in a fraction of a microsecond and vaporizes, melts and crushes the surrounding rock. A cavity forms and expands spherically around the blast center following the outward moving shock wave until the pressure of the gas in the cavity approaches equilibrium with the weight of the overlying rock. The molten rock that initially lines the cavity walls will flow and form a pool on the cavity bottom and as it cools, solidifying into a relatively inert glass, it traps and entrains up to 95% of the radioactive fission products generated by the explosion.

The explosion would be expected to result in a chimney of broken ore about 440 ft high and 200 ft in diameter containing about 1.3 million tons of ore. The chimney material is extremely permeable; in earlier Plowshare experiments, shattered granite has contained about 25% void space. Also, 75% of the fragments have been smaller than 12 in. in size. The force of the

explosion will also fracture rock beyond the chimney, increasing the original rock's permeability for a distance approaching three cavity radii.

The Sloop study proposes an experiment to evaluate the combined nuclear fracturing/*in-situ* leaching technique for recovery of copper from low grade orebodies. The Safford deposit of Kennecott Copper Corp., about nine miles northeast of Safford, Ariz., is suggested as the experimental site. The cost is estimated at more than $13,000,000, including construction of pilot processing plant facilities at the Safford site and its operation for one year. If the proposal is accepted by the AEC, terms of the joint project, including the division of costs between the government and Kennecott, would be negotiated.

It is estimated that 9 months would be required from the authorization date until detonation of the explosive. In an additional 9 months the leaching tests could begin. A minimum of one year of leaching would probably be required to accumulate sufficient data to evaluate the techniques. The overall project time from authorization to evaluation would approximate 30 months.

The plan is to place the nuclear explosive in a 20-in. diam hole drilled from the surface. The hole would then be plugged to prevent venting to the atmosphere and the explosive would be detonated at a depth of 1200 ft.

After the shot, holes would be drilled from the surface into the chimney to define its height, take samples of the atmosphere inside it and measure the void volume. Holes would also be drilled to investigate the extent and radius of fracturing outside the chimney. As soon as the post-shot safety requirements are satisfied, existing underground openings would be rehabilitated and facilities installed for the leaching tests.

For the leaching tests, leach liquid input holes would be drilled to the top of the chimney. An access drift and a system of drill holes would be installed beneath the chimney to collect the pregnant (metal-bearing) leach solutions. The copper would be recovered from the solution by treatment with iron to precipitate a copper powder. A precipitation plant using cone precipitators similar to those now used at Kennecott's western mines would be constructed near the shaft. The plant would be capable of treating a throughput of about 2600 gpm of solution obtained from the collection system, and of recycling the barren (stripped) solutions to the chimney zone.

The operation of the pilot leaching plant should produce a moderate amount of copper that, after suitable treatment, could be made available for ordinary usage. A portion of the copper precipitates would be used for developmental studies to determine the most efficient process for refining the crude copper for marketing on a commercial scale.

The feasibility study concludes that there appears to be no safety problems that cannot be satisfactorily managed and that the project can be conducted at the Safford site without hazard or serious inconvenience to the population of the area. Radioactivity in the leaching solutions should be at low enough levels that shielding for personnel protection would not be required. Any residual contaminants in the raw copper product would be removable by refining processes so that the finished copper would be virtually free of any radioactive material.

Project Sloop would be a joint effort of the U.S. Government and Kennecott Copper Corp., with the AEC providing the nuclear explosive and conducting the operation and program for the protection of public health and safety. Kennecott would be responsible for the leaching and copper recovery phase of the experiment. The U. S. Bureau of Mines would participate in all phases of the experiment, evaluating results, estimating applicability of the technique to other potential orebodies and cooperating with the other participants in reporting the results of the experiment.

At the present time the AEC is not authorized to supply explosives and the required support services on a commercial basis. The AEC can, however, under the Atomic Energy Act of 1954, utilize nuclear explosives in cooperative research and development arrangements with industry, including demonstrations of particular applications.

In order to assist industry in evaluating possible future uses, the AEC has published projected charges for nuclear explosives for use as a guide in evaluating Plowshare excavation applications.

Projected Costs for Thermonuclear Explosives

Yield, Kilotons	Approx. Charge
10	$350,000
50	425,000
100	460,000
350	500,000
500	535,000
1,000	570,000
2,000	600,000

The AEC believes that the projected charges are sufficiently representative of the future situation to warrant their use in feasibility studies.

These charges cover nuclear materials, fabrication and assembly, and arming and firing services. Significant related services which are not covered by these projected charges are safety studies, site preparation including construction of emplacement holes, transportation and emplacement of the explosives and support of the operations in the field. The charges would be produced in quantity for routine commercial utilization and it is possible that reductions in these costs could occur as a result of future technological developments.

The nuclear fracturing and "solution mining" concept, if successful, could greatly increase the mineable copper reserves in the United States by permitting development of low grade deposits which cannot be mined economically by conventional methods. In addition, it would keep disturbance of the natural landscape at a minimum. ME

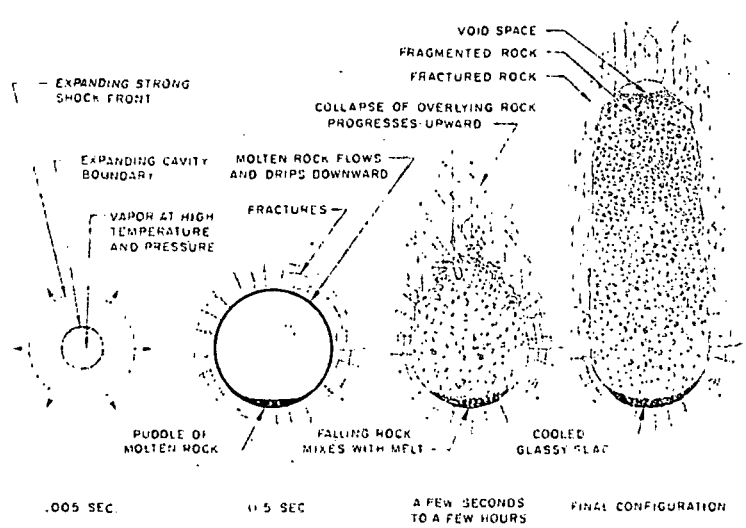

Sequence of cavity—chimney formation by a nuclear blast.

shear at the same strain values. The success of the theory of plastic bending (see Dolan and Sidebottom, for example[3]) indicates that this assumption is not greatly in error.

It is clear from Table I that fracture does not occur for a critical value of either the glide strain or the applied normal stress. Furthermore, most com-

Table I. Fracture of Zinc Crystals in Bending at —196°C (deflection rate = 1 ipm for beam 1 in. long)

Orientation χ_o, Deg	Radius at Fracture, Cm	Glide Strain at Fracture (Outer Fiber)	Corresponding Resolved Shear Stress fr. Tensile Test, G per Sq Mm	Normal Stress, G per Sq Mm
30	1.1	0.36	180	85
45	1.9	0.19	120	100
60	3.5	0.11	91	130
75	8.6	0.08	80	230

Orientation χ_o	Radius of Glide Planes at Fracture (Outer Fiber), Cm	Corresponding Excess Dislocation, Density, Lb per Sq Cm	Disl Density Times Normal Stress
30	1.2	3.2×10^7	2.7×10^9
45	1.6	2.4	2.4
60	2.1	1.8	2.5
75	2.9	1.3	3.0
			Avg = 2.65

SUBJ
MNG
KSDC

such as the strain times the normal stress ive good criteria. Complex combinations can be found which might serve as criteria, would have doubtful physical significance. est fracture criterion that was found was derived by correlating the fracture stresses with the dislocation contents of the crystals. The total dislocation content of the crystals is not known, but the density of excess positive dislocations can be calculated from the curvature of the glide planes. If $a = R_f \sin \chi_o$ and $L = R_f + d/2$, then the radius of curvature of the (0001) planes at the outer fiber is $r = (L^2 - a^2)^{1/2}$. The density of excess positive dislocations, ρ_E, is then given by $\rho_E = 1/rb$ where b = magnitude of Burgers vector.[1] The final column of Table I lists values of $\rho_E \sigma_f$ and it may be seen that this quantity has a fairly constant value, and therefore may be taken to be a fracture criterion.

Since fracture occurs in the bent crystals at relatively large strains the details of the geometry are complicated and unknown. Hence, detailed calculations are not possible. All that can be done is to postulate that dislocations have a specific weakening effect which is proportional to the dislocation density. Then the applied normal stress times the dislocation density should have a constant value as in Table I.

The fact that the fracture occurs along the curved glide surfaces is significant. It suggests that the glide plane of an edge dislocation is a particularly weak region in a crystal. It is thus consistent with the conclusion of a previous paper.[4]

Most of the experimental portion of this work was carried out by Mr. V. J. DeCarlo.

References

[1] J. F. Nye: "Some Geometrical Relations in Dislocated Crystals," *Acta Metallurgica*, 1953, vol. 1, p. 151.
[2] E. Schmid and W. Boas: *Plasticity of Crystals*; F. Hughes and Company, London, England, 1950, p. 59.
[3] T. J. Dolan and O. Sidebottom: "Raised (?) Yield Point in Bend Tests," *Metals Progress*, 1946, vol. 50, p. 653.
[4] J. J. Gilman: "Fracture of Zinc—Monocrystals and Bicrystals, submitted to AIME for publication.

A Kinetic Study of the Dissolution of UO_2 In Carbonate Solution

Sintered UO_2 samples were leached in carbonate solutions of various concentrations. A pressurized system was used so that it was possible to investigate the kinetics of the reaction to 200°C with oxygen overpressures as high as 800 psi. The surface active species in solution appears to be the undissociated acid H_2CO_3. Competitive adsorption between oxygen and H_2CO_3 occurs at the UO_2 surface resulting in an over-all rate decrease at high concentrations of H_2CO_3. Oxygen splits between two surface active sites and the slow step of the surface reactions involves a rearrangement or diffusion of oxygen on the mineral surface.

by Ray L. Pearson and Milton E. Wadsworth

THE dissolution of UO_2 in carbonate solutions can occur only if the tetravalent uranium is oxidized to the hexavalent state. The carbonate system is of particular interest because it provides a means whereby the oxidized uranium may be dissolved by forming the complex ion $UO_2(CO_3)_3^{-4}$. In the presence of oxygen the over-all reaction may be written

$$UO_2 + \tfrac{1}{2}O_2 + CO_3^{--} + 2HCO_3^- \rightarrow UO_2(CO_3)_3^{-4} + H_2O \quad [1]$$

UO_2 was used in this study because it could be obtained in high purity and also because it is representative of the most refractory of the primary uranium minerals. The mineral ulrichite is the natural counterpart of the synthetic UO_2 used. The kinetics of the leaching of UO_2 should be similar for any of the uraninite type minerals.

A pressurized system was used not with the hope it could be extended to commercial systems as a primary purpose but simply to provide the means whereby important temperature and pressure parameters could be varied for the evaluation of the kinetic processes. The importance of such pres-

R. L. PEARSON and M. E. WADSWORTH, Member AIME, are associated with Dept. of Metallurgy, University of Utah, Salt Lake City. This work was supported by the Atomic Energy Commission under Contract No. AT(11-1)-82.

TP 4631D. Manuscript, Sept. 17, 1956. New Orleans Meeting, February 1957.

surized systems has already been demonstrated by Forward, Halpern and Peters,[1,2,3] and the Beaver Lodge Processing plant in Saskatchewan, Canada, has incorporated the results of that research in a commercial uranium treatment plant.[4]

Peters and Halpern[2] carried out a kinetic study of the leaching of pitchblende (U_3O_8). The slow step proposed by these investigators was the adsorption and splitting of oxygen on the U_3O_8 surface, and the measured rates were found to be independent of the HCO_3^- and $CO_3^=$ solution concentrations under the conditions of their studies. This investigation was undertaken to determine the mechanism of the dissolution of the more refractory tetravalent uranium compound UO_2, with the hope that specific details regarding the role of oxygen and the various carbonate species present could be evaluated.

Experimental

The UO_2 as received* was found by spectroscopic analysis to have a purity of 99.94 pct ±0.03. It was ground in a mechanical agate mortar and screened through a 400 mesh sieve. Thin flat disks of UO_2 were prepared by pressing the sized powder in a specially constructed die at a total pressure of approximately 15 tons per sq in. These disks measured approximately 2.3 mm in thickness and 1.6 cm in diameter and weighed approximately 3.6 g. As pressed, the samples were approximately 65 pct of theoretical density. It was essential that a binder such as polyvinyl alcohol be added before pressing to prevent formation of strains and cracks when fired.

The disks were dried and fired in a molybdenum-wound furnace under hydrogen at 1800°C for 30 min. A careful X-ray diffraction study of the sintered disks showed them to be unaltered from the original unfired UO_2. The final density of usable samples had to be above 89 pct of theoretical density. At densities below 89 pct the void spaces were connected, resulting in a sample of high porosity. Porous disks are completely unsatisfactory because the geometric surface area is unknown and a large variation in area occurs during leaching. Samples above 89 pct of theoretical density had no measurable porosity based upon a 2-hr immersion in boiling water. These samples gave consistent and reproducible results.

* Mallinckrodt reagent, supplied by the Atomic Energy Commission.

Leaching studies were carried out in a specially designed autoclave. The details of this equipment have been presented elsewhere.[5] One milliliter samples removed from the autoclave during the course of a run were analyzed for U_3O_8 content with a Beckman Model DU spectrophotometer by the method of DeSesa and Nietzel.[6] Knowing the surface area of the sample by measurement with a micrometer, the time of reaction and the corresponding concentration of uranium in solution, rates were measured in mg U_3O_8/min/cm^2.

Experimental Results

The results presented in this paper are based upon 75 separate rate determinations. The range of conditions varied, extending up to 60 g per l of $Na_2CO_3 \cdot H_2O$ and 60 g per l $NaHCO_3$, temperatures from 127 to 203°C and oxygen partial pressures from 0 to 800 psia. Fig. 1 illustrates the results of three typical runs at three separate temperatures. The rates were linear under all of the conditions of this study indicating that no surface products were formed on the surface of the sample which inhibited the reaction.

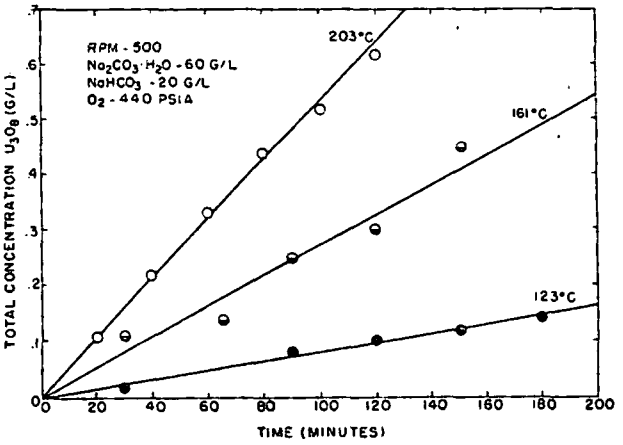

Fig. 1—Typical curves showing total concentration of U_3O_8 in solution versus time.

The effect of stirring is often of importance in a solution-dissolution study since solution diffusion must be eliminated if the kinetics of the surface reactions are to be evaluated. A series of rate versus speed of agitation runs was obtained at 175°C, 440 psi oxygen overpressure, with a solution concentration of 60 g per l $Na_2CO_3 \cdot H_2O$ and 20 g per l $NaHCO_3$. The rate of reaction increased with stirring speed to approximately 400 rpm under these conditions. Above 400 rpm the rate was independent of the speed of agitation. Subsequent runs were carried out at 500 rpm.

Fig. 2 illustrates the effect of oxygen overpressure on the rate of dissolution. These rate pressure isotherms were obtained at 127, 143, 161, 187 and 203°C. The solution in all cases contained 60 g per l $Na_2CO_3 \cdot H_2O$ and 20 g per l $NaHCO_3$.

A similar series of runs was carried out at constant oxygen overpressure but at various carbonate concentrations. Rate-concentration data are presented in Fig. 3 for 175, 161 and 143°C. The oxygen overpressure was maintained at 440 psi, and the concentration of $Na_2CO_3 \cdot H_2O$ was 60 g per l in all tests. Fig. 3 is a plot of measured rate versus the concentration of $NaHCO_3$ for the foregoing conditions. The rate-concentration isotherms go through a maximum. At lower temperatures, however, the height of the maximum diminished appreciably, and

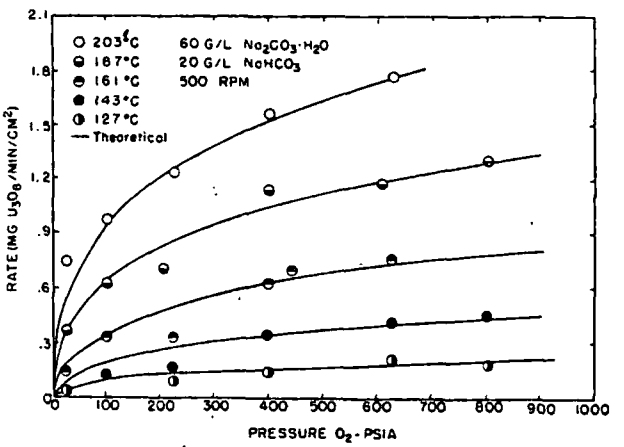

Fig. 2—Effect of O_2 overpressure on the rate of dissolution of UO_2.

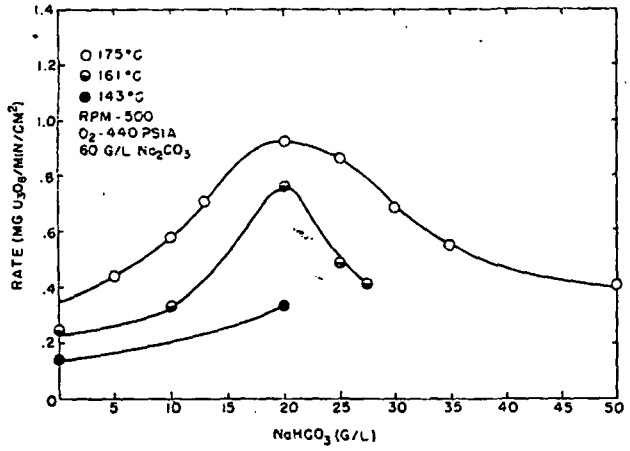

Fig. 3—Effect of varying $NaHCO_3$ concentration on the dissolution of UO_2.

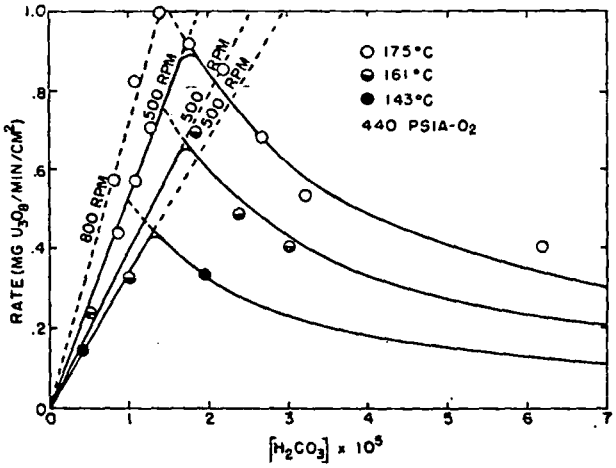

Fig. 5—Effect of H_2CO_3 concentration on the rate of dissolution of UO_2.

it is conceivable that at sufficiently low temperatures the rate may appear to be independent of solution concentration. This may explain the results obtained on pitchblende[2] in which the rate was independent of solution concentrations. Also the pressures used in this study were very much greater than those used for pitchblende. An alternate explanation, of course, is simply the inherent difference between UO_2 and U_3O_8. The rising portion to the left of the maxima of Fig. 3 could not be attributed to surface precipitation of insoluble sodium uranate (Na_2UO_4) as was found in the case of pitchblende since all rates measured in this region were linear. It was found, however, that at 175°C, 15 g per l $NaHCO_3$, and 42.5 g per l Na_2CO_3-H_2O a yellow precipitate was formed.

Discussion of Results

Although the carbonate system is quite complex, kinetically only one of the carbonate species ($CO_3^=$, HCO_3^- or undissociated H_2CO_3) is likely to be involved in the slow step of the reaction. Calculating the concentrations of each of these species presents a problem since the equilibrium constants have not been measured in the temperature range of this study. Equations have been developed[7,8,9] to explain the temperature dependence of the equilibrium constants at lower temperatures, however, and these equations were assumed valid for the temperature range covered in this investigation. This is a broad extrapolation and throws serious question on the absolute concentrations calculated. In spite of this, however, the interdependent relationship described by the equilibrium reactions between the species in question should remain self-consistent. This is particularly true since the equilibrium constants may be in error by as much as ±25 pct without seriously altering the calculated concentrations.

Fig. 4 is a plot of the 175°C data (Fig. 3) for rate versus $[CO_3^=]$ and $[HCO_3^-]$. Similarly, Fig. 5 is a plot of the rate versus $[H_2CO_3]$ for 175, 161 and 143°C. The maxima occur at 20 g per l $NaHCO_3$ and 60 g per l Na_2CO_3. This was the concentration used to investigate the effect of stirring speeds. As a consequence, additional stirring tests were necessary to determine if diffusion was rate controlling at the lower concentrations; i.e., at concentrations below the maxima of the curves of Fig. 3. The results are shown in the upper (dotted) curve of Fig. 5. An increase in stirring speed from 500 rpm to 800 rpm was found to increase the rate of dissolution for all concentrations to the left of the maxima of the rate versus concentration curves, indicating that diffusion in this region is rate controlling. At higher concentrations, increasing stirring speed had no effect upon the rate of dissolution, indicating that the slow step in this region is a surface reaction or possibly diffusion through a limiting boundary film. The latter possibility in this case may be eliminated, however, since the rate decreased as the H_2CO_3 concentration was increased.

The region of diffusion control is useful in this system since it provides a means whereby the reactive carbonate species may be identified. When diffusion is rate controlling the rate of reaction should be a linear function of the concentration of the diffusing ion or molecule. An examination of Fig. 4 and 5 shows that a linear relationship exists between rate and the concentration of undissociated H_2CO_3. The linear dependence of course assumes that the thickness of the diffusion boundary is constant for any one set of conditions. This condition is met by maintaining stirring speed constant. The 500 and 800-rpm curves (175°C) of Fig. 5 illustrate the linear dependence at two stirring speeds. Since initial straight slopes were obtained for more than one temperature the heat of activation for diffusion may be determined by plotting log $\mathcal{R}/(H_2CO_3)$ versus $1/T$. Fig. 6 is such a plot giving a value of approximately 4.7 kcal for ΔH_D of diffusion of H_2CO_3 through the solution. This is of the correct magnitude for solution diffusion and lends additional evidence that the rising portion of the curves of Fig. 5 involves solution diffusion as the slow step. It seems somewhat surprising that the diffusion of H_2CO_3 rather

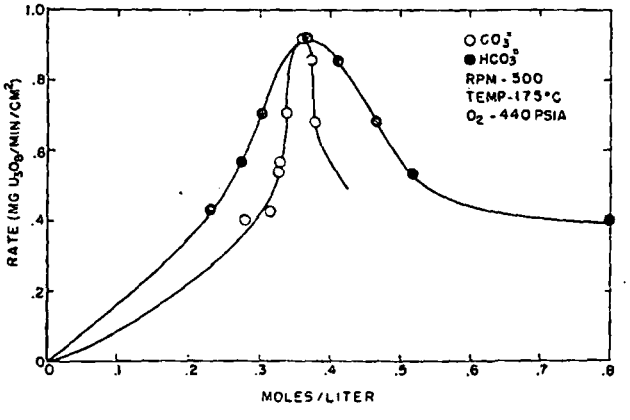

Fig. 4—Effect of $CO_3^=$ ion and HCO_3^- ion concentrations on the dissolution of UO_2.

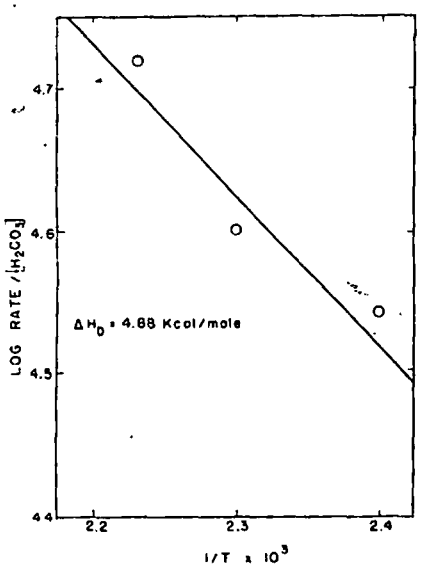

Fig. 6—Arrhenius plot for the solution diffusion of H_2CO_3.

than some other species is limiting because of the expected rapid formation of H_2CO_3 by hydrolysis of $CO_3^=$ and HCO_3^- which are present. In spite of this, the results depicted in Fig. 5 indicate that the reactive species in this system is the free or undissociated H_2CO_3. The importance of neutral molecule (hydrolytic) adsorption has been shown in other systems.[10,11,12] According to the foregoing interpretation, the behavior of H_2CO_3 in the surface reactions must be quite complex since the rate was found to decrease asymptotically as the H_2CO_3 concentration was increased. The decrease in rate at higher concentrations strongly suggests competitive adsorption between H_2CO_3 and oxygen.

The rate versus P_{O_2} curves of Fig. 2 are satisfied by the empirical equation

$$\text{Rate} = \frac{AP^{1/2}_{O_2}}{1 + BP^{1/2}_{O_2}} \qquad [2]$$

This is the form of equation of a typical Langmuir-type isotherm in which the concentration of the reactants involves chemisorption. The one-half power dependence indicates that oxygen splits between two active sites when it is adsorbed on the surface. A similar half-power dependence was observed by Peters and Halpern[2] for the dissolution of pitchblende. In that case, however, the value of B (Equation [2]) could not be evaluated since the pressure range investigated was such that $BP^{1/2}_{O_2}$ was very much less than 1. The temperature dependence of B is very important in evaluating the mechanism of the slow step of the surface reactions.

The following mechanism is proposed to explain the slow step associated with the surface reactions. It is consistent with the rate determinations made under the conditions of this study.

The absorption of oxygen by the solution is a fast step and may be considered to be at equilibrium according to the reaction

$$O_{2g} \overset{K_h}{\rightleftharpoons} O_{2l} \qquad [3]$$

where g and l refer to the gas and liquid phases, respectively. The term K_h is the Henry constant representing the equilibrium partition of Equation [3]. The adsorption of O_2 and H_2CO_3 may be represented by the equations

$$2\left|UO_2 + O_2 \rightleftharpoons 2\right|UO_2 \cdot O \qquad [4]$$

$$\left|UO_2 + H_2CO_3 \rightleftharpoons\right|UO_2 \cdot H_2CO_3 \qquad [5]$$

Equations [4] and [5] represent competitive adsorption of O_2 and H_2CO_3, respectively, for an active UO_2 surface site, represented by the notation $\left|UO_2\right.$. These reactions also may be considered to be at equilibrium. Such an assumption is valid and simply implies that the back reactions (desorption) of Equations [4] and [5] are fast compared to the rate of removal of the adsorbates as a result of a surface reaction. In order to explain the observed kinetics it was found necessary to propose as the slow step the rearrangement of oxygen on the surface according to a reaction of the type

$$\left|UO_2 \cdot O \overset{+}{\rightarrow}\right|UO_2 \cdot \text{(slow)} \qquad [6]$$

The notations used here are not intended to imply the actual structure of the surface groups.

According to absolute reaction-rate theory[13]

$$\text{Rate} = \kappa \frac{kT}{h} \prod_i C_i^{x_i} e^{-\frac{\Delta F^+}{RT}} = \prod_i C_i^{x_i} k' \qquad [7]$$

where κ is the transmission coefficient (conventionally taken as unity), k is the Boltzmann constant, h the Planck constant, $\prod_i C_i^{x_i}$ the product of the concentrations of the reactive species in the slow step, x_i is the order of the reaction in regard to the ith species, ΔF^+ is the free energy of activation and k' is the specific reaction rate constant. In Equation [7] the activity coefficients of the reactants and the activated complex are assumed to be unity. According to the model proposed the $\prod_i C_i^{x_i}$ term of Equation [7] includes the surface area, roughness factor (ratio of true surface area to geometric), and the concentration of $\left|UO_2 \cdot O\right.$ sites. Letting θ_1 be the fraction of potentially reactive sites containing adsorbed oxygen ($\left|UO_2 \cdot O\right.$), Equation [7] becomes

$$\mathcal{R} = \frac{kT}{h} k_o \theta_1 e^{-\frac{\Delta F^+}{RT}} = k_o \theta_1 k' \qquad [8]$$

where $\mathcal{R}$ is the rate per unit measured (geometric) surface area and k_o includes the surface-roughness factor, number of potentially reactive sites per square centimeter and conversion units to accommodate the units of the measured rate $\mathcal{R}$. The fraction of potentially reactive sites covered by adsorbed H_2CO_3 may be designated as θ_2. Accordingly the equilibrium constants of Equations [4] and [5] are

$$K_1 = \frac{\theta_1^2}{\phi^2} \frac{1}{P_{O_2}} \qquad [9]$$

$$K_2 = \frac{\theta_2}{\phi} \frac{1}{[H_2CO_3]} \qquad [10]$$

where ϕ is the fraction of the potentially reactive sites uncovered ($|UO_2$). The equilibrium constant K_1 includes the Henry constant K_A of Equation [3]. According to the total surface balance

$$\phi = 1 - \theta_1 - \theta_2 \qquad [11]$$

An expression for θ_1 may be derived from Equations [9], [10] and [11] whereby Equation [8] becomes

$$\mathcal{R} = k_o \frac{kT}{h} \left[\frac{K_1^{1/2} P_{O_2}^{1/2}}{1 + K_2 [H_2CO_3] + K_1^{1/2} P_{O_2}^{1/2}} \right] e^{-\frac{\Delta F^{\ddagger}}{RT}} \qquad [12]$$

At constant temperature (T) and $[H_2CO_3]$, Equation [12] may be written

$$\mathcal{R} = k_o k' \left[\frac{K' P_{O_2}^{1/2}}{1 + K' P_{O_2}^{1/2}} \right] \qquad [13]$$

where

$$K' = \frac{K_1^{1/2}}{1 + K_2 [H_2CO_3]} \qquad [14]$$

Equation [13] is of the same form as Equation [2] where $A = k_o k' K'$ and $B = K'$. The value of K' and $k_o k'$ may be calculated for each rate isotherm of Fig. 2 by selecting two points on the experimental curve and solving them simultaneously. An Arrhenius plot of log K' versus $1/T$ is shown in Fig. 7. The linear dependence means that the quantity $K_2 [H_2CO_3]$ is not of the order of magnitude of 1; that is, it must be much larger or much smaller than 1. Otherwise an Arrhenius plot would not result in a straight line as is evident from the form of Equation [14]. It is also significant that K' increases as temperature increases resulting in the negative slope of Fig. 7. If K' contained only the equilibrium constant for the adsorption of oxygen, an Arrhenius plot of log K' versus $1/T$ would have to have a positive slope giving a negative enthalpy (ΔH). The adsorption process of itself must be exothermic, particularly since the character of the rate isotherms, Fig. 2, indicates that the surface is approaching saturation. The negative slope of Fig. 7, therefore, indicates that $K_2 [H_2CO_3] >> 1$ and that the net ΔH calculated must contain enthalpy terms for more than one adsorption process. Equation [14] thus may be written

$$K' [H_2CO_3] = \frac{K_1^{1/2}}{K_2} = e^{-\frac{1}{RT}\left(\frac{\Delta H_1}{2} - \Delta H_2\right)} e^{\frac{1}{R}\left(\frac{\Delta S_1}{2} - \Delta S_2\right)} \qquad [15]$$

Fig. 8 is a plot of log $K_1^{1/2}/K_2$ versus $1/T$. From the slope, $\Delta H_1/2 - \Delta H_2 = 3.6$ kcal per mole. The positive value indicates that the enthalpy of adsorption of H_2CO_3 on the surface of UO_2 has a larger negative value than one half the enthalpy of adsorption of oxygen on the surface of UO_2. The very small enthalpy measured its additional evidence of the complexity of K'. Such a small value would be unreasonable for the enthalpy of adsorption of oxygen alone particularly in view of the fact that chemisorption occurs, as evidenced by the splitting of oxygen during adsorption.

At constant temperature and P_{O_2}, Equation [12] may be written

$$\mathcal{R} = k_o k' \left[\frac{1}{1 + K'' [H_2CO_3]} \right], \qquad [16]$$

where

$$K'' = \frac{K_2}{K_1^{1/2} P_{O_2}^{1/2}} \qquad [17]$$

The value of K'' may be calculated for any temperature and P_{O_2} from the curve of Fig. 8. The solid curves through the data of Fig. 5 to the right of the maxima were drawn using Equation [16] and K'' values calculated from the $K_1^{1/2}/K_2$ relationship determined from the pressure-rate isotherms of Fig. 2. The value of $k_o k'$ was determined by passing the theoretical curve through one point of the experimental concentration-rate isotherm. It is evident from Equations [13] and [16] that the values of $k_o k'$ have been determined for a series of temperatures for both the pressure-rate and the concentration-rate isotherms. The specific rate constant k' contains the heat of activation ($\Delta H^{\ddagger}$) which may be

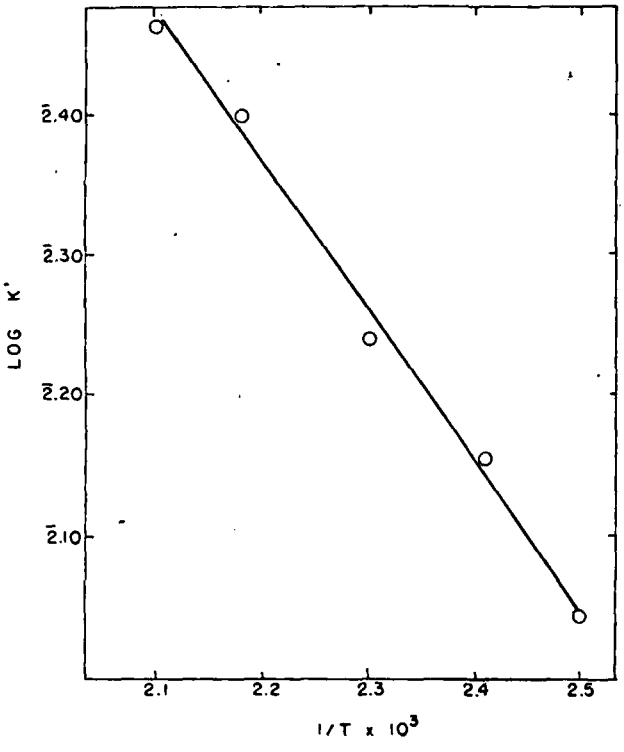

Fig. 7—Arrhenius plot of K' determined from the isotherms of Fig. 2.

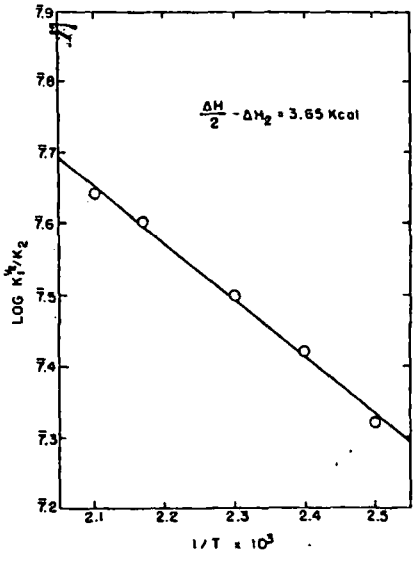

Fig. 8—Arrhenius plot for the determination of $\Delta H_1/2 - \Delta H_2$.

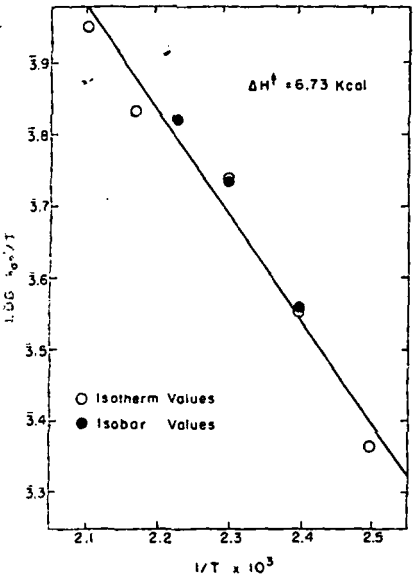

Fig. 9—Arrhenius plot of k_0k' determined from the isotherms of Figs. 2 and 5.

evaluated by plotting log k_0k'/T versus $1/T$. Fig. 9 is such a plot. The open circles represent k_0k' values determined from the pressure-rate isotherms, Fig. 2, and the solid points from the concentration-rate isotherms, Fig. 5. The value of $\Delta H^{\neq}$ was found to be approximately 6.7 kcal per mole. The small $\Delta H^{\neq}$ value representing the slow step of Equation [6] suggests that the slow process may not necessarily be the formation of $|UO_3$ but may simply involve surface diffusion of oxygen. The actual reactions following the slow step are purely speculative.

The value of $\Delta H^{\neq}$ for the dissolution of UO_2 is very much smaller than the $\Delta H^{\neq}$ for pitchblende reported by Peters and Halpern.[2] Their values ranged between 9.2 and 12.3 kcal per mole dependent upon the solution concentration. It was interesting to note in this study that, if rates at several temperatures were taken at constant pressure from the data of Fig. 2, plots of log $\mathcal{R}/T$ versus $1/T$ gave apparent heats of activation between 11 and 15 kcal/mole. The lower value resulted from rates measured at higher pressures. This is in the same range as the values reported by Peters and Halpern. The apparent higher activation energy results from the fact that the temperature dependence of K_1 and K_2 is included in the over-all Arrhenius plot. This is made clear upon examining Equation [12] under conditions of small $P^{1/2}_{O_2}$.

Under these conditions Equation [12] becomes

$$\mathcal{R} = k_0 \frac{kT}{h} \frac{K_1^{1/2}}{K_2} \frac{P^{1/2}_{O_2}}{[H_2CO_3]} e^{-\frac{\Delta F^{\neq}}{RT}}$$

$$= k_0 \frac{kT}{h} \frac{P^{1/2}_{O_2}}{[H_2CO_3]} e^{-\frac{1}{RT}\left(\Delta H^{\neq} + \frac{\Delta H_1}{2} - \Delta H_2\right)} e^{\frac{1}{R}\left(\Delta S^{\neq} + \frac{\Delta S_1}{2} - \Delta S_2\right)} \quad [18]$$

An Arrhenius plot of Equation [18] gives the value of the composite enthalpy

$$\Delta H^{\neq} + \frac{\Delta H_1}{2} - \Delta H_2 .$$

These values have been separated but the composite value determined from Figs. 8 and 9 is 10.4 kcal per mole. This value is in the same range reported for pitchblende.

According to the model proposed in which the surface slow step involves the rearrangement of atomic oxygen on the surface, the entropy of activation ($\Delta S^{\neq}$) should be very small, and may reasonably be considered to be zero. The only remaining unknown in the complete rate equation is k_0. Its solution is important since it contains the factors for the number of reactive sites per square centimeter and surface roughness. Its value for a surface-roughness factor of unity is approximately 10^{11} sites per cm^2. A surface-roughness factor of 10 would reduce this number to 10^{10} sites per cm^2. Since there are approximately 10^{15} UO_2 sites per cm^2 on the solid, the value of k_0 indicates that less than one site in 10,000 is an active site. These active sites are probably edges or corners on the surface of the solid and may be associated with edge or screw dislocations. If one assumes the reactive sites represent a sequence of steps, 1 molecular unit high, being removed in layers, there would be less than 3000 such steps per square centimeter of the surface.

It may seem surprising that oxygen and H_2CO_3 both adsorb on the same types of active sites since there are so few sites available. The fact they do is supported by the competitive model necessary to explain the observed kinetics. Also there does not seem to be a detectable change in the heat of adsorption with surface coverage. This may be due largely to the fact that there are relatively few sites present so that surface charge or strain effects are minimized.

Conclusions

The dissolution of UO_2 in carbonate solutions may be explained as involving competitive adsorption between oxygen and undissociated H_2CO_3. The oxygen upon adsorption splits between two surface sites. The following sequence of reactions is consistent with observed rates under various conditions of temperature, oxygen overpressure, and solution concentration

1) $2|UO_2 + O_2 \rightleftarrows 2\ UO_2 \cdot O$ (equilibrium)

2) $|UO_2 + H_2CO_3 \rightleftarrows |UO_2 \cdot H_2CO_3$ (equilibrium)

3) $|UO_2 \cdot O \rightarrow ||^{\neq} \rightarrow UO_3$ (slow step)

4) $|UO_3 + UO_2 \cdot H_2CO_3 \rightarrow UO_2(CO_3) \cdot H_2O + |UO_2$ (fast)

5) $UO_2(CO_3) \cdot H_2O + 2CO_3^{=} \rightarrow UO_2(CO_3)_3^{-4} + H_2O$ (fast)

The series of reactions following the slow step is only speculative. The presence of the neutral intermediate complex $UO_2(CO_3) \cdot H_2O$ is simply suggested as a possible step in the formation of the complex ion $UO_2(CO_3)_3^{-4}$. Such an intermediate complex would be very unstable and would be immediately removed at or near the solid surface.

The heat of activation is 6.7 kcal per mole, and the competitive adsorption of H_2CO_3 results in a reduction of the rate of dissolution at high concentrations of H_2CO_3. Fewer than one site in 10,000 is potentially reactive at any one time. Optimum conditions for the dissolution of UO_2 are provided under conditions of vigorous agitation with the concentration of undissociated H_2CO_3 at approximately 1×10^{-5} moles per liter.

References

[1] F. A. Forward and J. Halpern: *Canadian Mining and Metallurgical Bulletin Trans.*, 1953, vol. 56, p. 344.
[2] E. Peters and J. Halpern: *Canadian Mining and Metallurgical Bulletin Trans.*, 1953, vol. 56, p. 350.
[3] F. A. Forward and J. Halpern: *AIME Trans.*, 1954, vol. 200, p. 1408; JOURNAL OF METALS, December 1954.

[4] R. W. Mancantelli and J. R. Woodward: *AIME Trans.*, 1955, vol. 203, p. 751; JOURNAL OF METALS, June 1955.
[5] W. H. Dresher, T. M. Kaneko, W. M. Fassell, Jr., and M. E. Wadsworth: *Industrial and Engineering Chemistry*, 1955, vol. 47, p. 1681.
[6] M. A. De Sesa and O. A. Nietzel: U. S. Atomic Energy Commission Topical Report No. ACCO-54, 1954.
[7] H. S. Harned and S. R. Scholes, Jr.: *Journal American Chemical Soc.*, 1941, vol. 63, p. 1706.
[8] T. Shedlousky and D. A. MacInnes: *Journal American Chemical Soc.*, 1935, vol. 57, p. 1705.
[9] H. S. Harned and B. B. Owen: "The Physical Chemistry of Electrolytic Solutions," p. 492. Reinhold Publishing Corp. New York, 1950.
[10] M. A. Cook and G. A. Last: *Journal of Physical Chemistry*, 1952, vol. 56, p. 637.
[11] M. E. Wadsworth and D. R. Wadia: *AIME Trans.*, 1955, vol. 203, p. 755; JOURNAL OF METALS, June 1955.
[12] N. L. Jensen and M. E. Wadsworth: Technical Report No. XVIII, 1956, No. 1. N7-onr-45103. University of Utah.
[13] C. H. Pitt and M. E. Wadsworth: Technical Report No. XX, 1957, No. ONR N7-onr-45103. University of Utah.
[14] S. Glasstone, K. J. Laidler, and H. Eyring: "The Theory of Rate Processes," McGraw-Hill Co. New York, 1941.

Discussion of this paper sent (2 copies) to AIME by Aug. 1, 1958 will appear in AIME Transactions Vol. 212, 1958.

Technical Note

On Deformation Structures in Silver-Gold Alloys

by R. J. Block, J. B. Cohen, and M. B. Bever

RECENT investigations have shown that face-centered cubic metals may deform by twinning. Blewitt, et al[1] found that at 4.2°K the mode of deformation of single crystals of copper changed at large strains and markings formed on (111) planes. Later they[2] demonstrated by X-ray diffraction and metallography that the markings were twins and showed that favorably oriented single crystals of copper deformed by twinning at 78°K. They also observed twinning in silver and gold deformed at 4.2 and 78°K. Wagner[3] obtained evidence for twinning from the peak shape of diffraction lines of silver cold-worked at 78°K, but twins small enough to cause such effects are not likely to be detected metallographically.

In the work reported here lamellar structures were observed in deformed silver-gold alloys. They appeared to be mechanical twins, but metallography could not establish this conclusively. Their tendency to form depended on strain rate, temperature and composition.

Specimens of silver-gold alloys (0 to 83 wt pct Au) were deformed plastically. One set was worked by hammering under liquid nitrogen, at room temperature and at intermediate temperatures. Another set was compressed slowly in liquid nitrogen to the same reductions as those produced by hammering. Tensile specimens (0.015 x 0.120 x 1.5 in.) of various compositions and approximately equal grain size (0.011 to 0.016 cm) were tested at −195°C and at room temperature.

In microsections of all specimens deformed by hammering at −195°C thin lamellae appeared, Fig. 1. They were aligned in definite directions in each grain. In some grains they had two orientations. Where lamellae intersected, a displacement was apparent. Near the center of the left margin of Fig. 1 shear has taken place beyond the fully developed intersecting lamella.

Many lamellae resembled Neumann bands in alpha iron. They were parallel to one side of triangular etch pits in the matrix (as in Figs. 1 and 2). The individual lamellae were narrow and had little substructure. This suggested that they did not result from concentrated local slip. The shape of etch pits within the lamellae differed from that of pits in the matrix, as can be seen in Fig. 2; this indicated a difference in orientation.

Specimens slowly deformed at −195°C contained regions in which the lamellae were clustered. In these specimens some lamellae were bent and presumably had formed before the termination of the deformation. Structures of greater width than the lamellae were also seen.[4]

More lamellar structures formed on impact than during slow compression to a given reduction. This was true of all compositions. The structures became less abundant with increasing temperature of deformation. None was observed after extension to fracture at room temperature, but they could be pro-

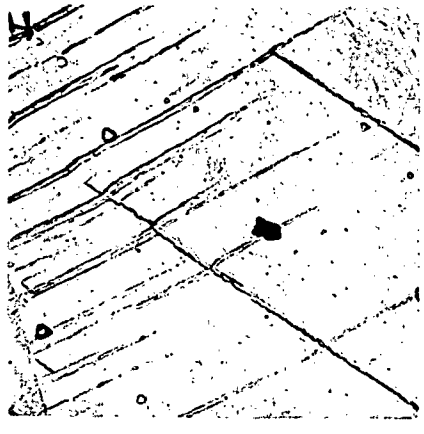

Fig. 1—Micrograph of specimen polished and etched after deformation by impact at −195°C. 83 pct Au. Oblique illumination. X500. Reduced approximately 39 pct for reproduction.

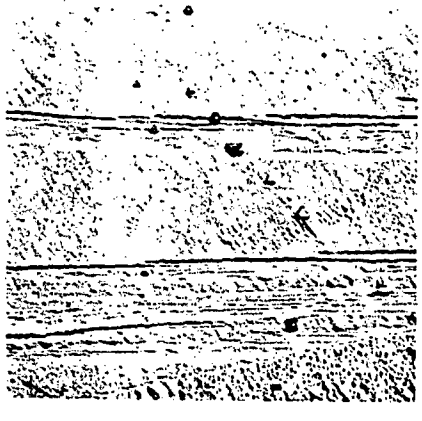

Fig. 2—Micrograph of specimen polished and etched after slow compression at −195°C. 83 pct Au. Oblique illumination. X1000. Reduced approximately 39 pct for reproduction.

R. J. BLOCK, teaching assistant in the School of Mines, Columbia University, New York, N.Y., was formerly an undergraduate at Massachusetts Institute of Technology, Cambridge, Mass. J. B. COHEN, presently a Fulbright Scholar at Conservatoire National des Arts et Mètiers, Paris, France, was formerly a Kennecott Copper Company Graduate Fellow at Massachusetts Institute of Technology. M. B. BEVER, Member AIME, is Professor of Metallurgy at Massachusetts Institute of Technology. Portions of this work were submitted by R. J. Block, in June 1956, in partial fulfillment of the requirements for the degree of Bachelor of Science at Massachusetts Institute of Technology.

TN 478 E. Manuscript, August 26, 1957.

ECONOMIC GEOLOGY
AND THE
BULLETIN OF THE SOCIETY OF ECONOMIC GEOLOGISTS

VOL. 71 DECEMBER, 1976 No. 8

A Kinetic Study of the Dissolution of Uraninite

D. E. GRANDSTAFF

Abstract

The kinetics of uraninite dissolution in water may be summarized by the equation:

$$R = \frac{-d(uran)}{dt} = 10^{20.25}(SS)(RF)^{-1}(10^{-3.33-10.8\,NOC})(a_{\Sigma CO_2})(D.O.)(a_{H^+})\exp(-7045/T)\ day^{-1}$$

where R is the rate of the dissolution reaction, SS is the specific surface area (cm^2-gm^{-1}), RF is an organic retardation factor, NOC is the mole fraction of nonuranium cations in the uraninite, D.O. is the dissolved oxygen content of the water (ppm), ΣCO_2 is the total dissolved carbonate, and T is the absolute temperature. Application of these data may allow better understanding of factors influencing oxidation of uraninite and the resulting mobility of uranium in natural waters.

Introduction

The oxidation of UO_2, U_3O_8, pitchblende, and uraniferous ore material has been studied by a number of investigators. The use of UO_2 as a fuel in nuclear reactors has prompted several studies of the oxidation of UO_2 or U_3O_8 under conditions simulating reactor failure (summary in Aronson, 1961). The use of carbonate and acid leaching in extraction of uranium from ore material has prompted several studies of oxidation to determine the kinetics of oxidation under the appropriate mill conditions (summary in Merritt, 1971).

Oxidation of uranium oxides in air or oxygen is quite slow, diffusion of oxygen through the oxide lattice being the rate determining step. UO_2 is oxidized to $UO_{2.8}$-$UO_{2.4}$ at temperatures up to 250°C. Above 250°C the $UO_{2.3}$-$UO_{2.4}$ is further oxidized to U_3O_8. Oxidation beyond U_3O_8 is more difficult in the laboratory.

In the presence of water the oxidation of uranium oxides proceeds in a completely different manner. A surface layer is oxidized directly to UO_3 (Gillies, 1946) or to a uranyl hydrate (Aronson, 1961). At low pH this oxidized layer may be taken into solution as a uranyl ion, UO_2^{+2}. At intermediate and high pH in the presence of carbonate the oxidized layer may react with aqueous carbonate species to produce a uranyl carbonate complex in solution (Merritt, 1971). Depending on the pH conditions either $UO_2(CO_3)_2(H_2O)_2^{-2}$ or $UO_2(CO_3)_3^{-4}$ is formed (Garrels and Christ, 1965). Removal of the oxidized layer permits further oxidation of the solid.

The oxidation of UO_2 and uraninite (represented as UO_2) at intermediate pH in the presence of dissolved carbonate probably takes place according to the overall formula

$$UO_2 + \tfrac{1}{2}O_2 + 2HCO_3^- + H_2O = UO_2(CO_3)_2(H_2O)_2^{-2} \quad (1)$$

Application of the results of the previous experiments to earth surface or near earth surface conditions might be extremely dubious due to the differences in temperature and reagent concentrations involved. Additionally, most of the studies used artificial UO_2 or U_3O_8 powders or sintered compacts. Natural uraninite is a complex mixture of elements. The kinetic rate measured from artificial preparations may not be reflected by natural products. Therefore, the present work has been undertaken using natural uraninite samples and has been carried out at temperatures of 23° and 2°C, under low oxygen and reagent concentrations, in order to reproduce more closely earth-surface conditions. This may permit application of the data toward a better understanding of factors influencing oxidation of uraninite in the natural environment and the result-

ing mobility of uranium in natural waters, as well as factors influencing secondary recovery of uranium from leaching of uraninite in mine dumps.

Material

Six samples of natural uraninite were used in this study. Four samples of pegmatitic uraninite (designated NC, M, N, and W) were purchased from Ward's Natural Science Establishment. The large uraninite crystals were crushed and handpicked to remove, so far as possible, secondary oxidation products and gangue minerals. The purity of the ultimate product was probably about 99 percent. No impurities were noted visually and no peaks, except those of uraninite, were found in X-ray diffraction traces. Two samples of uraniferous conglomerate from Blind River-Elliot Lake, Ontario, Canada (BR), and the Vaal Reefs West mine, Klerksdorp, Witwatersrand, South Africa (VR), were also obtained. These samples were crushed and the uraninite was separated by use of bromoform, Clerici solution, and the Frantz Isodynamic Separator. Because the quartz matrix could not be entirely separated from the uraninite, the two samples were probably not more than 95 percent pure.

The handpicked material was further crushed and sized by passing through sieves. The following U.S. standard mesh size fractions were used: $-200+325$, $-200+100$, and $-100+50$.

The geometric specific surface area of each fraction (the surface area per unit mass, expressed as $cm^2\text{-}gm^{-1}$) was calculated from measurement of the size of several hundred grains. Because uraninite has pronounced cubic cleavage, the crushed grains generally had the shape of tablets or laths. The length, width, and breadth of individual grains were measured under the binocular microscope. From these measurements the geometric specific surface area could be calculated. The estimate of the specific surface area is probably good to ±10 percent.

Chemical analyses of the uraninite samples were made by ARL-EMX microprobe. The measurements were made at 15 kV and 0.05 μA sample current with a 1 to 2 μm diameter beam. Artificial UO_2, ThO_2, glass, and natural silicate standards were used. Data were corrected for drift, which was negligible, background, and deadtime. Weight percent of oxides were calculated by the correction scheme of Bence and Albee (1968) and Albee and Ray (1970).

Four of the samples were homogeneous. However, the ore samples from the Blind River (BR) and the Witwatersrand (VR) were heterogeneous (Grandstaff, 1974).

Analysis for tetravalent uranium was made by

TABLE 1. Chemical Analyses and Unit Cell Dimensions of Uraninites Used in This Study
Elemental analyses by ARL microprobe, UO_2 analyses by titration.

	NC	M	N	W	BR[1]	VR[1]
	Weight percent					
UO_2	75.5	29.3	30.8	50.0	22.7	23.2
UO_3	12.3	59.8	51.0	20.1	42.6	46.9
ThO_2	2.0	3.2	4.1	15.3	6.1	3.9
CeO_2	0.2	0.3	0.4	0.8	1.0	1.1
PbO	5.8	5.5	10.9	13.9	22.6	21.0
La_2O_3	0.0	0.0	0.0	0.1	0.1	0.6
Y_2O_3	1.5	1.4	1.6	0.0	1.9	0.2
CaO	0.2	0.2	1.9	0.1	0.7	1.1
FeO	0.1	0.1	0.1	0.1	0.1	0.2
S	0.0	0.0	0.0	0.0	0.9	1.1
	97.6	99.7	100.1	100.4	98.5	99.3
a_0	5.4398 ±0.0008	5.4291 ±0.0020	5.4440 ±0.0002	5.4965 ±0.0007	5.4865 ±0.0010	5.4683 ±0.0005
	Cation mole fraction					
U(IV)	0.745	0.291	0.289	0.484	0.198	0.201
U(VI)	0.115	0.561	0.453	0.184	0.351	0.384
Th	0.020	0.032	0.039	0.152	0.055	0.034
Ce	0.003	0.005	0.006	0.012	0.014	0.015
Pb	0.069	0.066	0.124	0.163	0.239	0.221
La	0.000	0.000	0.000	0.002	0.001	0.009
Y	0.035	0.033	0.035	0.000	0.039	0.004
Ca	0.009	0.009	0.040	0.004	0.029	0.045
Fe	0.003	0.003	0.003	0.003	0.003	0.006
S	0.000	0.000	0.000	0.000	0.066	0.081

[1] Calculated from the average of grain analyses.

solution of uraninite in excess $Ce(SO_4)_2$ followed by titration with $FeSO_4$ (Rodden, 1950). In this procedure uranium (IV) undergoes an oxidation-reduction reaction with cerium (IV):

$$2Ce^{+4} + U^{+4} = 2Ce^{+3} + U^{+6} \quad (2)$$

The amount of cerium (IV) remaining may then be determined by titration with $Fe(SO_4)$:

$$Ce^{+4} + Fe^{+2} = Ce^{+3} + Fe^{+3} \quad (3)$$

The end point of the reaction (3) may be determined either by Eh electrode or by phenanthroline complex. The amount of U^{+4} may be determined from the amount of cerium oxidized in reaction (2). U^{+6} is determined by difference. In acidic solutions, Ce^{+3} is more stable than U^{+4} with respect to oxidation. Therefore, this procedure gives higher precision than direct determinations.

Table 1 provides some basic data for the samples investigated.

Experimental Procedure

Experiments were done in specially constructed 500 ml reaction cells. Details of construction are given in Grandstaff (1973). The top of the cell could be left open to admit ambient air or closed to permit special gas mixtures to be bubbled through the solution during experiments. The total pressure of gas mixture bubbled through the solution was maintained at one atmosphere. The base of the cell consisted of a fritted glass disk which allowed solutions to be removed from the cell without loss of uraninite grains. This enabled the rate of dissolution of samples to be measured repeatedly.

Prior to a dissolution experiment distilled water or previously prepared solutions were equilibrated with the ambient atmosphere or special gas mixtures (Table 2). The uraninite was then allowed to react with the solution for a period of time. After this period the resultant solution was separated from the uraninite by gravity filtration through the fritted glass filter. Reaction conditions were maintained during filtration. After filtration the solution pH was measured and the solution was acidified with hydrochloric acid to pH 1.6. This low pH enabled ions taken into solution during dissolution of the uraninite to be trapped by use of Reeve-Angel SA-2 ion-exchange loaded filter papers cut into disks.

Table 2. Composition of Gas Mixtures

Number	Percent N_2	O_2	CO_2
1.	97.87	2.10	0.03
2.	99.76	0.20	0.03
3.	97.50	2.10	0.40
4.	96.50	0.20	3.30

Table 3. Partial Analyses of Natural and Artificial Waters

	Artificial seawater[1]	Barnegat Bay	Oswego River
Chlorinity	19‰	17‰	—
HCO_3^-	2.4 meq/l	2.2 meq/l	0.01 meq/l
pH	8.18	8.15	3.95

[1] Prepared after Kester et al., 1967.

General specifications and use of the SA-2 filter paper have been described by Campbell (1963), Campbell et al. (1966), and Campbell et al. (1970). Recovery of uranium from test solutions by the SA-2 disks was greatest when the solution was approximately pH 1.6. Tests indicated recovery efficiency greater than 99 percent. During experiments two ion-exchange disks were exposed to each solution in sequence to insure quantitative recovery.

Uranium trapped in the ion-exchange papers was analyzed by the Norelco Universal Vacuum Spectrograph equipped with LiF crystal, scintillation counter, and Tungsten Target X-ray Tube.

Variables investigated during experiments included temperature, pH, P_{CO_2}, P_{O_2}, presence of inorganic ions and organic species, surface area, stirring rate, solution volume, and uraninite composition. The solution pH was varied by use of HCl, NaOH, and $NaHCO_3$ solutions. Other natural and artificial waters (Table 3) were also used to determine the possible effects of other inorganic and organic species.

Rates of reactions involving solutions can be estimated by taking aliquots of solution at intervals of time, stopping the reaction, and measuring the concentration or quantity of one or more of the species. The rate of the reaction is then given by the slope of the concentration-time line generated from the experimental points. This approach has proven generally impractical in this study because of the very slow reaction velocities, the small amount of uraninite taken into solution in reasonable periods, and the limits of sensitivity of the instrumental technique used. Instead, the uraninite was allowed to react for a period of time. After the reaction period all of the solution was taken from the reaction vessel and the amount of uranium was measured. The average rate of dissolution was calculated by the equations

$$R = d(\text{uran})/dt = \frac{M_{UO_2}(\text{soln})}{M_{\text{uran}} X_{UO_2} t} \ (\text{day}^{-1}) \quad (4)$$

or

$$R = d(\text{uran})/dt = \frac{M_{UO_2}(\text{soln})}{M_{\text{uran}} X_{UO_2} SSt} (gm_{\text{uran}} - cm^{-2} - day^{-1}) \quad (5)$$

where R = rate of the reaction; d(uran)/dt = the appearance of ions dissolved from uraninite in solution as a function of time; $M_{UO_2(soln)}$ = uranium as UO_2 in the solution (gm); M_{uran} = weight of uraninite undergoing oxidation (gm); X_{UO_2} = weight fraction of uranium as UO_2 in the uraninite; SS = specific surface area (cm^2-gm^{-1}); and t = time (days).

Equation (4) yields the rate of the reaction in terms of the fraction of uraninite destroyed per unit time (gm uraninite dissolved per gram of uraninite per day), while equation (5) takes into account the possible effects of surface area on the reaction rate (gm uraninite dissolved per cm^2 area per day).

The rate calculated from this method will be equal to the reaction rate if the amount of uranium in the initial solution is zero or negligibly small compared to the final concentration and if the rate is a constant.

Two sets of experiments were undertaken with the fastest reacting uraninite samples (M and NC) to test this method. In one, the more usual method of aliquot removal was employed. Aliquots were removed at intervals and analyzed for uranium. The total amount of uranium in solution was calculated, correcting for the amount removed in previous aliquots. The results (Fig. 1) indicate that the rate was constant during the period investigated. Oxidation rates calculated from these results agree well with those obtained from other experiments on the same material.

In a second set of experiments the uraninite was reacted in distilled water for varying periods of time. At the end of each experiment all of the solution was removed and analyzed for uranium and the mean rate calculated according to equations (4) and (5). The rates (Table 4) calculated were the same within experimental error for the various periods of time. Thus both of these sets of experiments show constant and reproducibly measurable reaction rates and justify the method used for the majority of experiments.

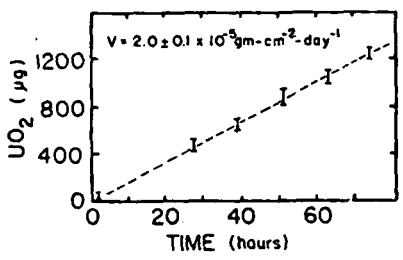

FIG. 1. Results of the rate test. The straight line obtained from the data suggests that the rate of dissolution was approximately constant during the experiment.

TABLE 4. Results of Rate Tests

Experiment number	Duration (days)	Rate (gm-cm^{-2}-day^{-1}) ($\times 10^6$)
L 4	1.0	4.2 ± 0.6
L 8	2.0	4.4 ± 0.6
L 9	2.5	4.2 ± 0.3
L 11	3.0	4.2 ± 0.3

During initial experiments the solution was stirred vigorously by polyethylene stirring rods. However, variation in the rate of stirring had no effect on the rate of dissolution, indicating that the reaction was not diffusion limited under the experimental conditions. Therefore, most of the experiments were carried out without stirring. In unstirred experiments, the rough fritted glass surface probably allowed contact between the downward-facing side of the uraninite grains, permitting dissolution to continue on that face, minimizing loss of effective surface area.

Most dissolution experiments were undertaken using 100 ml of solution. However, a few experiments were undertaken in solution volumes of 25 and 250 ml. The variation in solution volume did not have any discernible effect on the reaction rates.

The concentration of uranium in solution at the end of the experiments was generally less than 10 ppm. Although this concentration is much higher than that found in most natural waters (Wedepohl, 1969), the solutions appear to have been undersaturated with respect to uraninite (Bullwinkel, 1954). The undersaturation suggests that only "foreward" dissolution reactions were observed in this study. The absence of equilibrium and reactions precipitating uraninite can account for the lack of effect of uranium concentration and solution volume on the reaction rates observed.

After several experiments the relative concentrations of uranium, thorium, and lead in the solid uraninite were compared with the relative concentrations of these elements exchanged onto ion-exchange papers. The data indicate that the ratios of the three elements in the solid state and in solution are the same. Since the oxides of these three elements comprise the bulk of the uraninite, the data suggest that the uraninite oxidized and dissolved congruently under the experimental conditions.

Results and Discussion

The results of the experiments are tabulated in Appendix I. The tabulated analytical uncertainty

was calculated from the standard error based on X-ray fluorescence counting statistics.

The pH of distilled water used in the experiments varied between 5.5 and 5.7, consistent with the pH of distilled water in equilibrium with the atmosphere. However, the pH of the final solution in equilibrium with the atmosphere was usually about 5.9 to 6.3, averaging about 6.1. Therefore, the solution pH rose slightly during the runs. This pH variation was not noted in reaction breakers not containing uraninite. Therefore, the change in pH may be due either to the creation or destruction of hydrogen or hydroxyl ion during the reaction, or to addition of a species in the reaction products buffering the solution to a different pH.

The solution pH during a single experiment was measured at intervals as shown in Figure 2. The pH changed rapidly from pH 5.7 to a pH near 6.1, after which it remained constant. However, it appears that the uraninite dissolved at a more or less constant rate throughout.

Bullwinkel (1954) found that concentrated solutions of uranyl dicarbonate complex buffered the pH between 6 and 7. The buffering effect may be a result of the reactions

$$UO_2(CO_3)_2(H_2O)_2^{-2} + H^+ = HUO_2(CO_3)_2(H_2O)_2^{-1}$$
$$UO_2(CO_3)_2(H_2O)_2^{-2} + H^+ = H_2UO_2(CO_3)_2(H_2O)_2^{\circ} \quad (6)$$

The final concentration of uranyl dicarbonate in the experiments was greater than approximately 1×10^{-4} molar. The change in hydrogen ion concentration during the runs was approximately 1.5×10^{-6} M. If each uranyl dicarbonate ion is capable of reacting with two hydrogen ions, the uranyl carbonate should be capable of changing the hydrogen ion concentration to the degree observed. Thus these data are consistent with the interpretation that uranyl dicarbonate complex is formed by the oxidation reaction and that the pH is partially buffered by that complex. The presence of carbonate species and other ions in the solution may influence the buffering somewhat. Therefore, variations in the final pH from the different uraninite samples tested may be real and due to differences of the chemistry of the uraninite and hence of the solution. Variation between runs of the same sample are more likely a result of experimental errors.

TABLE 5. Summary of Rate Data (Distilled Water, Ambient Atmosphere)

Sample	Rate (gm-cm^{-2}-day^{-1}) ($\times 10^6$)	$\frac{R_1}{R_2}$	Temperature (°C)
NC	22.7 ± 0.4	2.69 ± 0.05	23
	8.4 ± 0.3		2
M	4.8 ± 0.2	2.66 ± 0.10	23
	1.8 ± 0.2		2
N	1.5 ± 0.1	2.54 ± 0.10	23
	0.59 ± 0.03		2
BR	0.24 ± 0.01	2.82 ± 0.25	23
	0.085 ± 0.008		2
W	0.066 ± 0.003	2.75 ± 0.25	23
	0.024 ± 0.003		2
VR	0.58 ± 0.03	2.50 ± 0.20	23
	0.20 ± 0.02		2
	Average	2.66 ± 0.12	

Effect of surface area

The dissolution of a solid differs from a homogeneous reaction of dissolved reactants primarily because not all of the atoms, but only those at the surface, are physically free to react. Consequently, the surface area unit mass (the specific surface) must appear in the rate expression, in analogy to the concentration or pressure in homogeneous reactions.

The data for variation of dissolution rate with

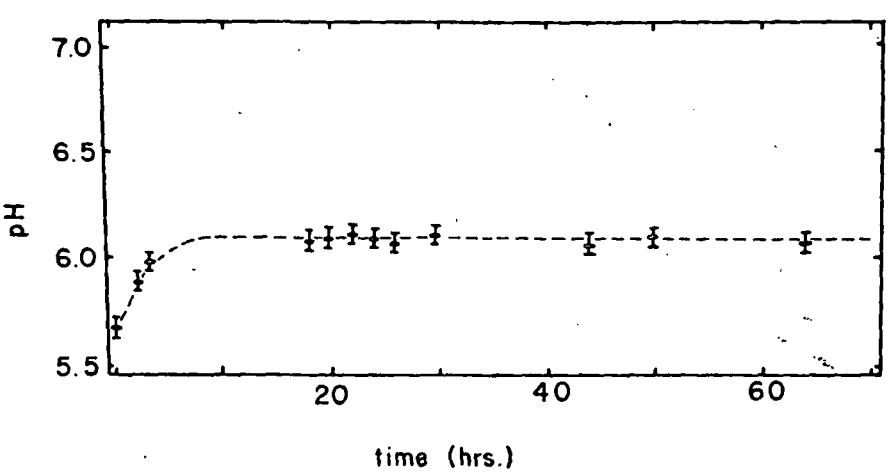

FIG. 2. Variation in pH during a single experiment.

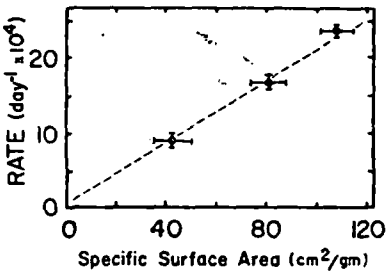

FIG. 3. Variation in dissolution rate with variation of the specific surface area of the uraninite grains. (Sample NC, T = 23°C, ambient air, distilled water.)

variation of specific surface are shown in Figure 3. The variation of rate appears to be first order with respect to surface area. This justifies tabulation of the reaction rate data in Appendix I in terms of the surface area ($gm\text{-}cm^{-2}\text{-}day^{-1}$).

Effect of composition

The effect of uraninite composition on the reaction rate was investigated by dissolution of the different uraninite samples in distilled water under ambient air at 23° and 2°C. The results are summarized in Table 5. Quite a wide variation of reaction rate was found in the uraninite samples investigated. For example, sample NC oxidized at a rate approximately 350 times faster than sample W. With all other experimental variables constant, the reaction rate is a function of the chemistry and crystallinity of the uraninite.

Because of the few samples investigated and the complex chemical system involved in the uraninite samples (UO_2-UO_3-ThO_2-$CeCO_2$-etc.), no unequivocal interpretation of the nature of the relationship between variation in chemistry and variation of reaction rate can be made. Several mechanisms may be proposed to explain the data but any conclusions must be empirical and tentative.

The oxidation state of the uranium in the uraninite could be an important factor in influencing the rate of dissolution. If U^{+6} could be taken directly into solution, any slow oxidation reaction steps might be avoided. If the oxidation state were a major factor, a correlation between the U^{+6} content or the U^{+6}/U^{+4} ratio and the rate of dissolution might be expected. In this case the highly oxidized samples M, VR, and BR (Table 1) would be the fastest reacting, while the less oxidized samples NC and W would be the slowest. However, no significant correlation between the extent of oxidation of the uranium in uraninite and the rate of dissolution was observed. This suggests that oxidation is not the only rate determining step and that release of materials from the uraninite surface into the solution may be an additional rate controlling factor.

Since thorianite is resistant to oxidation and exists as a detrital mineral (Frondel, 1958), Davidson (1960) speculated that the content of thorium in the uraninite influenced the rate of dissolution. Figure 4 shows a plot of the rate of dissolution versus the ThO_2 content. This figure does show a systematic decrease in the rate of dissolution with increasing ThO_2. However, this emphasis on the role of thorium ignores the possible stability of other end members and intermediate members with respect to oxidation.

Laxen (1971) has dissolved uranium dioxide crystals in strong acid. He compared the rate of dissolution of a crystal containing 8 percent ThO_2 with one pure UO_2. The rate of dissolution of the thorium-bearing crystal was about one third that of the pure uranium dioxide crystal. A much greater decrease in the reaction rate would be expected from consideration of data plotted in Figure 4. Therefore, unless the differing experimental conditions result in a change in the effect of chemical composition on the reaction rate, it appears that the effect of thorium content alone, as observed by Laxen (1971), is insufficient to account for the variation of rate observed in the present experiments.

The rate of oxidation of uraninite may be correlated with the total concentration of non-uranium oxides in the uraninite. This is shown in Figure 5. Although rates for the Witwatersrand uraninite (VR) and the Blind River uraninite (BR) were measured and are shown on the figure, they have not been used in the calculation of the rate equation (7) because of the marked heterogeneity of the samples.

The equation of the regression line is

$$R = k \exp_{10}(-3.38 - 10.8\ NOC) \qquad (7)$$

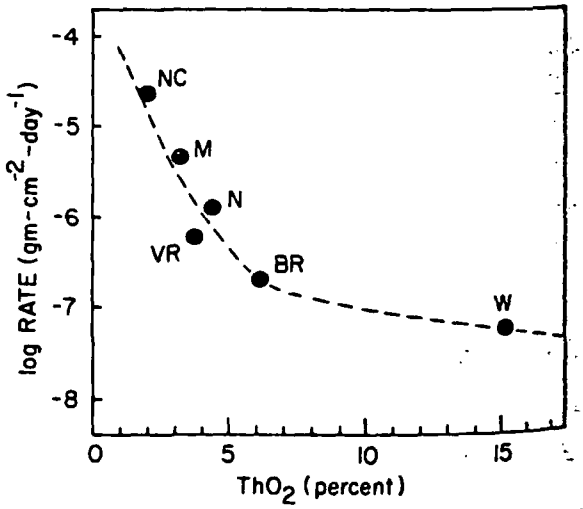

FIG. 4. Rate of uraninite dissolution as a function of uraninite ThO_2 content. (T = 23°C, ambient air, distilled water.)

where NOC is the mole fraction of non-uranium cations, primarily thorium and lead in the samples studied.

Analysis of the rate and compositional data by stepwise multiple regression analysis did not reveal any significant increase in correlation when the oxidation state of the uraninite was entered in the regression. This further suggests that the oxidation state of the uraninite is of only minor importance in determining dissolution rates.

One possible mechanism to explain the rate variation may be that the overall rate measued is a product of two steps or subreactions, an oxidation reaction involving the uranium (IV) atoms, and a solution or desorption reaction step involving both the uranium and non-uranium cations.

As the oxidation and solution reactions strip uranium cations from the uraninite surface, non-uranium ions will be encountered. If the rate of desorption of non-uranium ions is slower than that for the uranium ions, the reaction will be halted until the non-uranium ion can be removed, either by a solution reaction, or until the surrounding uranium cations are oxidized and the non-uranium ion is excavated from the surface. It seems reasonable that the more non-uranium cations are encountered the more the overall rate measured will be controlled by the desorption or excavation subreaction, slowing the overall solution rate.

The present treatment assumes that the different non-uranium cations are virtually identical in terms of their ability to reduce the rate of the overall reaction. That is, they are taken into solution or excavated from the surface at the same rate. This implies that a sort of steric hindrance is involved. However, it is well known that the lability and the rate of formation of soluble complexes is highly variable, depending primarily on the element forming the central atom of the complex (for example, Cotton and Wilkinson, 1966, p. 164, fig. 5.5). A more sophisticated approach might attempt to correlate variations in lability of the various impurity cations to variations in rate. In this case one or two cations might be rate determining. However, the data available are not sufficient to test such a model.

Another rate mechanism proposed by Laxen (1971) in experiments previously cited concerns the electric properties of the uraninite. UO_2 is a p-type semiconductor; Laxen proposed that addition of ThO_2 would make the UO_2 more p-type and therefore more difficult to dissolve. This explanation might also be generalized to include other components. Unfortunately, it appears difficult to assess the extent to which the dissolution rate might be altered by this mechanism.

Only by conducting kinetic experiments of this type on crystals along the various compositional joins (UO_2-ThO_2, UO_2-CeO_2, etc.) can a more complete relationship between chemistry and rate be determined.

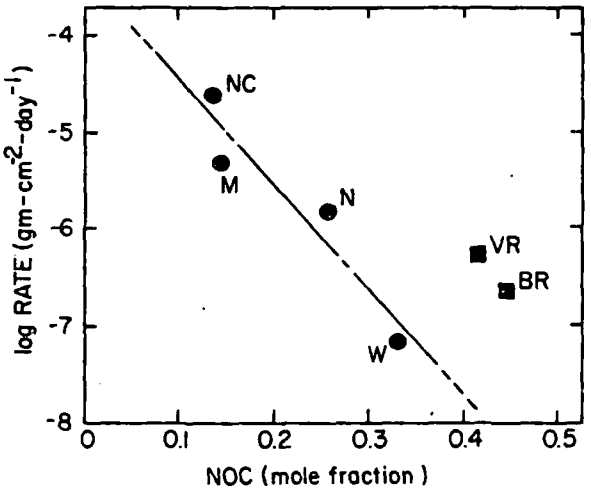

FIG. 5. Rate of uraninite dissolution as a function of non-uranium cation mole fraction (NOC). ($T = 23°C$, ambient air, distilled water.) Samples indicated by square symbols (BR and VR) were not considered in the analysis because of marked sample heterogeneity.

Chemical variables are probably not the only factors influencing the reaction rate. Differences in crystallinity, the number of growth defects, and defects caused by nuclear recoil following radioactive decay may all change its susceptibility to oxidation. For example, Gillies (1946) ascribed differences in the oxidation rate of different U_3O_8 samples to differences in crystallinity. Nel (1958) found that the resistance of uraninite to chemical attack by acid solutions could be improved by heating the uraninite in vacuo, thus annealing the uraninite. This suggests that the oxidation reaction may be at least partially localized on defects. These structural factors were not investigated in the present work. However, no significant differences in line broadening in X-ray traces, ascribable to variations in crystallinity, were noted in the samples investigated.

If radiation recoil damage to the uraninite structure were a major factor influencing reaction rates, and since structural radiation damage is proportional to the amount of radiogenic lead, and therefore the age of the uraninite, it would be expected that the samples of mid-Precambrian uraninite from the Witwatersrand (VR) and Blind River (BR) would be the fastest reacting, while the samples NC and M would be the slowest reacting. In fact, samples VR and BR dissolve much more slowly than NC and M, suggesting that structural effects in pegmatitic uraninites are subsidiary to the chemical effects.

The assumption that structural damage increases in proportion to the amount of radiogenic lead may

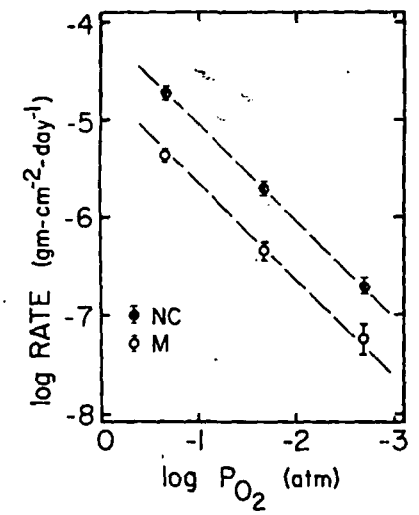

FIG. 6. Variation of dissolution rate as a function of oxygen partial pressure showing first order dependence. (Samples M and NC, T = 23°C.)

not be correct. Uraninite does not become metamict as do thorite, zircon, or some other minerals containing high concentrations of uranium and thorium. This suggests that structural damage in uraninite may reach a limiting value, short of that in-metamict minerals.

Effect of oxygen partial pressure

The effect of oxygen partial pressure on the rate of dissolution was determined by reacting two samples of uraninite with water equilibrated with ambient air and with mixtures (Table 2) containing less oxygen than the ambient air.

A plot of the logarithm of the dissolution rate vs the logarithm of the oxygen pressure gives a straight line having near unit slope (Fig. 6). The rate of dissolution is therefore directly proportional to the partial pressure of oxygen, at least at 23°C and oxygen partial pressures less than 0.2 atm.

Effect of hydrogen ion

The effect of hydrogen ion concentration on the rate of dissolution was determined by reacting uraninite under ambient atmosphere in dilute solutions of HCl and distilled water having a pH range from about pH 4 to pH 6. The interpretation of the results is complicated slightly by the change in pH due to the formation of the uranyl ion.

A plot of the logarithm of the dissolution rate versus pH is shown in Figure 7. The horizontal bars indicate the variation of pH during the runs. Ideal lines for half, first, and second order dependency are superimposed. The data demonstrate a first order dependence for the dissolution rate with hydrogen ion concentration in the range pH 4 to 6.

Effect of carbonate species

In two experiments the effects of carbonate were examined by direct variation in the pressure of carbon dioxide. However, variation in P_{CO_2} also produces a variation in the pH of the distilled water due to the formation and dissociation of carbonic acid. Therefore, variation of carbonate concentration was also created by variation of the concentration of $NaHCO_3$. Concentrated solutions of freshly prepared sodium bicarbonate ($> 10^{-3}$ M) have a pH of 8.35, independent of concentration (Olson et al., 1956). Therefore the effect of changes of bicarbonate concentration could be investigated without simultaneous change in the initial pH.

The data are shown in Figure 8. The effect of bicarbonate on the rate is first order at lower concentrations and becomes zero order at higher concentrations. This behavior can be explained by the requirements of adsorption of reactant species from solution onto the uraninite surface. The reaction is probably dependent on the amount of carbonate adsorbed onto the surface of the uraninite grains. Mathematically this may be expressed as

$$R = k\,\Theta \qquad (8)$$

where R is the rate of the reaction, k is a rate constant, and Θ is the surface coverage of the adsorbed species, in this instance bicarbonate (Thomson and Webb, 1968). If the extent of surface coverage is related to solution concentration as approximated by the Langmuir adsorption isotherm, as the simplest example, the relationship between surface coverage and solution concentration will be expressed by the equation

$$\Theta = bX/(1 + bX) \qquad (9)$$

where b is a coverage constant and X is the concentration of the species in solution. Substitution of

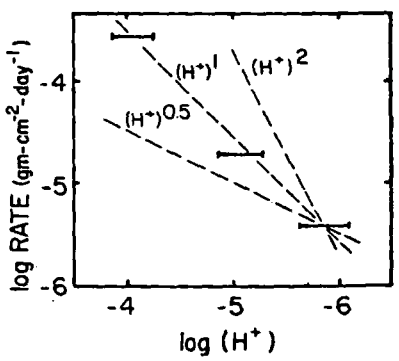

FIG. 7. Variation of dissolution rate as a function of hydrogen ion concentration. Trend lines for half, first, and second order relations are superimposed. The horizontal lines indicate the variation of hydrogen ion concentration during the various experiments. (Sample M, T = 23°C ambient air.)

quation (9) into (8) yields

$$R = kbX/(1 + bX) \qquad (10)$$

t low concentrations the surface is sparsely covered, $bX \ll 1$ and $(1 + bX) \approx 1$ and equation (10) reduces to

$$R = kbX \qquad (11)$$

he reaction is first order. Conversely at high surface coverage and high reagent concentrations the surface becomes saturated with the adsorbed species and further increases of the concentration of the species if solution fails to raise the concentration adsorbed to the grain surface. Mathematically, at high reagent concentrations $bX \gg 1$ and $(1 + bX) \approx bX$ and equation (10) reduces to

$$R = k \qquad (12)$$

he reaction becomes zero order, independent of the icarbonate concentration in solution. The reaction ata shown in Figure 9 fit a Langmuir equation (10) aving constants, $k = 1.0 \times 10^{-4}$ gm-cm^{-2}-day^{-1}, and $= 13.2$ molar^{-1}. Most natural waters have bicarbonate concentrations on the order of 10^{-3} molar or ess. This is in the region in which the rate is first rder. Extrapolation of the rate data to concentrations of 1.6×10^{-5} molar, the concentration of otal dissolved carbonate ($\Sigma CO_2 = H_2CO_3 + HCO_3^- + CO_3^{-2}$) in distilled water at pH 6 in contact with mbient air, yields a rate of $1.6 \pm 0.4 \times 10^{-8}$ gm-m^{-2}-day^{-1} in good agreement with the rate value xtrapolated on the basis of the pH dependency.

This suggests that the reaction rate is dependent n the total dissolved carbonate, rather than H_2CO_3 r HCO_3^- alone. This is reinforced by the data om the experiments in which P_{CO_2} was varied. Variation of the dissolution rate is apparently dependent on H_2CO_3 in these experiments, since, at he lower pH of these experiments, carbonic acid is he major carbon-bearing species.

These experiments suggest that, in the first order

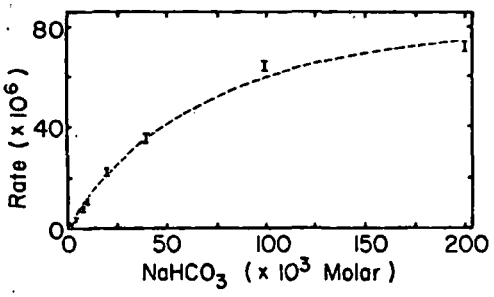

Fig. 8. Variation of dissolution rate as a function of HCO_3 concentration. (Sample M, ambient air T = °C)

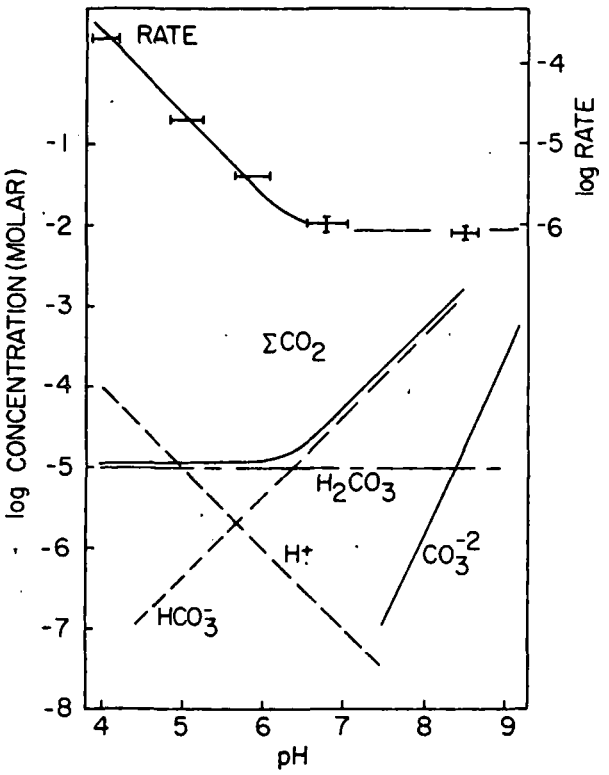

Fig. 9. Interaction of hydrogen ion and carbonate species at intermediate pH. (Sample M, ambient air, T = 23°C.) Horizontal bars indicate variation in pH during the various experiments, vertical bars indicate analytical uncertainty, where appreciable.

region, the equation has the form

$$R = k\ (a_{H^+})\ (a_{\Sigma CO_2}) \qquad (13)$$

This interpretation is parallel with that of Shortmann and DeSesa (1958). They found that, as long as some bicarbonate was present, the reaction was broadly dependent on total dissolved carbonate rather than HCO_3^- or CO_3^{-2} alone.

Interaction of hydrogen ion and carbonate species

Dissolution rate data are shown in Figure 9 for the range of pH 4 to 8.5 for reactions open to the atmosphere. These data are superimposed on a theoretical line based on rate equation (13).

At low pH, carbonic acid is the dominant dissolved carbon-bearing species. The total dissolved carbonate may be approximated by carbonic acid alone ($\Sigma CO_2 \approx H_2CO_3$). At constant temperature and ionic strength the concentration of carbonic acid in solution is a function only of the carbon dioxide pressure of the atmosphere. This is expressed as

$$(H_2CO_3) = BP_{CO_2}$$

where concentration and pressure substituted for activity and fugacity. B is the Henry's Law co-

efficient relating the pressure of carbon dioxide in the atmosphere to the concentration of carbonic acid. At low pH equation (13) may therefore be rewritten

$$R = k\ (H^+)(BP_{CO_2}) \qquad (14)$$

If the carbon dioxide pressure is constant, this reduces to

$$R = k'\ (H^+)$$

The velocity of the reaction varies with the concentration of hydrogen ion as shown in Figure 7.

At intermediate pH, however, above approximately pH 6.3, the concentration of total dissolved carbonate rises as bicarbonate ion becomes the dominant carbon-bearing species. The bicarbonate increases with decreasing hydrogen ion concentration according to the equation

$$(HCO_3^-) = \frac{K_1 BP_{CO_2}}{(H^+)}$$

This may be substituted into the rate equation (13), yielding

$$R = k(H^+)\frac{K_1 BP_{CO_2}}{(H^+)} = K_1 BP_{CO_2} \qquad (15)$$

Therefore, at intermediate pH, between approximately 6.3 and 10.4, the rate should be constant, dependent only on the carbon dioxide pressure of the atmosphere. This is shown by data in Figure 9.

Extrapolation from equation (13) suggests that under high pH conditions the oxidation rate might be inversely related to a_{H^+}. However, results of dissolution experiments under alkaline conditions (Merritt, 1971) suggest that different reaction mechanisms may be involved at high pH and such extrapolation may not be valid.

Therefore, for open systems, such as rivers, where a near approach to equilibrium with the atmosphere would be expected, the rate of oxidation of uraninite will be constant between pH 6.3 and 10.4 for constant oxygen pressure and temperature. Rivers today generally have pH values of between 4.5 and 8.5. Rivers draining crystalline terrains have pH ranges between 6.5 and 7.5. This is in the constant rate region.

For closed systems, such as ground waters, not in contact with the atmosphere ΣCO_2 rather than P_{CO_2} must be considered. Under these conditions the rate will tend to fall parallel to the line of pH variation, if the total carbonate content of the water is constant.

Effect of temperature

For most chemical reactions, the rate varies exponentially with the reciprocal of the absolute temperature. This fact is expressed mathematically by the Arrhenius equation

$$\frac{dR}{dT} = k\exp(-E_a^*/RT) \qquad (16)$$

where dR/dT is the change of reaction rate with change in temperature, E_a^* is the activation energy, and R is the gas constant. Proof that the reaction follows the Arrhenius relation is usually obtained by acquisition of a straight line in a plot of the logarithm of the rate vs the reciprocal of the absolute temperature. Several studies of the oxidation of UO_2 at high P and T have found that the reaction does obey the Arrhenius relation (Shortmann and DeSesa, 1958; Mackay and Wadsworth, 1958). Since, in this study, the reaction has been investigated at only two temperatures, proof of this cannot be obtained, and it must be assumed that the reaction will follow the Arrhenius rate law.

For analysis at two temperatures the following form of the Arrhenius equation may be used

$$\ln\frac{R_1}{R_2} = \frac{E_a^*}{R}\left[\frac{1}{T_2} - \frac{1}{T_1}\right] \qquad (17)$$

where R_1 and R_2 are the rates at temperatures T_1 and T_2 respectively. Values R_1/R_2 are gathered in Table 5. R_1/R_2 for the various uraninite samples appear to be the same within the experimental limits. This allows the interpretation that all of the uraninite samples studied have the same rate determining step and that the dissolution mechanism is the same for all them. The average for the samples is 2.66 ± 0.12. This yields an apparent activation energy near 8 kcal/mole. However, this is not the true value. Although the experiments at both temperatures were undertaken under ambient atmospheric conditions, the solubility of oxygen and carbon dioxide changes between 23° and 2°C. The solubility of oxygen increases by about 50 percent while the solubility of carbon dioxide nearly doubles (Garrels and Christ, 1965; Stumm and Morgan, 1970). The increased solubility of carbon dioxide at low temperature causes a decrease in the pH, although the value of the first dissociation constant decreases slightly at lower temperatures. All of these factors have an effect on the rate. When the reaction conditions are recalculated to equi-dissolved oxygen, dissolved carbonate, and pH with linear corrections, the activation energy calculated is 14 ± 2 kcal/mole.

Organic molecules and inorganic ions

Several experiments were done in natural and artificial waters (Table 3) containing inorganic and organic species to determine if these had any effect on the reaction rate. The rate expected was calculated from the concentration of hydrogen ion and total dissolved carbonate, on the basis of the kinetic

TABLE 6. Organic Retardation by Various Waters

Experiment number	Observed rate (gm-cm^{-2}-day^{-1}) ($\times 10^6$)	Calculated rate (gm-cm^{-2}-day^{-1}) ($\times 10^6$)	RF	Water sample
HSA	3.0 ± 0.3	3.2 ± 0.6	1.1 ± 0.1	Artificial seawater
PSA	15.0 ± 1.0	15.0 ± 2.0	1.0 ± 0.1	Artificial seawater
PSW	0.42 ± 0.06	15.6 ± 2.0	37.0 ± 6.0	Barnegat Bay
NSW	0.49 ± 0.06	18.5 ± 0.5	38.0 ± 6.0	Barnegat Bay
LOX	72.0 ± 6.0	420.0 ± 80.0	6.0 ± 1.0	Oswego River

equation (13). The expected rate was compared with the observed rate and a retardation factor was calculated by

$$RF = \frac{R_{calc}}{R_{obs}} \tag{18}$$

The results are summarized in Table 6. The results indicate that inorganic species present in the artificial seawater, other than hydrogen ion and dissolved carbonate, had very little effect on the reaction rate. In contrast the reaction rate observed in natural water was less than that expected. New Jersey seawater gave a retardation of approximately 37 times while Oswego River water gave a reaction rate approximately 6 times less than expected. This effect may be due to organic molecules. Apparently they bond with and block the surface oxidation sites. Essentially, they appear to decrease the effective surface area of the uraninite grains. In this way they act analogously to a poison on a catalyst.

Chave (1965), Chave and Schmaltz (1966), and Suess (1970) found that polar organic matter interacts with calcium carbonate to form surface complexes. These surface complexes partially isolated the calcium carbonate minerals from seawater and decreased rates of nucleation, growth, and dissolution. Berner (1971) postulated that complexing of surfaces caused the apparent supersaturation of calcium carbonate in natural waters.

The large difference in the amount of retardation between the Oswego River water and the seawater may be due to a difference in the organic species present, the organic content, or the pH of the two waters. Rothstein and Meier (1951) noted that the stability of some uranyl-organic complexes was decreased at low pH. Therefore, the tendency to form surface uraninite-organic complexes may be less at low pH. This would result in a decrease in the retardation factor. Therefore, the lower retardation factor calculated for Oswego River water may be due, in part, to the low pH of this water.

In clay minerals, those having greater isomorphic substitution or lattice imperfections, including broken bonds, are generally favored for adsorption and bonding with organic molecules (Rashid et al., 1972). The surface of a particle undergoing dissolution should therefore be ideal to provoke bonding between the crystal and the organic molecule.

Experimental rate expression

The information obtained from the experiments elucidating the effects of surface area, composition, oxygen, carbonate, organic molecules, pH, and temperature may be summarized by writing a single rate equation. In the first order regions, such an equation is

$$R = 10^{20.25}(SS)\,(RF)^{-1}\,(10^{-3.89-10.8})\,(DO)\,(a_{\Sigma CO_2})\,(a_{H^+})\exp(-7045/T)\ \text{day}^{-1} \tag{19}$$

where SS = specific surface area (cm^2 − gm^{-1}); RF = organic retardation factor; NOC = mole fraction of non-uranium cations in uraninite; DO = dissolved oxygen (ppm); and Σ_{CO_2} = total dissolved carbonate (molar).

It is impossible to specify the limits within which this rate equation is applicable to uraninite dissolution. Radical changes in the reaction parameters are likely to result in changes in the reaction mechanism (Merritt, 1971). The equation is unlikely to be applicable at much higher temperature, gas pressure, or pH. The rate equation must also break down under conditions in which $P_{O_2} > 0$ and $\Sigma CO_2 \rightarrow 0$. Under these conditions the rate equation suggests that the dissolution rate would go to zero as well. However, it is likely that under such conditions the formation of the uranyl ion, UO_2^{+2}, would proceed at a finite rate, providing another mechanism for dissolution. However, such conditions are unlikely to be encountered in geological situations.

Tentative Reaction Mechanisms

Because the intermediate compounds in the reaction are not well known, the exact rate mechanism must remain speculative. However, some points are fairly clear.

One rate determining step appears to be that of adsorption of molecular oxygen onto the uraninite surface at an adsorption site. Schematically

$$UO_2 + O_2 = UO_2 - O_2 \ \text{(slow)} \tag{20}$$

This gives rise to the first order dependence on the oxygen partial pressure This reaction is followed by

faster steps involving possible migration of the oxygen from an adsorption site to an oxidation site, if the two are not identical, and splitting of the oxygen molecule:

$$UO_2 + O + H_2O = UO_3 \cdot H_2O \quad \text{(fast)} \quad (21)$$

Data of Gillies (1946) and Nel (1958) suggest that crystal dislocations or radiation defects may serve either as adsorption or oxidation sites.

The intermediate compound of the reaction (21) at room temperature is unknown. Aronson (1961), in experiments at temperatures of 87° to 177°C, found that a uranyl hydrate, approximately $UO_3 \cdot 0.8 H_2O$ was formed (represented here as $UO_3 \cdot H_2O$). This has been used in the present interpretation. However, at room temperatures in the presence of excess water the dihydrate, $UO_3 \cdot 2H_2O$, is the thermodynamically favored phase. This composition corresponds roughly to the minerals ianthiaite, bequerelite, schoepite, and masuyite (Frondel, 1958). Therefore, it is possible that a different uranyl hydrate is formed at room temperatures.

Because the reaction is dependent on both oxygen and carbonate concentration, this first rate determining reaction (20) must be followed in steady state by a second reaction involving the addition of carbonate and creation of a uranyl carbonate complex (Shortmann and DeSesa, 1958). Although the stoichiometry of the reaction (equation 1) indicates that two carbonate molecules are added during the reaction, the first order dependence found in this investigation suggests that one carbonate is added faster than the other:

$$UO_3 \cdot H_2O + HCO_3^- = UO_2(CO_3)(H_2O)(OH)^- \text{ (slow)} \quad (22)$$

$$UO_2(CO_3)(H_2O)(OH)^- + HCO_3^- = UO_2(CO_3)_2(H_2O)_2^{-2} \text{ (fast)} \quad (23)$$

Here the addition of the first carbonate is suggested as the slow step. The first rate determining reaction (20) creates an oxidized surface on the uraninite grain. The second reaction then scavenges this surface, removing the oxidized layer and exposing a fresh surface.

The nature of the hydrogen ion dependence is much more obscure. Mackay and Wadsworth (1958) have suggested a mechanism similar to the one suggested here. When the uraninite is placed in water the fresh surface becomes hydrated:

$$UO_2 + H_2O = UO(OH)_2$$

This hydrated surface could then undergo dissociation, the extent of the surface dissociation being a function of the solution pH. Thus at low pH the surface would be highly associated while at higher pH the surface hydrated complex would become increasingly dissociated:

$$UO_2(OH)_2 = UO_2OHO^- + H^+ \quad \text{(first dissociation) (equilibrium)} \quad (24)$$

and

$$UO_2(OH)O^- = UO_3O^{-2} + H^+ \quad \text{(second dissociation) (equilibrium)} \quad (25)$$

If the oxygen molecule could only adsorb on a fully associated surface site or if the fully associated site was the site for oxidation, the first order dependence on the solution hydrogen ion concentration might be explained.

Acknowledgments

This paper is based on a Ph.D dissertation presented at Princeton University. I am grateful to Dr. H. D. Holland for supervision of the thesis work. I greatly appreciate the generosity of Dr. S. A. Antrobus of Anglo-American Corporation of South Africa and Rio Algam Mines Limited for samples of high grade uranium ores.

Financial support for the work was provided by a fellowship granted under Title IV of the National Defense Education Act, by Princeton University Department of Geological and Geophysical Sciences, and by grants to the Princeton University computer center.

Department of Geology
Temple University
Philadelphia, Pennsylvania 19122
August 7, 1975; April 15, 1976

REFERENCES

Albee, A. L., and Ray, L., 1970, Correction factors for electron probe microanalysis of silicates, oxides, carbonates, phosphates and sulfates: Anal. Chemistry, v. 42, p. 1408–1414.

Aronson, S., 1961, Oxidation and corrosion of uranium dioxide, *in* Belle, J., Uranium dioxide: Properties and nuclear applications: U. S. Atomic Energy Commission, Washington, D. C., U. S. Government Printing Office, 726 p.

Bence, A. E. and Albee, A. L., 1968, Empirical correction factors for the electron microanalysis of silicates and oxides: Jour. Geology, v. 76, p. 382–403.

Berner, R. A., 1971, Principles of chemical sedimentology: New York, McGraw-Hill Book Company, 240 p.

Bullwinkel, E. P., 1954, The chemistry of uranium in carbonate solutions: U. S. Atomic Energy Commission, Raw Materials Division Topical Report RMO-2614, 66 p.

Campbell, W. J., 1963, Fluorescent X-ray spectrographic analysis of trace elements including thin films, *in* Symposium on X-ray and electron probe analysis: American Society for Testing and Materials, Spec. Tech. Pub. 349, p. 28–34.

—— Green, T. E., and Law, S. L., 1970, Ion exchange papers in X-ray spectroscopy: Am. Laboratory, June 1970, p. 28–34.

Campbell, W. J., Spano, E. F., and Green, T. E., 1966, Micro and trace analysis by a combination of ion exchange resin-loaded papers and X-ray spectrography: Anal. Chemistry, v. 38, p. 987–996.

Chave, K. E., 1965, Carbonates: Association with organic matter in surface seawater: Science, v. 148, p. 1723–1724.
— and Schmalz, R. F., 1966, Carbonate–seawater interactions: Geochim. et Cosmochim. Acta, v. 30, p. 1037–1048.
Cotton, F. A., and Wilkinson, G., 1966, Advanced inorganic chemistry: New York, Wiley Interscience, 1136 p.
Davidson, C. F., 1960, The present state of the Witwatersrand controversy: Mining Mag., v. 102, p. 84–95, 149–159, 222–229.
Frondel, C., 1958, Systematic mineralogy of uranium and thorium: U. S. Geol. Survey Bull. 1064, p. 400.
Garrels, R. M., and Christ, C. L., 1965, Solutions, minerals, and equilibria: New York, Harper and Row, 450 p.
Gillies, D. M., 1946, Some studies of the reactions of uranium oxides with hydrogen, oxygen, and water: Unpub. Ph.D. dissertation, Univ. Pennsylvania.
Grandstaff, D. E., 1973, Kinetics of uraninite oxidation: implications for the Precambrian atmosphere: Unpub. Ph.D. dissertation, Princeton Univ.
— 1974, Microprobe analysis of uranium and thorium in uraninite from the Witwatersrand, South Africa, and Blind River, Ontario, Canada: Geol. Soc. South Africa Trans., v. 77 (3), p. 291–294.
Kester, D. R., Duedall, I. W., Connors, D. N., and Pytkowicz, R. M., 1967, Preparation of artificial seawater: Limnology Oceanography, v. 12, p. 176–179.
Laxen, P. A., 1971, The dissolution of UO_2 as an electron transfer reaction, *in* The recovery of uranium: International Atomic Energy Agency, Vienna, 478 p.
Mackay, T. L., and Wadsworth, M. E., 1958, A kinetic study of the dissolution of UO_2 in sulfuric acid: Am. Inst. Mining Metall. Petroleum Engineers Trans., v. 212, p. 597–603.
Merritt, R. C., 1971, The extractive metallurgy of uranium: Golden, Colorado, Colorado School Mines Research Inst., 576 p.
Nel, H. J., 1958, Discussion of the attrition of uraninite, by G. M. Koen: Geol. Soc. South Africa Trans., v. 61, p. 194.
Olson, A. R., Kock, C. W., and Pimentel, G. C., 1956, Introductory quantitative chemistry: San Francisco, W. H. Freeman, 470 p.
Pearson, R. L., and Wadsworth, M. E., 1958, A kinetic study of the dissolution of UO_2 in carbonate solution: Am. Inst. Mining Metall. Petroleum Engineers Trans., v. 212, p. 294–300.
Rashid, M. A., Buckley, D. E., and Robertson, K. R., 1972, Interactions of a marine humic acid with clay minerals and a natural sediment: Geoderma, v. 8, p. 11–25.
Rodden, C. J., 1950, Analytical chemistry of the Manhatten project: New York, McGraw-Hill Book Co., 748 p.
Rothstein, A., and Meier, R., 1951, The relationship of the cell surface to metabolism: Jour. Cellular Comp. Physiology, v. 38, p. 245–270.
Shortmann, W. E., and DeSesa, M. A., 1958, Kinetics of the dissolution of uranium dioxide in carbonate-bicarbonate solutions: Second United Nations International Conference on the Peaceful Uses of Atomic Energy, Geneva, Proc., v. 3, p. 333–341.
Stumm, W., and Morgan, J., 1970, Aquatic chemistry: New York, John Wiley and Sons, Inc., 583 p.
Suess, E., 1970, Interaction of organic compounds with calcium carbonate, I. Association phenomena and geochemical implications: Geochim. et Cosmochim. Acta, v. 34, p. 157–168.
Thomson, S. J., and Webb. G., 1968, Heterogeneous catalysis: New York, John Wiley and Sons, Inc., 197 p.
Wedepohl, K. H., ed., 1969, Handbook of geochemistry: New York, Springer-Verlag, p. 442.

APPENDIX 1. Results of Dissolution Experiments

Number	Sample[1]	Surface area (cm^2-gm^{-1})	Duration (days)	T (°C)	Atm.[2]	pH[3] (±0.05)	Rate (gm-cm^2-day^{-1}) ($\times 10^5$)
T 14	NC	81	2.0	23 ± 2	A	6.27	1.9 ± 0.3
T 15	NC	81	1.0	23 ± 2	A	6.11	2.0 ± 0.3
T 16	NC	81	2.5	23 ± 2	A	6.18	2.0 ± 0.3
T 17	NC	81	2.5	23 ± 2	A	6.18	2.0 ± 0.3
R 7	NC	81	2.0	2 ± 1	A	5.92	0.7 ± 0.1
R 8	NC	81	3.0	2 ± 1	A	5.93	0.7 ± 0.1
R 9	NC	81	2.0	2 ± 1	A	5.96	0.7 ± 0.1
P 5	NC	43	2.0	23 ± 1	A	6.02	1.8 ± 0.2
P 7	NC	43	2.0	23 ± 1	A	5.94	1.7 ± 0.2
X 1	NC	104	1.0	23 ± 1	A	6.18	2.0 ± 0.2
X 2	NC	104	1.0	23 ± 1	A	6.18	2.0 ± 0.2
W 4	W	50	5.0	23 ± 2	A	6.15	0.0044 ± 0.0006
W 5	W	50	5.0	23 ± 2	A	5.99	0.0048 ± 0.0006
W 6	W	50	5.0	23 ± 2	A	6.11	0.0048 ± 0.0006
W 11	W	50	15.0	2 ± 1	A	5.87	0.0017 ± 0.0003
W 12	W	50	16.0	2 ± 1	A	5.96	0.0016 ± 0.0003
VR 1	VR	76	15.0	23 ± 2	A	6.08	0.041 ± 0.006
VR 2	VR	76	15.0	23 ± 2	A	6.05	0.037 ± 0.006
VR 4	VR	76	40.0	2 ± 1	A	5.90	0.016 ± 0.002
N 4	N	53	3.0	23 ± 2	A	6.34	0.12 ± 0.02
N 5	N	53	4.0	23 ± 2	A	6.29	0.12 ± 0.02
N 7	N	53	4.0	2 ± 1	A	6.09	0.05 ± 0.01
N 8	N	53	15.0	2 ± 1	A	6.14	0.05 ± 0.01
BR 4	BR	52	17.0	23 ± 2	A	6.06	0.015 ± 0.002
BR 5	BR	52	10.0	23 ± 2	A	5.98	0.016 ± 0.002
BR 6	BR	52	10.0	23 ± 2	A	5.92	0.015 ± 0.002
BR 9	BR	52	22.0	3 ± 2	A	5.89	0.006 ± 0.001
Br 10	BR	52	24.0	2 ± 1	A	5.93	0.005 ± 0.001
L 4	M	50	1.0	23 ± 2	A	6.16	0.42 ± 0.06
L 8	M	50	2.0	23 ± 2	A	6.08	0.44 ± 0.06
L 9	M	50	2.5	23 ± 2	A	6.10	0.42 ± 0.03
L 11	M	50	3.0	23 ± 2	A	6.05	0.42 ± 0.03
L 12	M	50	4.0	2 ± 1	A	5.92	0.16 ± 0.02

APPENDIX 1.—(*Continued*)

Number	Sample	Surface area (cm^2-gm^{-1})	Duration (days)	T (°C)	Atm.	pH_i[4] (±0.05)	pH_f	Rate ($gm\text{-}cm^{-2}\text{-}day^{-1}$) ($\times 10^5$)
L 5	M	50	3.0	23 ± 2	1	5.59	5.78	0.048 ± 0.008
L 6	M	50	4.0	23 ± 2	1	5.68	5.99	0.042 ± 0.008
L 7	M	50	4.0	23 ± 2	1	5.65	5.98	0.042 ± 0.008
K 10	M	50	7.0	23 ± 2	2	5.64	5.95	0.006 ± 0.002
K 100C	M	50	1.0	23 ± 2	4	4.72	5.21	4.5 ± 0.2
K 10C	M	50	1.0	23 ± 2	3	5.20	5.78	1.3 ± 0.1
L 13[5]	M	50	1.0	23 ± 2	A	3.86	4.32	24.0 ± 1.0
L 14[6]	M	50	1.0	23 ± 2	A	4.92	5.38	1.9 ± 0.2
L 15[6]	M	50	0.5	23 ± 2	A	7.04	6.53	0.10 ± 0.02
P 9	NC	43	3.0	23 ± 2	1	5.63	6.11	0.20 ± 0.02
P 10	NC	43	4.0	23 ± 2	1	5.59	5.95	0.20 ± 0.02
P 11	NC	43	7.0	23 ± 2	2	5.63	5.98	0.02 ± 0.01
HSA[7]	M	50	1.0	23 ± 2	A	8.19	8.20	0.30 ± 0.03
PSA[7]	NC	43	1.0	23 ± 2	A	8.18	8.19	1.5 ± 0.1
PSW[8]	NC	43	1.0	23 ± 2	A	8.15	8.16	0.042 ± 0.006
XSW[8]	NC	50	0.1	23 ± 2	A	8.15	8.15	0.049 ± 0.006
LOX[9]	M	50	0.1	23 ± 2	A	3.95	4.20	7.2 ± 0.6

Number	Sample	Surface area (cm^2-gm^{-1})	Duration (days)	T (°C)	Atm.	pH_i (±0.05)	pH_f	$NaHCO_3$ ($\times 10^3$ M)	Rate ($gm\text{-}cm^{-2}\text{-}day^{-1}$)
L 24	M	50	1.0	23 ± 2	A	8.34	8.38	1.0	0.10 ± 0.02
L 25	M	50	1.0	23 ± 2	A	8.35	—	2.0	0.22 ± 0.04
L 27	M	50	1.0	23 ± 2	A	8.34	8.52	4.0	0.38 ± 0.04
L 32	M	50	1.0	23 ± 2	A	8.34	8.42	8.0	0.80 ± 0.07
L 33	M	50	0.5	23 ± 2	A	8.35	8.44	10.0	1.1 ± 0.1
L 34	M	50	0.5	23 ± 2	A	8.33	8.56	20.0	2.2 ± 0.2
L 35	M	50	0.5	23 ± 2	A	8.35	8.55	40.0	3.5 ± 0.2
L 36	M	50	0.25	23 ± 2	A	8.34	8.55	100.0	6.4 ± 0.3
L 37	M	50	0.25	23 ± 2	A	8.35	8.87	200.0	7.2 ± 0.3

[1] Sample designations as in Table 1.
[2] Atmosphere. "A" refers to ambient atmosphere, other designations as in Table 2.
[3] The pH measured at the end of the experiment.
[4] The pH measured at the beginning of the experiment.
[5] Weak HCl solution.
[6] Weak NaOH solution.
[7] Experiment in artificial seawater.
[8] Experiment in Barnegat Bay, New Jersey, coastal seawater.
[9] Experiment in Oswego River water.

Profile of proposed test site

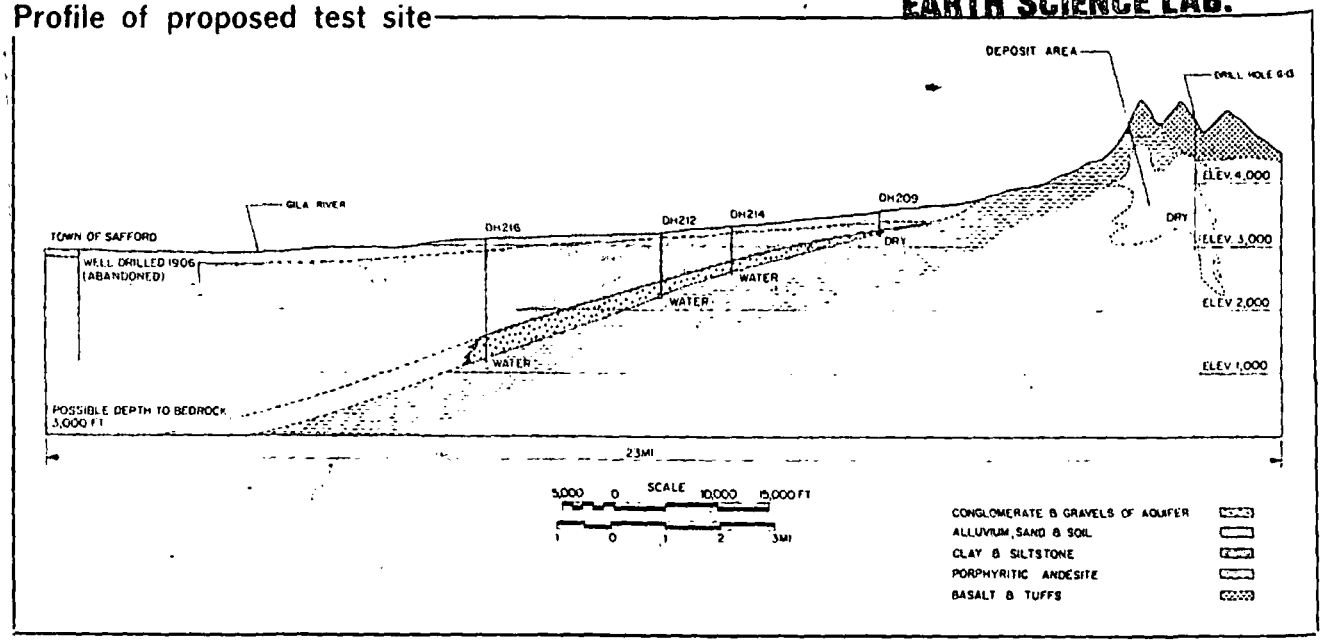

Thermonuclear explosive would be placed at about 3,700 ft elevation in hole adjacent to Kennecott's exploration bore G-13 in Gila Mountains. Deposit is above water table and the test would pose little problem with water contamination.

Kennecott sets sights on nuclear test for

Studies indicate 20 kiloton device would break 1.3-million tons in contained explosion at 1,200 ft depth.

PROJECT SLOOP moved one step closer to reality last month when Kennecott Copper Corp. disclosed details of a proposal that it submitted to the U.S. Atomic Energy Commission for a joint $13-million contained nuclear blast and solution mining experiment at its Safford, Ariz., copper porphyry. The anticipated budget would also cover construction and operation of a pilot precipitation plant capable of handling 2,600 gpm of pregnant solution flow and side studies concerned with radiation, blast effects and methods for refining cement copper.

The test would involve the emplacement of a 20-kiloton device at a depth of 1,200 ft below the surface in an oxide zone of a low-grade deposit that KCC has been investigating since 1955. It is anticipated that the shot would produce a nuclear chimney measuring some 200 ft in diameter and 440 ft in height containing 1.3-million tons of broken rock running 0.41% copper.

The nuclear device would be placed in a suitable plugged 20-in. dia hole at a site where the sub-outcrop is covered by some 750 ft of basalts and andesites in Arizona's Gila Mountains. Following the detonation, a cluster of solution input holes would tap the chimney and a set of solution recovery holes and piping in underground access drifts below the chimney would collect the pregnant solution for pumping to the surface precipitator. The latter would be equipped with KCC's now-famous cone units similar to those installed at other of its Western Mining Divisions. The barren effluent would be returned to the solution mining holes.

The conceptual study on which the proposal was based has been underway for over two years as a joint effort of KKC, the AEC, the U.S. Bureau of Mines, and Lawrence Radiation Laboratory. A summary report was released last month.[1]

Short and long range objectives

Project Sloop aims primarily at determining the practicability of using nuclear explosives in a new environment and as a means for recovering copper. The immediate goals include: (1) The determination of the amount of the contained copper that can be recovered by leaching a nuclear explosion chimney; (2) the investigation of how radionuclides generated by the explosion behave during the leaching process and what measures, if any, are necessary to provide for radiation control and decontamination of the copper; and (3) the testing and demonstration of the ability to predict the physical effects of a nuclear explosion in a new medium and new location.

For the long-run, the test, if approved, may lead to the development of an entire new mining technology—one in which the surface is left undisturbed and in which vast amounts of mechanical horsepower and expense can be eliminated simply to handle overburden and waste. If the initial objectives of the test are attained it may provide the information necessary to extrapolate the results to a large-yield explosive or a multiple detonation application of this technology.

Evidence from preliminary studies suggests that nuclear explosives may lower the cost structure for recovering copper and thereby create new ore reserves in many areas of the U.S. Development of a nuclear stoping capability for in-place leaching operations would be particularly timely because USBM studies predict continued declines in grade of average U.S. copper ores (now about 0.7%) to the 0.5% copper level in 1985.

The premise for analyzing a nuclear-assisted technology is based on the use of explosives of larger yield than the device contemplated for Sloop. For instance, Lawrence Radiation Laboratory states that thermonuclear charges, up to 100 kilotons, could be used to prepare a 240-million ton leaching reserve averaging 0.55% copper in a deposit similar to Safford.

The growth of a nuclear chimney

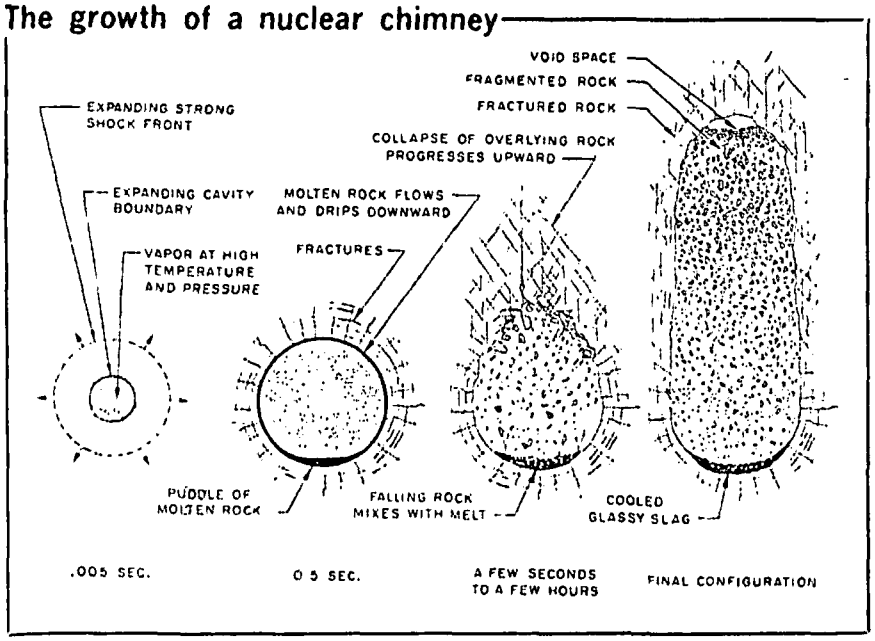

Dilation of vapor cavity reaches full radius in half a second after the shot, then rock collapse feeds growth of chimney to an equilibrium state.

in-situ recovery of copper

Conservative estimates of facilities and operating costs, using current levels of labor, material and construction, for a plant sized to treat 5-million gallons of solution indicated a recovery of 100 tpd of marketable pure copper. The analysis suggested that a commercial-size fracturing-leaching installation would be able to produce copper from lower-grade ores at today's cost levels competively with the metal now recovered from higher grade ores.

Congress must approve the test

KCC's proposal needs both AEC and Congressional approval. Built-into the suggested program is a $750,000 site and safety study to insure adequate public health safeguards. This six-month investigation (Phase 1 of the project) would delve into the field of underground water supplies, geologic formations, soil structures, weather and potential hazards. If Phase 1 cleared the AEC with approval, another nine months would be required to bore the emplacement hole and other satellite holes that are necessary for monitoring the operation and to prepare the site.

It would be 1969 at the earliest before the shot could be triggered. Another year, at a minimum, would be necessary for solution mining and precipitation studies along with collateral investigations. If AEC failed to give its approval on completion of Phase 1, the test would have to be modified, dropped, or another location considered.

The summary report that led to the proposal makes several general observations with regard to the technical feasibility of the project.

1) Chimney material formed by nuclear explosions in granitic rocks is very permeable and has been observed to be about 25% void space with 75% of the fragments smaller than 12-in. in size.

2) It is expected that 90% of the radionuclides would be trapped in a slag glass that forms at the bottom of the cavity as the melt flows down the chimney walls.

3) Contamination of copper appears to be a manageable problem. During leaching, the primary concern underground and in the plant would be with tritium vapors. It is felt that acid soluble radioactive elements would not be a problem. The only long-lived radioisotope that would precipitate with copper is ruthenium 106, but it would be essentially removed during smelting and electrolytic refining.

5) Based on borehole studies to date the possibility of contamination of ground water supplies appears exceedingly remote.

Project management

How would this shot compare with other big blasts in mining? It wouldn't break as much ore as some but this is

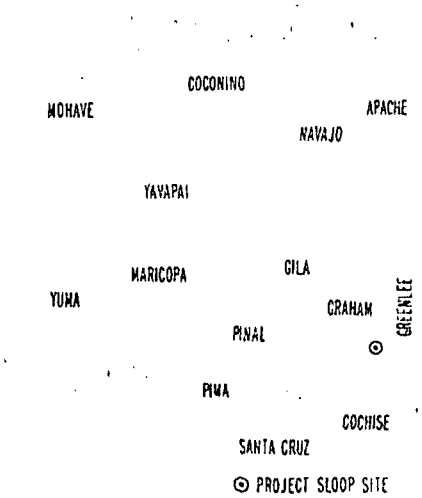

Cost estimates for Project Sloop

Phase 1

Field start-up and initial support facilities	
Pre-shot sampling holes	
Site safety studies	
Total Phase 1	$750,000

Phase 2

Project start-up and support facilities	
Rehabilitation of existing workings	
Scientific program and explosive diagnostics	
Emplacement hole	
Emplacement, stemming	
Operational support	
Communications	
Post-shot drilling, re-entry and testing	
Miscellaneous construction	
Engineering inspection	
Total Phase 2	$5,750,000

Phase 3

Underground re-entry and rehabilitation	
Leach solution and recovery system	
Post-shot sample and solution input holes	
Underground process piping and pumping system	
Copper precipitation plant	
Process water supply	
Leach plant operating costs—one year	
Public and industrial safety monitoring	
Project evaluation	
Total phase 3	$6,675,000
Total Project Sloop	**$13,175,000**

As yield goes up the cost of nuclear explosives levels-off

Yield Kilotons	Approximate Charge
10	$350,000
50	425,000
100	460,000
350	500,000
500	535,000
1,000	570,000
2,000	600,000

Table is based on data published by AEC which projected charges for nuclear explosives as a guide for evaluating Plowshare excavation applications. The above charges cover nuclear materials, fabrication and assembly, and arming and firing services. They do not include safety studies, site preparation, hole emplacement, transportation and emplacement of the explosives or support of operations in the field. The charges are based on a projection to a time when explosives would be produced in quantity for routine utilization, but do not consider potential reduction in cost as a result of future technological development.

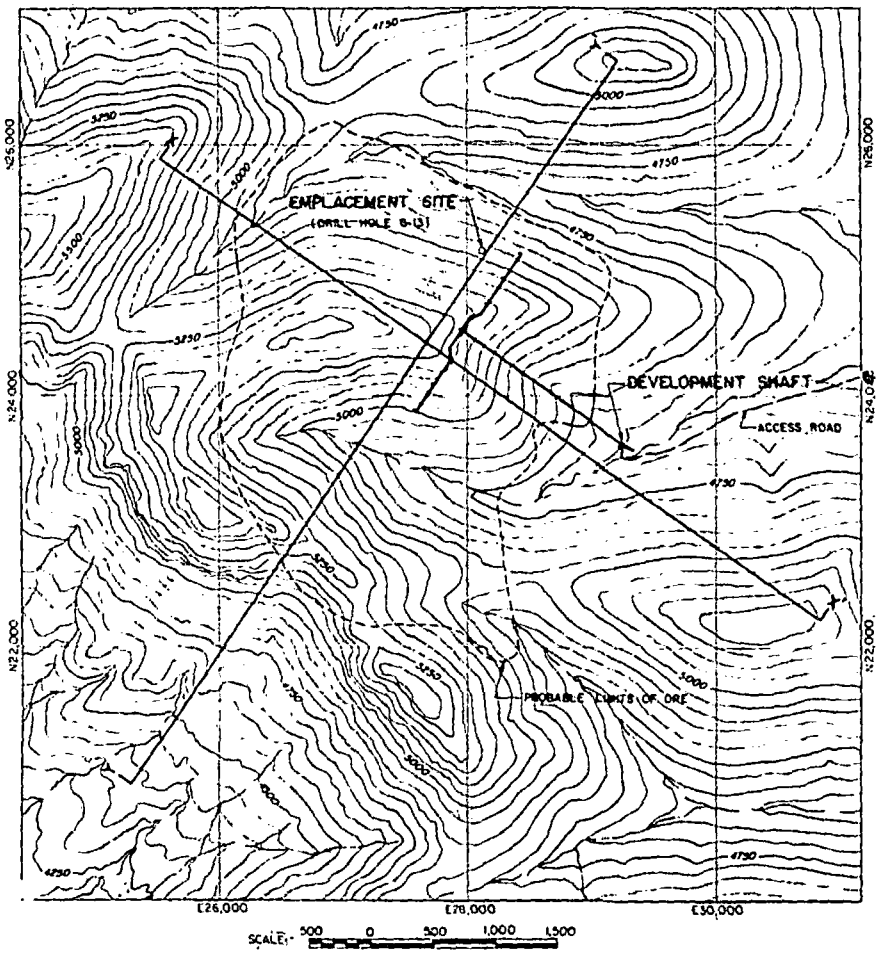

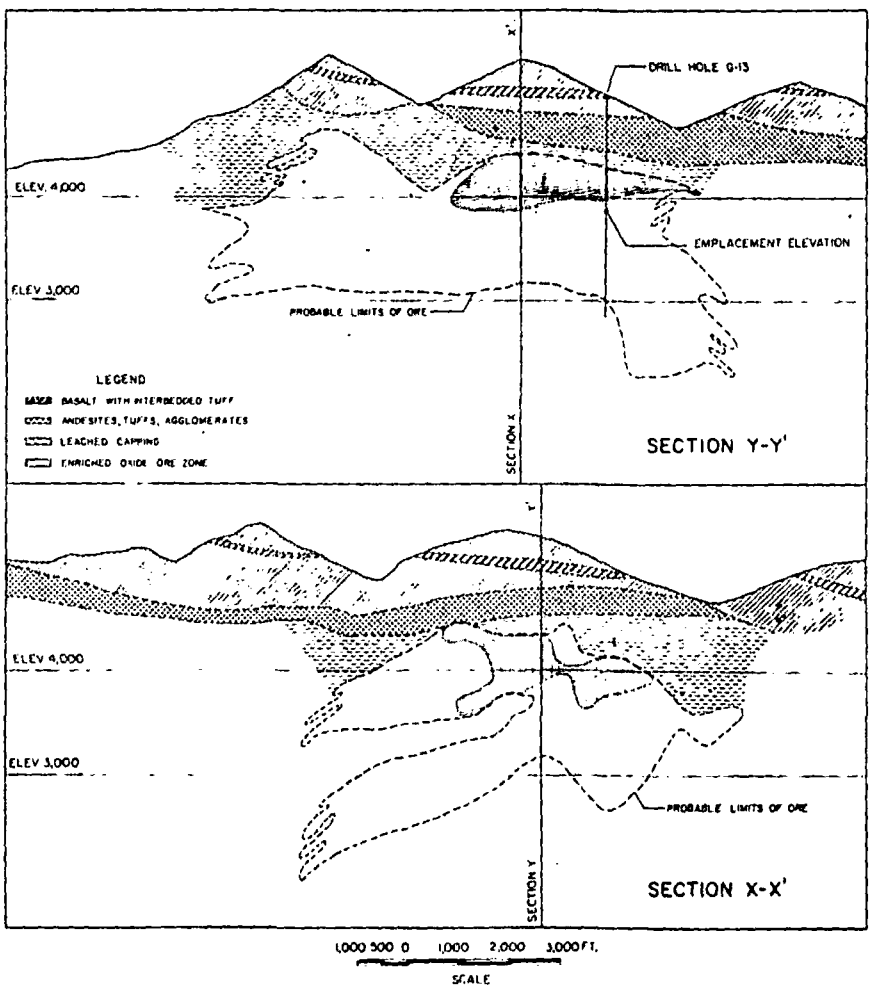

Geometry of overlying volcanic wastes, enriched oxide and underlying sulphide zones of deposit, plus absence of water table, makes orebody an ideal test site.

because all production blasts have been planned to break to one or more free faces, and/or boundary-weakened planes. Here are a few comparative yardsticks. International Nickel Co. of Canada broke 5.25-million tons at the Frood Stobie mine in 1965 with 464 tons of powder. Climax Molybdenum Co. broke 1.25-million tons in a glory hole blast in May 1964 with 208 tons of explosive. Hercules Powder Co. reported that 850 tons of high energy slurry distributed in 1,118 jet-pierced holes in Minnesota taconite broke 1.3-million tons in 1966.

In planning and design of Project Sloop this is how the responsibilities would be divided. The AEC would provide the nuclear explosive, conduct the nuclear operations and the programs for the protection of public health and safety. KCC would be responsible for the leaching and copper recovery phase of the test and USBM would participate in all phases of the test, help evaluate results and would cooperate with the other participants, including AEC's Lawrence Radiation Laboratory, in reporting the results.

The Safford deposit has a number of factors working in its favor as a site for a nuclear blast for researching a commercial scale in-situ leaching operation. It is typical of disseminated porphyry deposits containing oxide, sulphide, and mixed oxide-sulphide ores of a grade that will soon have to be developed in the U.S. as a source of copper. KCC has already conducted years of detailed investigative work that spans reconnaissance drilling, close-grid drilling, and underground drilling and development. Kennecott has also accumulated considerable processing experience with Safford ore in a 1-tpd pilot plant equipped for continuous leach and wash cycles and an electrolytic recovery section. It was set-up to study the possibility of a full-scale conventional oxide recovery plant.

2-billion tons of 0.41% copper

Located in Arizona's Lone Star mining district, Kennecott's disseminated deposit contains a large reserve of low-grade copper. The test site is centered on the north flank of the mineral zone, which is situated within the Gila Mountains at an elevation of 5,000 ft.

After four years of geological and exploration reconnaissance, Kennecott purchased the property in 1959 when

ft became clear that work had indicated the possibility of a large porphyry copper at depth. At the conclusion of development drilling, an estimated 2-billion-ton reserve had been indicated consisting of oxide, mixed oxide-sulphide and sulphide mineralization that averaged a probable 0.41% total copper.

The formations exposed in the Lone Star District are predominantly volcanics with some intrusives. The oldest pre-mineral rocks are primarily andesitic volcanics believed to be Cretaceous. They are cut by several strong, broad, northeasterly trending fracture zones. Most of the fractures were intruded by Early Tertiary igneous bodies of rhyolite, latite, quartz monzonite, granodiorite and quartz diorite.

This complex is overlain by two series of post-ore volcanics with a total thickness ranging from 200 to 800 ft. The older of these consists of flows of andesite and dacite. The youngest volcanic rock, which caps the Gila Mountain Range, consists of Quaternary basalt flows and some interbedded tuff beds. These rocks decrease in thickness and pinch out in the vicinity of Kennecott's deposit, and are not found on the south side of the range.

Copper mineralization occurs in the Cretaceous and Early Tertiary volcanics under generally rugged surface topography (see accompanying maps and sections). In cross section the deposit is like an irregular ellipsoid some 3,600 to 4,000 ft long and about 1,600 ft thick. It is overlain with a leached capping and barren volcanics that vary from 500 to 1,300 ft in thickness. Kennecott says that about one-half of the indicated reserve is relatively enriched oxide ore. The principal copper minerals in this portion are chrysocolla and brochantite. Another one-third of the total ore consists of a mixture of oxides and primary and secondary sulphides. In addition to the foregoing oxide minerals, other ore minerals include chalcopyrite, chalcocite, covellite and minor amounts of bornite and molybdenite at depth in the sulphide zone.

The climate is typical of the southwestern desert areas of the U.S., with little rainfall, hot summers and mild winters. Kennecott's ore environment is dry and above any known water table. Exploration holes on the north flank of the deposit, near the proposed test site, have penetrated to depths of 3,000 ft and no ground water has ever been encountered there or in the underground workings. A water well field has been drilled near the town of Safford that is estimated to be capable of developing an 8,000 gpm supply, although the flow is rather saline for an electrolytic section.

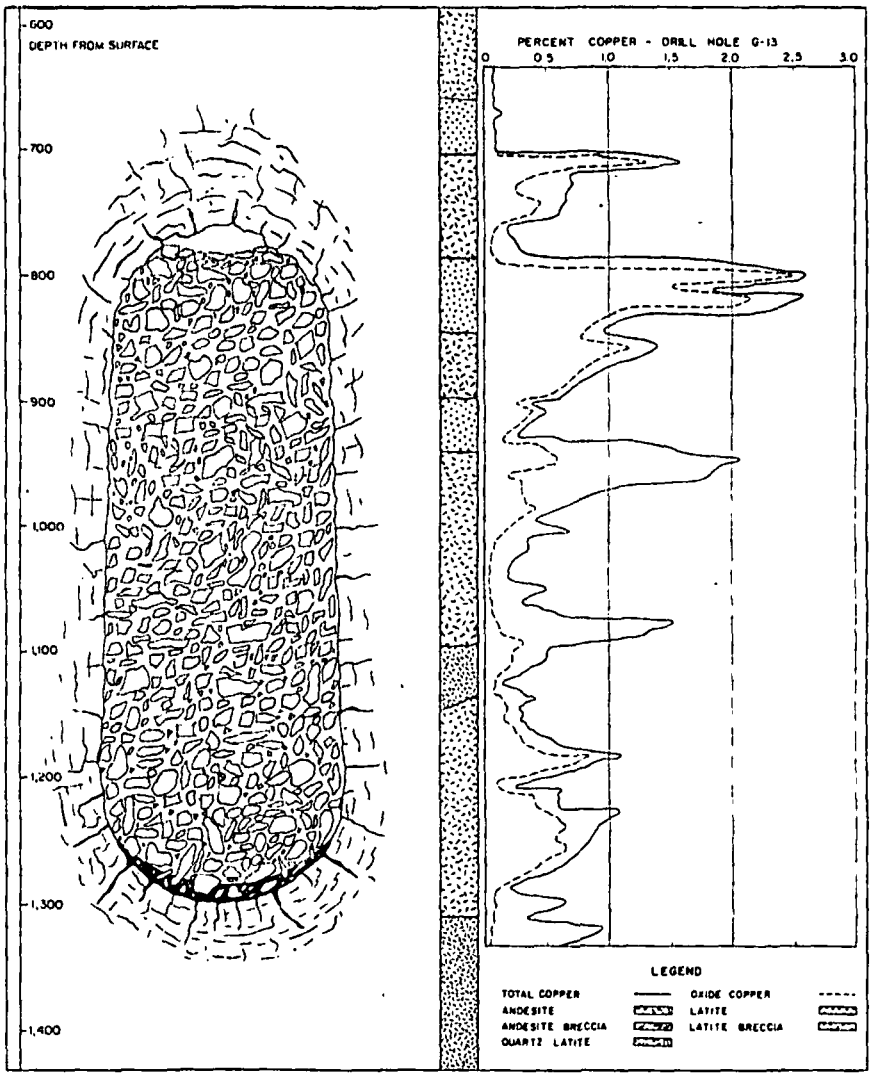

Total and oxide copper content of ore is flashed against the chimney site from data collected in one of Kennecott's earlier exploration drill holes.

How ore responds to leaching

Although Kennecott's pilot plant test work was aimed at design of a leaching plant for a conventional mining operation, these conclusions can be drawn concerning behavior of the ore in an in-situ leaching situation, according to the Project Sloop report.

(1) Safford ore can be treated for the recovery of copper by a moderate strength sulphuric acid leaching process. (2) In pilot plant testing, overall copper recovery on oxide ore grade material ranged from 70% to 80%. In an in-situ environment a somewhat lower recovery may be anticipated. (3) Overall acid reagent consumption in the test work averaged 40 lb per ton of ore. (4) High purity copper, approaching that of electro-refining methods, can be produced by electrolysis of strong leach solutions with no special purification of the feed solution indicated other than a dechloridization step.

Kennecott started initial metallurgical studies on Safford ore in 1957 using samples of diamond drill core from earlier exploration holes. These laboratory scale results when projected to a vat leaching cycle suggested a recovery of 76% of the copper from ores assaying 0.96% copper, and 85% recovery for higher grade ores averaging 1.00% copper.

As part of Kennecott's evaluation of the Safford deposit, an 800-ft development shaft and 3,000 ft of underground working were driven into the oxide ore horizons. From these openings some 52,000 ft of underground core drilling were completed in 1961. The core and excavated material furnished bulk samples for the 1-tpd pilot leaching plant that was constructed adjacent to the shaft site. The principal objective of the pilot was to try the vat leaching and electrolytic studies on a level larger than laboratory scale and to determine the effects, if any, of the saline well water developed by the company near Safford since it would likely be the only

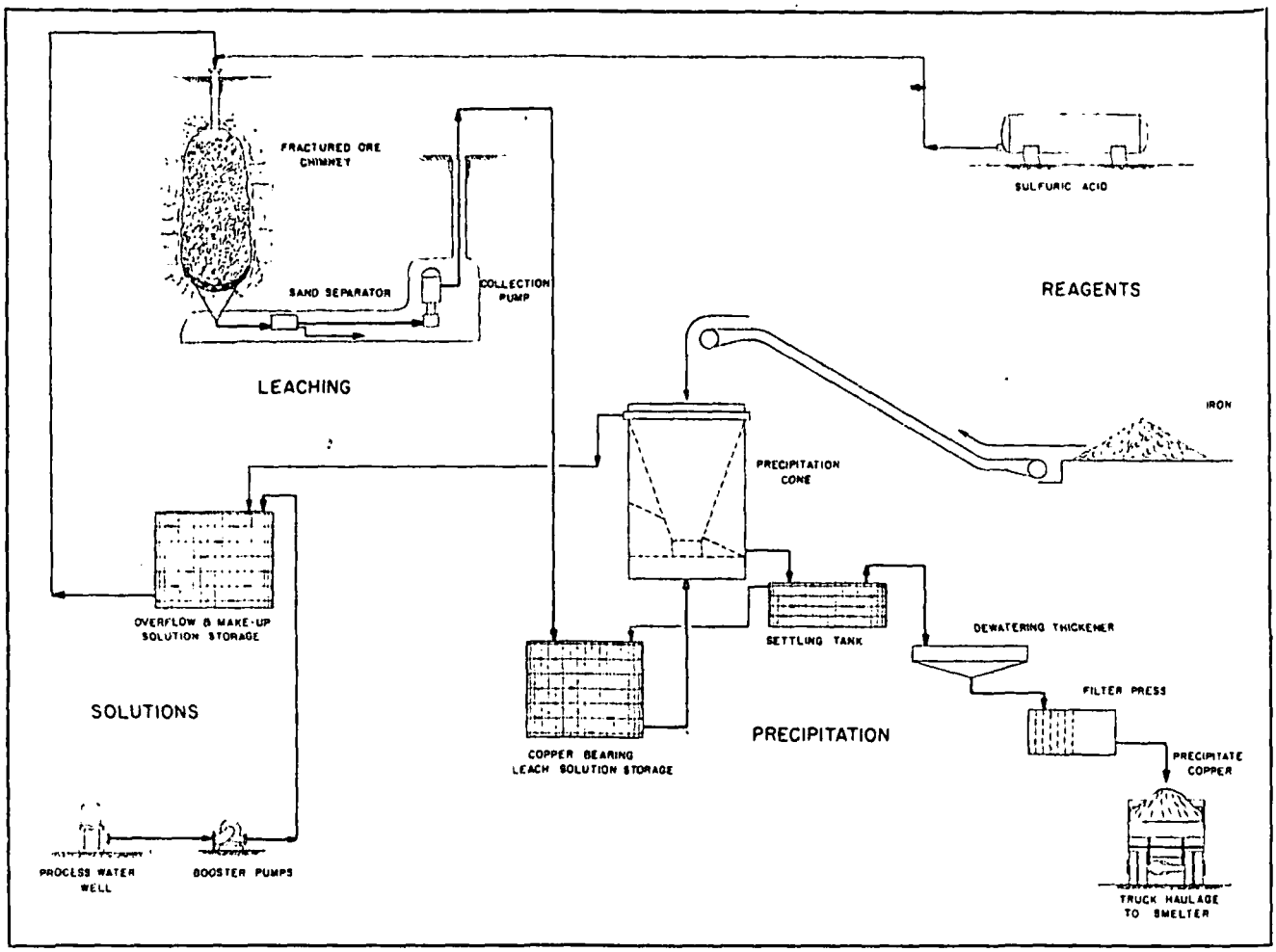

Surface precipitation plant would be sized to handle 2,600 gpm of pregnant solution and equipped to return the barren liquor with make-up water and acid to the chimney input holes. Plant will be forced to use saline water.

process water available for a production operation.

How the chimney is formed

For rock breaking, the Project Sloop report expains that a fully contained nuclear blast underground breaks only about one-seventh of the rock that might be shattered with a near-surface detonation that heaves fragments into an inverted cone. The latter, however, obviously vents radioactive gases to the atmosphere.

On detonation of a contained nuclear explosive, the energy is released in a fraction of a micro-second. It vaporizes, melts and crushes surrounding rock with the formation of spherical cavity that expands around the blast center until the cavity gas pressure approaches equilibrium with the weight of overlying rock.

The molten rock that initially lines the cavity walls flows to a pool on the bottom. As this slag cools and solidifies into a relatively inert glass, it traps up to 90% of the radioactive fission products generated by the explosion. The cavity roof is fractured by the shockwave and effectively undercut starting a caving action. The chimney has a radius approximating the cavity, and normally extends to a height of four or five cavity radii.

The AEC, which has experience with over 225 nuclear shots, points out that similar explosions in granite yield an extremely permeable rubble with 75% of the fragments under 12-in. in size. Outside fracturing beyond the chimney walls may increase original permeability of surrounding formations for a distance approaching three cavity radii. Without the physical displacement of cavity collapse, however, this fringe permeability would be much lower than the cavity with its 25% void space.

Experimental design of Sloop

The tentative location for the test shot is Kennecott's exploration drill hole G-13 (see maps), which is far enough from the existing shaft to minimize damage, according to the report. Lawrence Radiation Laboratory has recommended a group of pre- and post-shot holes for control and monitoring of the explosion and its effects.

Four pre-shot surface holes would be drilled in the chimney area 200 ft below the shot depth to establish the distribution and amount of copper. Cores and geophysical logs would be obtained to make studies of the chemical and physical characteristics of the rock. Borehole photography and drill stem pressurization tests would be conducted to determine in-situ fracture distribution and permeability. A fifth pre-shot hole would be bored outside of the chimney area to verify geologic data and would be instrumented for shock time-of-arrival, pressure, and particle velocity measurements.

The nuclear device would be emplaced from the surface in an approximate 20-in. dia uncased hole at the planned 1,200-ft depth. At this level, it would be about 100 ft below the existing drift horizon in the mine. Stemming could be accomplished by grout plugs and pea gravel. The shaft would be stemmed for approximately 50 ft with local surface material and 50 ft of sand, charcoal, and asphalt. Physical effects measurements would be made in the shot hole and in the satellite hole. The mine workings and ground surface would be instrumented for earth motion, and seismic data would be recorded at various stations.

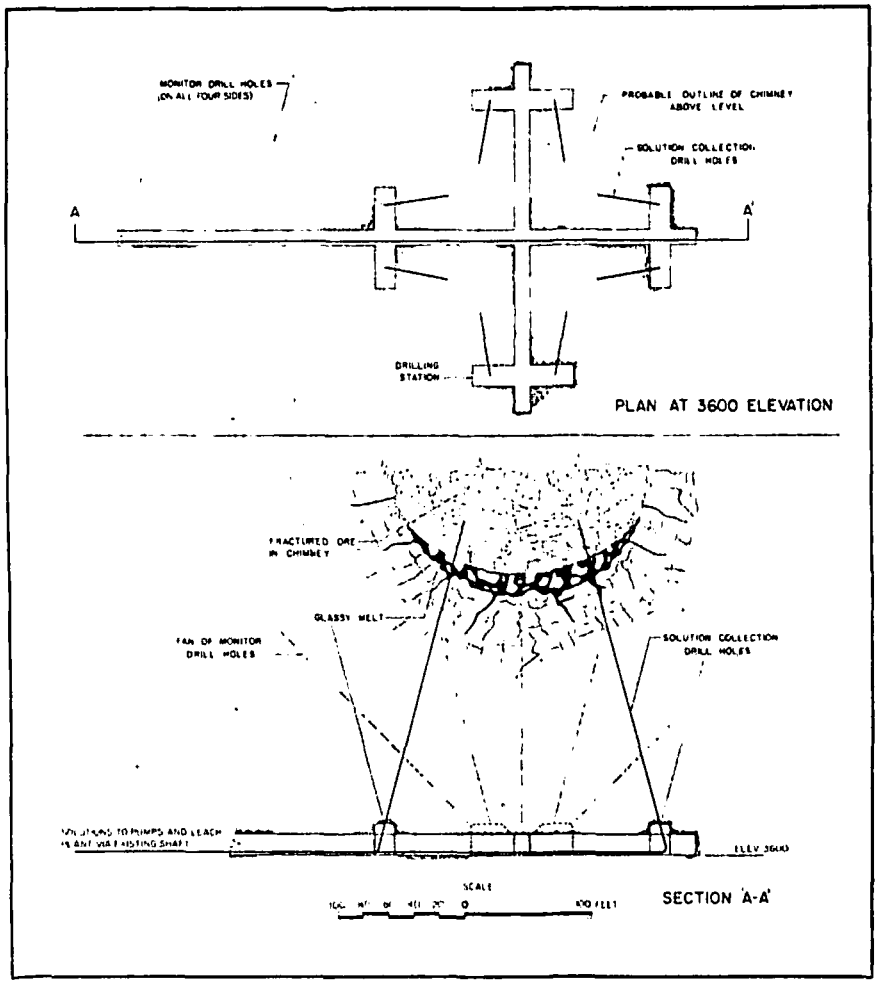

Solution recovery and monitor holes would be drilled from development headings located about 100 ft below the lower end of the nuclear cavity.

All holes within 1,000 ft of the shot would be stemmed.

While the AEC believes the Safford site could contain explosive yields of up to 100 kilotons, the use of a device with this much energy would not be considered until results of the smaller 20 kiloton device were fully evaluated.

For post-shot studies, LRL suggested an 8¾-in. vertical hole near the emplacement hole to enter the void at the top of the chimney. It would be used for defining chimney characteristics and for leaching studies. LRL also recommended two 6⅞-in. holes to a depth of 1,400 ft outside the chimney area. Two whipstock holes would then be drilled from each of the last holes to intersect the chimney edge and cavity bottom.

Samples of the atmosphere and a complete set of geophysical logs, cores, downhole photos and TV will be taken in all holes. Chimney volume and fracture permeability will be studied by pumping compressed air into one of the holes intersecting the chimney. The collected data would provide an assessment of the distribution of heat energy and radioactivity, chimney particle size distribution, and associated permeability in the fracture zone after the blast is detonated.

The leaching program

Three leach solution input holes would be drilled from the surface to tap the top of the chimney zone. Underground drift and cross-cut development would be driven 200 ft below the shot point to establish drill stations for holing the bottom of the cavity with a solution recovery system. This development would be about 100 ft below the bottom of the cavity. In addition to cone precipitators capable of handling a daily throughput of 2,600 gpm, the surface plant will include facilities for make-up water, solution pumping, acid storage, and iron and copper precipitate handling and storage.

The leaching studies would take one to three years. A primary concern during this stage would be potential industrial radiological safety problems that might be encountered as a result of solution treatment of the broken rock. These would be primarily due to tritium and to acid soluble fission products entering the circulating leach solution. Investigations indicate, the report states, that radiation from the leach solutions would be at such low levels that no shielding would be required for personnel protection. Very little additional operating cost would be incurred by the housekeeping type precautions required to assure complete operational safety in handling the solutions.

Treated water vapor from leach solutions could constitute a hazard in the underground workings or in the precipitation plant, if allowed to collect or concentrate where it could be inhaled or absorbed through the skin. Process plant design specifying enclosed pipeline handling of solutions and adequate ventilation would minimize the potential hazard.

The tritium content of process solutions could be greatly reduced by initially flushing the chimney with water prior to the start of leaching. The flushing fluids would be chemically controlled in order to dissolve a minimum amount of copper, and if they become contaminated, they would be disposed of in accordance to AEC and State regulations.

Extensive laboratory studies at Oak Ridge have investigated the possibility of radioactive contamination of the finished copper causing a health or marketing difficulty. Copper itself is not rendered radioactive for any significant time because its radionuclides are very short lived and decay rapidly.

The 5% to 10% fraction of the fission products that are not trapped in the relatively insoluble glass slag at the bottom of the cavity would be dispersed in the chimney in a more leachable form. Many of these products, however, would be strongly held on the ore by adsorption mechanisms and would not build-up to significant concentrations in circulating solutions.

A portion of the copper precipitates would be used for studies to determine the most efficient process for refining the metal commercially. Solvent extraction methods, electrolysis of dissolved precipitates in acid and conventional smelting followed by electro-refining methods would be investigated.

Substantial quantities of cement copper would be produced from the test program. After the experimental requirements of Project Sloop are satisfied, commercial usage of copper could be permissible under suitable regulatory arrangements with the parties involved in the test.

Distribution of radioactivity

In developing a concept for Project Sloop, LRL points out that the only long-lived soluble fission products which may interfere are: Cs 137, Ru 106, Zr-Nb 95, Ce 144, Ce 141, Y 91, Pm 147, Sr 90 and Sr 89. Of the

radionuclides trapped in the glass matrix at the bottom of the cavity, less than 5% is solubilized in normal leaching of the glass at pH of 1.5 to 2.0. Ce 141, Sr 90, and Cs 137, however, have gaseous precursors, and Ru 103-106 is a volatile compound that can be deposited on readily accessible broken rock at considerable distances from the melt zone. These four, particularly the Sr, are more readily leachable and in laboratory experiments have constituted the bulk of the activity in the first increment of solution through the leach bed. Ce and Ru are about 10 times more soluble at a pH of 1.5 than at 3.1.

Irradiation of Safford ore at Oak Ridge National Laboratory indicated that Sc 46, Co 60, Mn 54, Fe 59, Zn 65 and Se 75 would probably be the most important induced long-lived radionuclides. Sc and Fe are significant at early times, but Co, Zr and Se are most important later.

Personnel from Oak Ridge say that the ion exchange properties of the copper ore are highly important in regulating the quantities of certain radionuclides that dissolve from the ore. Safford ore adsorbed Cs 137 and Zr-Nb 95 very strongly from leach liquors. Sr was adsorbed much less, although still significantly.

They also say that the rubble-filled chimney in a continuous leaching cycle will function as an ion exchange column. Radionuclides dissolved from the ore early in the leach cycle would tend to be adsorbed on the ore in later leach cycles. This would limit the build-up in concentration of certain radionuclides in the leach solution to levels far below those that would be predicted on the basis of simple batch tests. The radionuclides formed by neutron activation of the ore should not be of importance in the processing cycle.

Contamination of copper

Cementation tests showed that only Ru 106 and Zr-Nb 95 precipitate with the copper to a significant extent. Certain potential activation products, such as mercury and silver, cement quantitatively with copper, but after considering the quantities of each of the various radionuclides it was concluded that Ru 106 was the only radioisotope that was important in the contamination picture. Over 50% of the soluble Ru followed the copper and ORNL tests determined that 20% of the Zr-Nb followed copper.

Direct smelting of Ru-contaminated cement copper showed that all the Ru appeared in the blister copper. Electrolytic refining, however, gave a relatively pure copper cathode. Following electrolysis, 66% of the Ru remained with the electrolyte and 33% dropped out as anode mud. Only 1% of the contained Ru content followed the copper to the cathode. Of the total induced activity, only 5% went into solution and only 6% of this soluble fraction, principally Zr and Se, ended up with the cement copper and these dropped out in the slag during smelting.

Recovery of copper from leach solutions by solvent extraction is a potential alternative to cementation, and this route will be investigated if Project Sloop receives approval. Soluble copper taken into the extractant can be stripped by 2 mol H_2SO_4 and this solution can be fed directly to electrolysis. Preliminary solvent extraction tests have indicated a good separation of copper from ruthenium as well as all other important fission products with the possible exception of Zr-Nb 95.

Safety considerations

The scaled burial of the shot is greater than that which is normally required from the standpoint of containment of the energy.

The probability of a stemming failure would appear to be extremely small, however, the possibility of some minor venting cannot be ruled out says LRL. Because of the competence of the overlying formations, it has been estimated, for the worst credible case, no more than 5×10^7 curries at one minute could be released through a fissure and be injected into the atmosphere after the shot.

In such an eventuality, the predominant nuclides in the radioactive cloud would be Kr, Xe, I, and their decay products. The distribution and intensity of this fallout can be controlled by detonating the explosive under specified meteorological conditions.

It is the judgement of LRL that in no case will iodine levels exceed values which, with proper operational control and monitoring, could lead to excessive exposure to individuals in the public. In making this judgment, LRL assumes that radiation protection guidance published by the Federal Radiation Council would apply.

If Sloop demonstrates a new mining technology, here is a benchmark on what it might do for U.S. reserves. In 1965 USBM estimated the domestic total at 75-million tons of copper in ores of 0.86%; another 58-million tons may exist in 0.47% sub-ore.

[1] Project Sloop, PNE 1300 Nuclear Explosives—Peaceful Applications is available from the Clearinghouse for Federal Scientific & Technical Information, National Bureau of Standards, U.S. Dept. of Commerce, Springfield, Va. 22151, for $3 (printed copy) or 65¢ for microfiche.

SUBJ
MNG
KSSN

Profile of proposed test site

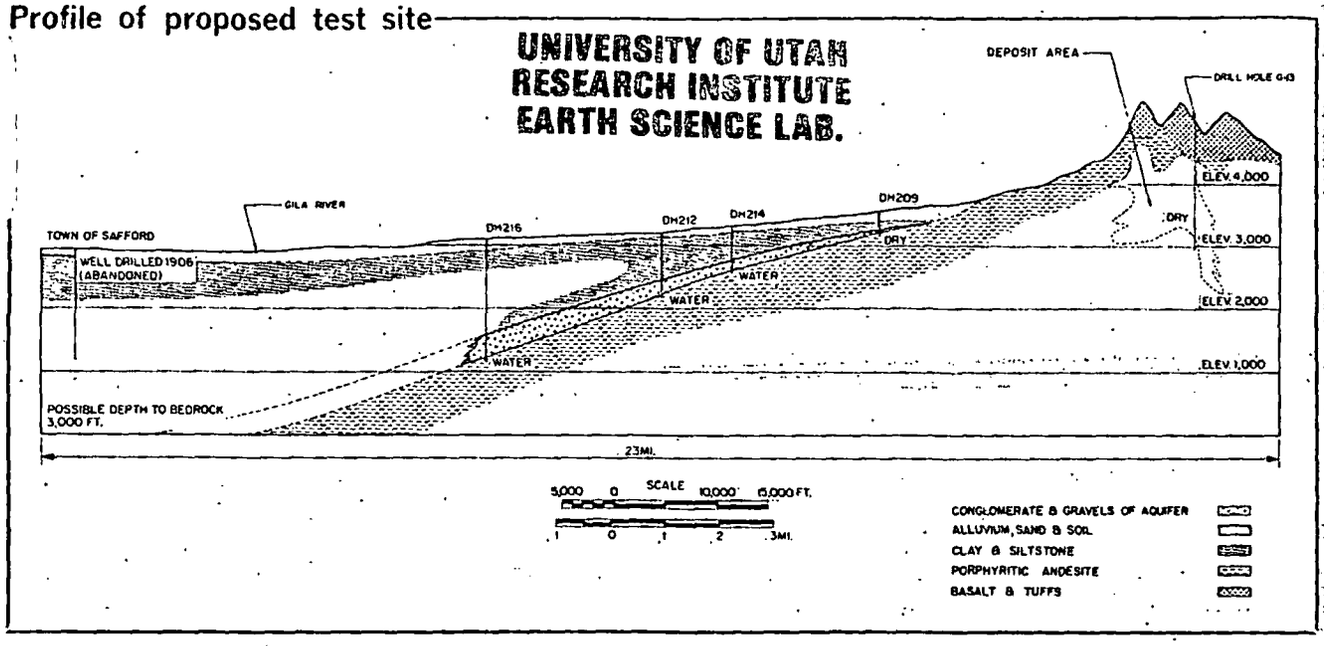

Thermonuclear explosive would be placed at about 3,700 ft elevation in hole adjacent to Kennecott's exploration bore G-13 in Gila Mountains. Deposit is above water table and the test would pose little problem with water contamination.

Kennecott sets sights on nuclear test for

Studies indicate 20 kiloton device would break 1.3-million tons in contained explosion at 1,200 ft depth.

PROJECT SLOOP moved one step closer to reality last month when Kennecott Copper Corp. disclosed details of a proposal that it submitted to the U.S. Atomic Energy Commission for a joint $13-million contained nuclear blast and solution mining experiment at its Safford, Ariz., copper porphyry. The anticipated budget would also cover construction and operation of a pilot precipitation plant capable of handling 2,600 gpm of pregnant solution flow and side studies concerned with radiation, blast effects and methods for refining cement copper.

The test would involve the emplacement of a 20-kiloton device at a depth of 1,200 ft below the surface in an oxide zone of a low-grade deposit that KCC has been investigating since 1955. It is anticipated that the shot would produce a nuclear chimney measuring some 200 ft in diameter and 440 ft in height containing 1.3-million tons of broken rock running 0.41% copper.

The nuclear device would be placed in a suitable plugged 20-in. dia hole at a site where the sub-outcrop is covered by some 750 ft of basalts and andesites in Arizona's Gila Mountains. Following the detonation, a cluster of solution input holes would tap the chimney and a set of solution recovery holes and piping in underground access drifts below the chimney would collect the pregnant solution for pumping to the surface precipitator. The latter would be equipped with KCC's now-famous cone units similar to those installed at other of its Western Mining Divisions. The barren effluent would be returned to the solution mining holes.

The conceptual study on which the proposal was based has been underway for over two years as a joint effort of KKC, the AEC, the U.S. Bureau of Mines, and Lawrence Radiation Laboratory. A summary report was released last month.[1]

Short and long range objectives

Project Sloop aims primarily at determining the practicability of using nuclear explosives in a new environment and as a means for recovering copper. The immediate goals include: (1) The determination of the amount of the contained copper that can be recovered by leaching a nuclear explosion chimney; (2) the investigation of how radionuclides generated by the explosion behave during the leaching process and what measures, if any, are necessary to provide for radiation control and decontamination of the copper; and (3) the testing and demonstration of the ability to predict the physical effects of a nuclear explosion in a new medium and new location.

For the long-run, the test, if approved, may lead to the development of an entire new mining technology—one in which the surface is left undisturbed and in which vast amounts of mechanical horsepower and expense can be eliminated simply to handle overburden and waste. If the initial objectives of the test are attained it may provide the information necessary to extrapolate the results to a large-yield explosive or a multiple detonation application of this technology.

Evidence from preliminary studies suggests that nuclear explosives may lower the cost structure for recovering copper and thereby create new ore reserves in many areas of the U.S. Development of a nuclear stoping capability for in-place leaching operations would be particularly timely because USBM studies predict continued declines in grade of average U.S. copper ores (now about 0.7%) to the 0.5% copper level in 1985.

The premise for analyzing a nuclear-assisted technology is based on the use of explosives of larger yield than the device contemplated for Sloop. For instance, Lawrence Radiation Laboratory states that thermonuclear charges, up to 100 kilotons, could be used to prepare a 240-million ton leaching reserve averaging 0.55% copper in a deposit similar to Safford.

The growth of a nuclear chimney

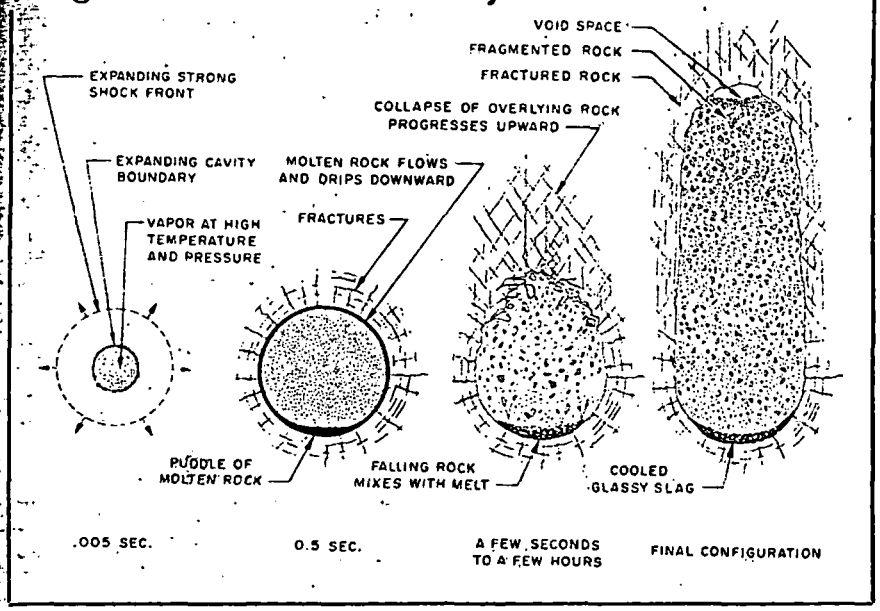

Dilation of vapor cavity reaches full radius in half a second after the shot, then rock collapse feeds growth of chimney to an equilibrium state.

in-situ recovery of copper

Conservative estimates of facilities and operating costs, using current levels of labor, material and construction, for a plant sized to treat 5-million gallons of solution indicated a recovery of 100 tpd of marketable pure copper. The analysis suggested that a commercial-size fracturing-leaching installation would be able to produce copper from lower-grade ores at today's cost levels competively with the metal now recovered from higher grade ores.

Congress must approve the test

KCC's proposal needs both AEC and Congressional approval. Built-into the suggested program is a $750,000 site and safety study to insure adequate public health safeguards. This six-month investigation (Phase 1 of the project) would delve into the field of underground water supplies, geologic formations, soil structures, weather and potential hazards. If Phase 1 cleared the AEC with approval, another nine months would be required to bore the emplacement hole and other satellite holes that are necessary for monitoring the operation and to prepare the site.

It would be 1969 at the earliest before the shot could be triggered. Another year, at a minimum, would be necessary for solution mining and precipitation studies along with collateral investigations. If AEC failed to give its approval on completion of Phase 1, the test would have to be modified, dropped, or another location considered.

The summary report that led to the proposal makes several general observations with regard to the technical feasibility of the project.

1) Chimney material formed by nuclear explosions in granitic rocks is very permeable and has been observed to be about 25% void space with 75% of the fragments smaller than 12-in. in size.

2) It is expected that 90% of the radionuclides would be trapped in a slag glass that forms at the bottom of the cavity as the melt flows down the chimney walls.

3) Contamination of copper appears to be a manageable problem. During leaching, the primary concern underground and in the plant would be with tritium vapors. It is felt that acid soluble radioactive elements would not be a problem. The only long-lived radioisotope that would precipitate with copper is ruthenium 106, but it would be essentially removed during smelting and electrolytic refining.

5) Based on borehole studies to date the possibility of contamination of ground water supplies appears exceedingly remote.

Project management

How would this shot compare with other big blasts in mining? It wouldn't break as much ore as some but this is

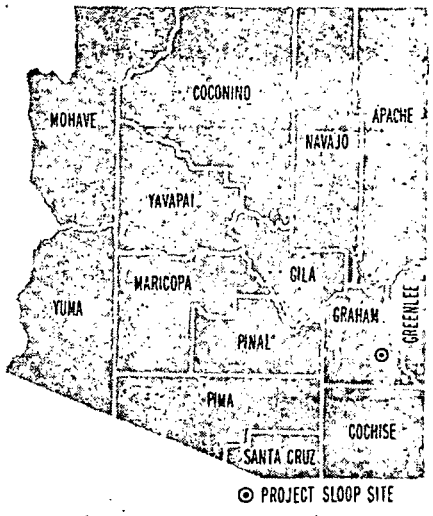

Cost estimates for Project Sloop

Phase 1	
Field start-up and initial support facilities	
Pre-shot sampling holes	
Site safety studies	
Total Phase 1	$750,000
Phase 2	
Project start-up and support facilities	
Rehabilitation of existing workings	
Scientific program and explosive diagnostics	
Emplacement hole	
Emplacement, stemming	
Operational support	
Communications	
Post-shot drilling, re-entry and testing	
Miscellaneous construction	
Engineering inspection	
Total Phase 2	$5,750,000
Phase 3	
Underground re-entry and rehabilitation	
Leach solution and recovery system	
Post-shot sample and solution input holes	
Underground process piping and pumping system	
Copper precipitation plant	
Process water supply	
Leach plant operating costs—one year	
Public and industrial safety monitoring	
Project evaluation	
Total phase 3	$6,675,000
Total Project Sloop	**$13,175,000**

As yield goes up the cost of nuclear explosives levels-off

Yield Kilotons	Approximate Charge
10	$350,000
50	425,000
100	460,000
350	500,000
500	535,000
1,000	570,000
2,000	600,000

Table is based on data published by AEC which projected charges for nuclear explosives as a guide for evaluating Plowshare excavation applications. The above charges cover nuclear materials, fabrication and assembly, and arming and firing services. They do not include safety studies, site preparation, hole emplacement, transportation and emplacement of the explosives or support of operations in the field. The charges are based on a projection to a time when explosives would be produced in quantity for routine utilization, but do not consider potential reduction in cost as a result of future technological development.

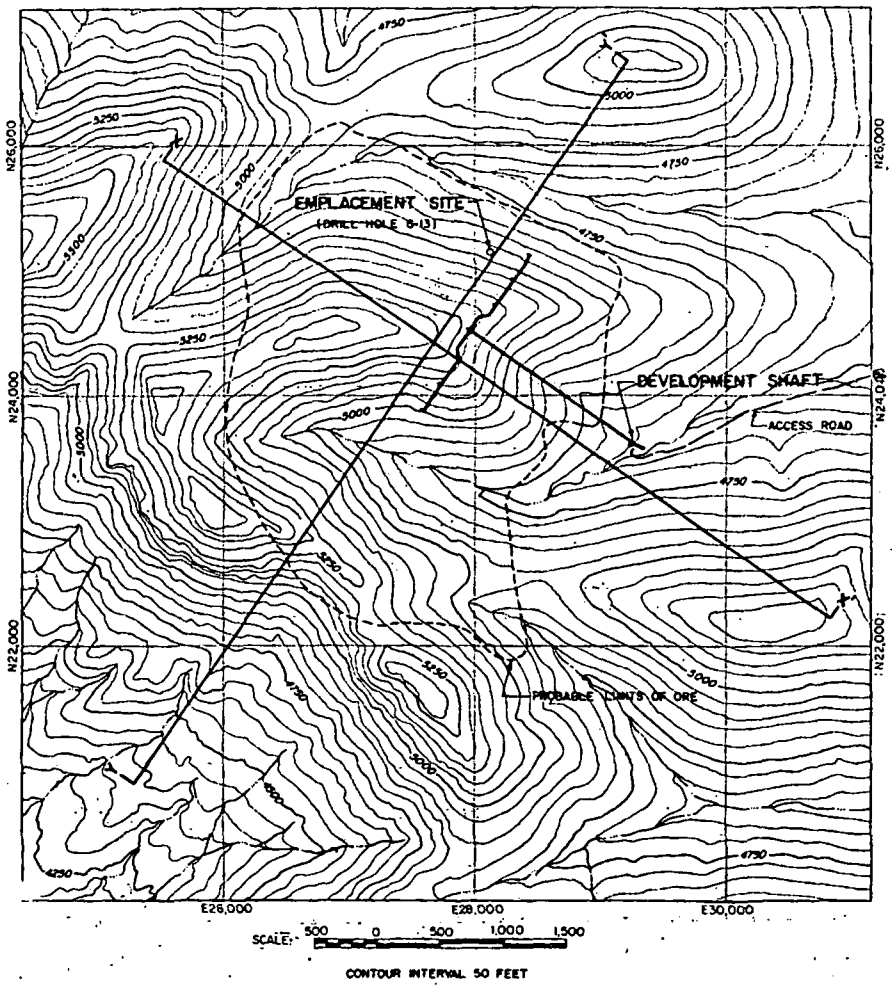

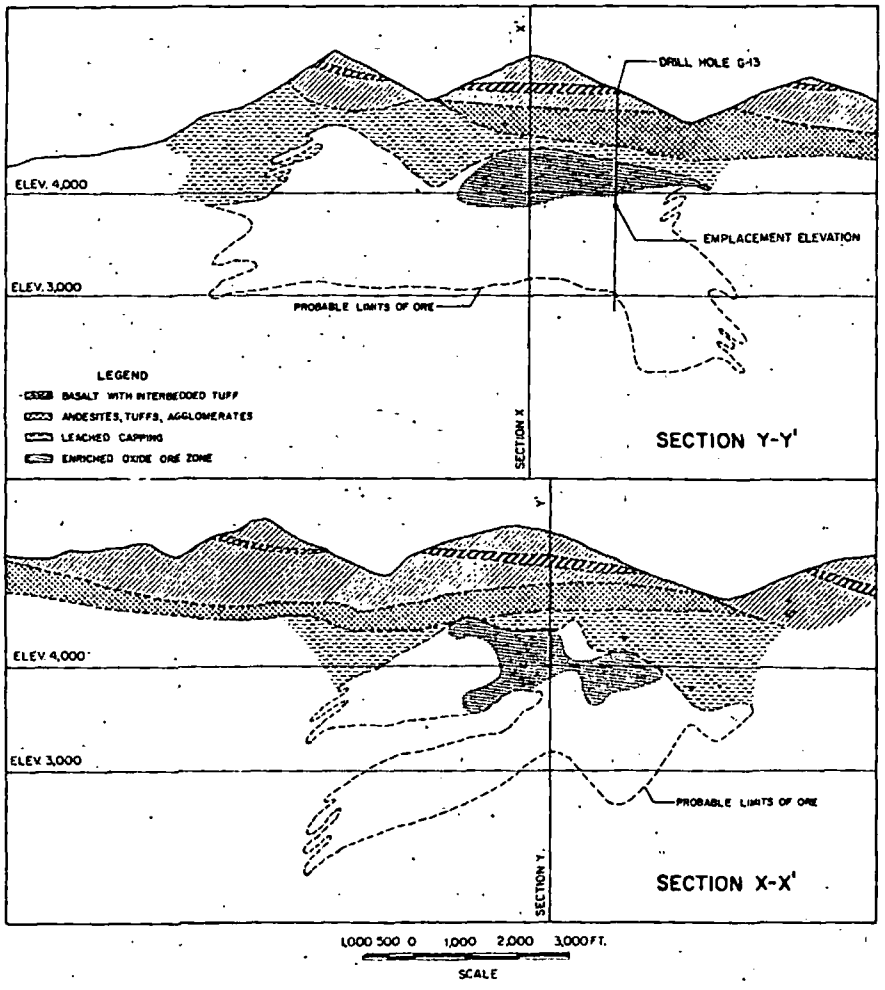

Geometry of overlying volcanic wastes, enriched oxide and underlying sulphide zones of deposit, plus absence of water table, makes orebody an ideal test site.

because all production blasts have been planned to break to one or more free faces, and/or boundary-weakened planes. Here are a few comparative yardsticks. International Nickel Co. of Canada broke 5.25-million tons at the Frood Stobie mine in 1965 with 464 tons of powder. Climax Molybdenum Co. broke 1.25-million tons in a glory hole blast in May 1964 with 208 tons of explosive. Hercules Powder Co. reported that 850 tons of high energy slurry distributed in 1,118 jet-pierced holes in Minnesota taconite broke 1.3-million tons in 1966.

In planning and design of Project Sloop this is how the responsibilities would be divided. The AEC would provide the nuclear explosive, conduct the nuclear operations and the programs for the protection of public health and safety. KCC would be responsible for the leaching and copper recovery phase of the test and USBM would participate in all phases of the test, help evaluate results and would cooperate with the other participants, including AEC's Lawrence Radiation Laboratory, in reporting the results.

The Safford deposit has a number of factors working in its favor as a site for a nuclear blast for researching a commercial scale in-situ leaching operation. It is typical of disseminated porphyry deposits containing oxide, sulphide, and mixed oxide-sulphide ores of a grade that will soon have to be developed in the U.S. as a source of copper. KCC has already conducted years of detailed investigative work that spans reconnaissance drilling, close-grid drilling, and underground drilling and development. Kennecott has also accumulated considerable processing experience with Safford ore in a 1-tpd pilot plant equipped for continuous leach and wash cycles and an electrolytic recovery section. It was set-up to study the possibility of a full-scale conventional oxide recovery plant.

2-billion tons of 0.41% copper

Located in Arizona's Lone Star mining district, Kennecott's disseminated deposit contains a large reserve of low-grade copper. The test site is centered on the north flank of the mineral zone, which is situated within the Gila Mountains at an elevation of 5,000 ft.

After four years of geological and exploration reconnaissance, Kennecott purchased the property in 1959 when

It became clear that work had indicated the possibility of a large porphyry copper at depth. At the conclusion of development drilling, an estimated 2-billion-ton reserve had been indicated consisting of oxide, mixed oxide-sulphide and sulphide mineralization that averaged a probable 0.41% total copper.

The formations exposed in the Lone Star District are predominantly volcanics with some intrusives. The oldest pre-mineral rocks are primarily andesitic volcanics believed to be Cretaceous. They are cut by several strong, broad, northeasterly trending fracture zones. Most of the fractures were intruded by Early Tertiary igneous bodies of rhyolite, latite, quartz monzonite, granodiorite and quartz diorite.

This complex is overlain by two series of post-ore volcanics with a total thickness ranging from 200 to 800 ft. The older of these consists of flows of andesite and dacite. The youngest volcanic rock, which caps the Gila Mountain Range, consists of Quaternary basalt flows and some interbedded tuff beds. These rocks decrease in thickness and pinch out in the vicinity of Kennecott's deposit, and are not found on the south side of the range.

Copper mineralization occurs in the Cretaceous and Early Tertiary volcanics under generally rugged surface topography (see accompanying maps and sections). In cross section the deposit is like an irregular ellipsoid some 3,600 to 4,000 ft long and about 1,600 ft thick. It is overlain with a leached capping and barren volcanics that vary from 500 to 1,300 ft in thickness. Kennecott says that about one-half of the indicated reserve is relatively enriched oxide ore. The principal copper minerals in this portion are chrysocolla and brochantite. Another one-third of the total ore consists of a mixture of oxides and primary and secondary sulphides. In addition to the foregoing oxide minerals, other ore minerals include chalcopyrite, chalcocite, covellite and minor amounts of bornite and molybdenite at depth in the sulphide zone.

The climate is typical of the southwestern desert areas of the U.S., with little rainfall, hot summers and mild winters. Kennecott's ore environment is dry and above any known water table. Exploration holes on the north flank of the deposit, near the proposed test site, have penetrated to depths of 3,000 ft and no ground water has ever been encountered there or in the underground workings. A water well field has been drilled near the town of Safford that is estimated to be capable of developing an 8,000 gpm supply, although the flow is rather saline for an electrolytic section.

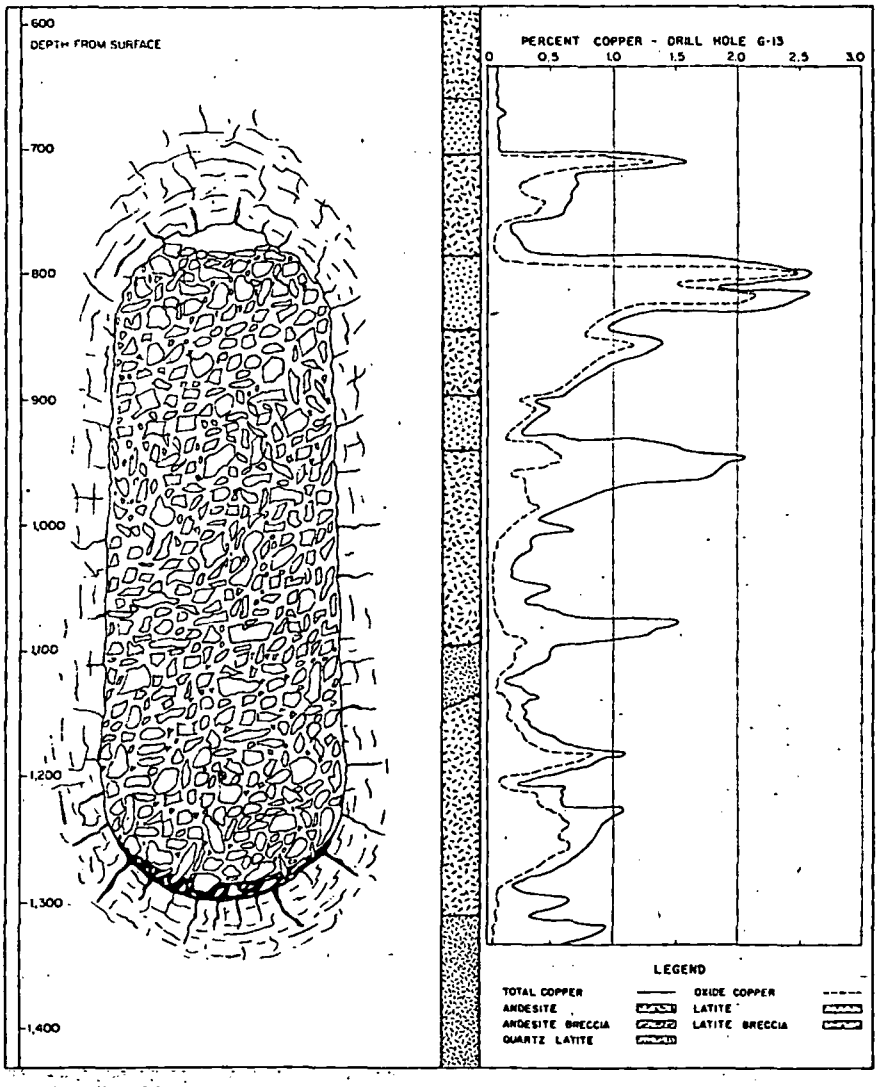

Total and oxide copper content of ore is flashed against the chimney site from data collected in one of Kennecott's earlier exploration drill holes.

How ore responds to leaching

Although Kennecott's pilot plant test work was aimed at design of a leaching plant for a conventional mining operation, these conclusions can be drawn concerning behavior of the ore in an in-situ leaching situation, according to the Project Sloop report.

(1) Safford ore can be treated for the recovery of copper by a moderate strength sulphuric acid leaching process. (2) In pilot plant testing, overall copper recovery on oxide ore grade material ranged from 70% to 80%. In an in-situ environment a somewhat lower recovery may be anticipated. (3) Overall acid reagent consumption in the test work averaged 40 lb per ton of ore. (4) High purity copper, approaching that of electro-refining methods, can be produced by electrolysis of strong leach solutions with no special purification of the feed solution indicated other than a dechloridization step.

Kennecott started initial metallurgical studies on Safford ore in 1957 using samples of diamond drill core from earlier exploration holes. These laboratory scale results when projected to a vat leaching cycle suggested a recovery of 76% of the copper from ores assaying 0.96% copper, and 85% recovery for higher grade ores averaging 1.00% copper.

As part of Kennecott's evaluation of the Safford deposit, an 800-ft development shaft and 3,000 ft of underground working were driven into the oxide ore horizons. From these openings some 52,000 ft of underground core drilling were completed in 1961. The core and excavated material furnished bulk samples for the 1-tpd pilot leaching plant that was constructed adjacent to the shaft site. The principal objective of the pilot was to try the vat leaching and eletrolytic studies on a level larger than laboratory scale and to determine the effects, if any, of the saline well water developed by the company near Safford since it would likely be the only

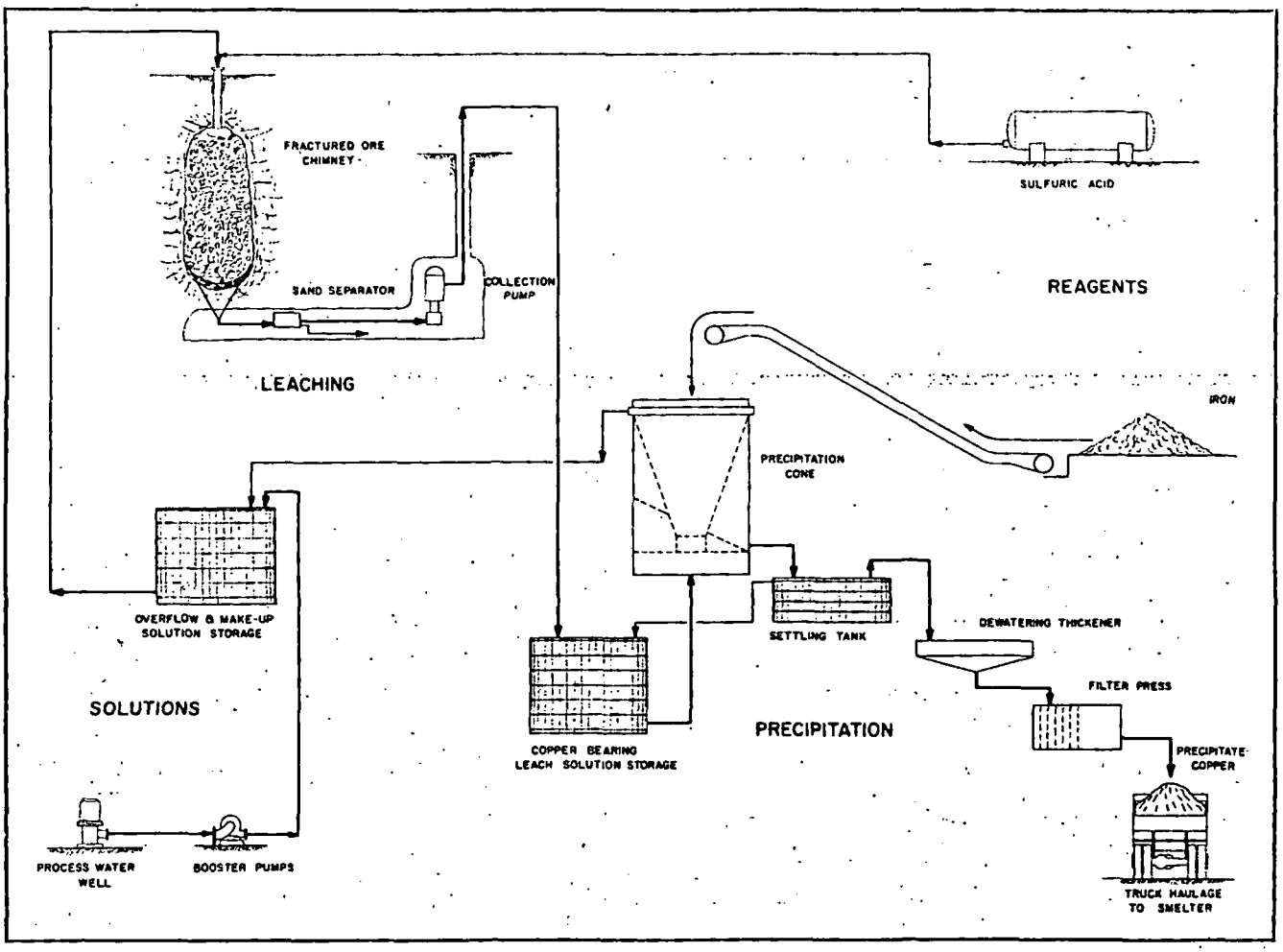

Surface precipitation plant would be sized to handle 2,600 gpm of pregnant solution and equipped to return the barren liquor with make-up water and acid to the chimney input holes. Plant will be forced to use saline water.

process water available for a production operation.

How the chimney is formed

For rock breaking, the Project Sloop report expains that a fully contained nuclear blast underground breaks only about one-seventh of the rock that might be shattered with a near-surface detonation that heaves fragments into an inverted cone. The latter, however, obviously vents radioactive gases to the atmosphere.

On detonation of a contained nuclear explosive, the energy is released in a fraction of a micro-second. It vaporizes, melts and crushes surrounding rock with the formation of spherical cavity that expands around the blast center until the cavity gas pressure approaches equilibrium with the weight of overlying rock.

The molten rock that initially lines the cavity walls flows to a pool on the bottom. As this slag cools and solidifies into a relatively inert glass, it traps up to 90% of the radioactive fission products generated by the explosion. The cavity roof is fractured by the shockwave and effectively undercut starting a caving action. The chimney has a radius approximating the cavity, and normally extends to a height of four or five cavity radii.

The AEC, which has experience with over 225 nuclear shots, points out that similar explosions in granite yield an extremely permeable rubble with 75% of the fragments under 12-in. in size. Outside fracturing beyond the chimney walls may increase original permeability of surrounding formations for a distance approaching three cavity radii. Without the physical displacement of cavity collapse, however, this fringe permeability would be much lower than the cavity with its 25% void space.

Experimental design of Sloop

The tentative location for the test shot is Kennecott's exploration drill hole G-13 (see maps), which is far enough from the existing shaft to minimize damage, according to the report. Lawrence Radiation Laboratory has recommended a group of pre- and post-shot holes for control and monitoring of the explosion and its effects.

Four pre-shot surface holes would be drilled in the chimney area 200 ft below the shot depth to establish the distribution and amount of copper. Cores and geophysical logs would be obtained to make studies of the chemical and physical characteristics of the rock. Borehole photography and drill stem pressurization tests would be conducted to determine in-situ fracture distribution and permeability. A fifth pre-shot hole would be bored outside of the chimney area to verify geologic data and would be instrucmented for shock time-of-arrival, pressure, and particle velocity measurements.

The nuclear device would be emplaced from the surface in an approximate 20-in. dia uncased hole at the planned 1,200-ft depth. At this level, it would be about 100 ft below the existing drift horizon in the mine. Stemming could be accomplished by grout plugs and pea gravel. The shaft would be stemmed for approximately 50 ft with local surface material and 50 ft of sand, charcoal, and asphalt. Physical effects measurements would be made in the shot hole and in the satellite hole. The mine workings and ground surface would be instrumented for earth motion, and seismic data would be recorded at various stations.

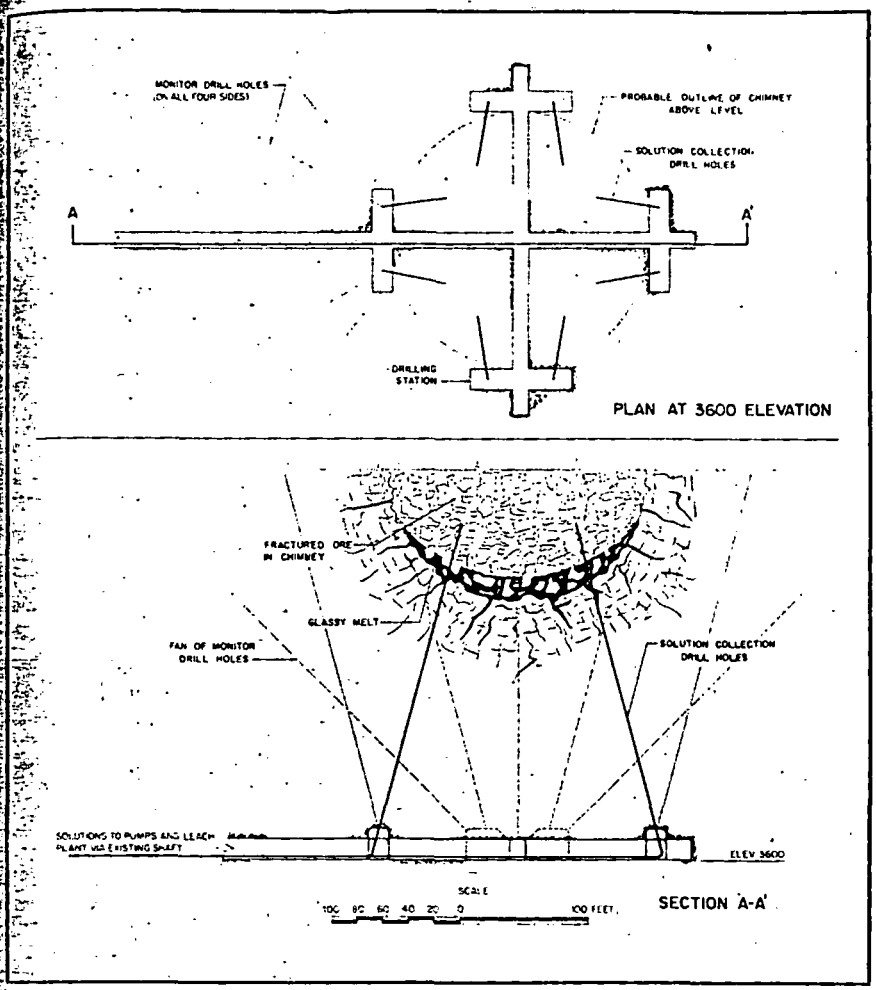

Solution recovery and monitor holes would be drilled from development headings located about 100 ft below the lower end of the nuclear cavity.

All holes within 1,000 ft of the shot would be stemmed.

While the AEC believes the Safford site could contain explosive yields of up to 100 kilotons, the use of a device with this much energy would not be considered until results of the smaller 20 kiloton device were fully evaluated.

For post-shot studies, LRL suggested an 8¾-in. vertical hole near the emplacement hole to enter the void at the top of the chimney. It would be used for defining chimney characteristics and for leaching studies. LRL also recommended two 6⅞-in. holes to a depth of 1,400 ft outside the chimney area. Two whipstock holes would then be drilled from each of the last holes to intersect the chimney edge and cavity bottom.

Samples of the atmosphere and a complete set of geophysical logs, cores, downhole photos and TV will be taken in all holes. Chimney volume and fracture permeability will be studied by pumping compressed air into one of the holes intersecting the chimney. The collected data would provide an assessment of the distribution of heat energy and radioactivity, chimney particle size distribution, and associated permeability in the fracture zone after the blast is detonated.

The leaching program

Three leach solution input holes would be drilled from the surface to tap the top of the chimney zone. Underground drift and cross-cut development would be driven 200 ft below the shot point to establish drill stations for holing the bottom of the cavity with a solution recovery system. This development would be about 100 ft below the bottom of the cavity. In addition to cone precipitators capable of handling a daily throughput of 2,600 gpm, the surface plant will include facilities for make-up water, solution pumping, acid storage, and iron and copper precipitate handling and storage.

The leaching studies would take one to three years. A primary concern during this stage would be potential industrial radiological safety problems that might be encountered as a result of solution treatment of the broken rock. These would be primarily due to tritium and to acid soluble fission products entering the circulating leach solution. Investigations indicate, the report states, that radiation from the leach solutions would be at such low levels that no shielding would be required for personnel protection. Very little additional operating cost would be incurred by the housekeeping type precautions required to assure complete operational safety in handling the solutions.

Treated water vapor from leach solutions could constitute a hazard in the underground workings or in the precipitation plant, if allowed to collect or concentrate where it could be inhaled or absorbed through the skin. Process plant design specifying enclosed pipeline handling of solutions and adequate ventilation would minimize the potential hazard.

The tritium content of process solutions could be greatly reduced by initially flushing the chimney with water prior to the start of leaching. The flushing fluids would be chemically controlled in order to dissolve a minimum amount of copper, and if they become contaminated, they would be disposed of in accordance to AEC and State regulations.

Extensive laboratory studies at Oak Ridge have investigated the possibility of radioactive contamination of the finished copper causing a health or marketing difficulty. Copper itself is not rendered radioactive for any significant time because its radionuclides are very short lived and decay rapidly.

The 5% to 10% fraction of the fission products that are not trapped in the relatively insoluble glass slag at the bottom of the cavity would be dispersed in the chimney in a more leachable form. Many of these products, however, would be strongly held on the ore by adsorption mechanisms and would not build-up to significant concentrations in circulating solutions.

A portion of the copper precipitates would be used for studies to determine the most efficient process for refining the metal commercially. Solvent extraction methods, electrolysis of dissolved precipitates in acid and conventional smelting followed by electro-refining methods would be investigated.

Substantial quantities of cement copper would be produced from the test program. After the experimental requirements of Project Sloop are satisfied, commercial usage of copper could be permissible under suitable regulatory arrangements with the parties involved in the test.

Distribution of radioactivity

In developing a concept for Project Sloop, LRL points out that the only long-lived soluble fission products which may interfere are: Cs 137, Ru 106, Zr-Nb 95, Ce 144, Ce 141, Y 91, Pm 147, Sr 90 and Sr 89. Of the

radionuclides trapped in the glass matrix at the bottom of the cavity, less than 5% is solubilized in normal leaching of the glass at pH of 1.5 to 2.0. Ce 141, Sr 90, and Cs 137, however, have gaseous precursors, and Ru 103-106 is a volatile compound that can be deposited on readily accessible broken rock at considerable distances from the melt zone. These four, particularly the Sr, are more readily leachable and in laboratory experiments have constituted the bulk of the activity in the first increment of solution through the leach bed. Ce and Ru are about 10 times more soluble at a pH of 1.5 than at 3.1.

Irradiation of Safford ore at Oak Ridge National Laboratory indicated that Sc 46, Co 60, Mn 54, Fe 59, Zn 65 and Se 75 would probably be the most important induced long-lived radionuclides. Sc and Fe are significant at early times, but Co, Zr and Se are most important later.

Personnel from Oak Ridge say that the ion exchange properties of the copper ore are highly important in regulating the quantities of certain radionuclides that dissolve from the ore. Safford ore adsorbed Cs 137 and Zr-Nb 95 very strongly from leach liquors. Sr was adsorbed much less, although still significantly.

They also say that the rubble-filled chimney in a continuous leaching cycle will function as an ion exchange column. Radionuclides dissolved from the ore early in the leach cycle would tend to be adsorbed on the ore in later leach cycles. This would limit the build-up in concentration of certain radionuclides in the leach solution to levels far below those that would be predicted on the basis of simple batch tests. The radionuclides formed by neutron activation of the ore should not be of importance in the processing cycle.

Contamination of copper

Cementation tests showed that only Ru 106 and Zr-Nb 95 precipitate with the copper to a significant extent. Certain potential activation products, such as mercury and silver, cement quantitatively with copper, but after considering the quantities of each of the various radionuclides it was concluded that Ru 106 was the only radioisotope that was important in the contamination picture. Over 50% of the soluble Ru followed the copper and ORNL tests determined that 20% of the Zr-Nb followed copper.

Direct smelting of Ru-contaminated cement copper showed that all the Ru appeared in the blister copper. Electrolytic refining, however, gave a relatively pure copper cathode. Following electrolysis, 66% of the Ru remained with the electrolyte and 33% dropped out as anode mud. Only 1% of the contained Ru content followed the copper to the cathode. Of the total induced activity, only 5% went into solution and only 6% of this soluble fraction, principally Zr and Se, ended up with the cement copper and these dropped out in the slag during smelting.

Recovery of copper from leach solutions by solvent extraction is a potential alternative to cementation, and this route will be investigated if Project Sloop receives approval. Soluble copper taken into the extractant can be stripped by 2 mol H_2SO_4 and this solution can be fed directly to electrolysis. Preliminary solvent extraction tests have indicated a good separation of copper from ruthenium as well as all other important fission products with the possible exception of Zr-Nb 95.

Safety considerations

The scaled burial of the shot is greater than that which is normally required from the standpoint of containment of the energy.

The probability of a stemming failure would appear to be extremely small, however, the possibility of some minor venting cannot be ruled out says LRL. Because of the competence of the overlying formations, it has been estimated, for the worst credible case, no more than 5×10^7 curries at one minute could be released through a fissure and be injected into the atmosphere after the shot.

In such an eventuality, the predominant nuclides in the radioactive cloud would be Kr, Xe, I, and their decay products. The distribution and intensity of this fallout can be controlled by detonating the explosive under specified meteorological conditions.

It is the judgement of LRL that in no case will iodine levels exceed values which, with proper operational control and monitoring, could lead to excessive exposure to individuals in the public. In making this judgment, LRL assumes that radiation protection guidance published by the Federal Radiation Council would apply.

If Sloop demonstrates a new mining technology, here is a benchmark on what it might do for U.S. reserves. In 1965 USBM estimated the domestic total at 75-million tons of copper in ores of 0.86%; another 58-million tons may exist in 0.47% sub-ore.

[1]Project Sloop, PNE 1300 Nuclear Explosives — Peaceful Applications is available from the Clearinghouse for Federal Scientific & Technical Information. National Bureau of Standards, U.S. Dept. of Commerce, Springfield, Va. 22151, for $3 (printed copy) or 65¢ for microfiche.

Kennecott and West German consortium consider cooperation in ocean mining

TALKS OVER POSSIBLE COOPERATION in ocean mining of manganese nodules are being conducted by a three-member consortium of West German mining firms—Preussag AG, Metallgesellschaft AG, and Salzgitter AG—with Kennecott Copper Corp. of the US. The talks are still at an "exploratory stage," according to Dr. Hans Amann, chief of Preussag's Ocean Technology Department.

Amann told E/MJ that "Kennecott has asked if we could chip in as much as $30 million to $50 million per year starting in 1974 for ocean projects." The German consortium is presently spending only $3.1 million per year for deep sea manganese nodule exploration and mining technology, and virtually concedes that it could not afford the ante without far greater assistance from the German government. Bonn's current plans envision support of only about $700,000 per year through 1975.

The German group, however, does not view the sums named by Kennecott as hard and fast. "But Kennecott has been active in ocean mining research since 1962, has the greatest experience in the field, and obviously is going to put a price tag on sharing in its knowhow," Amann said. According to the Preussag official, the talks with Kennecott are one in a series of bilateral and multilateral talks underway which could lead to a new major cooperative venture or ventures involving mining firms and oceanology institutes from the US, France, Japan, the USSR, and West Germany.

The German trio, which formally banded together in a consortium called AMR last December, has been active in Pacific manganese nodule exploration and technology for three years. In 1970 and 1971, it chartered the *RV Prospector* from Deepsea Ventures for Pacific research, and last December wrapped up what a Metallgesellschaft official describes as a "highly successful" four-month survey of manganese nodules over a 115,800-sq-mi Pacific parcel between the Clarion and Clipperton fracture zones, some 750 mi southeast of Hawaii. The group is now using the German ship *RV Valdivia*.

Last year's *Valdivia* expedition had succeeded in defining a right-angle chain 80 mi perpendicular and 310 mi east-west containing "sizable stores" of manganese nodules at depths of 16,400 to 19,700 ft. Some results are still being tallied and a complete report is slated to be released on April 15. But the official said that the nodules have averaged out to over 3% copper and nickel.

The consortium is presently carrying out a new, four-month research voyage southeast of Hawaii from March to July. And based on the promising results of the latest trip, Amann told E/MJ that the group is planning six months of exploration in the general region next year. Moreover, the German companies hope to complete a feasibility study of manganese nodule ocean mining by 1977 with about $3 million from the German government.

In ocean mining technology, Preussag geologist Fritz-Otto Poeppel said that Pacific tests by an international group last summer have "proven the potential," given the right circumstances, of Japan's Continuous Bucket Line (CBL) system for manganese nodule mining. Some 28 companies from six countries—Japan, the US, Australia, Canada, France, and West Germany—calling themselves the International CBL Syndicate, participated in the $1.2 million testing project.

Poeppel described a sufficiently level ocean bottom topography with relatively constant current conditions as prerequisites to use of CBL. Rough topography and changeable currents generally foiled success with the system, and entanglements of its 45,900-ft cable were common under unstable current conditions, as the bucket operated at depths of 16,400 ft and more.

Poeppel said that modifications are in order for some components of the CBL system—for example, the dredging buckets and friction drive of the hoisting cable. "But it is all but certain that the system will be used in regular production for removal of manganese nodules," he predicted. Other means of retrieval—probably more costly hydraulic systems—will have to be perfected for undersea conditions not suitable for the CBL system, Poeppel said.

In a roundup of other ocean mining projects by the German trio, Preussag's Dr. Harald Baecker reviewed 1971 and 1972 Red Sea trips aboard the *RV Valdivia* for exploration of sea bottom ore sludge. Though the bulk of exploration concentrated on the Atlantis I and Atlantis II deeps, the entire central region of the sea was studied. Sufficient concentrations of copper and zinc were found in sludge at several sites to suggest that mining could be feasible, and that even ore in place might lie beneath the sludge at some locations. "The main problem, however, is feasible technology for separation of the metals we want from the worthless substances."

Meanwhile, E/MJ has learned that a number of mechanical engineering firms from West Germany—such as Krupp and Demag—as well as other metal processing companies would soon join with the AMR consortium to give a financial boost, especially in ocean mining technology. □

EPA appoints effluent standards advisory committee

THE ENVIRONMENTAL PROTECTION AGENCY (EPA) announced in February that nine persons have been appointed by administrator William D. Ruckelshaus to form the Effluent Standards and Water Quality Information Advisory Committee. The committee was created by the Federal Water Pollution Control Act Amendments of 1972 to advise the administrator on the development of new effluent standards and water quality information. It will conduct public hearings and provide technical information to the administrator for making decisions on the effluent standards. The standards are used in the issuance of wastewater discharge permits as required by the new water law.

Following is a list of the names of the committee members and their affiliations:

- Don E. Bloodgood, 70, is professor emeritus of sanitary engineering at Purdue University, West Lafayette, Ind., and has had long experience in the fields of municipal and industrial waste treatment.

- William W. Eckenfelder, Jr., 58, who is distinguished professor of environmental and water resources at Vanderbilt University, Nashville, Tenn., is an expert on biological treatment of sewage and industrial wastes.

- Robert B. Grieves, 37, is a professor and chairman of the Dept. of Chemical Engineering at the University of Kentucky, in Lexington. He has specialized in industrial water and waste treatment.

- Ramon Guzman, 49, a chemical engineer with the School of Medical Science at the University of Puerto Rico, San Juan, is a specialist in industrial waste problems and is in charge of all water and sewage operations for the Puerto Rico Aqueduct Authority.

- Lloyd Smith, Jr., 63, a professor in the Dept. of Entomology, Fisheries, and Wildlife at the University of Minnesota in St. Paul, is an expert on the effect of water quality on fisheries and other aquatic life.

- Martha Sager is a professor and director of Environmental Systems Management Program within the Center for Technology and Administration, College of Public Affairs at American University, Washington, D.C. She specializes in sanitary engineering and industrial microbiology.

- Blair T. Bower, 47, is associate director of the Quality of Environment Program of Resources for the Future in Washington, D.C. A social scientist, he has worked with the Delaware River Basin Authority.

- Robert McCall, 59, is director of Environmental Health Services of the West Virginia Dept. of Health in Charleston.

- Glenn Paulson, 31, is a staff scientist with the Natural Resources Defense Council in New York City. He worked with Dr. Rene DuBois in the Dept. of Enviro-Biochemical Medicine at Rockefeller University in New York. □

(Continued on p 35)